Report LR-600

Essays on Stability and Control

October 1989

Edited by M. Baarspul and J.A. Mulder

TU Delft

Delft University of Technology

Faculty of Aerospace Engineering

ESSAYS ON STABILITY AND CONTROL

Edited by M. Baarspul and J.A. Mulder

ESSAYS ON STABILITY AND CONTROL
'Liber Amicorum'

Dedicated to Prof.Dr. O.H. Gerlach
on occasion of his retirement as professor
of the Faculty of Aerospace Engineering of
Delft University of Technology

October 27th, 1989

CONTENTS

Preface

The present report is a 'liber amicorum' dedicated to prof.dr. O.H. Gerlach on the occasion of his retirement as a professor at the Faculty of Aerospace Engineering of Delft University of Technology on November 1st 1989. After an appreciation of prof. Gerlach as an educator, scientist and leader, the report opens with a reprint of the 20th Lanchaster Memorial lecture which was delivered by prof. Gerlach himself to the Royal Aeronautical Society in 1977.
The title of the lecture 'Developments in mathematical models of human pilot behaviour', clearly reflects his main interest in aircraft stability and control, i.e. the role of the human pilot in flight management and control. The other contributions are by former students and co-workers, reflecting the wide variety of work, both scientific and technical, for which the education in Stability and Control under prof. Gerlach's supervision proved to be a sound foundation.

Prof.dr.ir. O.H. Gerlach - educator, scientist and leader

An appreciation

In 1945, just after World War II, Otto Herman Gerlach as a young student entered Delft University of Technology for the study of aeronautical engineer. Already during this study he obtained an appointment as student-assistant at the University and was also selected for training as professional pilot at the Dutch Government Flying School. In May 1951 he graduated cum laude at Delft and became a full staff member at the Aeronautical Department, in charge of flight test research and educational tasks.
In the same year I myself also became a staff member at the University and we both assisted the founder of the Department, prof.dr.ir. H.J. van der Maas. His field was flight mechanics, including flight testing. I still remember the discussions with Otto Gerlach about the choice of subjects to divide between us. He deliberately wanted the field of stability and control for himself, being convinced that this had a greater scientific content than the other branch of flight mechanics: the performance of aircraft. In the fifties his view was certainly right and in later years we became both satisfied by the original choice. The performance field extended to include aircraft design, propulsion and more recently even advanced optimization techniques. Our successors will meet each other again because in the latter mathematics and control theory plays an important role also!
Next to theoretical work, Gerlach had in his early years at the Department an active role in flight test work. He even introduced me, as a non-pilot, into some practical experience in flight. In the old Tiger-Moth airplane he took me up to show me looping and spin manoeuvres in an other way than on paper. I could stand this all up to the final part of the demonstration of very tight turns, which made me finally air sick. On another occasion he showed me the necessity of wheelbrakes by performing an unbraked landing run at the long runway of Maastricht Airport with the Auster test-airplane of the Department. When the Department obtained the De Havilland Beaver Aircraft for flight tests in 1958, Gerlach continued being one of the test-pilots. His early research was in the field of conventional flight testing in steady flight. But his mathematical interest, combined with practical knowledge, made him start the development of the theory and practice of measurements in non-steady flight, based on aerodynamic modelling of the aircraft and the propulsion system. This became the subject of his extensive thesis to obtain the Ph. Degree at Delft University of Technology in 1964. He pioneered with his able staff in the technique of non-steady measurements in actual flight testing with the Beaver aircraft. This technique made it possible to obtain performance and stability and control characteristics together in the one short flight manoeuvre, reducing the required flight-test time considerably in comparison with the technique of steady-flight measurements of the older days. Gerlach had lengthy discussions with his promotor, prof. Van der Maas, to convince his older colleague as a flight-test pilot of the usefulness and reliability of this new method of performing flight tests.
The work of Gerlach's group also brought about extensive work on dynamic flight testing at the National Aerospace Laboratory NLR in Amsterdam. After his promotion to senior-lecturer at the Department in 1959, Gerlach became full-professor at the University in 1965.

In the fifties and beyond Gerlach showed his broad scope as an aeronautical engineer and scientist, not only in his flight-test work but also in his view of the important role that flight simulation was to play in the field of stability and control in the early sixties. An analogue flight simulator with the cockpit of an old Second World War bomber was installed at the Department soon to be followed by another cockpit with moving base and visual system. In this moving base the hydrostatic bearing hydraulic servo's, designed by prof.dr.ir. T.J. Viersma of the Department of Mechanical Engineering of Delft University were applied. This unique device became known world-wide and was applied later by several flight simulator manufacturers abroad. Under the pushing guidance of professor Gerlach, the flight test simulation laboratory of the Department has developed from the analogue system with simple cockpit to a very modern set-up with digital techniques using a large Gould computer. Until today non-steady flight techniques and flight simulation are the key-stones of research on stability and control of aircraft. In the field of simulation techniques cooperation with NLR and other institutes abroad has been stimulated by Gerlach. In his inaugural speech in 1965 professor Gerlach paid also attention to the then new field of attitude control of spacecraft. At that time an inauguration was performed in a former church in the old inner city of Delft, without the at present normal practice of using visual presentations. He then took the unusual step of showing a small model of an airplane, at first hidden under his desk, to demonstrate the stable and unstable rolling motions, depending on the rolling velocity. Although his personal interest mainly stayed in aeronautics, he made arrangements in his group to start lectures on attitude control of spacecraft combined with some research topics, still part of the work at the Department.

In the educational program of the Department Gerlach played an important role. From the start of his career in Delft he lectured the basic course of aircraft stability and control for all students and, due to his initiative and efforts, several advanced courses on aircraft control system technology and aircraft response in disturbed flight conditions emerged. Many students of the Department selected and still select Stability and Control for their final study and they all enjoyed the thorough knowledge of prof. Gerlach and his staff-members during the lectures and their thesis work. This thesis work is mostly derived directly from ongoing research in the group and the contributions of students to the results of this research (by able conductance of their work) have been noticeable, not in the least by the able supervision. Since his appointment as professor about 210 students obtained their Delft degree in the discipline stability and control. But from the seventies on the scope of Gerlach's activities was very much widened up. He was prepared for these larger responsibilities not only by his work at the Department, but also by a long time membership of the Advisory Committee on flying qualities and aircraft operations of the NLR, of the Flight Mechanics Panel of AGARD and of the Dutch Civil Aircraft Accident Investigation Board.

When his academic 'father-teacher' professor van der Maas retired in 1971 from the chairmanship of the Board of the National Aerospace Laboratory in Amsterdam, Gerlach heritaged this very important position in the Netherland's aerospace research. As chairman of this Board he also became a member of the Board of the Netherlands Agency for Aerospace Programs NIVR, bringing him in close contact with the aircraft and spacecraft-development programs of this Board.

After his retirement of the University, Gerlach will end an active period as academic educator and scientist, but he will continue the chairmanship of the NLR-Board.

Since 1971 he has shown the leadership, which his predecessor had already foreseen. As a member of the NLR-Board myself, I have personally observed his intense efforts to further the research at the NLR, which is so very essential for the advancement of the development and operation of aircraft in the Netherlands. Financial constraints, imposed by the Government, have to be tackled in continuous efforts by talks with responsible persons in the Government.
As chairman of NLR Gerlach has been instrumental to foster international cooperation for the Netherland's aeronautical research activities. Under his NLR-leadership the German-Dutch Wind Tunnel (DNW) in the North-East Polder was built and brought in operation with much success as the largest subsonic wind tunnel in Western Europe.
As National Delegate for the Advisory Group for Aerospace Research and Development (AGARD), he became Chairman of the National Delegates Board in the three years term 1982-1985. At the twice-a-year meetings of the Board I noticed, being one of the panel chairman, his ability to guide international meetings with the thoroughness, which characterises his work continuously. In the international field Gerlach has held and still holds other important positions, among others Chief Representative in the Council of the Group of Aeronautical Research and Technology in Europe (GARTEUR), which brings the aerospace laboratories in Western Europe together in combined research projects.
During his career he published a number of papers among which the prestigious Twentieth Lancaster Memorial Lecture for the Royal Aeronautical Society in England in 1977. In this lecture he discussed the developments in mathematical models of the human pilot behaviour.
This paper is included in this book to honour his personal interest in man-machine relations in the aeronautical field, which I did not mention earlier. From personal discussions I know that he does sincerely hope that this subject will hold the interest of our Department in connection with the other research topics of his group.
This appraisal of the career of professor Gerlach at Delft University of Technology should not be ended without mentioning the personal support from his wife, Mrs. Annie Gerlach. With their two children, she gave him a family life, which is so important for a man who in his professional life is fulfilling tasks of great responsibility.
On the occasion of his retirement of Delft University of Technology, it is appropriate to thank professor Gerlach on behalf of the aerospace community in the Netherlands for his efforts to foster and to contribute to the education and the research in aeronautics in our country.
Respectfully the thanks of his colleagues, his staff members, his former students and all others at the Department of Aerospace Engineering are added to this vote of thanks.
But we not only acknowledge our respect, many of us deal feelings of friendship with prof. and Mrs. Gerlach, which will continue in the years to come. For these years we wish you both all the best. May Professor Gerlach continue his best efforts for Dutch aerospace, but may he also find time for his hobby in the photography and some personal research with his computer at home!

Prof. Hans Wittenberg,

Dean of the Faculty of Aerospace Engineering
and friend during a life-time.

DEVELOPMENTS IN MATHEMATICAL MODELS OF HUMAN PILOT BEHAVIOUR

O.H. Gerlach

Delft University of Technology

Contents .

1. Introduction

Presenting the Twentieth Lanchester Memorial Lecture certainly is an honourable and pleasant experience. The subject of my Lecture has several ties with the memory of Frederic William Lanchester.

By way of introduction, I suggest you consider for a moment four aircraft as dissimilar as a small general aviation aircraft, a large transport such as the Airbus, a glider and finally a fighter aircraft such as the Tornado. As regards handling in the air of these widely differing flying machines, their most significant common quality is perhaps, that they can all be flown by a human pilot.

In the definition of the desirable handling qualities of these aircraft, one might - in complete innocence - expect to find a description of such desirable qualities in terms of the behaviour, capabilities and limitations of the human pilot, which one would, of course, expect to be independent of class or category of aircraft.

As we all know, the actual situation is somewhat different. We have different sets of rules for each different class of aircraft. These rules are expressed in terms of th characteristics thereof, although implicitly they lean heavily on the capabilities and limitations of the human pilot. In this situation one cannot help wondering, whether more fundamental answers to the perennial question of what constitute good handling qualities, could not be given with the aid of more explicit studies of the behaviour of the human pilot, his capabilities and his limitations. Quite naturally in an engineering community such as ours, the results of such studies would be expressed in terms of mathematical models of the human pilot. Precisely the development of such mathematical models is the subject of this paper.

There is more than one connection between this subject and the work of Lanchester, whose name and work we honour tonight. Lanchester's contributions to the field of aircraft stability and control are well known. They have been described in the Memorial Lecture (1) two years ago. Perhaps not so well known is the fact, that Lanchester had more than a passing interest in human perception, as exemplified by his paper on Discontinuities in the Normal Field of Vision (2), published in 1934. Undoubtedly the most fascinating aspect of the works of Lanchester is the extremely wide range of human activities covered. In modern jargon, Lanchester's interests were truly multi-disciplinary. On a more limited scale, the present paper will draw from a number of different disciplines which had Lanchester's interests and this is a further link with his work.

The history of mathematical models of human controllers goes back some thirty years, when Tustin (3) published the results of his pioneering experiments. It was the time when control theory was rapidly developing. Right from the beginning of this development the control of an aircraft was clearly recognized as an excellent example of a closed-loop control situation. Mathematical description of the system required a mathematical model of all elements in the loop, including the pilot.

Since those early days, mathematical models of the behaviour of a human operator in a closed-loop control system have been much improved. They describe a very narrow, highly specialized area of human activities. Even within this small area, four distinct pilot activities can still be discerned :

1. sensing the data required to control the aircraft,
2. processing the sensed data in the nervous system and the brain,
3. decision making in the brain, based on the processed data,
4. actuating the aircraft's controls by implementing the decisions, through the

actions of the brain, nervous system, muscles and skeletal bones.

In the past, pilot models tended to concentrate on the more overt actions of the pilot, in particular on the actuation of the controls. The present and future emphasis in modelling the pilot's activities will increasingly be laid on predominantly mental aspects, such as flight monitoring and decision making. For this reason this paper pays much attention to the physiological and psychological parts of the pilot's task, viz. processing of sensed data and decision making.

2. Engineering models

2.1. Introduction

In the past, many efforts have been made to describe pilot's behaviour by means of mathematical models of varying complexity. In order to set the scene for later discussions, this Chapter briefly presents two of the better known engineering pilot models which are used on a wide scale, namely:

1. the cross-over model,
2. the optimal control model.

Essential for these models is the empirically established fact (3, 4), that the human operator behaves like an essentially linear element if he is the controller in a closed-loop control system as shown in Fig. 1. In common with most other engineering models, the two models to be discussed here, are strictly valid solely under certain restrictive conditions:

1. the forcing function, i in Fig. 1, is assumed to be stochastic, or at least to appear stochastic to the human operator,
2. the controlled element in the closed-loop - i.e. the aircraft - is assumed to be linear,
3. full operator's attention is assumed in the performing of a continuous compensatory tracking task.

The latter condition implies that the operator is presented only with the error signal, e in Fig. 1. He tries to compensate or null the error through suitable manipulation of the controlled variable, c in Fig. 1. As will be seen later, in experiments it is not always easy to fulfil the requirement of attracting and holding the operator's full attention. In many cases it leads to a forcing function of rather higher bandwidth than would occur in actual flight.

2.2. The cross-over model

This model has been developed by McRuer, Krendel, Elkind and several others (5, 6). It presents the pilot's behaviour in the frequency domain, in the form of a describing function. The pilot is assumed to be the controller in a time-invariant, single-display, single-control system, as shown in Fig. 1. The describing function relates the pilot's output, c, to his visually observed input, e. There are several excellent descriptions of this model in the literatur (7, 8, 4, 5).

Under the various restrictive conditions summed up in 2.1., the cross-over model

briefly summarized in Fig. 2 appears to be a very acceptable approximation of the open loop characteristics of the control system in the frequency range around the cross-ove frequency, ω_c, where the open-loop gain $|H(j\omega_c)|=1$. The cross-over model of the human pilot is complete only, if two additions are made to the model.

In the first place, the so-called "verbal adjustment rules" are needed to select suitable quantitative values for the parameters K_p, τ, τ_I, τ_L, τ_N, τ_e and ω_c in the model. It is assumed that the pilot, through previous experience as well as through practice in the actual control situation, adjusts his behaviour in the closed-loop. The adjustment rules are intended to describe his behaviour in this adjusted situation Since these rules can be found at numerous places in the literature (7, 8), they are not repeated here.

The second necessary addition to the above model takes the form of data on the so-called pilot's remnant, i.e. that part of the pilot's output not linearly correlate with his input signal. From experiments it has been found, that the remnant can be described as an uncorrelated stochastic signal, having a continuous and reasonably smooth spectrum (7, 8, 9).

As stated, e.g. in (7), the cross-over model has been applied in many pilot-vehicl system analyses and also in pilot-vehicle-display system analyses, both in design and in simulation problems. The model has been extended to multi-display, multi-control situations (7, 10, 11), based on classical multi-loop control theory. As such, the use of the extended model relies heavily on judgements concerning the closed-loop system structure.

2.3. The optimal control model

This model, attributable mainly to Baron, Kleinman and Levison (12, 13), is applicable under the restrictions already mentioned in 2.1. The optimal control model, however, is of more recent origin than the cross-over model. It has been formulated in the time-domain, by means of the statevariable notation. As a consequence, the model is, in principle, suited to describe multi-display, multi-control situations. The matrix notation employed makes calculations on the digital computer rather straigh forward (14). It has been stated (12), that the basic assumption underlying the optima control model is, that the well-motivated, well-trained human operator behaves in a near optimal manner, subject to his inherent limitations and constraints and his control task. As it appears, the difficulty in using the model often lies in defining the optimum and these inherent limitations and constraints.

The blockdiagram of the model given in Fig. 3 shows, that the model contains a number of distinct, mathematically formulated elements: a time-delay, a Kalman-Bucy filter, a predictor to compensate for the time-delay, an optimal control law, the neuromuscular dynamics, and finally the observation noise- and motor noise-parameters. Extensive descriptions of the optimal control model can be found in the literature already mentioned. Data have also been given on the selection of the various parameter in the model. The correct selection of the weighting factors in the cost function, whi is to be minimised to attain the optimum, and especially the selection of the noise levels, are important to match the model to experimentally determined pilot describing functions.

In the literature a number of successful applications of the model can be found (12, 15). In addition, several attempts have been made to extend the optimal control

model from the basic single-display, single-control situation to multi-display visual observations (16), to multi-model observations (17, 18), to include the human information processing and decision-making processes (19, 20), and finally to describe various aspects of task-interference and pilot workload (21, 22). It should be noted, however, that several of these extensions of the optimal control model still need much further substantiation.

2.4. Remarks on engineering models

Engineering models have been useful and continue to be so. They have found many successful applications, as can be judged from the cited references.

It is the unquestionable merit of the investigators who developed the cross-over model, that they defined, experimentally verified, and subsequently applied a number of basic notions related to the performance of the human operator in closed-loop control situations. An excellent summary of this work is presented in (7). Most further related work, also that performed by different schools of researchers, builds on many of these same notions.

Both models discussed in this Chapter, however, have their limitations. If the cross-over model is to be used as a design tool, the fact that the model has been applied mainly to single-display, single-control compensatory tracking tasks sometimes is a severe restriction. Applying the verbal adjustment rules in more complicated situations is not always as straightforward a process as might be desirable. Using the cross-over model as a diagnostic tool requires identification of the model parameters in the given control situation. To this end a test signal has to be employed having a bandwidth much higher than, and in many cases quite different from, the input signal occurring in actual life. This may badly impair the realism of the entire test.

The optimal control model has so far seen application mainly as a diagnostic tool. This may be due in part to the fact already mentioned, that it appears to be not always easy to define a priori the optimum cost function, which the human operator is assumed to minimize. The selection of the levels of remnant power often appears a matter of judicious selection a posteriori, to match experimentally obtained data.

A rather severe limitation of both engineering models lies in the fact that they lack a direct connection with the pilot's subjective opinion of the workload involved in a given control situation. In the end it is this expert opinion, which decides on the acceptability, or otherwise, of an aspect of the aircraft's handling qualities. There exists, as yet, no generally applicable method to derive the pilot's workload from the parameters of the engineering model. There are serious doubts whether such a method will ever be developed.

An explanation of this very real shortcoming of most existing engineering models is considered to lie in the fact, that such models portray primarily the control aspect of the human operator's activities, thereby ignoring or bypassing the equally important mental activities of data processing and decision making (23). It seems, therefore, that there is a need for new developments, explicitly combining into a single mathematical model the internal mental processes of data handling and decision making going on in the human brain, with the more overt control activities previously discussed.

In this paper the view is held, that such new developments should lean heavily on the vast amount of relevant knowledge available in physiology and experimental psychology. In doing so, it may be well to consider the admonition of Rasmussen (24):

"When entering a study of human performance in real-life tasks, one rapidly finds oneself rushing in where angles fear to tread. It turns out to be a truly inter-disciplinary study for which an accepted frame of reference has not yet been established, and iteration between rather general hypothesis, test of methods, and detailed analysis is necessary".

3. Physiological and psychological concepts

3.1. Introduction

Before a further developed mathematical model of the human pilot can be described, it is necessary to discuss some concepts to be incorporated in such a model. Emphasis in the following is, therefore, on certain physiological and psychological aspects of human pilot behaviour. Four categories of closely related activities of the pilot have been distinguished in Chapter 1. Of these four, the processing of sensed data, the decision making in the brain, and the actuation of the aircraft's controls are considered below.

It will be clear from the outset, that in this field the discussion cannot aim for completeness. Only a few topics of the very many possible can be mentioned, and attention is concentrated on those having a direct bearing on mathematically modelling the human pilot. A discussion on the fascinating subject of how the pilot senses with his visual, tactile and proprioceptive, and vestibular sensors the multitude of data he uses to control the aircraft, has to be omitted altogether. Several surveys on this subject are, however, available in the literature (25, 26, 27, 28).

The discussions in this Chapter are centered around Fig. 4. This figure depicts the relations between the human operator and his environment in a way not unlike several authors have done before (29, 30, 31, 32). It pretends to be a very crude description of what goes on in the pilot's sensors, brain and muscles when controlling an aircraft. In order to keep the picture as simple as possible, many simplifications have been implied in the figure. The environment with which the pilot interacts, i.e. the aircraft and its dynamic behaviour, is depicted in an abstract form at the bottom of the figure.

The pilot interacts through two different interfaces with his aircraft environment On the left side of the figure is indicated, that he senses the aircraft's behaviour through his various sensors (visual, tactile and proprioceptive, vestibular). In the language of the control engineer this is the input side of the pilot. The right side of the figure shows, that the second interface between pilot and aircraft is formed by the effectors, i.e. hands and feet, with which he moves the manipulators, primarily the stick and pedals. Thereby he actuates the controls of the aircraft, in order to influence the aircraft's motions according to his will. This is, of course, the pilot's output side. In a highly schematic way the figure shows how the flow of sensed data is processed in the nervous system and brain, and how it is ultimately transforme into output commands, resulting in the desired movements of the manipulators and finally of the aircraft itself.

3.2. Data processing and decision making

3.2.1. Characteristic features

A first impression of what happens with the visually sensed data may be derived

from the fact that the retina in the eye contains some 120 to 130 million individual photoreceptors, the well-known rods and cones, whereas only about 1 million separate nerve fibers leave the eye through the optic nerve, see Fig. 5. The inevitable conclusion is, that in the various layers of nerve cells also contained in the retina, as shown in Fig. 6, a significant reduction of the data flow originating from the individual photoreceptors has already taken place.

The psychophysical theory of space perception presented by J.J. Gibson, see e.g. (33, 34, 26, 32), discusses the subsequent data processing taking place in the brain. Gibson noted, that the data about the world around us, as sensed by the very many individual sensing elements in the various sensing organs of the human, contain a large redundancy. In the handling of these redundant data in the brain, the key effect is, that the redundancy is removed step by step through a process of successive data reduction, obtained through increasing selectivity of the brain cells. This is precisely what has been indicated schematically in the left hand side of Fig. 4. In this process of data reduction the most essential elements of what we sense are emphasized.

As an example it can be mentioned, that physiological experiments (35, 36, 26) have shown, that in the visual cortex of the brain, certain cells are exclusively sensitive to certain elements or features in the visual image projected on the retina. It has been found, for instance, that some brain cells respond only to a band of light having a particular orientation, sweeping over the visual image on the retina. This experimental fact and other similar evidence fortify the theory, that from the multitude of sensed data only the most relevant parts are retained and passed on. Less essential parts are ignored and do not reach the higher centers of the Central Nervous System. In more general terms, one might say, that we do not perceive in a neutral way. We extract those data which we expect to be most relevant to our interaction with the outside world. Through this process of data reduction, the human operator is able to filter from the enormous amount of sensed data about the world around him, merely those data he needs to perform his task.

For a pilot controlling an aircraft these data are derived mainly from the visual sense, but also from the vestibular, the auditory, the tactile and the proprioceptive senses. To a certain extent the decision between essential features to be passed on and non-essential features to be dropped, seems to be an individualistic one, depending on criteria which are applied largely subconsciously.

An illustration of this latter point is the fact, that some pilots are far more sensitive to imperfections in the motion qualities of a flight simulator than others. Apparently the more sensitive pilots attach greater importance to vestibular motion cues. Usually they are not at all conscious of their subjective weighting of the various cues their brain processes.

According to the theory of Gibson, the internal representation of the outside world in our brain is thus based on a collection of characteristic features, or cues. One can distinguish the visual characteristic features and also the aforementioned vestibular cues, which are an important part of the well-known, but rarely defined motion cues.

3.2.2. Internal models

The use of characteristic features or cues to reduce the redundancy of the sensed data is a first and highly important step in the data handling process going on in the brain. But it is by no means the final one. It has been stated by many physiologists

and psychologists (26, 30, 32), that perception cannot be separated from memory.

If we have in our memory an expectancy or estimate of what we are going to perceiv next, we can and will use this expectancy. We do this, in order to obtain a further reduction in the data flow needed to remain aware of the world around us. The uncertainty about the surrounding world, which we have to bring down to an acceptably low level through our observations, is drastically reduced by employing these expected vlaues. In nearly all day to day situations such an expectancy or estimate exists.

A pilot flying an aircraft also knows, or rather expects, in a general sense what will happen next. This expectancy stems from his general flying experience and from the flight plan he made before taking off. On a more limited time scale, the pilot expects certain motions from the aircraft in the next few moments, because of his previous observations of the aircraft's motion and because he remembers the subsequently applied control deflections.

From this example it follows, that the expectancy or estimate of what we will observe in the very near future, is obtained from knowledge residing in our memory. It can generally be said to be due to the internal representation in our mind of the world around us. This internal representation is commonly called our "internal model". Obviously, the term "internal model" is used here in an abstract sense, rather than in a pictorial sense. Observing the continuously changing world around us can thus be described as entailing the construction and regularly updating of a predictive interna model, using various parts of memory to incorporate past experience.

The idea of internal models is not at all new. It was proposed as early as 1943 by Craik (37). The concept is gaining more and more acceptance, see (38, 39, 40, 41, 42, 24, 32).

In the more particular case of a trained pilot flying an aircraft fully familiar to him, an internal model can be said to exist in his brain for each of the sensory channels. These internal models provide a prediction or estimate for each characteristic feature the pilot is paying attention to. The various partial models combined make up the total internal model mentioned above. The internal model is thus - subconsciously - employed to predict the impending motion of the aircraft.

Observations in the form of observed characteristic features serve to update this predicting internal model. Each subsequent observation updates the internal model anew Under suitable conditions, the observation of very few, but well selected, characteristic features may suffice to realign the internal model, and to keep it going for a while, without an immediate need for further sensory data processing. In this way the utmost reduction in the data flow in the brain is achieved.

To amplify on the above, it should be noted, that for the pilot to observe his own control actions - through characteristic features perceived by the tactile and proprioceptive senses - is quite essential. They help to provide him with a sufficiently accurate estimate of the aircraft's motions in the near future.

Returning once more to Fig. 4, it will be seen, that in the middle bottom part of the figure the receptors partly overlap with the effectors. This has been done intentionally, to indicate clearly, that some of the sensors, namely the tactile and some of the proprioceptive sensors, are located right inside the effectors. In this way these sensors provide the highly essential, direct feedback to the pilot's nervous system of the actual manipulator deflection applied to the aircraft.

Vestibular motion cues are used in the pilot's brain for the same purpose. In the absence of motions directly due to external disturbances, the vestibular motion cues may also help to improve knowledge about the most recent control actions, in order to

provide a more accurate prediction of the subsequent motion of the aircraft.

3.3. Actuating the aircraft's controls

3.3.1. The neuromuscular/manipulator system

The neuromuscular system is the interface between the pilot's brain and the aircraft's manipulator, i.e. the control stick, the wheel, or the side-arm controller. The input to the system is generated in the brain. The output signals are both the control force exerted on the manipulator and the manipulator deflection. Because of the close interactions between the characteristics of the neuromuscular system and those of the manipulator, a description of the neuromuscular system has to include the manipulator as well.

Mathematical models of the neuromuscular/manipulator system have been presented, e.g. in (23, 43). If known or estimated quantitative values of the various constants (44, 45) are substituted in such a model, it turns out, that this system should generally have a bandwidth of more than about 50 rad/sec. Carefully executed measurements on two widely differing neuromuscular/manipulator systems, reported in (46), showed in both cases a bandwidth of only 10-11 rad/sec. This fact clearly indicates, that the bandwidth of the system is not determined by the masses, spring constants and dampings of limb and manipulator alone, although these play a certain role.

It appears, that the bandwidth or speed of response of the neuromuscular system is restricted rather severely in higher centers of the brain. According to (30) and others, this activity takes place in the part of the brain called the cerebellum, where an important part of our control of limb movements resides. In terms of a mathematical model, the mechanism accomplishing this fact might be called a shaping network or, more specifically, a low-pass filter.

3.3.2. Standard output motions patterns

In further discussing the way in which the pilot effectuates the desired motions of the aircraft's manipulator, another psychological aspect has to be mentioned, apart from the various physiological items discussed in the previous paragraph.

It is of course well known, that highly skilled and heavily practised, complex patterns of limb movements play a major role in most manual systems, including manual control systems. Such situations comprise, for instance, playing a musical instrument, or practising a physical sport, or - indeed - controlling a car or an aircraft.

To perform any of these skills the human operator has built up a large repertory of skilled movement patterns of sequences, which he can evoke when needed (39, 41, 30, 32). Typical examples are: striking a golf ball, returning a tennis ball, playing the violin, or even writing one's signature.

The human operator response programs incorporate such motion patterns without the necessity for consciously planning in detail the individual movements that make up each pattern. As a consequence, a selection of output motion patterns made at a sufficiently high level in the brain, need not involve specification of the details of execution at the muscular level. This implies, that at a sufficiently high level in the brain the pilot's entire response pattern may be represented by just a few elements characteristic for that response pattern. These elements have been called the motor features (41) or characteristic output features. At the pilot's output side they are the equivalents to the previously discussed characteristic (input) features, or cues at the pilot's input side. In the control engineer's jargon the relation

between the input features and the output features may be described as the control law.

It is postulated and discussed in detail in (30), that the necessary translation of the characteristic output features coming from the highest centers, into the desired complex motion patterns takes place in the cerebellum part of the brain. It has further been suggested (30), that the patterns of stimulation, which the spinal chord receives from higher levels, such as the motor sensory cortex and the cerebellum in the brain, still do not yield twitches of individual muscles. They still consist of co-ordinated patterns of movement, which may involve a number of muscles. It is here, that the neural shaping network introduced in the previous paragraph comes into play again,

The standard output motion patterns experimentally recorded at the pilot's output are - according to the foregoing - commanded by the Central Nervous System through relatively simple commands, the characteristic output features. These command cause the neural "shaping network" to generate the desired complex output motions. Vi the actions of the muscular/manipulator system these desired limb movements are finally transformed into the actual aircraft's manipulator deflections.

4. A Biomorphic model

4.1. Introduction

Based upon the knowledge presented in the previous Chapter, a mathematical model of the pilot's behaviour will now be discussed. The purpose is not primarily to add yet another model to the many already in existence. The emphasis is rather on an attempt to describe - however crudely - how the data handling as well as the decision making processes going on in the pilot's brain may be modelled in mathematical terms, along with the third component of the pilot's activities, the control process proper on which most of the existing engineering models concentrate.

The aim of the new model is to obtain a closer and more detailed mathematical description of what actually goes on in the living organism. This more life-like model is named here a biomorphic model, to clearly distinguish it form the engineerin models previously discussed. The term "biomorphic" has been used before - at least by Serebriakoff (31) - in a similar, although not quite identical connotation.

Stated more explicitly, the aim of the biomorphic model is twofold.

1. The model should obviously show a control behaviour, as expressed in the usual terms, such as describing function, cross-over frequency, remnant power etc., which is comparable to the behaviour of actual pilots.
2. Equally important, and perhaps even more so than the requirement regarding the overt control behaviour, is the facility of the biomorphic model to allow conclusions to be drawn about the level of difficulty a well-trained human pilot would experience in controlling the given aircraft configuration to the same level of performance subject to the same level of external disturbances. This facility of the biomorphic model should provide a link with the pilot's subjective opinion and thus with some of the factors making up the pilot workload. The data handling and decision making processes have been explicitly included in the model in an effort to permit this connection with the pilot's workload to be made more satisfactorily, than has been proved possible with the existing engineering models.

A pilot model fulfilling these aims inevitably will be more complex than most of the customary engineering models. Provided the complexity of the biomorphic model

remains well organized, it is felt, that in the present age of powerful electronic computers, simplicity need not necessarily be the foremost virtue of a mathematical model intended to describe certain activities in the brain, the most complex computer-like organism we know.

In attempting to describe the behaviour of the human pilot in a closed-loop control situation, one soon finds, that a relatively complete model consists of various elements or sub-models, which can be developed more or less independently, and which can then be joined to describe the overall behaviour. The optimal control model of Fig. 3 already shows this characteristic.

Whereas basically the closed-loop control situation under consideration is still as shown in Fig. 1, the block labelled Human Operator in this figure can now be further elaborated, as shown in Fig. 7. First of all it is indicated, that a model is needed of the Observation Process, comprising the various senses. Such an observation model would describe the data handling process as well part of the human decision making process along the lines indicated in Chapter 3.

If a pure monitoring task is to be modelled, the Observation Model is also needed. As indicated in Fig. 8, it must then be followed by a model of the final part of the decision making process. A model of the latter type has been described - in relation with the optimal control model - as the so-called Subjective Expected Utility Model (20, 22).

If, on the other hand, a pure control task is to be modelled, a Response Model portraying the pilot's physical control actions is required, see Figs. 7 and 8. The Observation Model and Response Model are linked by another sub-model, essentially describing the Control Law.

If the task to be modelled is a multi-control and/or multi-display task, the complications for the pilot - resulting from the fact that he has to divide his attention - are reflected in the model by the need for an element (indicated in Fig. 8), called the Task Interference Model. Such a model has also been described in connection with the optimal control model (21, 22).

In order to limit the discussion in this paper to a manageable size, rather severe restrictions have to be accepted in the scope of the model to be considered here. The description will be confined to pure control tasks of the single-display, single-control compensatory type, see Fig. 1. This implies that only the human operator model shown in Fig. 7 will be considered. Although the intended application is of course the control of aircraft in actual flight, consideration of the sometimes highly important vestibular observations regrettably has to be omitted as well.

A difference between the usual engineering models and the biomorphic model should be mentioned, before going into some of the details of the elements shown in Fig. 7. For reasons to be explained below, the biomorphic model operates in a sampling way, rather than continuous like most engineering models. Like the optimal control model, and in line with modern control theory, the biomorphic model is described in the time domain.

4.2. The sampling process

Sampling models of pilot control behaviour have appeared more or less regularly throughout these thirty years of study of pilot models. Sheridan and Ferrell (23) give a short account of these developments. Various reasons have prompted several authors to propose sampling models. The main reason was usually the desire to improve the correspondence between human operator response data and the results obtained from

the model (47). In particular it was desired to accommodate experimentally observed discontinuities in the eye motions, viz. the saccadic motions (48), as well as discontinuities noted under certain circumstances in the recordings of the exerted control forces (49).

The reasons for choosing a sampling operation in the present model are partly the same. In particular the existence, noted in Chapter 3, of standard output patterns in the human operator behaviour, points in the direction of intermittent operation, at least at a certain level in the Central Nervous System. At the input side of the human operator, the extraction of characteristic features from sensed data, as discussed in Chapter 3, may also be described more convincingly in a sampling model. There is, however, yet another and perhaps overriding argument. In the cockpit, in actual flight, sampled observation of the various instruments, resulting in more or less discontinuous responses are the rule rather than the exception. Conversely, paying continuous and full attention to a single display for any length of time, appears to be quite an extraordinary situation in actual flight.

Experimental data on display scanning (50) has shown, that the visual sampling occurring in multi-display tasks is never perfectly periodic. The average sample interval differs for each instrument and depends on the flight task. Apart from the sample interval one has to distinguish a dwell-time for each instrument in the display. It is the time during which the pilot fixates foveally on that particular instrument. Like the sample interval, the dwell-time varies about an average value for a given instrument. More complex and higher bandwidth displays require larger dwell-times. The sample interval and the dwell-time also appear to depend very significantly on the individual test subject.

In a sense, the case of a full attention, single-display control task can be considered an extreme of a sampled operation. It is the case where the dwell-time for the single display equals the entire sample interval. If the difficulty of the control task so requires, the sample interval may become as short as the duration of the saccadic eye motions, i.e. some .2 to .3 sec. As Bekey has shown (51), even relatively small fluctuations in the sample interval completely mask the sampling operation from any experimental evidence taken from the human operator in such a full attention, single-display task.

Fig. 9 shows, that a sampling model of the type discussed in more detail below, can indeed produce a control behaviour comparable to the behaviour of actual pilots. In the single-display, compensatory tracking task used as an example. the controlled element was a simple integrator. The random appearing forcing function was the sum of ten sinusoids of 1.5 rad /sec bandwidth, conform to (4). The two test subjects were experienced pilots. Since the control responses (c in Fig. 1) to identical parts of the input signal are reproduced in the figure, the run-to-run variability of pilot K can be seen, as well as the differences with pilot L, who appears to have a slightly different "signature" in his responses. The mathematical model shows a behaviour well comparable to that of both human pilots. At a certain point in the model, the response is made up simply from small incremental steps, and to a much lesser extent from impulses occurring once per sample interval. The model had a sample interval averaging at .25 sec, and varying with a standard deviation of 20%. Analysis of the recorded data from the two test subjects, as well as from the sampling model, gave results as regards the describing function, cross-over frequency and remnant power, which agreed entirely with the experimental data presented in (4).

4.3. The Observation Model

After the preceding general remarks it is now possible to discuss one of the more important sub-models of the human model shown in Fig. 7, the Observation Model. It describes mathematically the sensing of the input signals entering the various human sensors, as well as the subsequent reduction of this multitude of sensed data into a form suitable to base the selection of appropriate output responses on. The data processing as well as part of the decision making process in the brain are thus embodied in the Observation Model.

In order to limit the scope of this presentation, only visual observations shall be described here in any detail. In the case of a single-display compensatory control task, as shown in Fig. 10, the visually observed variable can be thought of as the error in angle of pitch, θ, whereas the control variable going into the controlled element, the aircraft, would be the longitudinal manipulator position, s_e.

Pursuing the discussions in Chapter 3, the first step in the observation process is the extraction of the characteristic features. These are the most essential or characteristic elements in the time-history of an observed variable. In the case of visual sampling, the obvious characteristic features are the values of θ and $\dot{\theta}$ at a particular instant during the dwell-time. By way of definition this instant marks the beginning of the sample interval (t=0). Consequently, the sensed characteristic features are $\theta(0)$ and $\dot{\theta}(0)$.

The observed characteristic features, indicated as $\overset{o}{\theta}(0)$ and $\overset{o}{\dot{\theta}}(0)$, are obtained in the biomorphic model using an internal model for the visual observations as discussed in in Chapter 3. The observed characteristic features serve a twofold purpose as outlined in Chapter 3 and shown in Fig. 10. In the first place, they serve as the basis on which the output responses are selected via the control law. In the second place, the observed characteristic features are needed to regularly up-date the internal model.

The aforegoing leads up to a discussion of the way in which the internal model for the visual observations in the human brain is mathematically modelled in the biomorphic model. It is the function of the internal model - both in the actual brain, as well as in the biomorphic model - to provide a continuous prediction or estimate of the visually observed variable and also of its first time derivative, see Fig. 10. It is not yet quite clear how this is actually accomplished in the living brain. The obvious way to obtain such an estimate in a mathematical model, however, is to employ a set of ordinary, linear differential equations.

At the beginning of each sample interval, the differential equations representing the internal model are restarted, using as the initial conditions the visually observed characteristic features, $\overset{o}{\theta}(0)$ and $\overset{o}{\dot{\theta}}(0)$, sampled at the beginning of that interval. The solution of the differential equations generated as time proceeds, provides the needed estimates, $\hat{\theta}(t)$ and $\hat{\dot{\theta}}(t)$, as functions of time. At the end of the sample interval the next set of observed characteristic features becomes available to up-date, or rather to restart, the internal model, etc.

An internal model provides a replica of the dynamics of the system to be modelled. In this case the system is the visually observed aircraft motion. Usually the internal model is limited to simpler dynamic characteristics than the actual system. This is a consequence of the fact, that under normal conditions a human observer can visually extract no higher derivate than the first - i.e. the velocity - from a time-varying display. Here, only the error in angle of pitch, θ, and its rate of change, $\dot{\theta}$, can be visually observed. Hence the mathematical internal model for the visual observations can be a differential equation of second order at most.

A significant contribution to the changes in the visually observed error in pitch angle is due to the action of the control variable, the longitudinal manipulator deflection. This control variable is sensed, primarily in the form of the control force, via the tactile and proprioceptive sensors. In the pilot's brain the observed control deflection is used as an input to the visual internal model to estimate the changes in the error in pitch angle. Exactly the same occurs in the mathematical model, as shown in Fig. 10. The exact model by which the varying control deflection is observed in the biomorphic model, using a separate internal model, will not be discussed here.

With the exception of one important aspect, the foregoing describes the operation of the visual internal model. The single remaining item deals in some detail with the manner in which an observation is finally arrived at in the human brain.

From the foregoing it follows that in the Observation Model discussed here, observing a characteristic feature, say $\overset{o}{\theta}(0)$, requires the simultaneous availability of a sensed value, $\theta(0)$, and an estimate provided by the internal model, $\hat{\theta}(0)$. It is of some consequence to discuss how these two are combined into the resulting observed value, $\overset{o}{\theta}(0)$. The same applies to $\overset{o}{\dot{\theta}}(0)$, derived from $\dot{\theta}(0)$ and $\hat{\dot{\theta}}(0)$. Fig. 11 illustrates this process by further detailing the Decision Element in the Observation Model.

From daily life we know that the human mind needs some time to make a decision. This fact has been confirmed by many quantitative tests in psychology. The more options there are, the longer it takes to arrive at a decision. Formulated more precisely: man has a limited capacity to handle information. The word "information" is used here advisedly in the connotation given by Shannon and Weaver (52), meaning a measure of entropy or uncertainty. The limitation of the human mind in information handling capacity is perhaps one of the most fundamental and far reaching limitations of the human mind.

Using simple terms, a person deciding on the basis of perceived data which of two equally likely events has occurred, handles, in so doing, just one bit. Deciding on one out of four equally probable events means handling two bits, one out of eight implies handling three bits, etc. A more precise formulation of these rather loose statements can, of course, be found elsewhere (52, 53). For simple tasks and given the full attention of the test subject, experimental data indicate a remarkably linear relationship between the number of bits the brain handles and the time it takes to do so. This important empirical fact was discovered as early as 1885 by Merkel, see (23), although described in slightly different terms at the time.

The uncertainty in a variable to be observed, resides before the observation in the difference between the sensed and the estimated value, the so-called estimation error. After the observation, the remaining uncertainty in the observed value lies in the residual observation error. The statement that the human operator has a limited information handling capacity, can now be interpreted as meaning that the operator needs some time to reduce the observation error from the initial value of the estimation error to a smaller residual value. The observation time is assumed to be part of the externally measurable dwell-time, during which the pilot looks foveally at the display.

It is relatively easy to show that the linear relation between the number of bits to be handled and the time required to do so, leads to an exponential decrease to the variance of the observation error from that of the initial estimation error to a final, reduced value in the time during which attention is given to the observation. Fig. 12 shows such a relation. The figure shows, however, a number of exponential curves with varying time constants. This requires a further explanation.

Attention is the key notion in this respect. It must be mentioned, that attention always exists at a certain level of intensity. It can vary from full attention to no attention at all (53).

To a certain extent the human observer can opt where to focus his attention and also, at what level of attention he will do so. Consequently, it is reasonable to assume, that the observation error decrease more rapidly to a small value, if full attention is given to the observation, than if only partial attention is given. The mathematical assumption made in Fig. 12 is, that the time constants of the exponential curves are inversely proportional to their corresponding levels of attention. This statement might of course also be taken as an attempt to mathematically define such an illusive concept as "level of attention".

Finally, from Figs. 11 and 12 it can be seen how the observed values are obtained from the sensed and the estimated values, by allowing some finite observation time to arrive at an acceptably small residual observation error. Implications of this model of a decision process in the human brain on the pilot's mental workload will be referred to again in Chapter 5.

4.4. The Response Model

The second sub-model in the model of the human operator, see Fig. 7, is the Response Model. Pursuing the discussion in Chapter 3, the Response Model describes the actions of the neuromuscular/manipulator system. The determining element in the Response Model is the neural shaping filter, modelled here as a low-pass second order filter, having an undamped natural frequency of about 10 rad/sec and a damping of .7 to .8 of critical damping. Since the muscular/manipulator elements can usually respond much faster, it is the response of the neural shaping filter, that essentially determines the standard output patterns of the biomorphic model discussed in Chapter 3.

When it comes to actually deciding on the general shapes of these output patterns, it should be noted that in many cases the control output time-histories of human operators can be taken as being made up of two basic elements: small incremental steps and pulse-type patterns. In many situations the human operator uses combinations of these two basic types of responses.

Experimental data indicate that the actual mixture of the two basic types of response patterns used in a particular closed-loop control situation strongly depends on the dynamics of the controlled element. The pure integrator of Fig. 9 is controlled almost entirely by small incremental steps, whereas a double integrator would evoke predominantly pulse-type responses. Clearly, individual differences between different operators manifest themsleves also in their selection of these standard output patterns, as evidenced in Fig. 9.

The two standard output patterns of the Response Model are, therefore, the responses of the neuromuscular/manipulator system to an incremental step input and to an impulse input signal. As discussed in Chapter 3, the magnitudes of the impulse and the incremental step - A and B respectively - are the two characteristic ouput features of the Response Model.

4.5. The Control Law

The function of the Control Law - the remaining element in Fig. 7 - is to relate, for each sample interval anew, the magnitudes of the output characteristic features, i.e. the commanded impulse, A, and incremental step, B, to those of the observed

characteristic features, $\overset{o}{\theta}(0)$ and $\dot{\overset{o}{\theta}}(0)$. Assuming a linear control law, the desired ralations are expressed by a 2x2 matrix. The four elements of the matrix are found quantitatively by minimizing a suitably selected cost function, in which a trade-off is made of the precision of control against some reasonable measure of the control effort needed to achieve that precision.

Considering once more the variability between different human operators, one should not expect one single definition of such a cost function to lead to an acceptable control behaviour of the model. On the other hand, it is a stringent requirement, that the cost function one selects should yield - for as wide a range of controlled elements as possible - a behaviour of the model well comparable to that of actual human operators.

5. Relations with pilot workload

In the context of this paper, the ultimate goal in building models of human pilot behaviour is to use these models in the evaluation of aircraft handling qualities. It needs not to be emphasized here, that good handling qualities are essential for efficient flight operations; and of course, they are vital for flight safety. At present the common method of assessing handling qualities still relies heavily on the subjective opinions of experienced test pilots (54). These opinions have proved to be quite reliable, but they are sometimes difficult to use for design purposes.

A pilot's opinion is expressed primarily in the form of a pilot rating. The well-known Cooper-Harper scale (55) is widely used for this purpose, whereas other useful subjective rating scales have been studied e.g. by McDonnell (56, 57). An essential complement to a pilot's subjective rating are his more or less detailed verbal comments, often given in the form of a reply to a prepared questionnaire. Rating and comments combined reflect the pilot's opinion of the total workload imposed on him. They determine the suitability of the aircraft under test for a given mission.
The essential point of this commonly used procedure is, that the pilot's opinion is considered primarily an index for evaluating his workload. Obviously, it is the required workload which determines the acceptability of certain handling qualities.

There are several definitions of the notion:"pilot's workload". Cooper and Harper (55) define it as: the integrated physical and mental effort required to perform a specified piloting task. Another author, Jahns (58) - in a study on workload - defines workload in a more general way as: the extent to which an operator is occupied by a task. As Howitt (59) has pointed out, workload can be divided in three distinct areas:

1. the immediate workload, i.e. the workload experienced over any particular short period of time, e.g. take-off, descent, landing etc.,
2. the duty-day workload,
3. the long-term load.

Clearly, what interests us here, is the immediate workload. As expressed in the definition given by Cooper and Harper (55), this immediate workload consists of a physical and mental component. Of these two, the physical workload can usually be neglected in present-day aircraft: modern control systems permit the frequent use of trimming devices, resulting in relatively low remaining control forces.

Therefore, the sole factor of concern is the mental workload, describes by Bernotat and Wanner (60) as the processing of information by the human being. This aspect of workload is, of course, also important if the pilot performes the purely mental

task of monitoring, e.g. when keeping an eye on the control over the aircraft exercised by the automatic pilot during an approach. But as Firth (61) has pointed out, there is a lack of knowledge about the nature of mental workload, because of the complexity and covert nature of mental functions such as information processing and decision making.

Delving deeper into this mental workload, three related aspects should be distinguished, according to Jahns (58):
1. input load, 2. operator effort and 3. output performance. The relation between these three aspects is shown very schematically in Fig. 13. Somewhat in line with the discussion in Section 4.3. and (53), the operator attention required to perform a task has been used here as a measure of operator effort or mental workload. One of the obvious qualitative conclusions that can be drawn from this figure is, that the workload of a pilot will be quite different, if he tries to obtain different levels of ouput performance or control precision from the same aircraft at different input disturbance levels. Also, the assumption of full pilot attention is an evident limitation of present pilot models. This requirement will, of course, be met only very rarely in actual flight, normal operations taking place mostly at much lower levels of attention.

Attempts have been made in the past (62,63), to correlate workload (as expressed by pilot's opinions or subjective ratings) with the parameters of the cross-over model. For a variety of reasons these efforts have not been very successful. Mostly perhaps, because the concept of mental workload needs more model refinement in the areas of data processing and decision making than the cross-over model can offer.

It appears, at present, that pilot models operating in the time domain, such as the optimal control model or the biomorphic model, are more amenable to further development in measuring pilot mental workload. The biomorphic model, discussed at some length in the present paper, seems to be particularly well suited to generate measures of mental workload, because of its sampling type of operation and its explicit modelling of the data handling and decision making processes.

At present, however, there is no generally accepted measure of mental workload. As a consequence, there is also no direct method for continuous, precise measurement of the mental workload - in flight or in a simulator - although several authors, e.g. (59), have been confident that some physical measures can be developed, allowing a reasonable assessment of immediate workload.

From this brief account of the state of affairs it may be clear, that further progress in the area of aircraft handling qualities requires, above all, a better understanding of what constitutes mental workload. The concerted efforts of pilots, psychologists and engineers will be needed to perform experimental as well as theoretical work. The results of the studies would have to be expressed - for the benefit of the humble engineer at any rate - in the form of further developed mathematical models of the pilot's behaviour.

Finally, but very clearly, a sobering word on mathematical pilot models should be said. Several authors (39, 24, 64) have repeatedly stated, that great care is needed in using such pilot models. This applies particularly when extrapolating to new situations, such as for design purposes. Our mathematical techniques are but one method, and sometimes a rather inadequate one, to formulate the results of our research on human behaviour. As Christensen (64) has rightly said: "A model is never the real thing, otherwise it wouldn't be called a model".

6. Concluding remark

The title of this paper on mathematical models of human pilot behaviour intentionally includes the word "development". It emphasizes what has hopefully emerged from the foregoing: this fascinating subject is in full development and much imaginative and dedicated work is still required. It is the sincere hope that this paper may help to stimulate such work, and thus pay a fitting tribute to the memory of Frederic Lanchester, whose works have often had such inspiring effects.

7. References

1. DOETSCH, K.H. The Proper Symbiosis of the Human Pilot and Automatic Flight Control Eighteenth Lanchester Memorial Lecture. The Aeronautical Journal. Vol. 79, p. 247, June 1975.
2. LANCHESTER, F.W. Discontinuities in the Normal Field of Vision. Journal of Anatomy Vol. 68, p. 224, 1934.
3. TUSTIN, A. The Nature of the Operator's Response in Manual Control and Its Implications for Controlled Design. J.I.E.E. Vol. 94, Part II A, No. 2, 1947.
4. McRUER, D.T., KRENDEL, E.S., REISENER Jr., W. Human Pilot Dynamics in Compensatory Systems. AFFDL TR-65-15, 1965.
5. McRUER, D.T., KRENDEL, E.S. The Human Operator as a Servo System Element, J. Franklin Institute. Vol. 267, No. 5, p. 381, May 1959 and No. 6, p. 511, June 1959
6. ELKIND, J.I. A Survey of the Development of Models for the Human Controller, in: R.C. Langford, C.J. Mundo, eds., Guidance and Control-II, Vol. 13 of Progress in Astronautics and Aeronautics, p. 263. Academic Press, New York, 1964.
7. McRUER, D.T., KRENDEL, E.S. Mathematical Models of Human Pilot Behaviour. AGARDograph No. 188, AGARD, Neuilly, 1974.
8. McRUER, D.T., JEX, H.R. A Review of Quasi-Linear Pilot Models. IEEE Trans. Vol. HFE-8, No. 3, p. 231, 1967.
9. LEVISON, W.H., BARON, S., KLEINMAN, D.L. A Model for Controller Remnant. IEEE Trans. Vol. MMS-10, No. 4, p. 137, 1969.
10. STAPLEFORD, R.L., McRUER, D.T., MAGDALENO, R.E. Pilot Describing Function Measurement in a Multiloop Task. NASA CR-542, 1966.
11. LEVISON, W.H., ELKIND, J.I. Studies of Multivariable Manual Control Systems: Two-Axis Compensatory Systems with Separated Displays and Controls. NASA CR-875, 1967.
12. KLEINMAN, D.L., BARON, S., LEVISON, W.H. An Optimal Control Model of Human Respons Part I: Theory and Validation. Automatica. Vol. 6, p. 357, 1970.
13. BARON, S., KLEINMAN, D.L., LEVISON, W.H. An Optimal Control Model of Human Respons Part II: Prediction of Human Performance in a Complex Task. Automatica, Vol. 6, p. 371, 1970.
14. KLEINMAN, D.L., BARON, S. Manned Vehicle System Analysis by Means of Modern Contro Theory. NASA CR-1753, 1971.
15. WEWERINKE, P.H. Effort Involved in Single- and Two-Axis Control Systems. NLR TR 75060 U, Amsterdam, 1975.
16. KLEINMAN, D.L., BARON, S. Analytic Evaluation of Display Requirements for Approach to Landing. NASA CR-1952, 1971.
17. MERHAV, S.J. On Optimality in Human Control Tasks. ICAS Paper No. 76-54, Ottawa, 1976.
18. CURRY, R.E., YOUNG, L.R., HOFFMAN, W.C., KUGEL, D.L. A Pilot Model with Visual

and Motion cues, in: Twelfth Annual Conference on Manual Control. NASA TM X-73, 170, p 851, 1976.

19. BARON, S. KLEINMAN, D.L. The Human as an Optimal Controller and Information Processor. NASA CR-1151, 1968.
20. LEVISON, W.H., TANNER, R.B. A Control-Theory Model for Human Decision Making. NASA CR-1953, 1971.
21. LEVISON, W.H., ELKIND, J.I., WARD, J.L. Studies of Multivariable Manual Control Systems: A Model for Task Interference. NASA CR-1746, 1971.
22. WEWERINKE, P.H. Human Control and Monitoring - Models and Experiments. NLR MP 76015 U, Amsterdam, 1976.
23. SHERIDAN, T.B., FERRELL, W.B. Man-Machine Systems: Information, Control, and Decision Models of Human Performance. The MIT Press, Cambridge, Mass., 1974.
24. RASMUSSEN, J. Outlines of a Hybrid Model of the Process Plant Operator, In: NATO Science Committee Symp. on Monitoring Behavior and Supervisory Control. Berchtesgaden, p. 288, 1976.
25. PIRENNE, M.H. Vision and the Eye, Science Paperback SP 47, Chapman and Hall, London, 1971.
26. HABER, R.N., HERSHENSON, M. The Psychology of Visual Perception. Holt, Rinehart and Winston, London, 1974.
27. CORSO, J.F. The Experimental Psychology of Sensory Behavior, Holt, Rinehart and Winston, London, 1967.
28. KORNHUBER, H.H. (ed.) Handbook of Sensory Physiology. Vol. VI/2: Vestibular System Part 2. Springer Verlag, Berlin, 1974.
29. ARBIB, M.A. On Modelling the Nervous System, in: Principles and Practice of Bionics. AGARD CP-44, Neuilly, 1970.
30. ECCLES, J.C. The Understanding of the Brain. McGraw-Hill, New York, 1973.
31. SEREBRIAKOFF, B. Brain. Davis-Poynter, London, 1975.
32. STADLER, M., SEEGER, F., RAEITHER, A. Psychologie der Wahrnehmung. Juventa Verlag, München, 1975.
33. GIBSON, J.J. The Perception of the Visual World. Houghton Mifflin, Boston, 1950.
34. GIBSON, J.J. The Senses Considered as Perceptual Systems. Houghton Mifflin, Boston, 1966.
35. HUBEL, D.H., WIESEL, T.N. Receptive Fields, Binocular Interaction, and Functional Architecture in the Cat's Visual Cortex. J. of Physiology. Vol. 160, p. 106, 1962.
36. HUBEL, D.H. The Visual Cortex of the Brain. Scientific American. Vol. 222, p. 54, Nov. 1963.
37. CRAIK, K.J.W. The Nature of Explanation. Cambridge University Press, 1943.
38. McKAY, D.M. Internal Representation of the External World. Paper presented at the AGARD Avionics Panel Symposium on Natural and Artificial Logic Processors, Athens, 1963.
39. KELLEY, C.R. Manual and Automatic Control. John Wiley and Sons, New York, 1968.
40. GREGORY, R.L. On how so little information controls so much behaviour, in: Towards a Theoretical Biology, 2 Sketches. C.H. Waddington, ed., Edinburgh University Press, 1969.
41. ARBIB, M.A. The Metaphorical Brain, John Wiley and Sons, New York, 1972.
42. MORAY, M. Attention, Control, and Sampling Behavior, in: NATO Science Committee Symp. on Monitoring Behavior and Supervisory Control, Berchtesgaden, p. 168, 1976.
43. MAGDALENO, R.E., McRUER, D.T., MOORE, G.P. Small Perturbation Dynamics of the

Neuromuscular System in Tracking Tasks. NASA CR-1212, 1968.

44. DRILLES, R., CONTINI, R., BLUESTEIN, M. Body Segment Parameters, in: Selected Articles from Artificial Limbs. R.E. Krieger Publishing Co., Huntingdon, N.Y., 1970.
45. DREYFUSS, H. Measure of Man. Whitney Publications, New York, 1959.
46. MAGDALENO, R.E., McRUER, D.T. Experimental Validation and Analytical Elaboration for Models of the Pilot's Neuromuscular Subsystem in Tracking Tasks. NASA CR-1757 1971.
47. BEKEY, G.A. The Human Operator as a Sampled-Data System. IRE Trans. HFE-3, p. 43, September 1962.
48. YOUNG, L.R., STARK, L. Variable Feedback Experiments Testing a Sampled Data Model for Eye Tracking Movements. IEEE Trans. HFE-4, No. 1, p. 38, 1963.
49. LEMAY, L.P. WESTCOTT, J.H. The Simulation of Human Operator Tracking Using an Intermittent Model. Proc. IEEE Symp. Human Facotrs in Electronics, 1962.
50. ALLEN, R.W., CLEMENT, W.F., JEX, H.R. Research on Display Scanning, Sampling, and Reconstruction Using Separate Main and Secondary Tracking Tasks, NASA CR-1569, 1970.
51. BEKEY, G.A., BIDDLE, J.M. The Effect of a Random-Sampling Interval on a Sampled Data Model of the Human Operator. Third Annual NASA-University Conference on Manual Control. NASA SP-144, 1967.
52. SHANNON, C.E., WEAVER, W. The Mathematical Theory of Communication. The Universit of Illinois Press, Urbana, 1964.
53. KAHNEMAN, D. Attention and Effort. Prentice-Hall, Englewood Cliffs, N.J., 1973.
54. GERATEWOHL, S.J. Definition and Measurement of Perceptual and Mental Workload in Aircrews and Operators of Air Force Weapon Systems: A Status Report, in: Higher Mental Functioning in Operational Environments. AGARD CP-181, Neuilly, 1975.
55. COOPER, G.E., HARPER, R.P. The Use of Pilot Ratings in the Evaluation of Aircraft Handling Qualities. NASA TN-5153, 1969.
56. McDONNELL, J.D. Pilot Rating Techniques for the Estimation and Evaluation of Handling Qualities. AFFDL TR-68-76. 1968.
57. McDONNELL, J.D. An Application of Measurement Methods to Improve the Quantitative Nature of Pilot Rating Scales. IEEE Trans. Vol. MMS-10, No. 3, p. 81, 1969.
58. JAHNS, D.W. A Concept of Operator Workload in Manual Vehicle Operations. Forschungsinstitut für Anthropotechnik, Forschungsbericht Nr. 14, Meckenheim, 197
59. HOWITT, J.S. Flight-Deck Workload Studies in Civil Transport Aircraft, in: Measurement of Aircrew Performance, AGARD CP-56, Neuilly, 1969.
60. BERNOTAT, R.K., WANNER, J.C. Pilot Workload, in: Handling Qualities Criteria. AGARD CP-106, Neuilly, 1971.
61. FIRTH, P.A. Psychological Factors Influencing the Relationship Between Cardiac Arrythmia and Mental Load. Ergonomics. Vol. 16, No. 1, p. 5, 1973.
62. DILLOW, J.D. The Paper Pilot - A Digital Computer Program to Predict Pilot Rating for the Hover Task. AFFDL TR-70-40, 1971.
63. ANDERSON, R.O. Theoretical Pilot Rating Predictions, in: Handling Qualities Criteria. AGARD CP-106, Neuilly, 1971.
64. CHRISTENSEN, J.M. Human Engineering Considerations in Systems Development, in: Measurement of Man at Work. W.T. Singleton, J.G. Fox, D. Whitfield, eds. Taylor and Francis, London, 1971.

ooo0ooo

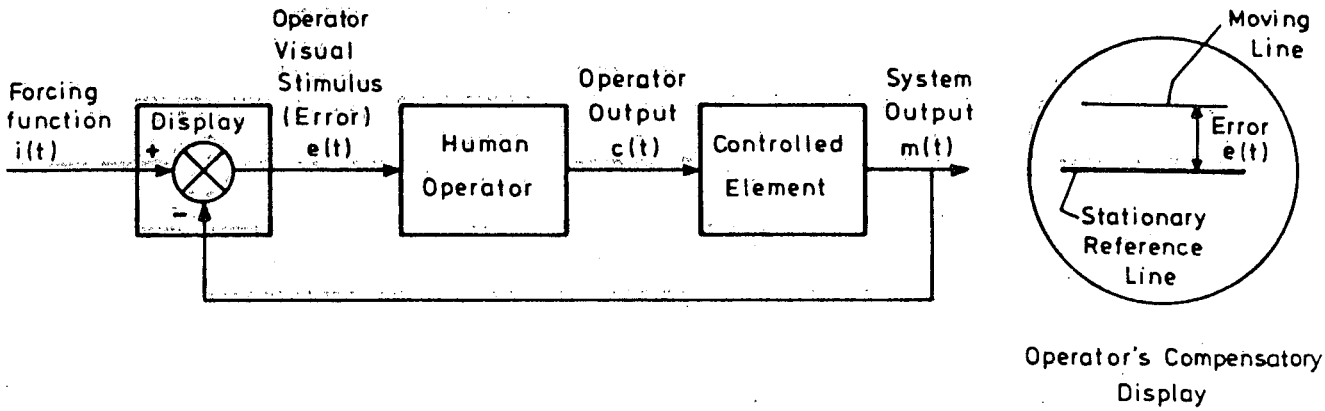

FIG. 1 : BLOCK DIAGRAM OF COMPENSATORY MANUAL CONTROL SYSTEM

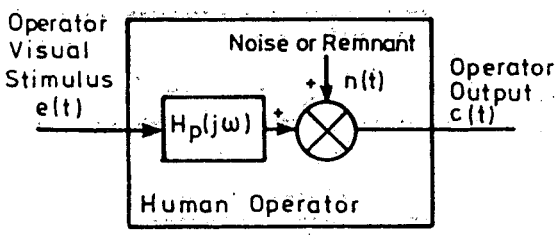

Cross-Over Model

$$H(j\omega) = \omega_c \cdot \frac{e^{-j\omega\tau_e}}{j\omega}$$

$$H(j\omega) = H_p(j\omega) \cdot H_c(j\omega)$$

Human Operator linear transfer function : $$H_p(j\omega) = K_p \cdot \frac{e^{-j\omega\tau}}{1+j\omega.\tau_N} \cdot \frac{1+j\omega.\tau_L}{1+j\omega.\tau_I}$$

Controlled element linear transfer function : $H_c(j\omega)$

FIG. 2 : THE CROSS-OVER MODEL

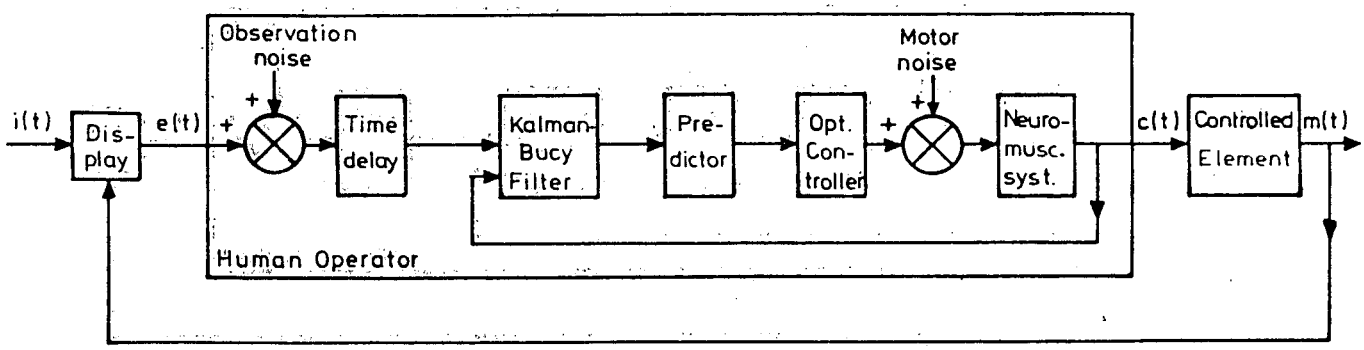

FIG. 3 : THE OPTIMAL CONTROL MODEL

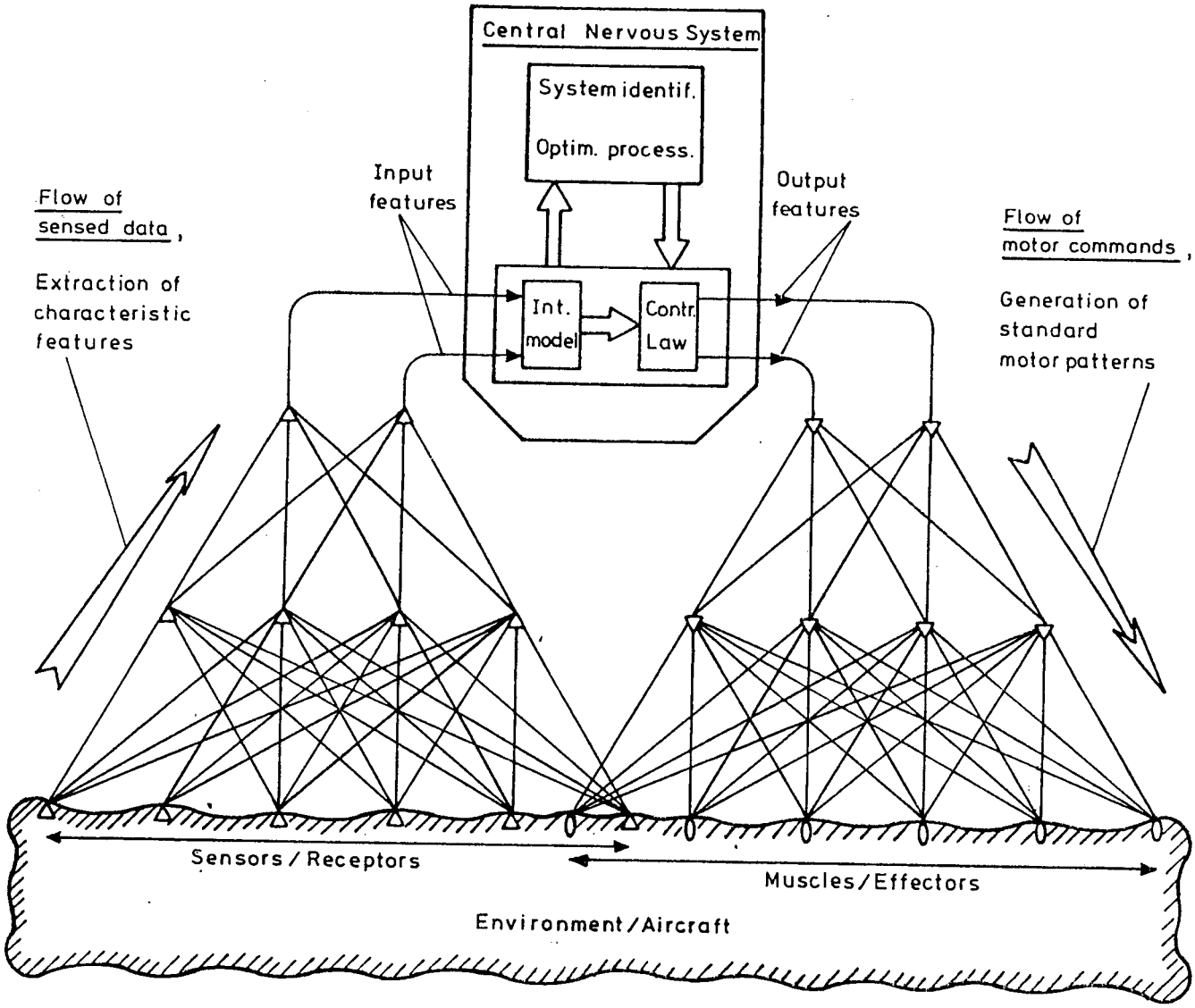

FIG. 4 : DATA PROCESSING IN THE HUMAN OPERATOR

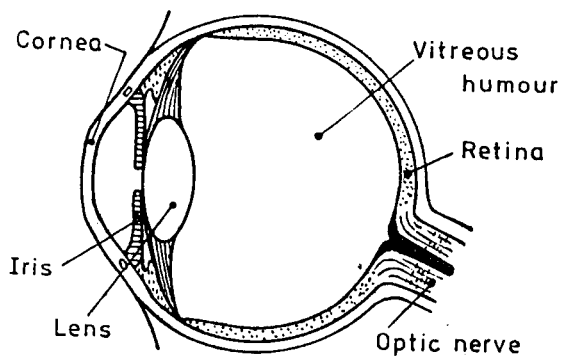

FIG. 5 : SECTION OF THE HUMAN EYE

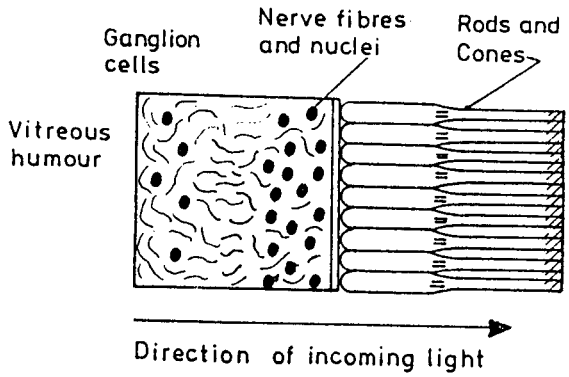

FIG. 6: SECTION OF THE RETINA

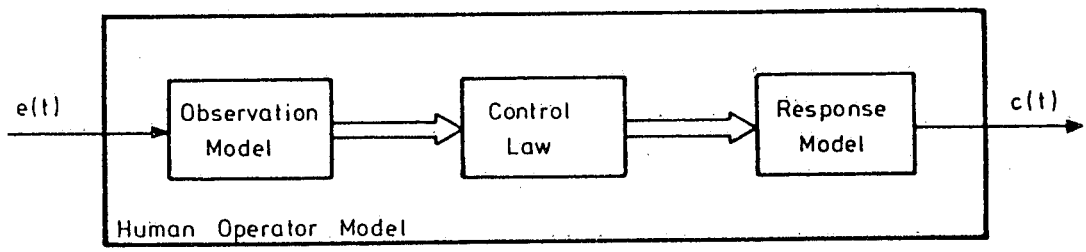

FIG.7 : ELEMENTS OF THE HUMAN OPERATOR MODEL IN A SINGLE-VARIABLE CONTROL TASK.

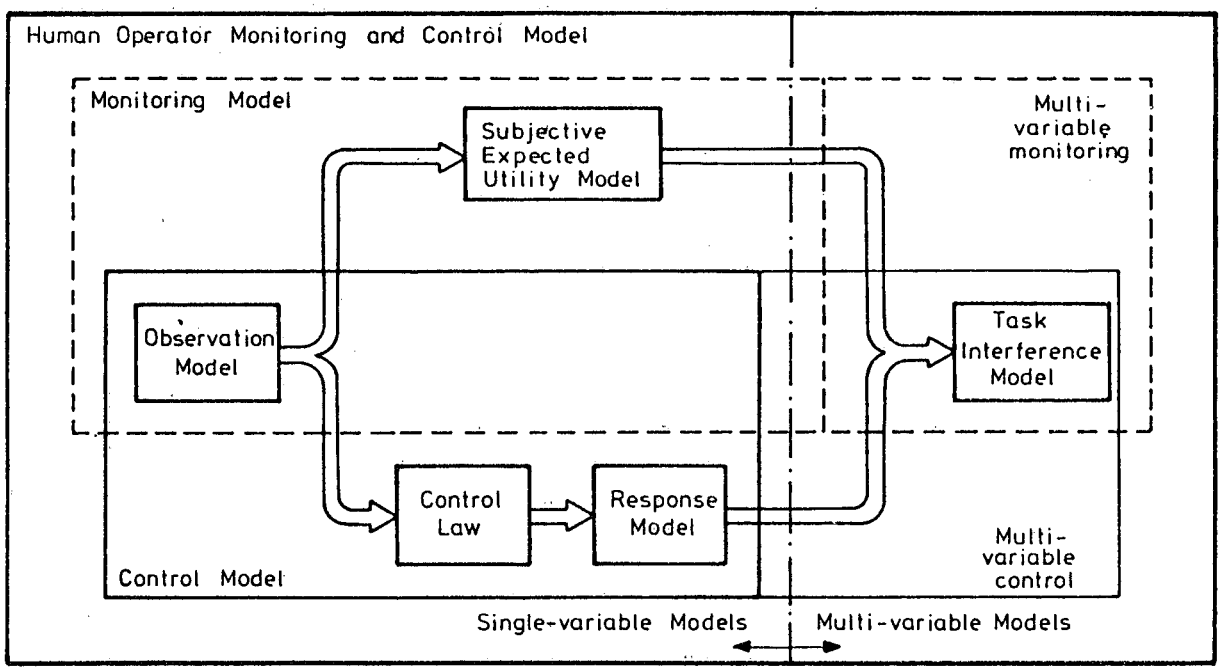

FIG.8: ELEMENTS OF HUMAN OPERATOR MODELS.

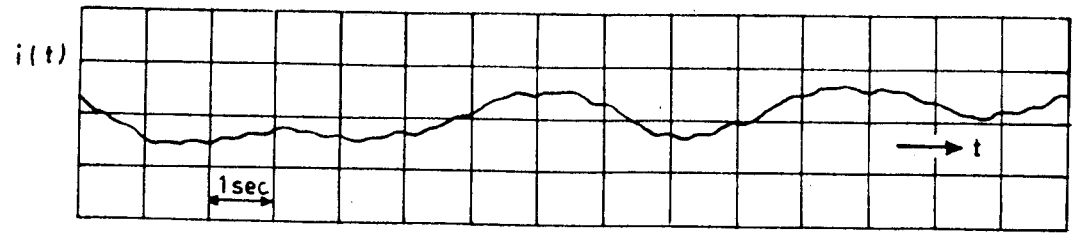

FORCING FUNCTION

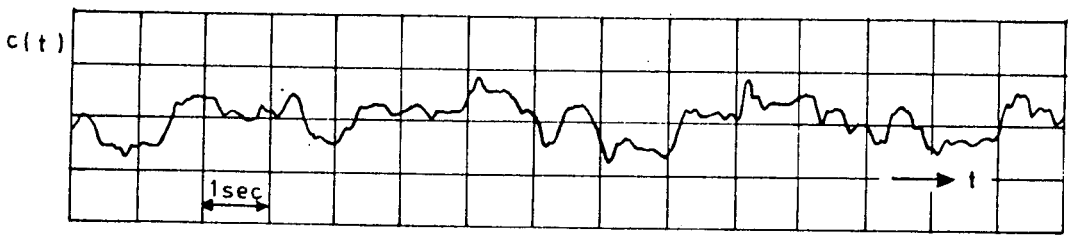

PILOT K

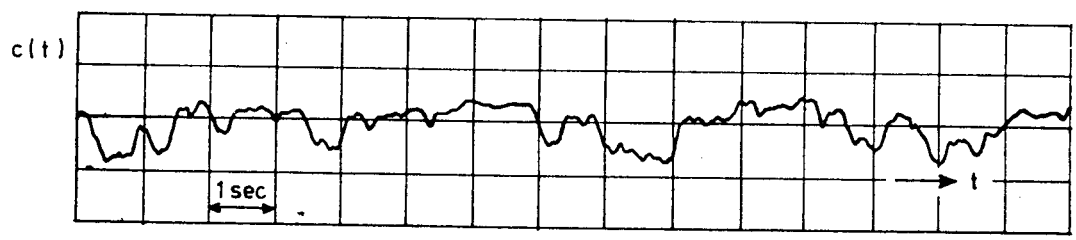

PILOT K

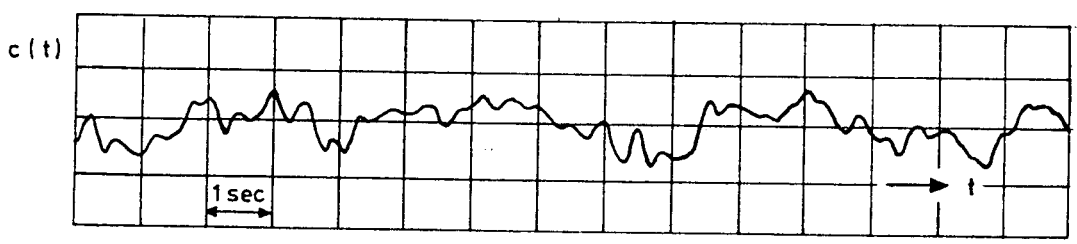

MODEL

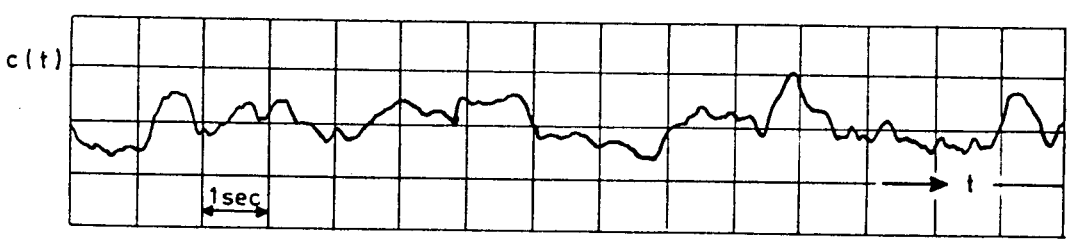

PILOT L

FIG.9 : RECORDED OUTPUT SIGNALS OF TWO PILOTS AND THE BIOMORPHIC MODEL

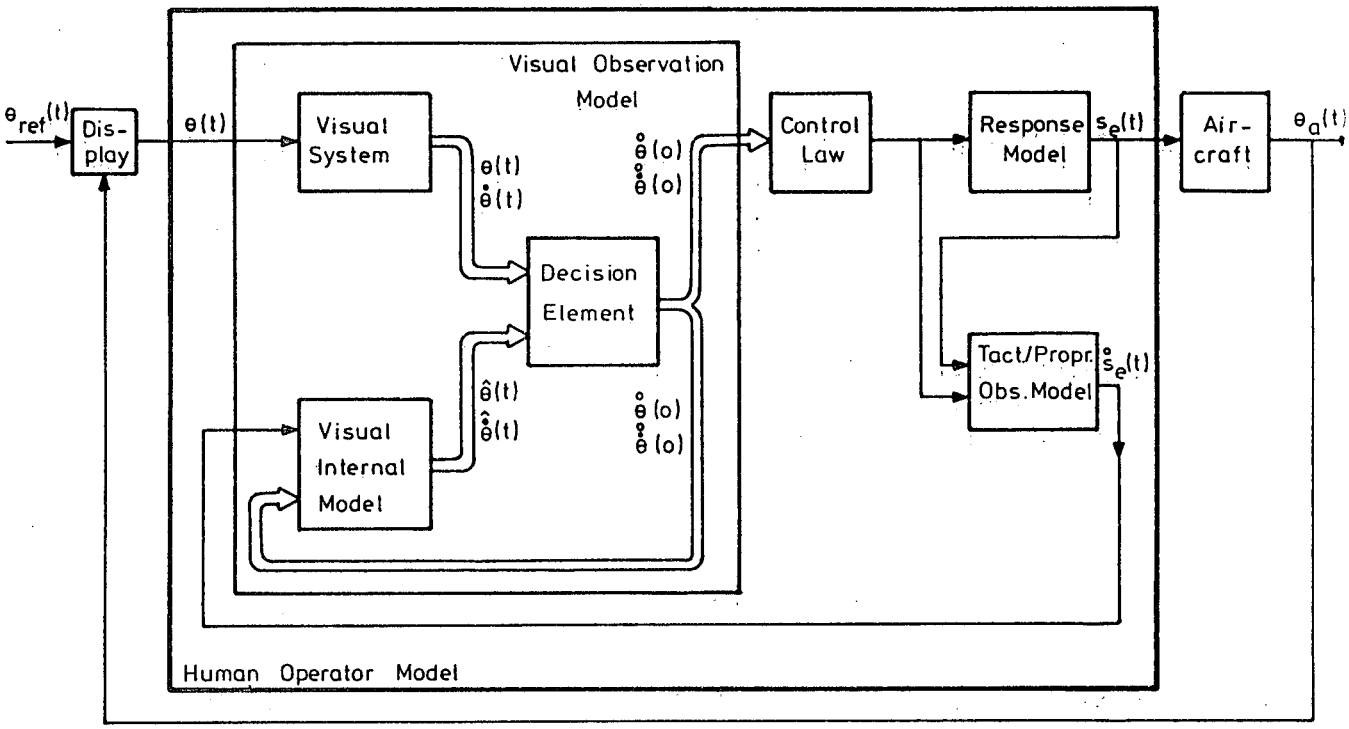

FIG. 10 : THE BIOMORPHIC MODEL IN A SINGLE-VARIABLE AIRCRAFT CONTROL TASK .

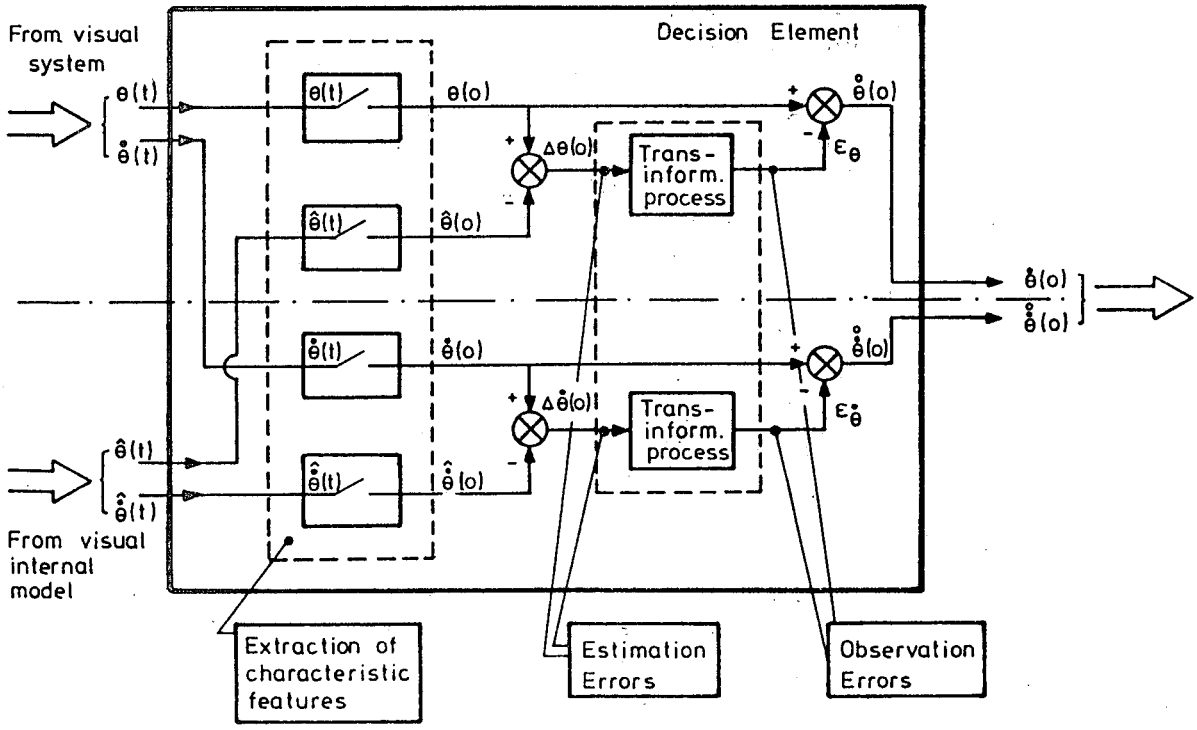

FIG. 11 : THE DECISION ELEMENT OF THE VISUAL OBSERVATION MODEL .

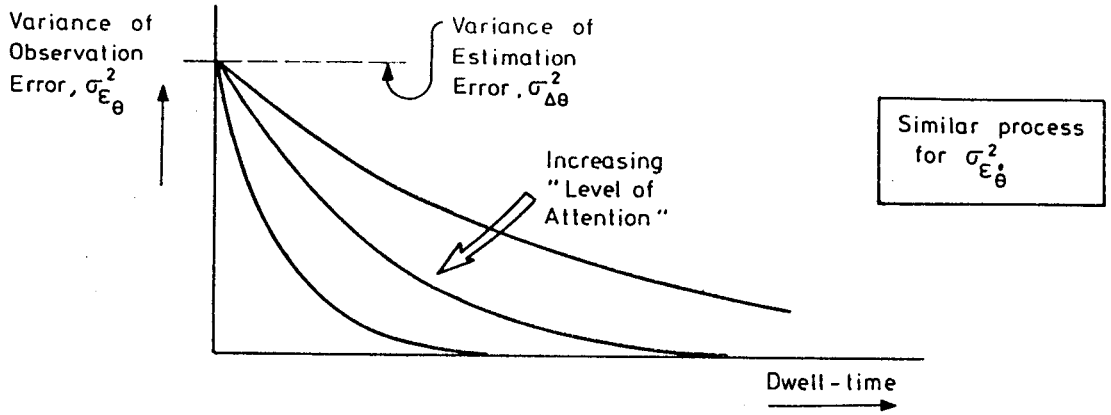

FIG. 12 : THE TRANSINFORMATION PROCESS OF VISUAL OBSERVATIONS.

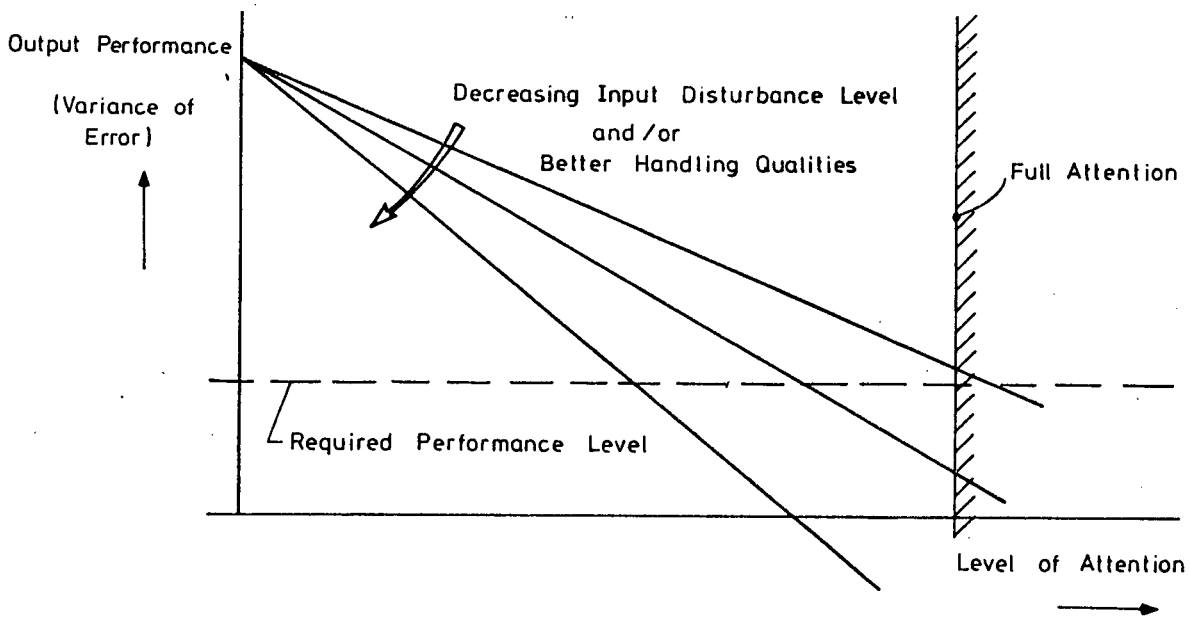

FIG. 13 : QUALITATIVE RELATIONS BETWEEN
INPUT DISTURBANCE LEVEL, HANDLING QUALITIES,
OUTPUT PERFORMANCE AND OPERATOR'S ATTENTION.

INSTRUMENTATION REQUIREMENTS AND PRESAMPLE FILTER DESIGN FOR MEASUREMENTS DURING NON STEADY MANOEUVRES WITH THE HAWKER HUNTER MK VII, PH-NLH

K. van Woerkom

Delft University of Technology

Instrumentation requirements and presample filter design for measurements during non steady manoeuvres with the Hawker Hunter MK VII, PH-NLH

by K. van Woerkom

Preface

Dear Professor Gerlach,

On the occasion of your leave as a Professor of Delft University of Technology, the initiative was taken to offer you this book. I gladly complied with the request to add my contribution in my own way.

Thirty years of cooperation in our Department, now called Faculty of Aerospace Engineering, is a very long time. Within the Disciplinary group for Stability and Control important research has been done in the field of Flighttest techniques.

Professor H.J. van der Maas, your teacher, was the moving force with regard to the development of the Fokker F-27 Friendship. You were the one who developed the NSM method, which was later applied by the NLR to the flighttesting of the Fokker F-28 (NSM is a Dutch acronym for Non Stationary Measurements).

The development of the NSM technique, which started for me in 1960, determined to a large extent my work in the Disciplinary group for Stability and Control. On the technical level I was enabled to contribute to this development. Step by step a high accuracy instrumentation system was designed, assembled and tested in the laboratory aircraft of the Faculty, the De Havilland DHC-2 Beaver. The first succesful flighttests were carried out in 1967/1968. The program consisted of measurements in nonsteady longitudinal flighttest manoeuvres. The promising results made it desirable to apply the NSM technique to a fast jet propelled aircraft. This led in 1974 to a series of flighttests in close cooperation with NLR with the Hawker Hunter MK VII, PH-LNH laboratory aircraft. For this program a new high accuracy instrumentation system was designed. The challenging problem to be solved was the mounting of the data acquisition system in the underwing pod of the Hunter.

Later a new series of longitudinal and lateral flighttests were conducted with the Beaver in 1978 in cooperation with DFVLR (now called DLR) and NLR. Additional instrumentation consisted of an electro-hydraulic control system, enabling the application of reproducable testsignals for longitudinal and lateral manoeuvres.

The latest NSM program in which we were involved concerned the RLS Cessna Citation 500, PH-CTA in cooperation again with NLR. My responsibility in this project was to develop various new transducers in the limited time available, in cooperation with the design departments of NLR and the Faculty of Aerospace Engineering.

The time passed at the NLR location in Amsterdam, at Eelde Airport and later at Schiphol Airport during the actual flighttests was an exciting one.

Considering the experience gained during the long time of cooperation in various flighttest projects, I look forward to an even closer cooperation between NLR and our Faculty of Aerospace Engineering, with a new and jointly operated laboratory aircraft.

The paper presented here describes the requirements for the instrumentation for the 'Hunter Measurements' with the emphasis put on the design of the presample filters.

1. Introduction

In 1967 in 1968 flight test programs were carried out with the DHC-2 Beaver laboratory aircraft of the Delft University of Technology, Department of Aerospace Engineering.
Relative short (< 60 sec) symmetric non steady manoeuvres demonstrated the flight test technique developed at this Department. To investigate the feasibility of this technique for the class of high subsonic jet propelled aircraft, a cooperative program was started with the National Aerospace Laboratory (Amsterdam) enabling flight tests to be performed with the Hawker Hunter MK VII, see fig. 1 and fig. 2.
The applied data collection system described in this report has a sample rate of 400 measurements per sec and an overall accuracy of 0.02%. The transducers used have different accuracies depending on the type and application, from 0.01 to 5%. To monitor the accuracy during the flight test period, rather extensive calibrations were carried out before, between and after the actual measurement flights.
The inflight measurements are recorded on magnetic tape in digital form, this tape is indicated as 'tape 0'. With special groundequipment and a digital computer the 'tape 0' is converted into IBM compatible tape, indicated as 'tape 1'. This tape contains transducer output voltages and administrative data recorded in sequential form. 'Tape 1' is subsequent by converted into 'tape 2' which contains the physical quantities, computed by the application of calibrations.
The instrumentation system is designed and developed at the Department of Aerospace Engineering in Delft, whereas the installation of the system including transducers is carried out at Schiphol Airport in close cooperation with the National Aerospace Laboratory, Amsterdam. For ease of installation and to reduce the installation time as much as possible, it was decided to install the data collection system in an underwing container (pod) of the 'Hunter'. Transducers used in the system were located at different places, in order to maintain accessibility. A small operators panel mounted in the cockpit provided the necessary controls of the instrumentation system.
The architecture of the instrumentation system as shown in fig. 3 is rather conventional. Much care however is devoted to the design and manufacture of all the separate components for maximum accuracy, precision and reliability. In fig. 4 a diagram is presented of the accompanying ground equipment. At the time of design few components were available in modular form, so several parts of the system had to be synthesized from discrete high quality components. Some components which were available had to be adapted to meet the rather severe environmental requirements. As follows from fig. 3, conceptually the operation of the system is straight forward. The analog d.c. voltage output signals of transducers or signal conditioners are passed through low-pass filters. Filtered signals are fed to a multiplexer, the output of which is converted to a digital signal. The parallel digital output of the analog to digital converter is serialized and recorded on magnetic tape simultaneously with some administrative data. On the ground this tape is replayed and the information is passed to a digital computer (EAI 640) in parallel format. The computer finally produced a nine-track IBM compatible tape as well as quick look time histories.
In section 2 formal requirements for flighttest instrumentation systems are discussed. The method used for the design of the required electronic filters is described in section 3.

2. REQUIREMENTS OF THE INSTRUMENTATION SYSTEM

2.1. Introduction

The requirements of the instrumentation system were accumulated during several meetings of a project group in which experts from NLR as well as DUT took part. The group was formed by pilots, flight test engineers, instrumentation technicians, aircraft technicians and software programmers. During the specification phase of the project the following aspects concerning the onboard system received attention.

2.2. Number of channels to be recorded

The number of channels to be recorded was established at 19. During the preparation phase of the program it turned out however, that two additional transducers would be essential for accurate post flight engine net thrust calculation. Because some of the essential hard ware was already completed at that time, it was decided that these transducers would each share one measuring channel with an already planned for but not very essential transducer. Consequently a rational choice of transducers to be actually recorded had to be made before each measurement flight.

2.3. Sample rate

The sample rate of each measured variable was fixed at 20 measurements per sec. For reason of system simplicity no attempts have been made to design a random address facility for the multiplexer applied, so all measuring channels had equal sample rate.
The sequence of the measured variables was also fixed, therefore no individual channel numbers had to be added during the recording process.

2.4. Measurement accuracy and resolution

Accuracy is considered to be of prime importance for the non-steady flight test technique. This holds in particular for the inertial measurements (A_x,A_y,A_z and q).
The accuracy of the data collection system was specified to be 0.02% for each measuring channel. Hence the combined stability of scale factor and zero of the applied analog to digital converter, with a range from 0 to 10V, had to be within ± 2 mV over the entire design temperature range, from -25 to +30 °C. The transducers applied in the system had different accuracies, depending on type and measurement range.
The resolution of the data collection system was determined by the analog to digital converter. The applied converter has a 4 digit BCD output, the least significant bit equals 1 mV or 0.01%.

2.5. Dynamic performance

The frequency response of the measuring channels is important with respect to aircraft motions to about 0.5 Hz introduced during non-steady flight manoeuvres. Due to the limited sample rate of the data collection system aliasing errors have to be considered. In each measuring channel, linear presampling filters attenuate the transducer output signal contents at frequencies above the filter 'cut-off' frequency. The sample rate should be high enough to avoid significant aliasing errors. The flight test manoeuvres at the other hand should be designed such as to avoid

significant errors of omission. The low pass frequency characteristics of the filters are selected such as to minimize difficult to recover distortions.

2.6. Environmental conditions

The environmental specifications of the instrumentation system were based on the environmental conditions expected and measured during exploratory flight tests. The data collection system including the tape recorder had to operate properly in an ambient temperature range from -25° up to 30°C. Vibration was considered to cause no mechanical problems. Shock mounting of the electronic boxes was expected to effectively eliminate any effect of airframe vibrations. Accelerameters and rate gyro's were strapped down dorsally mounted to the aircraft. Exploratory flight test showed the vibration level here low enough as to eliminate the need for any mechanical damper, this in contrast to earlier flight test programs with a piston engined aircraft.

2.7. Size and weight of the systems

The individual components of the systems were designed to be placed in a drawer which would easily fit into the underwing pod. The total weight of all components was approximately 60 kgf.
The pressure transducers were placed in one of the former ammunition boxes in the fuselage of the aircraft, for easy access and maintenance. The total weight of the 'pressure transducers box' was 22 kgf.

2.8. Electrical power supply

The instrumentation system was powered by 28 V dc and 115 V ac. The required dc power of 200 W was taken from the aircraft's dc bussystem, the ac power about 200 VA being supplied by a three phase rotary inverter.

2.9. Operation during flight

A first idea on the operation of the instrumentation system during flight was to have only a very basic control panel by the pilot. Later, it was throught that this would increase pilot workload to an undesirable level. Consequently an extra crew member would have to operate the instrumentation system. A second version of the operators panel was designed with more control and check facilities, such as a digital measuring channel voltage output display and a manual channel selector.

2.10. Calibration procedure

No separate components but rather the entire measuring channels were calibrated: transducer with associated signal condition including filters, multiplexer and analog to digital converter. For obvious reasons, the T and EGT transducers and measuring channels were calibrated separately as exceptions to this general procedure.
Calibrations were performed at least twice prior to the flight tests, one more during the flight test period and finally two after completion of the flight test program. As a consequence of the high ratio of transducer bandwidth to signal frequency contents only static calibrations were required.
All calibrations were carried through in the laboratory except for the elevator deflection - and stabilizer deflection transducer, the angle of attack - and the EGT transducer. These latter calibrations were performed with the transducers installed in the aircraft. After installation of the pressure measurement system and the pneumatic

tubing, dynamic characteristics of the complete pneumatic system were evaluated. It turned out that each pneumatic system consisting of pneumatic tubing, valves, connections and probes could adequately be described by a first order linear filter. All the associated time constants were subsequently measured.

2.11. Mechanical work

The mechanical work was devided into two parts. One part consisting of transducer installation, routing of electric cabeling and installation of pneumatic tubes was carried out at Schiphol Airport. The other part consisting of the construction of the drawer for the wing pod and of transducer systems was performed at DUT. The elevator- and stabilizer deflection transducers were manufactured by NLR.

2.12. Installation in the aircraft

The installation of the entire instrumentation system was eased by the fact that the data collection system was located in the under wing pod. Only one multipole connector served as an electrical connection to the aircraft. Access to the tape recorder was provided by an inspection hatch on the pod. The pressure transducer box was easily installed through the ammunition bay door. Installation of the inertial package as well as of the control surface deflection transducers however required the removal of aircraft spline fairings.

3. ELECTRICAL FILTERS OF THE INSTRUMENTATION SYSTEM

3.1. Introduction

Filtering transducer output signals is usually necessary before recording the data with a sampling digital recording system. Filters are used to attenuate the amplitude of the high frequency contents of the signals. The higher frequencies in the signals are considered as noise due to structural vibration, transducer noise and electromagnetic interference.
In the present flight test program, pilot induced motions had frequencies from zero to about 0.5 Hz.
Attenuation of high frequency signal components is required to reduce aliasing errors caused by the finite sample rate of the data collection system. This sample rate equalled 20 measurements per second for each variable.
Two conflicting requirements arise in designing pre-sampling filters. On the one hand, the filter cut-off frequency should be high as compared to the frequency range of the signal of interest, in order to obtain a flat frequency response and a constant group delay over the specified frequency range. On the other hand the filter cut-off frequency should be low as compared to the sample rate in order to keep the amplitude of fold back frequencies withing the required accuracy limits.

3.2. Filter specification

The required bandwidth was 0.5 Hz minimum with an amplitude ratio of input- and output signal between 0.998 and 1.002 in the specified frequency range. The time delay of the filters should be equal within ± 2 msec. The static gain was not too important for this value is taken into account during the static calibration proces. The gain stability required however equalled ± 0.02%. The aliasing error should be less then 0.1% with a sample rate of 20 measurements per second. The expected ambient temperature variations ranged from -25° to +50°C.

3.3. Filter design

Filter design is commenced with an attempt to establish the required order of the filters. This calculation carried through is based on the aliasing specification of 0.1% with the given sample rate of 20 s/sec. Further more it is obvious that the filter cut-off frequency is much smaller then the sample frequency.
For a n-th order low pass filter the following equation is valid when $f_i >> f_o$

$$\log M \tilde{=} - n \log \frac{f_i}{f_o} \qquad (1)$$

The first image depends on the difference between the sample frequency f_s and the signal frequency f_i, see also fig. 5.

Substitution of $f_s - f_o = f_i$ in (1) yields:

$$\log M \tilde{=} - n \log \frac{f_s - f_o}{f_o} \qquad (2)$$

Now for different values of n and fixed values of M and f_s, the highest allowable filter cut-off frequency f_o can be calculated.
$M = 0.001$ and $f_s = 20$ substituted in (2) results in

$$f_o \tilde{=} \frac{20}{10^{3/n} + 1}$$

The values of f_o for different values of n are given in the following table:

n	f_o(Hz)
1	0.02
2	0.6
3	1.8
4	3.0
5	4.0

From the results above it is clear that the first order or second order filter will not satisfy the amplitude requirements with signal frequencies up to above 0.5 Hz at the same time satisfying the time delay requirements. Practical considerations (simplicity in design and component selection) lead to the choice of a 4-th order filter, to be realized with identical 2-nd order filters connected in series. The cut-off frequency was established at 19.0 rad/sec or practically 3 Hz.

The next problem to be solved was the determination of the damping coefficient of the filter. The following is a description of the method used.

The output-input ratio of a 2-nd order system is described by the equation:

$$M = \{ (1 - N^2)^2 + (2\zeta N)^2 \}^{-\frac{1}{2}} \tag{3}$$

The phase angle between output and input is given by:

$$\varphi = - \text{arctg } 2\zeta N \, (1 - N^2)^{-1} \tag{4}$$

Now in order to achieve a bandwidth as high as possible, with the amplitude ratio M between the gain limits, it is necessary to apply a damping smaller then critical. So the gain will increase to the upper limit of M at a certain signal frequency. From this frequency the gain will decrease, passes M = 1 and reaches the lower limit of M at the maximum allowable signal frequency. An illustration is given in fig. 6.

The required value of ζ is computed as follows. From setting the derivative of (3) to zero and solving for N is the result:

$$N = (1 - 2\zeta^2)^{\frac{1}{2}} \tag{5}$$

With this value for N the maximum of the frequency characteristic is obtained henceforth the maximum value for M. When now the value of N from (5) is substituted in (3) and ζ is solved in the result:

$$\zeta = \{ \tfrac{1}{2} - (M^2 - 1)^{\frac{1}{2}} \cdot (2M)^{-1} \}^{\frac{1}{2}} \tag{6}$$

With the maximum value for M being equal to 1.001 the calculated required value ζ_r equals:

$$\zeta_r = 0.691$$

This value of ζ_r and the minimum value for M substituted in (3) and solving for N yields:

$$N = [1 - 2\zeta_r^2 + \{4\zeta_r^2 (\zeta_r^2 - 1) + M^{-2}\}^{\frac{1}{2}}]^{\frac{1}{2}} \tag{7}$$

With the real values $\zeta_r = 0.691$ and $M = 0.999$

$$N = 0.329$$

Henceforth the maximum allowable signal frequency in accordance to:

$$f_i = N.f_o$$

$$f_{max} \tilde{=} 1 \text{ Hz}$$

Having established the cut-off frequency and the damping ratio, the time delay of the filter as function of the impressed frequency can be calculated, referring to equation (4):

$$\varphi = - \text{arctg } 2\zeta N \, (1 - N^2)^{-1} \tag{4}$$

the time shift equals:

$$\Delta\tau = - \frac{\varphi}{\omega_i} \tag{8}$$

Combining (4) and (8) yields:

$$\Delta\tau = \frac{\text{arctg } 2\zeta N \, (1 - N^2)^{-1}}{\omega_i}$$

The negative sign denotes that the output is lagging with respect to the input.
For different values of N the time shift is calculated with the following results:

ω_i(r.sec^{-1})	f_i (Hz)	N	φ (rad)	$\Delta\tau$(sec)
0	0	0	-	0.0727
1	0.1592	0.0526	0.0728	0.0728
2	0.3183	0.1053	0.1460	0.0730
3	0.4775	0.1579	0.2202	0.0734
4	0.6366	0.2105	0.2905	0.0739
5	0.7958	0.2632	0.3726	0.0745
6	0.9549	0.3158	0.4515	0.0752
7	1.1141	0.3684	0.5324	0.0761

From the results it can be seen that the time shift increases with about 2 msec for frequencies to 1 Hz. A plot of the time shift characteristic is presented in fig. 7. As a result, for the frequency range relevant to flight testing, the time shift was established to 73.5 ± 1 msec for one second order filter.

3.4. Realization of the filters

The 2-nd order low-pass filters are realized by using operational amplifiers and stable R-C networks. The basic component configuration is given in fig. 8 which shows a multiple feedback circuit. This kind of filter has the advantage of mathematical simplicity and is based on the behaviour at low frequencies compared to cut-off frequency, with good phase and amplitude response.

The following equations describe the low-pass circuit:

$$\omega_o = (R_2 R_3 C_1 C_2)^{-\frac{1}{2}} \tag{9}$$

$$\zeta = \left\{ \frac{(R_2 + R_3 + \frac{R_2 R_3}{R_1})^2}{4R_2 R_3} \cdot \frac{C_2}{C_1} \right\}^{\frac{1}{2}} \tag{10}$$

$$A = -\frac{R_2}{R_1} \tag{11}$$

The static gain (zero frequency) required is nominally unity, so the circuit produces a signal inversion which adds an extra constant phase of 180° to the input-output phase relation.

Substitution of $R_2 = R_1$ and solving R_1 and R_3 from (9) and (10) yields:

$$R_1 = \{\zeta + (\zeta^2 - 2\frac{C_2}{C_1})^{\frac{1}{2}}\} \cdot (\omega_o C_2)^{-1} \tag{12}$$

$$R_3 = \{\zeta - (\zeta^2 - 2\frac{C_2}{C_1})^{\frac{1}{2}}\} \cdot (2\omega_o C_2)^{-1} \tag{13}$$

The calculation of the component values is initiated with the selection of the capacitors, because there are fewer standards of high quality capacitors than there are resistors. Also resistors are more easily used for final adjustment of the complete circuits.
Some trial and error work is required to select the proper capacitors in relation to acceptable resistor values. This is done with respect to circuit input impedance and amplifier characteristics, e.g. voltage and current drift due to temperature changes. The capacitor values determined are:

$C_1 = 0.47\ \mu F$ and $C_2 = 0.1\ \mu F$

The required resistor values are calculated with $\zeta = 0.691$ and $\omega_o = 19$ rad sec^{-1} substituted in eq. (12) and (13). The nominal component values calculated this way are listed in the following table:

Component	Value	Unit
R_1	484	KΩ
R_2	484	KΩ
R_3	122	KΩ
C_1	0.47	μF
C_2	0.1	μF

It is necessary to look at the sensitivity of resistor values in respect to capacitor tolerance, the selected capacitors only having a tolerance of 1% and the requirement of all filters being equal. With a simple program the extreme values of resistors were calculated, thereby taking into account the capacitor tolerance. The calculated values are:

Component	Minimum	Maximum	Unit
R_1	470	500	KΩ
R_2	470	500	KΩ
R_3	118	127	KΩ
C_2^1	0.465	0.475	μF
	0.099	0.101	μF

The actual resistors are assemblies of a fixed part and an adjustable part with the following values:

Component	Fixed part	Adj. part	Unit
R_1	470	25	KΩ
R_2	470	25	KΩ
R_3	120	10	KΩ

The resistor R_4 from fig. 8 is not yet mentioned in the description but for the measurement of bipolar input signals this resistor is needed to achieve an unipolar output. This resistor when connected to the -5 V reference voltage provided a bias to the output of the second stage of the filter circuit. The value of R_4 calculated to provide +5 V output is 728 KΩ.

3.5. Filter construction

Four second order filters are assembled on one printed circuit board of 30 x 6 cm^2 , which is enclosed in a dural frame work. A total of 10 units is placed in the filter box. Four switches and four screwdriver potentiometers on the front panel of each unit provide for initial offset adjustment of the operational amplifiers. The signal- and the power supply connections are made through one connector on the backpanel of each filter unit, see fig. 9.

3.6. Filter components

Chopper stabilized amplifiers type 210 from Analog Devices are used because of the stability requirements. These amplifiers have a voltage offset drift of 1 μV per °C and a current drift of 3 pA per °C over a temperature range from -30 to +50°C. One disadvantage of this type of amplifier is the unbalanced power input resulting in current flowing through power ground leads. This effect however was reduced by the application of suitable bleeding resistors.

Polystyrene capacitors are preferable in precision filter circuits for low frequencies because of their low temperature sensitivity, usually below 25 ppm per °C. Their physical dimensions hower are much larger compared to polycarbonate capacitors. Metallized polycarbonate capacitors, type MKB-3, are chosen for the filter circuits, they exhibit a reasonable long term stability 3.10^{-4} per y and a temperature sensitivity of 50 ppm, per °C. The tolerance available at the time of construction was ± 1%.

Stability and low temperature sensitivity are the requirements of the resistors, the resistance values being of less importance. The resistors used are from Ultronix, type 205 RP, having a temperature sensitivity of 10 ppm per °C, tracking 2 ppm, a long term stability of 1.10^{-4} per y and a tolerance of ± 1%. The resistors are small bifilarly would

with radial leads for printed circuit mounting. The variable resistors are from Beckman Helipot. The small diameter potentiometers have cermet resistance elements and the necessary infinite resolution. Temperature sensitivity depends on the range used but is in the order of 100 ppm per °C.
A complete scheme of one filter unit with four 2-nd order filters is presented in fig. 11.

3.7. Adjustment of the filters

The final adjustment procedure is carried out with the analog computer EAI 680 of the Department of Aerospace Engineering. An analog model of the filter was made with the calculated values of gain, damping and cut-off frequency. Precision components with a nominal accuracy of 0.01% are used in this computer. Fig. 10 shows the block diagram of the adjustment sett-up. Model and filter were excited with the same input, a low frequency sine wave or a square wave signal. During the adjustment with the three filter potentiometers, the output of the summing amplifier was monitored. When equality of model and filter was achieved, this signal remained zero for every input. A peak to peak output of 2 mV was considered to be acceptable for full scale input signals.

3.8. Filters with voltage gain

Because of the ± 2 V full scale output of some transducer systems, six filters are required with a static gain of 5. This is realized in the first stage of the filter unit. Component values of these circuits, determined with the method described for the standard filters, are listed in the following table.

Component	Fixed part	Adj. part	Unit
R_1	286	20	KΩ
R_2	1430	100	KΩ
R_3	116	10	KΩ
C_1	0.47	-	μF
C_2	0.033	-	μF

The adjustment procedure is carried out in the way described, only the potentiometer setting in the analog computer being changed. The input signal of course was reduced to an acceptable level.

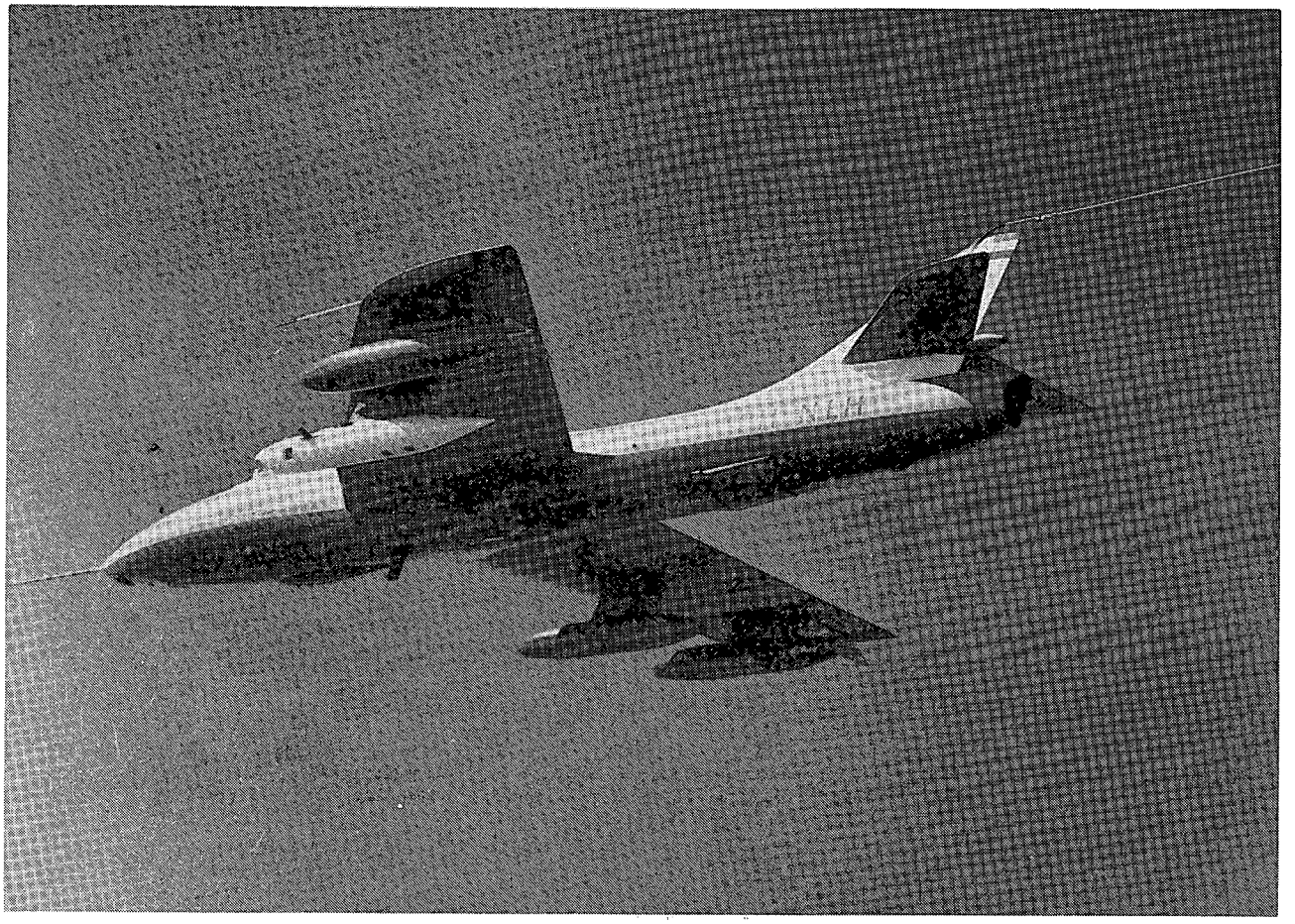

FIG. 1: HAWKER HUNTER MK VII WITH TRAILING CONE TUBE.

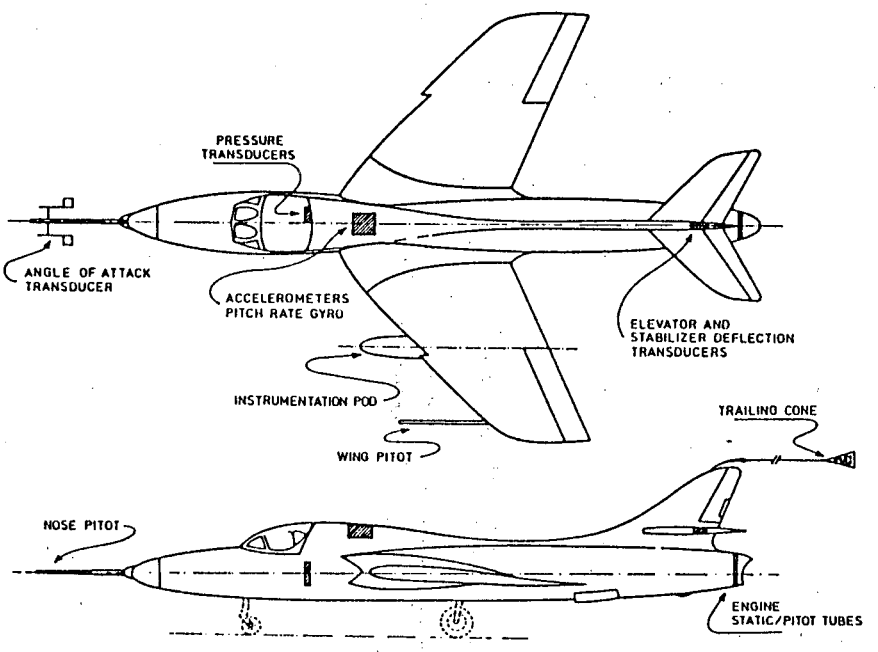

FIG. 2: TRANSDUCER LOCATIONS IN THE HUNTER MK VII.

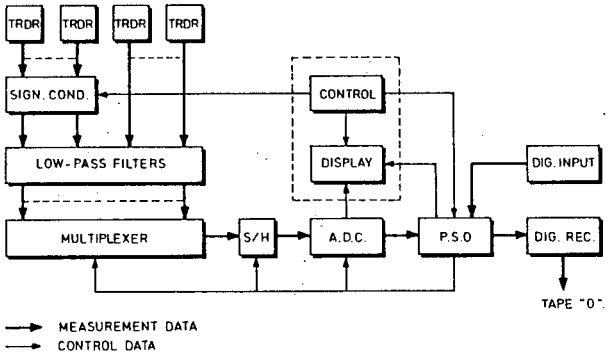

FIG. 3 : GENERAL ARRANGEMENT OF THE INSTRUMENTATIONSYSTEM.

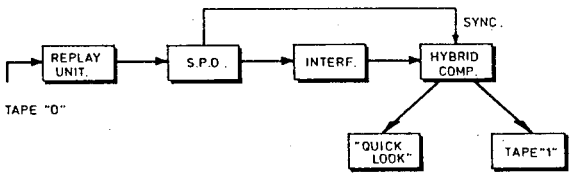

FIG. 4 : GENERAL ARRANGEMENT OF THE GROUND EQUIPMENT.

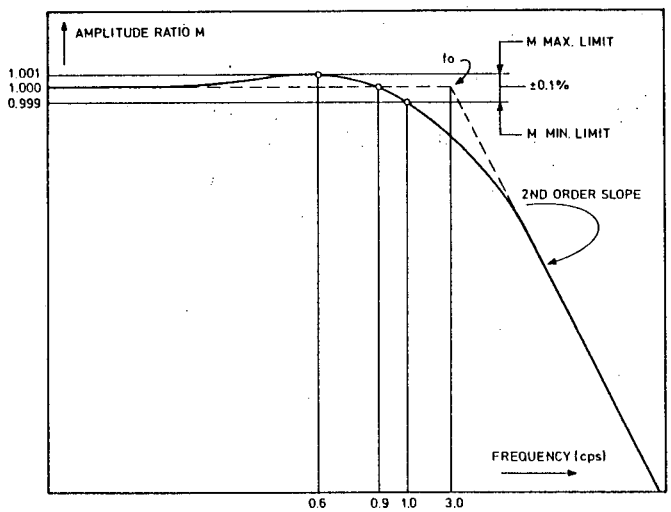

FIG. 6 : FREQUENCY CHARACTERISTIC OF 2ND ORDER FILTER.

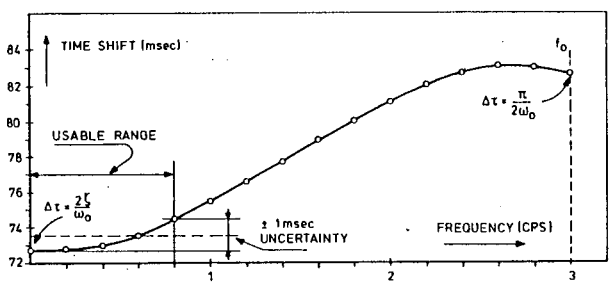

FIG. 7 : TIME SHIFT CHARACTERISTIC OF 2ND ORDER FILTER.

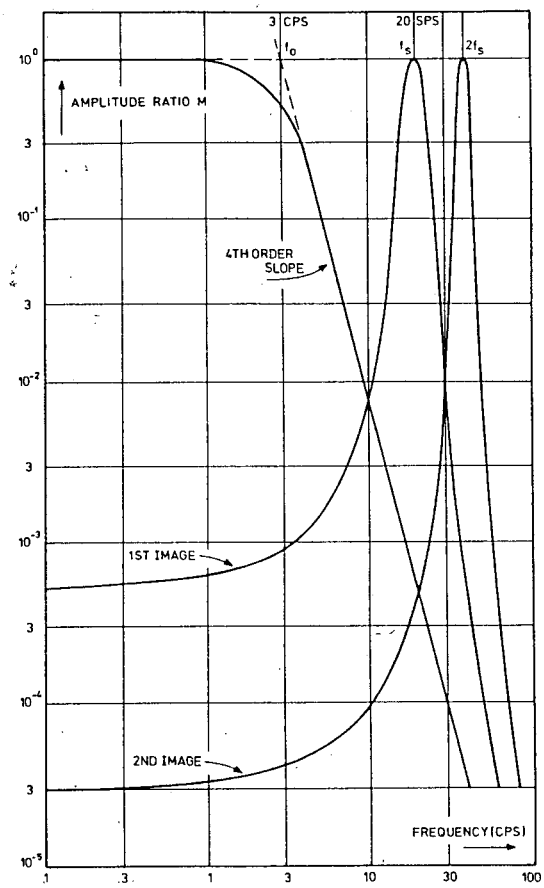

FIG. 5 : IMAGES PRODUCED BY SAMPLING OF 4TH ORDER DATA

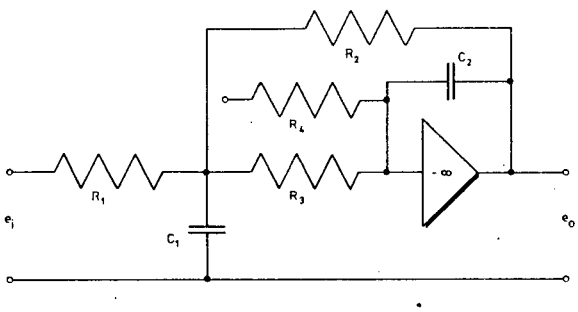

FIG. 8 : BASIC COMPONENTS OF 2ND ORDER FILTER.

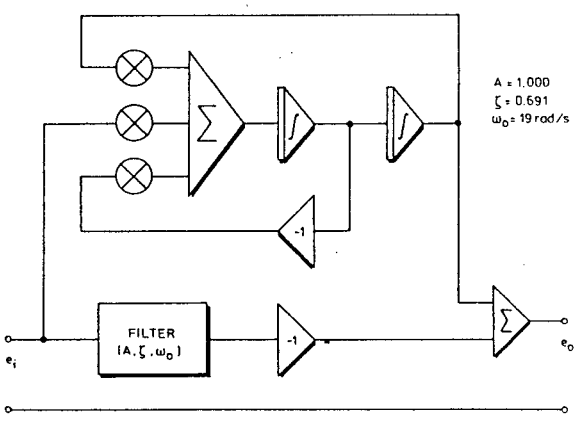

FIG. 10 : ANALOG COMPUTER ARRANGEMENT FOR FILTER ADJUSTMENT.

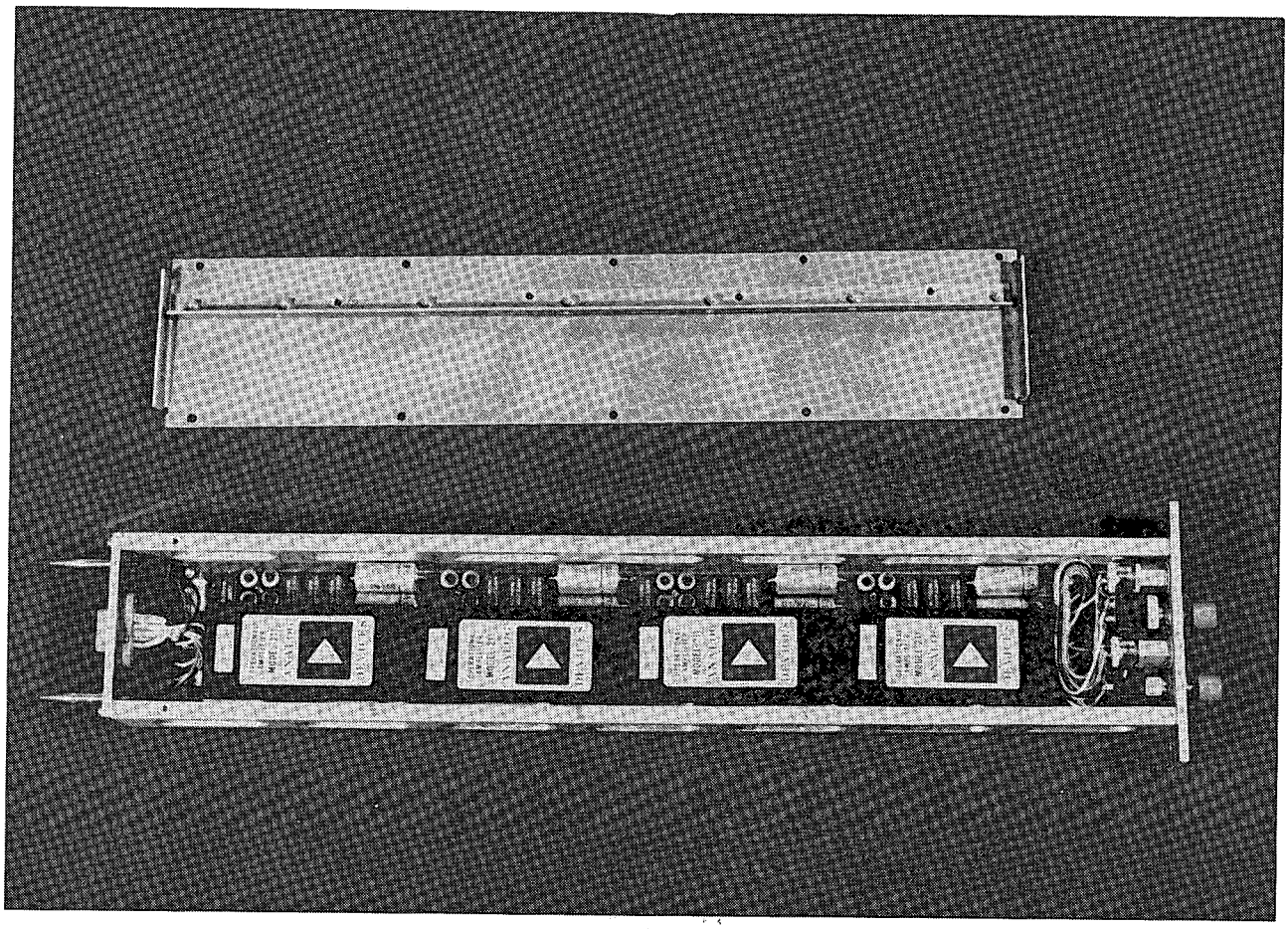

FIG. 9 : ELECTRONIC FILTER MODULE.

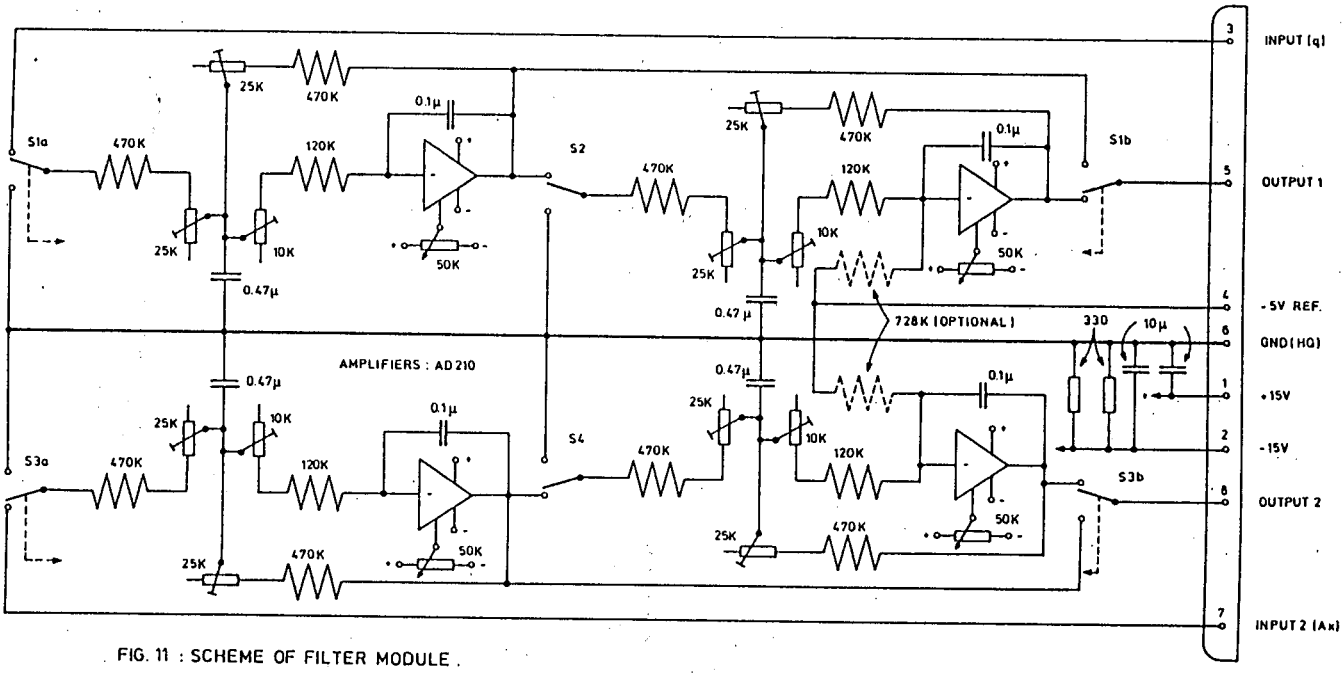

FIG. 11 : SCHEME OF FILTER MODULE.

SPECIFYING, BUYING AND ACCEPTING A FLIGHT SIMULATOR

J.M. van Sliedrecht
M.L. Wijnheijmer
R.P.A.M. Teunissen

Royal Dutch Airlines

ABSTRACT

A brief description is given of the process of specifying, buying and accepting a flight simulator by an Airline.
Special emphasis is put on the acceptance of the simulator and the specific role of the engineering pilot.
Some examples are given of the contributions of the engineering pilot to the quality of the flight simulator.
To conclude this paper, some final remarks are made on the task of the engineering pilot in a flight simulator project.

INTRODUCTION

Between the moment an order for a new flight simulator is given to a simulator manufacturer and the moment it is ready for training at the airline training centre, one to three years go by, depending on the type of simulator and the specific airline requirements.

A number of project phases can be distinguished: Drafting of the simulator specification, the gathering of aircraft data, the development and build up of simulator components, the integration,the acceptance by the airline and the introduction of the simulator as a training tool within the airline.

A considerable input from the airline is required in the different project phases. Generally, a simulator is not an off the shelf product, as specific airline requirements have to be incorporated. For instance, the instructor station is "airline unique" and very often based on the instructor station of a previously built simulator, in which technical enhancements are incorporated. In doing this, switching from one simulator to another by pilot instructors is relatively easy. Further all necessary malfunctions for the specific aircraft type have to be defined (including side-effects) by the airline.

Pilot input has always been required in order to make a simulator-project successful. The pilot is always responsible for the finishing touch of the flight program, the autoflight system, the flight controls and the motion system. He is the only one who can take that responsibility, because he has the operational experience, needed to judge the flying qualities of the simulator.
When a pilot has an engineering background, it very often turns out that existing problems with, or deficiencies of the simulator can be dealt with much more easily. That is because the engineering pilot and the responsible engineers will be able to communicate at the same level. They talk each others language!

In the following chapters the specific role of the engineering pilot will be highlighted, not only during the acceptance of the simulator, but also during the other project phases.

THE SIMULATOR SPECIFICATION

One of the most important documents of a simulator project is the contract between manufacturer and buyer. It contains mainly financial, liability and warranty matters.
Another one is the so called Technical Specification. This document contains the technical matters of the flight simulator project and is therefore of paramount importance to the acceptance team. This chapter deals with the latter of the two documents mentioned.
First we will try to answer the question why a Technical Specification, or "Spec" as it is affectionally called, is needed at all.
During the contract negotiations the buyer states his wishes and the manufacturer defines his abilities. The manufacturer will issue a Spec to give the customer an idea of what he may expect. This Spec is subject to changes during the contract negotiations.
As all simulator manufacturers will issue such a Spec, it gives the buyer a perfect opportunity to compare the various offers. In this phase of a simulator project the Spec mainly serves the purpose to enable comparison of different offers. After the contact has been awarded to a certain manufacturer, the Spec is firm. It states very specifically what the manufacturer will deliver. This Spec is from then on in principle no longer subject to any changes.
The Spec contains subjects like:

- software architecture
- hardware specifications
- limitations and tolerances
- systems data
- computer input, output organization and architecture
- linings and colour schemes, etc. etc.

After a simulator project has been started, the Spec is the guide line by which both the manufacturer and the buyer (i.e. the acceptance team) work. The question raised continuously is whether "the product meets the Spec". And if any discussion arises pertaining to a technical subject, the first thing to be done is to check the Spec.
The Spec also gives the acceptance team the possibility to fairly judge the work done by the manufacturer. In this respect there are only two possibilities: either a certain item meets the Spec or it does not. What will happen if the latter is the case will be discussed in the chapter: Development and build up.

THE AIRCRAFT DATA

Generally the configuration data, needed to construct the simulator consist of hardware data and software data. Both are a responsibility of the aircraft manufacturer (i.e. a simulator will always be built to reflect a certain tailnumber of the operator's fleet). The aircraft manufacturer derives these data from the aircraft specification. If, during the production of the simulator, certain aircraft specification items change, it is the responsibility of the aircraft manufacturer to update the configuration data and to disclose this information to the simulator manufacturer through update revisions of the applicable data package.
If, during build-up or check-out of the simulator, the data show inconsistencies, a data-request to the aircraft manufacturer should correct this. Replies on these data-requests are part of the approved data, and responsibility for correctness remains with the aircraft manufacturer.

The hardware is more than only the cockpit lay-out, see the figure at the end of this paper. In fact this is only a small part of the hardware. A very important part of the hardware data consist of inside cockpit dimensions, position of panels, seats and controls and also proper datum-lines to define the correct pilot's eye position. To achieve utmost reality, it is best to use actual aircraft parts for all visual components in the simulator flight compartment. However, as this would increase the cost of the simulator dramatically, the simulator manufacturer will produce certain parts, based on aircraft drawings and delivered as part of the data-package. Critical and/or complicated parts like the forward pedestal, all primary and secondary controls, the glareshield panel and all cockpit linings, are purchased as aircraft parts. Also a number of instruments and control boxes are purchased as aircraft parts. The hardware data delivered should therefore reflect all necessary information to control these aircraft parts and, these data should disclose all necessary information to simulate specific hardware, e.g. pressurization and airconditioning indicators.

Apart from hardware data the data package also contains software data. These data consist of modelling and check-out data for all aircraft systems, i.e. electrics, hydraulics, airconditioning, pressurization and fuel supply. But also a sound recording of typical aircraft sounds is part of the data. Besides these data, the simulator manufacturer delivers all information needed to drive actual aircraft indicators through the "interface control documents" (ICD). These documents enable the simulator manufacturer to let aircraft instruments in the simulator operate as in the aircraft. It is self-evident that a very important part of the software data is the aerodynamic model, representing the aircraft's flight characteristics. In a modern simulator not only all normal flight characteristics are covered, but also the aircraft behaviour with flight controls failed, engine failure, gear failure, etc. The necessary data are gathered during flight tests and windtunnel tests. Although generally the accuracy of the data is sufficient, it is possible that during check-out of the simulator, as an integrated product of many software programs the result may be different from the real aircraft.

A particular subject is the definition of malfunctions. These are failures in any aircraft system. This subject is mentioned here, because proper malfunction definition is closely related to the application of the approved data. One may distinguish two main reasons for malfunction definition. The first one is obvious and is only an operational one, i.e. those malfunctions defined to meet the necessary training requirements. The second reason is purely because of check-out purposes, i.e. by defining a malfuction in a certain part of an aircraft system, one can determine if the extent of the simulation is sufficient and therefore future modifications to the aircraft can be incorporated in the simulator relatively easy.
Malfunctions are defined by the customer, although the effects of failing parts of an aircraft system are governed by the information laid down in the hardware and software data.

DEVELOPMENT AND BUILD-UP OF SIMULATOR COMPONENTS

In this project phase the engineering pilot's main task is to check what has been done and what still has to be done. He will discuss with the assigned engineers those parts of the data-package which seem to be weak or even incorrect. If necessary, this will result in a meeting with the aircraft manufacturer in order to get the data right and in the correct format. By looking at the data and knowing the aircraft characteristics, it is often possible to define weak areas and correct those, in cooperation with the aircraft manufacturer. This can be done before one can actually "fly" the simulator. This of course will enhance the quality of the simulator and will save time later on in the project.

Furthermore a continuous check is required whether the manufacturer is building the simulator according to the specification or not. Very important is that both parties do have the same understanding and interpretation of the Spec. If, in spite of the foregoing both parties do not agree, it will be the decision of the engineering pilot and his staff, either to force the simulator manufacturer to change his mind or to give in. In the latter case credit is built up with the simulator manufacturer. Obviously this situation will repeat itself many times in the course of a project.

In the beginning of this project phase the hardware (layout) and the software of the complete instructor station have to be defined. A major task, as the success of the introduction of the simulator in the company depends heavily on the completeness and userfriendliness of the instructor station.

In other words: even when the simulator does have good flying qualities, but the instructor station is not liked by the instructors, the simulator will be rated as a bad one.

THE SIMULATOR INTEGRATION

During the production of the simulator components, many parallel activities take place. The engineering part consists of the production of all the necessary drawings, the design of the wiring and the hook-up of peripheral equipment like interface, motion, visual and communication with the host computer. The simulation software is designed on a system per system basis. This means that for each system to be simulated, there is a dedicated engineer, who is basically responsible for the proper performance of the system assigned to him.
Before considering the simulator under acceptance, it is of utmost importance that every system is checked-out seperately. For this purpose several documents are used: Acceptance Test Manuals (ATM) and the Approval Test Guide (ATG).

An ATM consists of a set of test set-ups, by which a simulated aircraft system can be checked. For purposes of convenience, the ATM's are set-up also on a system per system basis. Generally they consist of the following chapters:

- on ground checks
- in flight checks
- circuit breaker checks
- malfunction checks

The basic ATM is drafted by the responsible system engineer. In review sessions with the engineers of the customer and the simulator manufacturer, the ATM's are made as complete and as correct as possible. In this respect the engineering pilot plays an important role, as far as the feasibility of the suggested tests is concerned. He gives inputs how to execute the tests where flight manoeuvres are considered. He also evaluates malfunction effects and the impact to be achieved on the training. He therefore has to give input to optimize the training effect of suggested malfunctions. The basis for each ATM is, of course, the data delivered by the aircraft manufacturer.

The ATG consists of numerous aircraft configuration and set-ups by which the flight characteristics of the simulator can be validated. The tests are fully automated i.e. input signals and aircraft conditions are dictated and output signals are automatically recorded. By comparing the output signals to the actual aircraft responses, the simulator characteristics can be judged.
It must be shown that the ATG "matches", i.e. simulator responses, are in tolerance with the aircraft responses with all simulation programs running. The reason for this is that, due to the execution time, as opposed to the iteration rate of the computer, scheduling of programs has to take place. This means that not every simulation program will be executed each iteration. Some programs run at an iteration rate of half, one third, or even a quater of the host computer's basic iteration rate. By scheduling the most important programs in the basic iteration band, possible effects of time delays are suppressed. In this critical band a.o. at least flight, flight controls and landing gear should be scheduled.

THE SIMULATOR ACCEPTANCE

The acceptance of the simulator in the plant of the manufacturer is a job of eight till twelve weeks. The airline acceptance team consists of:

the engineering pilot (leader)
a second engineering pilot
a flight engineer
a software engineer
a hardware engineer
a visual engineer

The team accepts six to eight hours a day, five days a week. The simulator deficiencies found have to be cleared by the manufacturer. Usually, the manufacturer needs all the time available to cope with the number of deficiences. The simulator will be fully booked, twenty four hours a day, seven days a week. A typical number of generated deficiences will be fifteenhundred.

The sequence in which the different systems are tested is very important in order to acquire a simulator with all the systems properly integrated.
First of all, the instructor station should be checked out and work properly. This step should be finished before accepting the simulator as a flying machine.
This being done, the simulator environment should be checked (atmosphere).
Next, the engine, supplying electric, pneumatic and hydraulic power, should be checked.

Thereafter the electric, pneumatic and hydraulic systems and finally the flaps/slats, flight controls, gear, etc. should be checked.
Herafter, checking of flight, motion and autoflight can be started. At the same time the abnormal operation of the system can be checked. The earlier discussed Acceptance Test Manuals are the basis for the acceptance of the different systems, however, the finishing touch is done by the acceptance team, by using all its knowledge of the real aircraft.

A typical example of what turned out to be very critical data during the acceptance, is the landing flare of the Boeing 737-300. During acceptance it became evident that the flare was not according to that of the aircraft, in spite of the fact that all parameter trajectories were within the tolerances, prescribed by the FAA.
By manipulating not less than six parameters, related to groundeffect, and all parameter trajectories still within limits, the landing flare was still not correct.
The question remains, whether or not the (FAA) tolerances were chosen correctly.

A completely different approach was needed for the ground model of the same aircraft. The very pronounced -well known- "skating" effect on the runway could be greatly reduced, by doubling the iterating frequency, whereupon it turned out to be possible to increase tyre side forces to the required value, without the model getting unstable.

THE COMPANY INTRODUCTION OF THE SIMULATOR

After the flight simulator has been installed in KLM's training department facilities, the acceptance certificate has been signed and the inauguration festivities are over, the simulator engineering pilot will get a somewhat different task.
The flight simulator as such is not his primary responsibility anymore, since it has been handed over to the Chief-Pilot Instructor of the aircraft type concerned and to the assigned simulator engineer. Both will work in close cooperation and will take care of maintenance and training availability of the new simulator.
The first three to six month a flight simulator is used for training, are of utmost importance for its future, since it is in this period that a lot of deficiences will come (and ought to come!) out. These deficiences or "snags" will be recorded by the individual pilot-instructors using the flight simulator for training.
Tje "snags" written in this period are a mix of valid, newly found system deficiences, valid old and already known deficiencies (so-called "hold items") and invalid ones, originating from insufficient knowledge of the (new) aircraft type and its systems or from "mishandling" of the flight simulator.
Since all deficiency reports are written in a pilot's operational language and must be adressed by the assigned maintenance engineer, there is a possibility that the latter will spend a lot of his time trying to establish operational priorities of deficiency reports that need not be adressed at all. It is the simulator engineering pilot's task during this period to act as a "filter" between the operational crew (i.e. the pilot instructors and their students) and the technical crew (the simulator engineer and his maintenance crew).
This requires a lot of both operational and technical knowledge, and a great deal of tact and diplomacy as well.
A second task for the engineering pilot during this period is to review and test proposed solutions to reported deficiencies, and once these solutions appear satisfactory, to clear the outstanding deficiency.

FINAL REMARKS

It will now be clear that accepting a new flight simulator for an airline is a job that requires a mix of skills and talents.
Firstly the pilot concerned must be operationally "seasoned". Secondly he must have a profound technical knowledge and thirdly a certain dosis of tact and diplomacy is needed, together with some managerial skills.

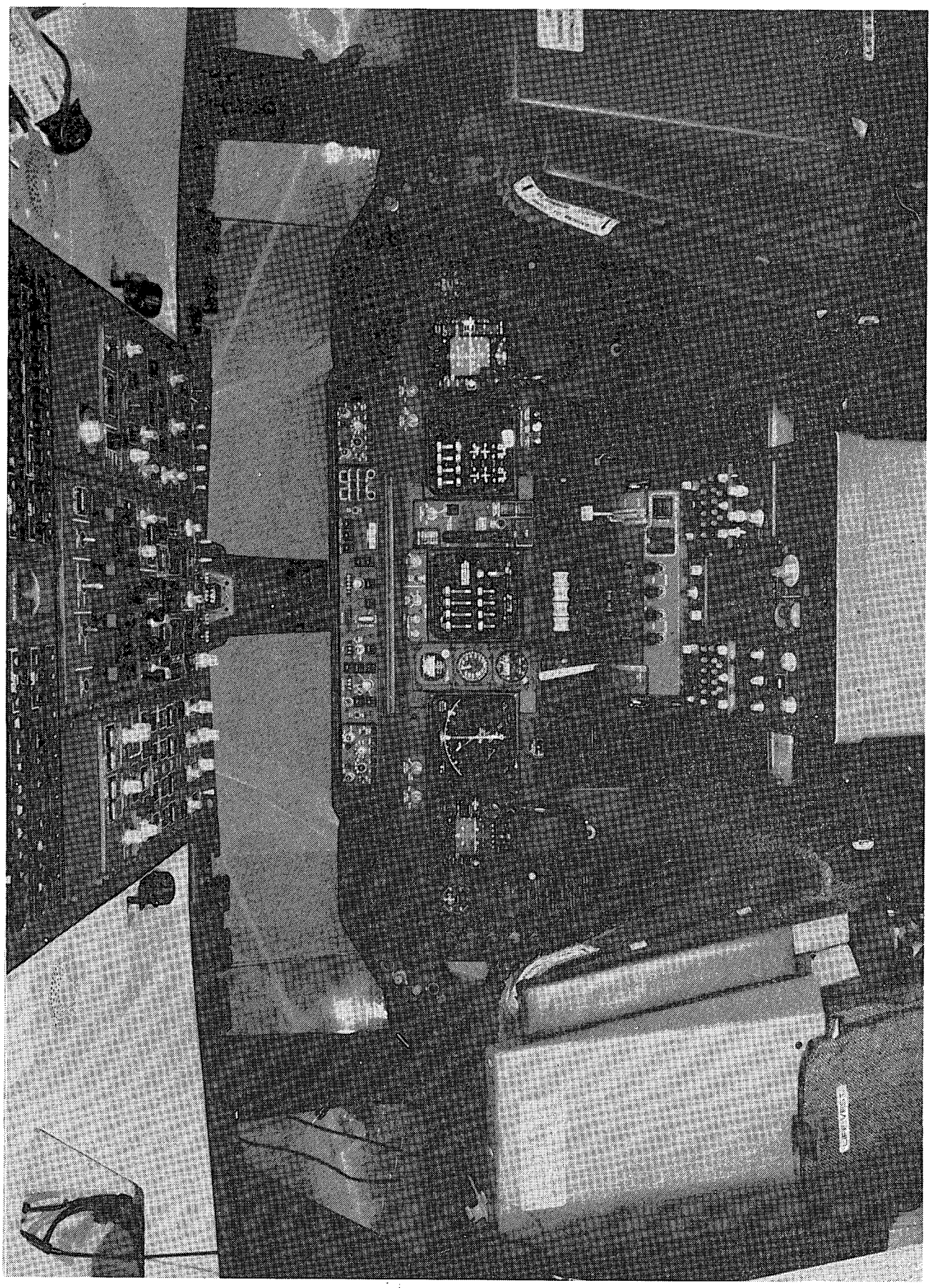

PHASE II FLIGHT SIMULATOR MATHEMATICAL MODEL & DATA-PACKAGE, BASED ON FLIGHT TEST & SIMULATION TECHNIQUES

A.M.H. Nieuwpoort
J.H. Breeman
National Aerospace Laboratory

M. Baarspul
J.A. Mulder
Delft University of Technology

PHASE II FLIGHT SIMULATOR MATHEMATICAL MODEL AND DATA-PACKAGE, BASED ON FLIGHT TEST AND SIMULATION TECHNIQUES

by
A.M.H. Nieuwpoort and J.H. Breeman
National Aerospace Laboratory NLR, Netherlands

M. Baarspul and J.A. Mulder
Delft University of Technology (DUT)
Faculty of Aerospace Engineering

Abstract

The Dutch Government Civil Aviation School (RLS) operated six Cessna Citation 500 aircraft in the final stage of the training of civil aviation pilot students. In the spring of 1986 RLS decided to purchase a phase II approved flight simulator to transfer parts of the training from flight to the ground. As a result of this only three aircraft would be necessary for actual flight training. However, because the aircraft was developed in the late sixties no mathematical model and data package were available with the required accuracy for a phase II flight simulator. Therefore RLS contracted the National Aerospace Laboratory (NLR) and the Faculty of Aerospace Engineering of Delft University of Technology (DUT) to install an accurate instrumentation system in one of the RLS Cessna Citation 500 aircraft, to execute a flight test programme and to process and analyse the resulting flight test data in order to generate the required mathematical simulation models and corresponding data.

In order to acquire the necessary information in the relatively short period of time available for the execution of the flight tests and the analysis, use was made intensively of dynamic flight test techniques in relation with computer data processing.

The mathematical models to be identified must give an adequate description of the aerodynamic forces and moments, the engine characteristics, the flight control system and the landing gear characteristics. In order to evaluate and test the generated models, both off-line and on-line (pilot in the loop) simulations were performed on the computer and moving base flight simulator owned and operated by the Stability and Control Group of the Faculty of Aerospace Engineering of DUT. Here also the comparisons were made, the so-called proof of match, between the measured flight test time histories and the computed model responses.

In the paper a survey is presented of the employed instrumentation system, the flight test programme, the data processing and corresponding parameter identification and the synthesis of the various models.

1. Introduction

It is a well-known fact, that flight hours are expensive and in-flight training imposes certain restrictions due to safety considerations. As a consequence already at an early stage tools were developed to shift at least parts of the training to the ground. As a result of the growth of technical skills this tool finally emerged into what is now called the ground based flight simulator. Due to the tremendous advances in computer technology both with respect to memory capacity and computation speed, flight training relies more and more upon this device. However, with the increase of tasks also the demands with respect to fidelity become more severe.

Present flight simulators consist of very complex systems;

1. Digital computers
2. Fully instrumented cockpit, including control loading system
3. Visual system
4. Motion system
5. Model software describing the various mathematical models of the simulated aircraft
6. System software interacting the various systems.

The fidelity of the complete flight simulator not only depends on the fidelity of the individual systems, but also on the integration of all parts. In concreto this means, that the flight simulator can be considered as a chain of which all links (systems) must be equally weighted.

The model software represents a very important link in this chain. Furthermore it is the least subjective part, because off-line analysis can be performed using the same real-time simulation software. The characteristics of the vehicle are laid down in various submodels embedded modular within the simulation programme. The most important submodels, related directly to the aircraft, are models with respect to:

1. Aerodynamics
2. Engine
3. Flight control system
4. Landing gear
5. Atmosphere, wind and gust
6. Navigation.

At present most mathematical models of transport aircraft are based on windtunnel measurements, theoretical analysis, data of engine manufacturers, updated with flight test results.

In the course of time the FAA has established various requirements for correlating simulator aerodynamic responses to airplane data. These requirements are legislated through Advisory Circular AC 120-40A (Ref. 1).

In the early days of simulator evaluations, an FAA pilot would subjectively evaluate a simulator by flying it and give his comments on the handling characteristics. Because each pilot will interpret these characteristics to his own standard, tuning may lead easily to very different flight simulators for the same type of aircraft.

Therefore in order to define more objective criteria, in 1980 the Advanced Simulation Plan was established as a joint effort of FAA, NASA, ALPA, airlines and simulator manufacturers. This

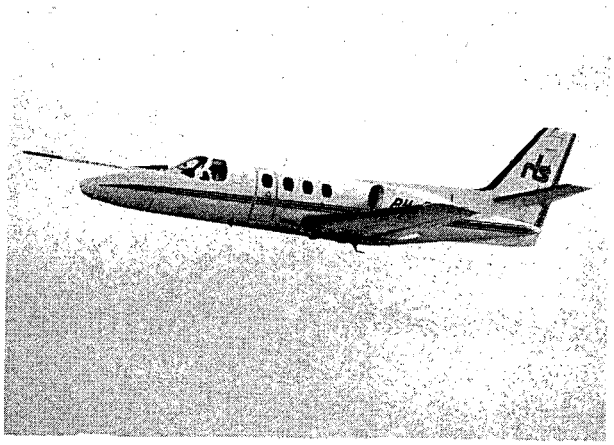

Fig. 1 Cessna Citation (PH-CTA) in flight

plan offered three major levels of approval defined as Phase I, II and III. If, for example, a flight simulator has fulfilled phase II requirements it is allowed to let pilots receive an airplane type rating without ever flying the aircraft.

Apart from the requirements for the various levels of approval the FAA also specifies a so-called Acceptance Test Guide (ATG), containing all kinds of tests with respect to aerodynamics, engines, systems and ground handling. This document is drafted by the simulator manufacturer in cooperation with the operator as a guarantee to the flight simulator customer. Parts of this ATG (so-called Proof of Match (POM) data) are evaluated by the FAA to award a certain level of approval.

The Cessna Citation 500 executive jet aircraft is operated by the Dutch Government Civil Aviation School (RLS) in the final stage of civil aviation pilot training.

In the spring of 1986 the RLS decided to purchase a flight simulator for the aircraft, which should have a Phase II approval. This made it possible to reduce the fleet from six to three aircraft.

Because the Citation 500 was developed in the late sixties no mathematical model and data package was available, which was of such quality that it could be used to obtain Phase II approval. Therefore RLS contracted NLR and DUT to install an accurate instrumentation system in one of the Citation 500 aircraft (PH-CTA) (Fig. 1), execute a flight test programme, analyse the data, evaluate the a priori mathematical models of the aerodynamics, engine, flight control system and landing gear and finally generate the

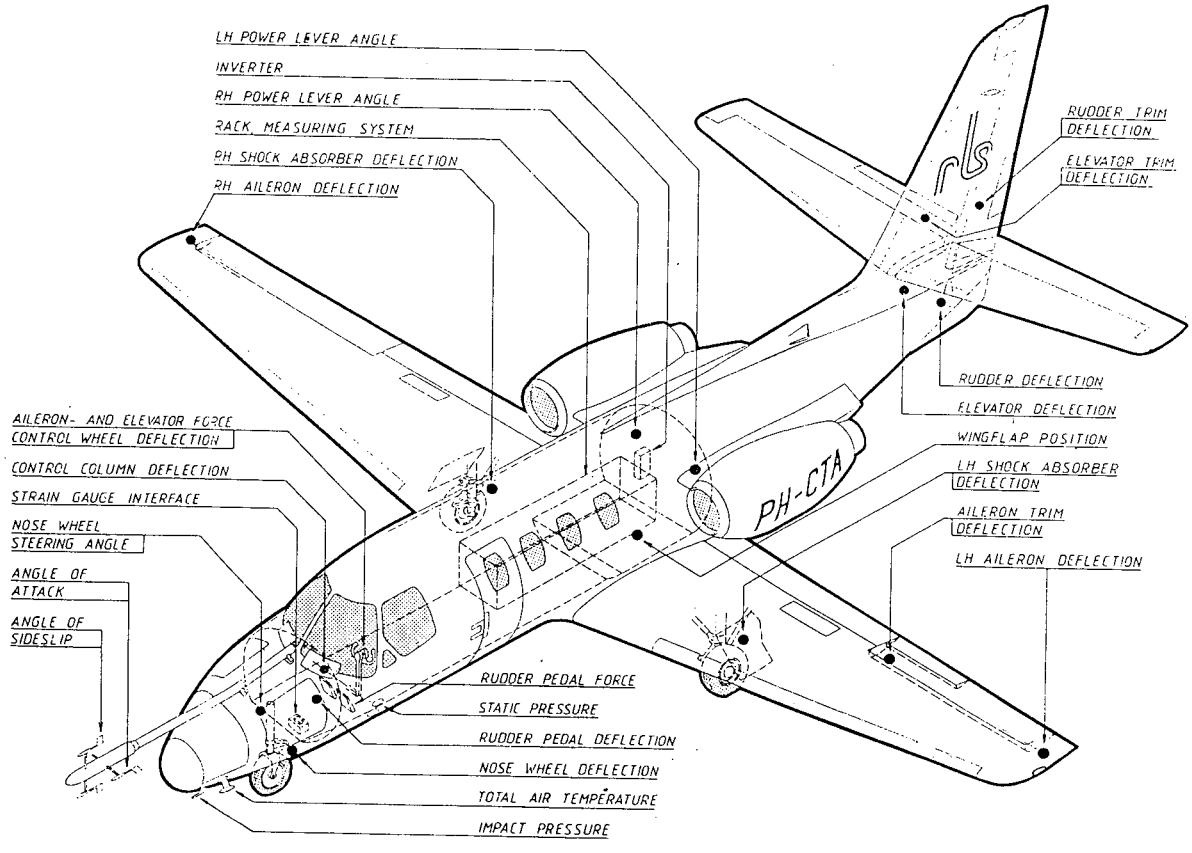

Fig. 2 Sensors in test aircraft

necessary data for these models, based on the results of the flight tests.

Before the flight test programme a priori models were developed based on literature (Ref. 2), comparable aircraft and engineering judgement.

In the paper the instrumentation system is discussed in section 2. Section 3 contains a short survey of the executed flight test programme, whereas section 4 yields the description of the data processing. In section 5 as an example the data analysis and modelling is described for the aerodynamics valid for the normal flight envelope. Finally in section 6 results are shown of some proof of match recordings.

2. Instrumentation

The instrumentation system required for flight tests incorporating dynamic manoeuvres must be more accurate than usually is employed with conventional methods. However, todays commercially available instrumentation systems can fulfill these requirements.
Five more or less independent sensor systems can be distinguished:

1. Inertial measurement system
2. Air-data measurement system and vanes to measure the aerodynamic angles
3. Transducers for measuring engine parameters
4. Transducers for measuring control surfaces and trim deflections
5. Transducers for the measurement of control forces and deflections and gear parameters such as shock absorber deflections and nosewheel steering angle.

Figure 2 shows the positions of the various sensors in the aircraft.

The inertial measurements are performed with a strapped-down Honeywell laser-gyro Inertial Reference System (IRS). For the measurements of static pressure and impact pressure the standard aircraft pitot tube and static sources have been used. However, accurate values of these pressures were obtained by very accurate Garrett barometric transducers, that were held at a constant temperature.

With respect to the engine parameter system, where possible standard on-board systems and transducers were employed. Also for the measurement of fuel flow, fuel quantity, stick shaker, radar altitude and events like gear up/down and speedbrakes retracted/extended use was made of existing instrumentation in the aircraft.

The transducers required to measure the control surface and trim tab positions and the shock absorber deflections were positioned as close as possible to the parameter to be measured.

As can be noted from figure 2 the angle of attack and slip angle vanes were mounted on a special designed boom, which was placed on top of the nose compartment. This design was chosen from a construction point of view and to attenuate the vane position errors.

Apart from the above-mentioned instrumentation three accelerometers were installed in the cockpit in order to measure vibration and buffet levels at the flight deck.

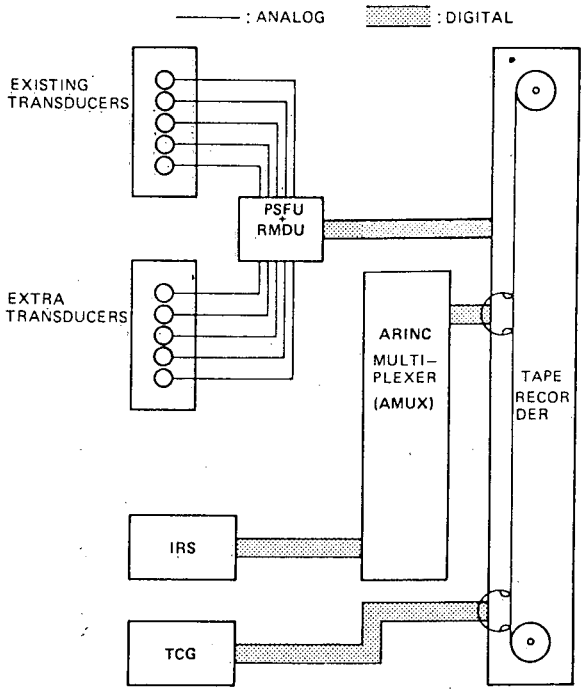

Fig. 3 Instrumentation system

The analog transducer outputs were digitized by means of a Pre-Sample Filter Unit (PSFU) to correct for aliasing and a standard NLR Remote Multiplexer Digitizer Unit (RMDU). The IRS output is converted to ARINC format by means of an ARINC multiplexer (AMUX) and just as the RMDU signals stored on a 14 track taperecorder. A reference time signal from a time code generator also is recorded on a separate track. This signal is used to synchronize all data on the various tracks to the same time grid, which is a requisite for the recording of dynamic manoeuvres. In figure 3 a schematic view is presented of the recording process.

Different sampling rates are employed for the various parameters dependent on the frequency contents. As a result of this, parameters were recorded with a sample rate varying from 2 Hz to 50 Hz, the accelerometers in the cockpit were sampled with 256 Hz.

Figure 4 shows the IRS unit, signal conditioning, operating panel and data recorder mounted in special racks in the aircraft.

Before the start of the actual flight test programme, an instrumentation checkout flight was performed in which the various system were tested and during which a number of manoeuvres were executed. During this test flight and also during the flight test programme the instrumentation functioned without significant problems. At a regular basis calibration checks were performed in order to safeguard the functioning of the instrumentation system. The smooth operation contributed significantly to the ability to execute the flight tests within the tight time schedule.

The flight test programme was executed in the period between January 28 until April 4, 1987. In total approximately 52 hours were flown.

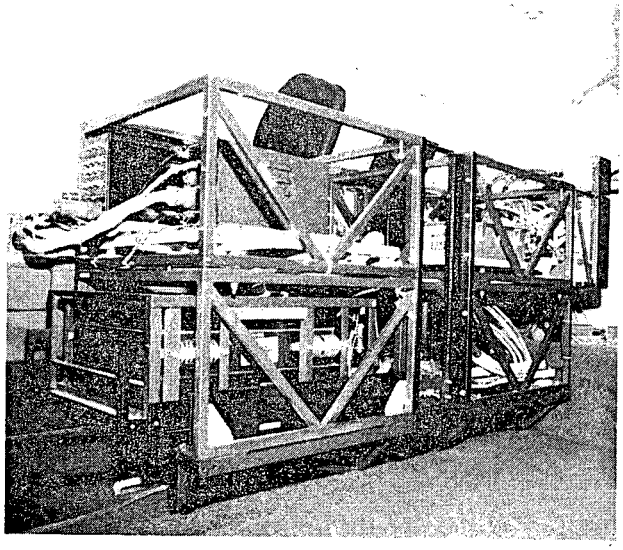

Fig. 4 Instrumentation in test aircraft

Finally it must be mentioned, that two flights were devoted to the determination of the position error correction as a function of configuration setting, speed and altitude. The corrections were determined by comparison of data obtained from the NLR Metro research aircraft and data obtained from the Cessna Citation aircraft. The measurements were executed during formation flights of the two aircraft. Hereby the Metro functioned as a pacer equipped with a tail cone for static pressure and a special pitot tube for impact pressure measurements.

3. Flight Test Programme

The flight test programme was drafted with two different objectives in mind:

A. Test flights to obtain data for the evaluation of the mathematical flight simulation model.
B. Test flights in order to fulfill a number of requirements of the simulator manufacturer and the FAA. These are the already mentioned ATG and POM requirements.

Five topics had to be covered by the flight test programme with respect to the mathematical modelling viz.:

1. Aerodynamics
2. Engine dynamics
3. Flight control system
4. Aircraft performance and handling on the ground
5. Flight deck cues, such as the levels of sound, vibration and buffeting present in certain conditions.

Obviously, a comprehensive programme would be necessary to acquire the data for the modelling of the topics mentioned under label 1 to 4. The only way to perform this challenging task successfully within the limited time available to execute the flight tests, was the ample use of dynamic flight test techniques in combination with a high accuracy instrumentation system. These new techniques comprising measurements in quasi-steady and non-stationary flight (NSM) have been developed by DUT and NLR to reduce the valuable test time while maintaining the same fidelity of the results (Ref. 3).

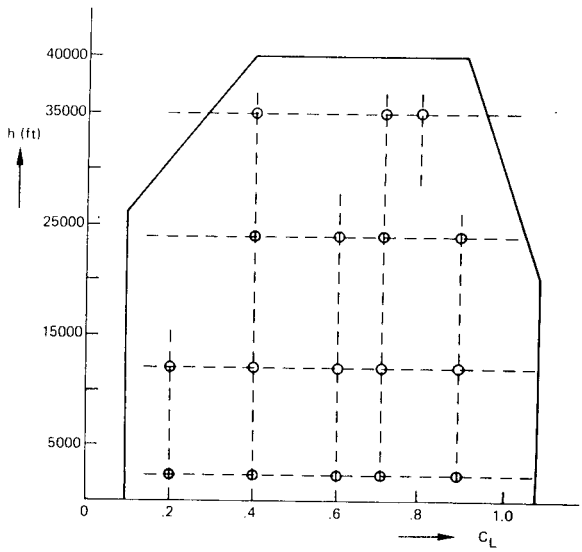

Fig. 5 Testpoints within flight envelope

Taking into account the configuration considered a grid of altitudes and speeds was placed upon the flight envelope of interest (Ref. 4). This is schematically shown in figure 5. This resulted in a set of testpoints, labelled by a particular configuration, centre of mass, altitude and lift coefficient, at which a train of specific manoeuvres was executed. This train of manoeuvres tailored to the various objectives (performance, stability and control, FCS, etc.) is described hereafter. The sequence of the manoeuvres lasted not more than 13 minutes per testpoint. Per altitude a maximum of 5 testpoints was selected at more or less equal angle of attack interspaces.

The tests for the aerodynamic modelling can be split up into three parts. Measurements are required with respect to:

1. Performance model
2. Stability and control model
3. Stall, ground effect and buffet model.

As already has been mentioned the train of manoeuvres contains manoeuvres useful for the determination of the performance model. This performance model can be split up in a symmetric

and asymmetric part. The latter comprises mainly steady flight conditions in which a sideslip angle is present. The following "manoeuvres" can be distinguished:

1. Quasi-steady rectilinear horizontal reference conditions of the test points and the angle of attack excursions of the dynamic manoeuvres, that are initiated from these conditions.

2. Quasi-stationary flight conditions, during which for each axis separately the appropriate trim tab deflection slowly is increased and decreased. At the same time the steady reference condition in maintained by means of the corresponding elevator, aileron or rudder deflection. The manoeuvre lasts as long as the control forces are considered acceptable to the pilot. In fact here an exchange between trim tab and control effectivity takes place.

3. Asymmetric quasi-stationary manoeuvres. These are nominally rectilinear sideslipping flights with "relatively slowly" varying slip angle, roll angle and heading. Positive and negative slip angle excursions are required.

4. Quasi-steady wind-up turn manoeuvre. In nominally horizontal flight and constant airspeed the roll angle is slowly increased and decreased to approximately 60°. Both left and right turns are executed.

When both the longitudinal and lateral performance models are available, the "performance" envelope of the aircraft has been covered. This means, that each steady state condition within the flight envelope, characterized by configuration, centre of mass, speed and altitude can be computed including the required angle of attack, sideslip angle, thrust-setting and trim deflections for moment control. However, in this model no terms are present yet, describing the aerodynamic effects, when deviations are made from this performance model. In particular these deviations determine the flying qualitites of the aircraft.

Therefore it is necessary to add terms in the longitudinal and lateral performance models, so that the stability and control characteristics are described accurately for the flight envelope of interest. This results in the addition of coefficients to the force and moment coefficients. The force models in this aspect are less critical than the moment models, because it is a well-known fact, that these determine to a large extent the flying qualitites. In order to be able to evaluate this part of the mathematical model the following manoeuvres were selected.

1. Symmetric non-stationary manoeuvres. Hereby the aircraft was excited manually by means of rectangular shaped elevator doublets, varying in amplitude and time.
2. Asymmetric non-stationary manoeuvres. Also here rectangular shaped aileron or rudder doublets, manually applied, were used, varying in amplitude and time.

The arguments to use these type of inputs rather than more "optimal" inputs were of a practical nature. Firstly the aircraft has no automatic flight control system, which could be used to implement these optimal signals. Furthermore because of the tight time schedule it would not be possible to tailor these signals throughout the flight envelope. Also budget constraints excluded the installation of special equipment, which could artificially manipulate the controls. Because the inputs had to be performed manually and several pilots participated in the flight test programme, it was decided, that only a rather simple input signal was suitable. The block type input was chosen because it is capable of exciting the aircraft over a rather large frequency range.

Ground effect measurements were executed for three configuration settings with landing gear down. For a number of preselected heights varying from 2 to 10 m above the ground rectilinear flights were executed at constant airspeed and height. During the run small excitations were evoked by means of elevator, aileron and rudder. Both the steady parts of the runs and the excitations can be used to evaluate the ground effect.

Both static and dynamic effects can be represented as increments models e.g. as a function of height above the ground superimposed on the coefficients valid for free flight. In the flight test programme also landings were included in which the final parts of the landing could be used for the evaluation of the ground effect. Therefore the aircraft was landed hands-off (as far as possible) at a number of configuration settings and at various constant sink rates.

Stalls were performed for four different configurations at approximately 12000 ft using different entry techniques.

Because it is not a Phase II requirement, no specific tests were planned to determine buffet phenomena. However, during stall and manoeuvres, in particular during some of the elevator doublets with large amplitude, these effects were encountered and logged on the test cards.

One test flight was dedicated to special tests with respect to the engine dynamic responses. The tests included throttle chops at several altitudes and speeds, throttle slams from idle to maximum continuous, small throttle steps, in-flight engine shut-downs and starts at several points in the flight envelope. Finally also constant power ratings were recorded on the ground and video recordings of the engine instruments were made of the engine start-up on the ground.

For the evaluation of the flight control model no specific manoeuvres were planned, because during all manoeuvres performed for aerodynamic modelling also the control forces and control wheel and pedal displacements were recorded. However, on the ground at rest control column and wheel sweeps have been performed. These measurements give information with respect to the dynamics of the control system. The flight recordings mainly provide the necessary information for the determination of the hinge moments.

Besides tests performed in the air also tests were executed on the ground in order to analyse the undercarriage dynamics. Apart from the use of the ground rolls of take-off and landing for this, also special taxi trials have been done incorporating turns at different speeds and turn rates as well as left/right braking exercises. Finally shock absorber deflections were measured during static tests under various mass and fuel distributions.

For the ATG flight test programme, reference 5 was used as a guide from which the flights were grouped and the test cards drafted. Reference 5 specifies a complete set of manoeuvres over the flight envelope of interest, including how the manoeuvre has to be performed, the conditions and configurations for which the test is required and finally the parameters that have to be recorded.

With the aid of this information the various tests were grouped as optimal as possible within a number of ATG flights. In principle the instrumentation system allowed the recording of parameters from engine start-up until engine shut-down. By this it was possible to perform take-offs, in-flight tests, landings and taxi trials in one test flight lasting no more than approximately two hours.

4. Data Processing

The procedure of the data processing is schematically indicated in figure 6.

After the test flight the tape and additional documentation is transported to the data processing facility of NLR (DVSV). If necessary quick-look plots can be generated within less than twelve hours after the flight, so that it is possible to check on a short term basis if all instrumentation systems have functioned correctly. At DVSV the data is converted to physical equivalents of the measured signals, including the calibrations required. Furthermore additional parameters are computed based on physical relationships between measured variables.

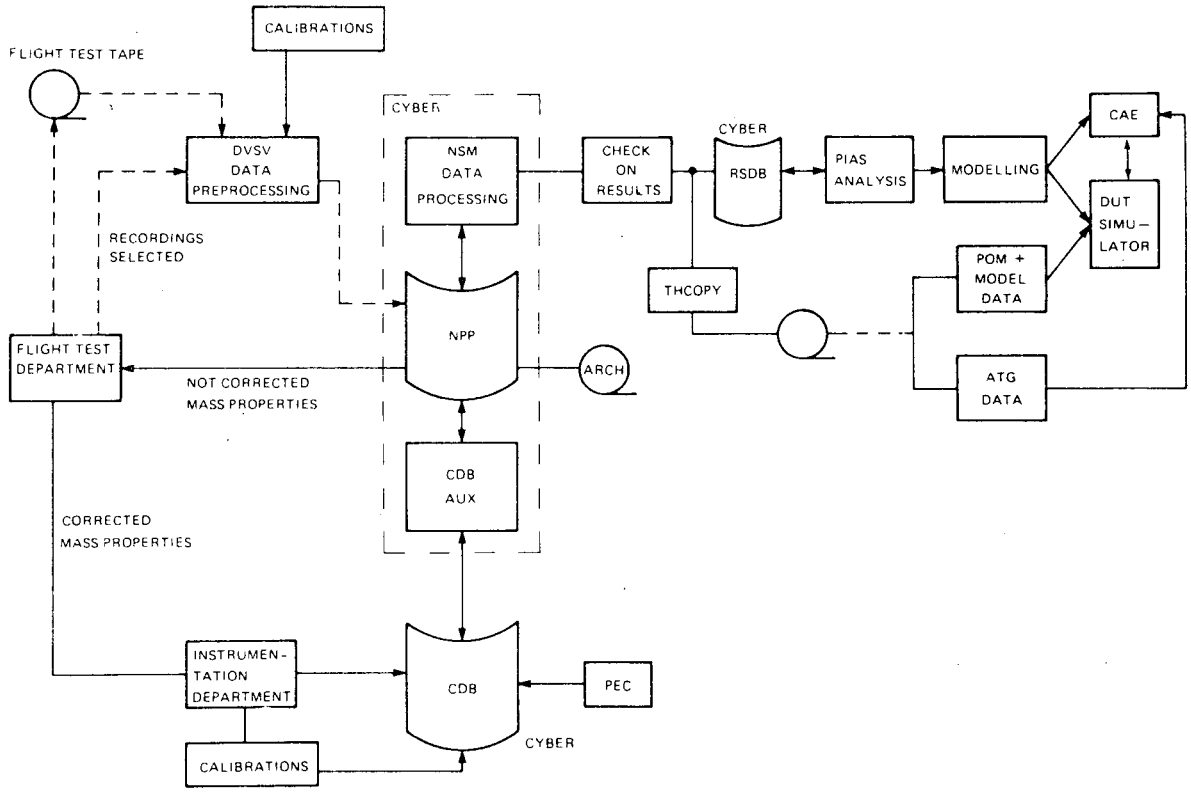

Fig. 6 Data processing of Citation flight test programme

After this all parameters as a function of time are sent to a database in the central computer (Control Data Cyber 170-855) of NLR. This database forms the backbone of the NLR Post-processing Process (NPP), which is a part of the NLR Measurement, Recording and Processing System (MRVS).

In the dataprocessing it is necessary to know the instanteneous gross weight, centre of mass position and the inertias during a particular test flight. In order to compute these parameters as a function of time the recorded fuel quantities and recording times are required. Therefore these data are taken from the database and handed to the flight test department. Here the required parameters are calculated as a function of time, based on the mass properties model, that was developed. Then these corrected auxiliary data are included in the so-called Central Data Base (CDB), which also contains the data with respect to instrumentation including PEC. In the CDB also physical constants and geometric aircraft data are stored.

The information in the CDB can be transmitted to the NPP database through a procedure called CDBAUX. Because in the CDB data can be present applicable to more than one aircraft and instrumentation systems this procedure is attached uniquely to a particular aircraft, flight and recording.

At this point all required information is available to start up the so-called NSM data processing sequence. In the NSM data processing four important submodels can be distinguished:

1. COR
2. FPR
3. CAP
4. PPM.

In module CORrection the following actions are performed:

1. All data are accurately synchronized to the same time grid.
2. Because motion about the centre of mass is considered, transformations are performed to the actual centre of mass for measurements obtained from vanes, pressure transducers and accelerometers, which are situated at various places in the aircraft.
3. The pressure measurements are corrected for time lags in the tubes.
4. The position error correction (PEC) is applied.
5. Sensor calibrations are applied to the vanes.

Per recording in module FPR (Flight Path Reconstruction), the trajectory of the mass centre through the air during steady, quasi-steady and unsteady motion is reconstructed. This process is based upon the use of the flight test measurements, both inertial and with respect to the local atmosphere (air data system), and the kinematic equations of motion governing the rigid body modes.

For steady conditions the determination of the flight path is rather simple and straightforward, because a number of time dependent variables are eliminated in the equations of motion. However, in quasi-steady and unsteady conditions the flight-path reconstruction is more complicated.

The variable which is crucial in this respect is the angle of attack, which can be measured accurately in steady conditions by means of a vane. Due to upwash of the flow, rotations of the aircraft, elastic deformations and the dynamics of the vane itself, this method is not suitable for the other conditions. Consequently an alternative manner had to be found.

The flight path of an aircraft can be described mathematically by the force equations of motion with respect to an inertial frame. Only three equations describing the translations of the mass centre are required.

Expressed in body axes the force equation can be represented in matrix form as:

$$[\vec{a}]^B_{mc} = \frac{[\vec{f}]^B}{m} = [\vec{A}]^B_{mc} - [\vec{g}]^B \qquad (4.1)$$

in which:

$[\vec{a}]^B_{mc}$: specific forces as measured by accelerometers attached to the body axes frame.

$[\vec{f}]^B_B$: aerodynamic and propulsive forces expressed in body axes.

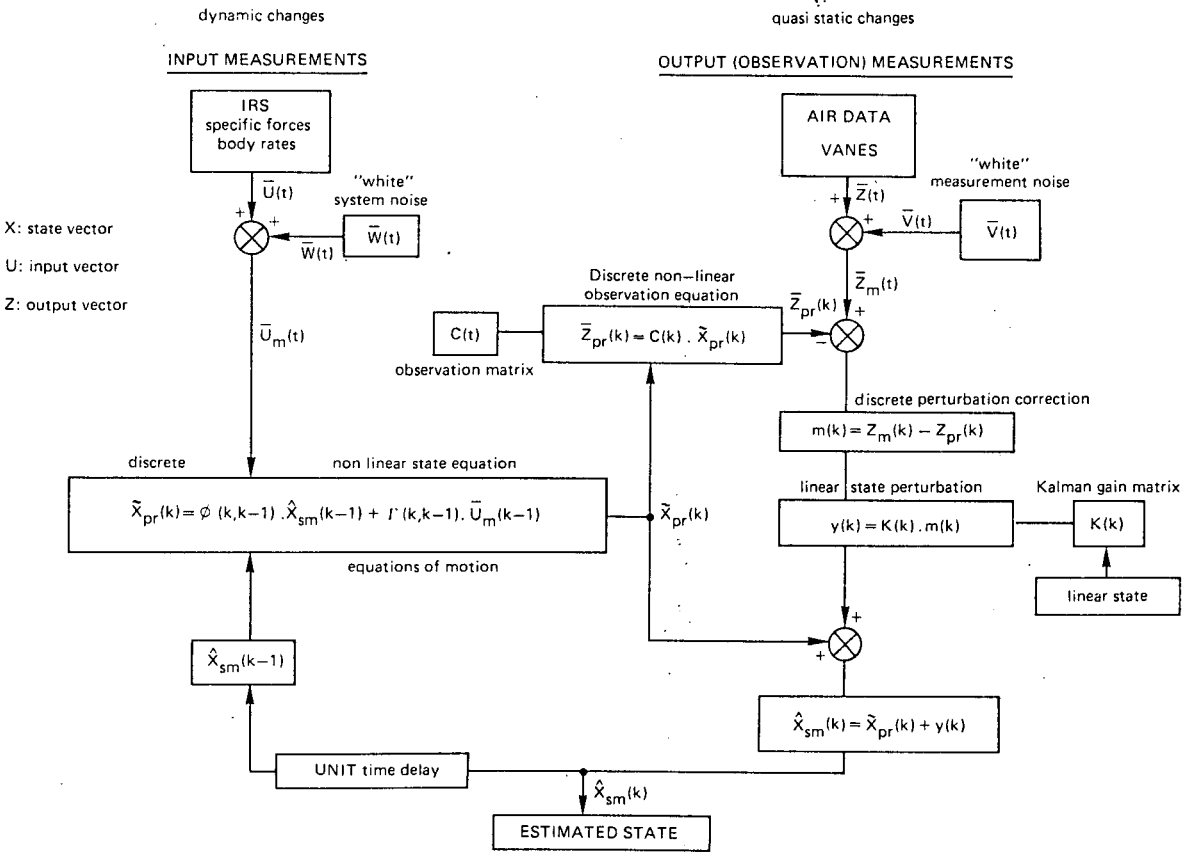

Fig. 7 Kalman filtering in NLR fligh test data processing

$[\vec{A}]^B_{mc}$: kinematical acceleration vector of the mass centre.

$[\vec{g}]^B$: acceleration vector due to gravity along the body axes.

$[\vec{A}]^B_{mc}$ consists of the kinematical accelerations along the body axes.
Expression (4.1) represents a non-linear set of differential equations with respect to time, which in principle can be integrated when either the specific forces and angular velocities or the aerodynamic and propulsive forces are known.
The flight path reconstruction in the data processing in fact is based on the integration of (4.1) (state) employing the measured time histories of the specific forces, angular rates, airspeed and the height. A schematic view is presented in figure 7. The specific forces and angular rates directly result from the inertial measurement unit (input measurements), whereas the air velocity and height increment or decrement can be derived from the air data measurement system (output measurements).

However, the measurements are corrupted with errors and the exact initial conditions necessary for the start of the integration are not known. Therefore, statistical procedures are required to attenuate the effects of these errors on the time histories of the state variables. In the data processing of the flight tests the well-known Kalman filtering and smoothing technique is employed (Ref. 6).

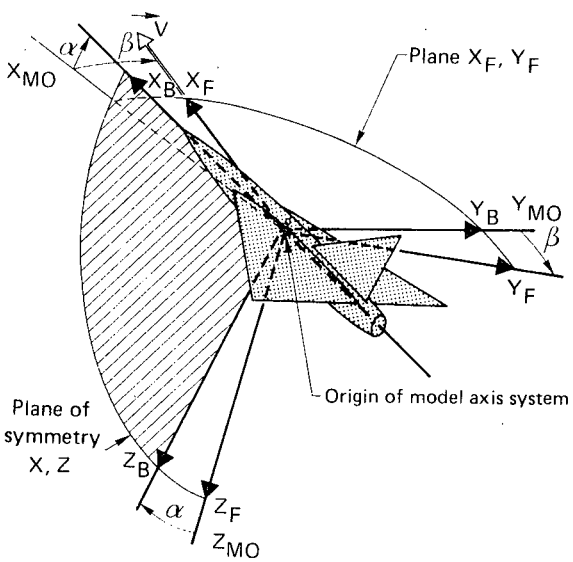

Body axis system (X_B, Y_B, Z_B)
Flight-path system (X_F, Y_F, Z_F)
Model axes system (X_{MO}, Y_{MO}, Z_{MO})

Fig. 8 Model axes reference frame

In the flight path reconstruction the most important quantities to be reconstructed are the air velocities u, v and w along the body axes and the Euler angles Θ, φ and ψ. Actual distances are not important in this respect. From the reconstructed velocities the angle of attack and side slip angle can be derived.

As a result of module FPR smooth time histories are obtained of the state variables, which are included in the NPP database.

In module CAP (Calculation of Aerodynamic Parameters) results of COR and FPR are used to compute additional parameters, which are necessary for the identification of the mathematical models. Amongst these are the dynamic pressure, Mach number and time derivatives of angle of attack and slip angle. Furthermore dimensionless specific forces and moment coefficients are computed. Finally the dimensionless specific forces are transformed to the so-called model axes frame (Fig. 8) and the moment coefficients are reduced to a reference centre of mass position. The results of CAP are added to the NPP database.

In module PPM (Power Plant Model) the static engine thrust is determined from measured engine parameters, such as fan speed and Mach and atmospheric measurements such as static air temperature and static pressure. A performance deck valid for the JT 15D-1 turbo fan was available developed by the engine manufacturer (Pratt & Whitney) based on test data. Both gross thrust and ram drag are computed in this programme as a function of compressor speed an Mach.

Finally the gross thrust and ram drag are also transformed to the model axes frame, so that lift, drag and other dynamic coefficients can be derived.

After this two possibilities for further processing were present. If data had to be processed for POM purposes and/or, for the identification of the FCS and gear models, they were converted to another tape format (THCOPY) suitable for implementation on the computer of DUT. After this the data was written to magnetic tape and transported to DUT. However, if data was required for the evaluation of the aerodynamic and thrust models the data was written to the so-called Result Storage Data Base (RSDB) for further analysis with the module PIAS (Processing of dynamic manoeuvre measurements with an Interactive Adaptive System).

The ATG data, consisting of time histories of selected parameters, were processed in the same way as the modelling data and transported to the simulator manufacturer according to the same procedure as the model/POM data transport to DUT.

When the NSM data processing for a particular recording is finished and the results stored in the RSDB all time histories for the aerodynamic modelling are present, viz.:
1. The aerodynamic coefficients
2. The state variables
3. The control and trim tab angles.

With respect to the FCS and undercarriage modelling, also time histories are available of the control forces and displacements, shock absorber deflections and nosewheel steering angle.

At the PIAS analysis stage the coefficients appearing in a postulated submodel structure, representative for the description of the aerodynamics in the various test points, are estimated by means of an equation error technique.

The regression algorithm is based upon the theory of the solution of linear least squares (Ref. 7).

In this procedure (so-called two step method) during the first step, which is mathematically the most complex part, the state of the aircraft is reconstructed as a function of time expressed in characteristic flight mechanical variables. Hereby the aerodynamics are not used to compute these variables. The flight path reconstruction has to be performed once for a particular recording.

The parameters of the aerodynamic models are estimated in the second step of the procedure, which is mathematically rather straightforward. Thus the separation of the trajectory reconstruction and the parameter identification process makes it possible to select and evaluate models in a flexible way. Hereby use is made to a great extent of both computer plotting and "batch" processing.

Finally in the modelling phase the submodel coefficients as a result of the PIAS analysis of the flown test points are integrated into a complete model. This final model then is converted to tables, suitable for implementation in the simulation programme at DUT. The complete model and corresponding data are also sent to the simulator manufacturer for implementation on the actual Citation 500 flight simulator.

5. Data analysis and modelling

To gain insight in a preliminary stage it was decided to build an a priori model of the Citation 500, based on the available wind tunnel and flight test information, completed with data of comparable aircraft and engineering judgement. At that stage it was not clear, which terms within the models were relevant for the Citation 500. Therefore rather comprehensive models were developed, including all kinds of non-linearities and dependencies on the aircraft state. Also from a software managing point of view it was thought a better philosophy to develop this comprehensive model in advance where time was less restrictive than during the rather short period available for analysis and modelling.

If particular parts of the model appeared to be insignificant or could not be identified from the test data, it would be much more simple to set the corresponding coefficients to zero instead of expanding the model by means of software changes.

The a priori models were implemented on the Gould/Sel computer of the moving base flight simulator operated by the Stability and Control Group of the Department of Aerospace Engineering of DUT. As a result a complete a priori model for the Citation 500 was available preceding the flight test programme.

After integration of the model within the simulation software and off-line testing, it was possible to fly an "a priori" Citation on-line with the pilot in the loop.

Although, in principle, no on-line simulation is required for the models and data, it was considered as a very valuable option both for the a priori, and final models. In case of the a priori model confidence could already be built up with respect to the flyability and/or functioning of the various models. Furthermore pilots can be familiarized more easily with the manoeuvres that are planned in the test flights.

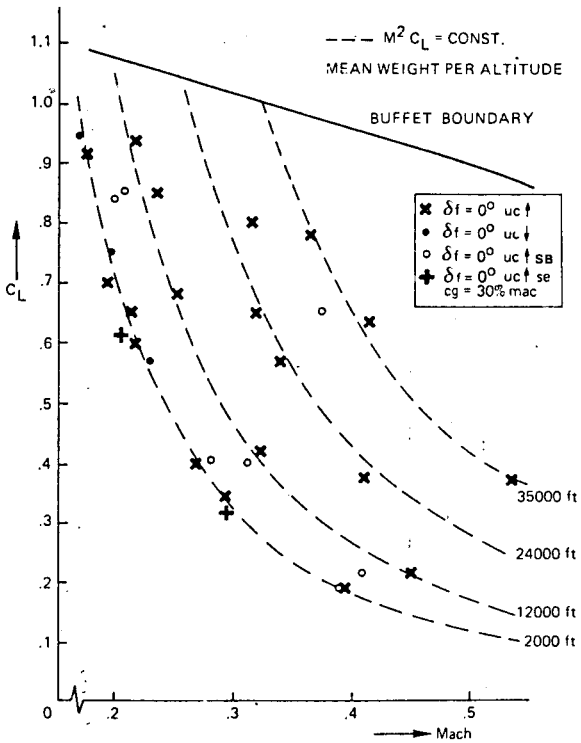

Fig. 9 Testpoints for δ_f=0 as a function of altitude

At the start of the analysis it was decided to concentrate at first on the quasi-stationary horizontal symmetrical reference conditions of the test points and the corresponding dynamic manoeuvres, both for the evaluation of the performance model and the additional stability and control parts. In figure 9 for the zero flap configuration, the test points are indicated in a lift coefficient versus Mach plot. As a reference also plotted herein are $M^2C_L \div W/\delta$ curves at four test altitudes. The weight appearing in this formula is chosen to represent the mean value of the test weights at that altitude.

Applicable to the reference mass centre (30% mac) in figure 9 the test points are indicated for the clean configuration (19 pts), configuration with flaps up and gear down (3 pts) and the configuration with flaps up, gear up and speedbrakes extended (7 pts).

Because in flight the inertial sensors always measure the simultaneous effects of the aerodynamics and thrust, there is always the issue, which effects must be contributed to thrust and which to drag. As already has been mentioned in section 4 for this project it was assumed, that the thrust could be computed with sufficient accuracy by means of a performance deck valid for the Pratt and Whitney turbofan. The input for this curve reading programme are measured parameters of which the fan speed is the most direct variable.

As a result, in the data processing the aerodynamic parts transformed to the model axes system (Fig. 8) can be isolated from the measurements. The aerodynamic model is described in the model axes frame, because this corresponds to the

way windtunnel measurements are performed. Partly as a result of this, the aerodynamic models used in simulation programmes are expressed also in this frame.

The static performance thrust model used in the flight test data processing also is implemented in the simulation software. The rationale behind this is, that the simulation process more or less can be considered as the inverse of the NSM data processing (Ref. 8). The integration of the equations of motion incorporating the sum of the outputs of the aerodynamic and thrust model, theoretically must lead to the same flight path as in actual flight. By this construction it was attempted to enhance the correlation between simulation and flight.

For the test points involved a submodel was postulated for the three force and three moment coefficients. These submodels are valid for and around the reference condition and can be described as follows:

1. Longitudinal submodel structure

$$C_{D_{MO}} = C_{D_0} + C_{D_\alpha}\cdot\alpha + C_{D_{\alpha^2}}\cdot\alpha^2 + C_{D_{q_{MO}}}\cdot\frac{q_{MO}\cdot\bar{c}}{V} + C_{D_{\delta_e}}\cdot\delta_e + C_{D_{\beta^2}}\cdot\beta^2$$

$$C_{L_{MO}} = C_{L_0} + C_{L_\alpha}\cdot\alpha + C_{L_{\alpha^2}}\cdot\alpha^2 + C_{L_{q_{MO}}}\cdot\frac{q_{MO}\cdot\bar{c}}{V} + C_{L_{\delta_e}}\cdot\delta_e \qquad (5.1)$$

$$C_{m_{MO}} = C_{m_0} + C_{m_\alpha}\cdot\alpha + C_{m_{\alpha^2}}\cdot\alpha^2 + C_{m_{q_{MO}}}\cdot\frac{q_{MO}\cdot\bar{c}}{V} + C_{m_{\delta_e}}\cdot\delta_e + C_{m_{\beta^2}}\cdot\beta^2 + C_{m_{\delta_{r^2}}}\cdot\delta_r^2 + C_{m_{\delta_{e_t}}}\cdot\delta_{e_t}$$

2. Lateral submodel structure

$$C_{y_{MO}} = C_{y_o} + C_{y_\beta}\cdot\beta + C_{y_{p_{MO}}}\cdot\frac{p_{MO}\cdot b}{2V} + C_{y_{r_{MO}}}\cdot\frac{r_{MO}\cdot b}{2V} + C_{y_{\delta_r}}\cdot\delta_r$$

$$C_{\ell_{MO}} = C_{\ell_o} + C_{\ell_\beta}\cdot\beta + C_{\ell_{p_{MO}}}\cdot\frac{p_{MO}\cdot b}{2V} + C_{\ell_{r_{MO}}}\cdot\frac{r_{MO}\cdot b}{2V} + C_{\ell_{\delta_r}}\cdot\delta_r + C_{\ell_{\delta_a}}\cdot\delta_a + C_{\ell_{\delta_{a_t}}}\cdot\delta_{a_t} \qquad (5.2)$$

$$C_{n_{MO}} = C_{n_o} + C_{n_\beta}\cdot\beta + C_{n_{p_{MO}}}\cdot\frac{p_{MO}\cdot b}{2V} + C_{n_{r_{MO}}}\cdot\frac{r_{MO}\cdot b}{2V} + C_{n_{\delta_r}}\cdot\delta_r + C_{n_{\delta_r}}\cdot\delta_r + C_{n_{\delta_{r_t}}}\cdot\delta_{r_t}$$

These submodels are valid within the normal flight envelope. Stall phenomena, buffeting, ground effects etc. are not represented by this formulation.

The mathematical model as postulated by (5.1) is based on the type of aircraft, that is investigated and the experience, which parameters can be identified accurately within a chosen model structure.

The Cessna Citation 500, a small executive jet transport, has a straight, tapered wing optimized for the low speed flight regime. The maximum speed in horizontal flight is approximately .62 Mach. Because of the size of the aircraft, the speed regime of interest and the objective of the mathematical model, it was assumed, that the aircraft could be considered as rigid.

The aircraft has a fixed tailplane setting with an elevator used both for trimming and manoeuvring. Control forces existing at a selected steady condition can be eliminated by means of a small trim tab in the right elevator surface. In a steady rectilinear symmetric flight, which usually is present, the lateral coefficients are zero. Therefore the aerodynamic coefficients representing the longitudinal performance model can be described by:

$$C_{D_{MO}} = C_{D_0} + C_{D_\alpha}\cdot\alpha_{tr} + C_{D_{\alpha^2}}\,\alpha_{tr}^2 + C_{D_{\delta_e}}\cdot\delta_{e_{tr}}$$

$$C_{L_{MO}} = C_{L_0} + C_{L_\alpha}\cdot\alpha_{tr} + C_{L_{\alpha^2}}\,\alpha_{tr}^2 + C_{L_{\delta_e}}\cdot\delta_{e_{tr}}$$

$$C_{m_{MO}} = C_{m_0} + C_{m_\alpha}\cdot\alpha_{tr} + C_{m_{\alpha^2}}\,\alpha_{tr}^2 + C_{m_{\delta_e}}\cdot\delta_{e_{tr}} + C_{m_{\delta_{e_t}}}\cdot\delta_{tr} \qquad (5.3)$$

Herein the subscript tr indicates the angle of attack, elevator angle and trim tab angle at the reference condition of a particular test point. It is assumed, that the effects of the trim tab on lift and drag are small enough to be neglected. The above described equation models are written as a linear function of α, α^2, δ_e and δ_{tr}. It is well-known, that the drag coefficient usually can be represented by a quadratic function of angle of attack. Because of the wing shape and flaps employed on the Citation 500 it is expected that the lift and pitching moment coefficient exhibit a linear relation with respect to angle of attack for a large part of the angle of attack range. However, at high angles and higher Mach numbers quadratic terms may be required also.

Frequently windtunnel measurements are executed as a function of angle of attack, whereby the trim and control deflections are equal to zero. If the same is done in (5.3), omitting the $\delta_{e_{tr}}$ and δ_{tr} contributions, this will lead to the same representation.
In this context it must be mentioned, that only the "geometric" contributions of thrust are accounted for in C_D and C_L. Aerodynamic effects due to thrust are assumed to be negligible on C_L and C_D. The rationale behind this is the fact, that the powerplant is a jet engine. Furthermore the position of the engines on the aircraft is such, that no large impact on C_L and C_D can be expected. For the contribution of the thrust on

the pitching moment a somewhat different philosophy is followed. Hereby it is assumed, that the geometric and aerodynamic effects are such, that they more or less are balanced. This conclusion was derived from analyses of flight test data in which throttle transients were present. If no aerodynamic effects due to thrust would be present (thus only thrust x arm) manipulations of the throttles would lead to a step response particular noticable in the angle of attack. However, this trend could not be found consistently in the timehistories of the flight test data. The thrust arm affecting the pitching moment is such, that an increase in power results in a nose down moment, However, augmenting thrust leads to a higher nozzle velocity and consequently to the phenomenon of jet entrainment. Hereby the surrounding air is affected by the jet in such a way, that the downwash is enforced at the horizontal tailplane leading to a decrease of tailplane angle of attack and this in a reduction of tailplane lift. This results in a pitch up moment opposite to the nose down geometric moment. Therefore in the mathematical model it is assumed, that the effective thrust arm is equal to zero.

As has been indicated in section 3, 5 à 6 testpoints at an approximately constant altitude were chosen.

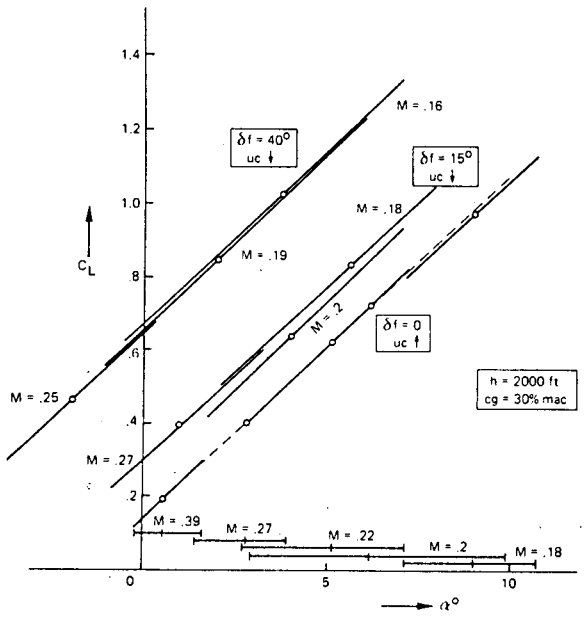

Fig. 10 C_L-α curves following from submodels for various flap settings

As an example in figure 10 it is indicated for C_L how these points are located as a function of angle of attack. Because the testpoints are flown at different airspeeds possible (Mach) speed effects are embedded. In the figure apart from the reference conditions also the α-sweeps are shown as result of the elevator doublets. In accordance with windtunnel presentations the control and trim tab deflections are set equal to zero, just as the dynamic effects due to pitch rate, so that only the angle of attack terms remain, now valid for the angle of attack range, covered by the manoeuvre.

Thus the α-sweeps as shown in figure 10 are described by the following equations and are valid around α_{tr}:

$$C_{D_{MO}} = C_{D_0} + C_{D_\alpha}\cdot\alpha + C_{D_{\alpha^2}}\cdot\alpha^2$$

$$C_{L_{MO}} = C_{L_0} + C_{L_\alpha}\cdot\alpha + C_{L_{\alpha^2}}\cdot\alpha^2 \qquad (5.4)$$

$$C_{m_{MO}} = C_{m_0} + C_{m_\alpha}\cdot\alpha + C_{m_{\alpha^2}}\cdot\alpha^2$$

The integration of the various submodels will be described hereafter. As an example here the lift coefficient is discussed. However, the same philosophy applies for the drag and pitching moment coefficient.

From the equilibrium condition in horizontal flight it follows:

$$W = C_L\cdot q_c\cdot S \approx C_{L_\alpha}(\alpha-\alpha_o)\cdot q_c\cdot S \qquad (5.5)$$

showing, that for constant values of C_{L_α}, α_o and airplane weight the dynamic pressure is the same at constant angle of attack. In other words for constant EAS the angle of attack is the same at each altitude. Obviously the weight during the testflights varied. As a result of this and the fact, that C_{L_α} and α_o variations may occur, lines of constant α do not coincide with all testpoints flown at that particular EAS. Now the assumption is made, that the submodel also is able to represent steady reference conditions deviating from the actual testpoint. These deviations, however, must be relatively small, otherwise a reduction to a particular steady state must take place. Then from a plot as given in figure 11 (in the analysis all available submodels have been used) for a number of constant angle of attack lines the lift coefficients can be plotted as a function of Mach. Using least-squares techniques this results in a family of curves of constant α as a function of Mach.

From this set of curves again C_L-α plots can be constructed for a set of constant Mach numbers. As can be noticed from figure 11 because of the low subsonic range the variation due to Mach is relatively small.
In this way plots are obtained, which are comparable to windtunnel results. Because here, in contrast to flight, Mach and angle of attack are not coupled kinematically to each other, measurements can be performed in which the Mach number remains constant during α-variations directly.

In the same way as described here the submodels for the drag and pitching moment coefficients are integrated.

For all configurations of interest in the same way as described the coefficients in the submodels are determined by means of regression analysis and integrated to $C_L(M)$-α, $C_D(M)$-α and $C_m(M)$-α plots. In total six sets are constructed for the flight envelope of interest, viz.:

1. clean uc↑
2. clean uc↑ speedbrakes extended
3. clean uc↓
4. 15° flaps uc↑
5. 15° flaps uc↓
6. 40° flaps uc↓

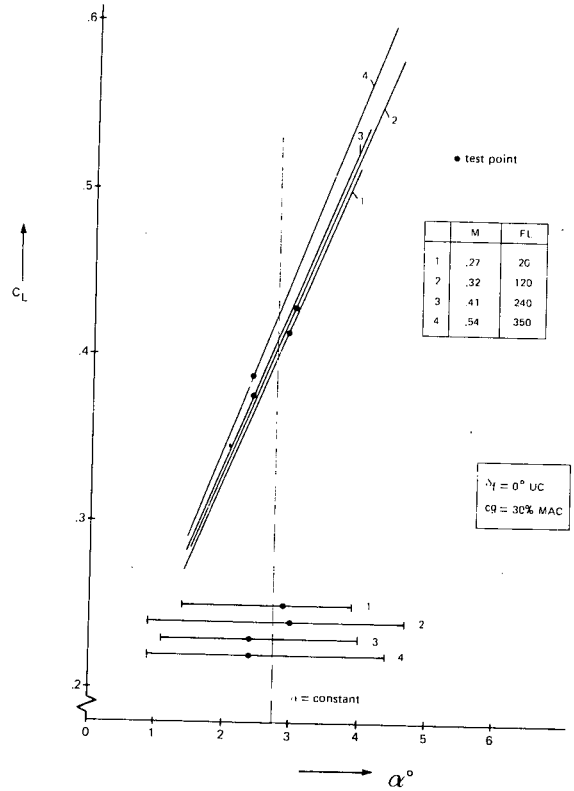

Fig. 11 C_L-α submodels as function of altitude

Set 1 (clean, uc†) was considered as a base model, which consistently was subtracted from the other sets. By this, effects due to flap manipulations, gear extension/retraction and speedbrake operation could be modelled as incremental contributions, which are superimposed on the base models of C_L, C_D and C_m.

The base model and increment families of curves are modelled as a function of angle of attack. This would allow a rather easy integration of the stall and ground effect submodels.

Finally the models are digitized and converted to tables. It appeared, that the structure of the a priori model was such, that these tables directly could be implemented in the software, employing table look-up techniques.

The coefficients in the C_L, C_D and C_m submodels, that effect stability and control primarily are the terms with respect to angle of attack and elevator. However, also the pitch rate coefficients are very important. Frequently also coefficients are modelled, that represent the non-stationary behaviour of the flow over the wings, which in stability and control considerations usually is represented by the quasi-steady $C_{L_{\dot\alpha}}$, $C_{D_{\dot\alpha}}$ and $C_{m_{\dot\alpha}}$ coefficients of which the latter is the most relevant.

Because in the identification process use is made of regression techniques and the fact, that a strong correlation exists between pitch rate and $\dot\alpha$ coefficients, an accurate identification of both parameters directly is very difficult. For this project it was decided to identify the effect of $\dot\alpha$ and q_B simultaneously in one pitch rate coefficient, so that the $\dot\alpha$ effects, although in principle quite different from nature than the pitch rate effects, are embedded. It is well known, that both pitch rate and $\dot\alpha$ have a large impact in the damping (for which the sum of C_{m_q} and $C_{m_{\dot\alpha}}$ is required) and frequency of the short period mode. In particular this applies to the C_{m_q} and C_{L_q} coefficients.

Also for these parameters,as a result of the data processing, a large set of data was obtained valid for the test points. In accordance with the performance model and for simulation purposes these coefficients were formulated as a function of angle of attack. Hereby again the clean configuration was considered as a base model on which effects due to configurations changes were superimposed. Then the plots of these models were digitized to numerical tables and implemented in the existing aeromodel structure. Also for these coefficients only minor modifications were required in the structure of the a priori aerodynamic model.

In contrast to the longitudinal model no "performance" model was considered for the lateral aerodynamic model. As a result of this only flight test data were analysed yielding responses to aileron and rudder doublets.

As can be noticed from (5.2) the aerodynamic coefficients are written as a linear function of sideslip, dimensionless roll and yaw rate and the control deflections. This formulation frequently is postulated, when describing the lateral aerodynamics about a steady state reference condition.

It is assumed, that $\dot\beta$-effects are embedded in the yaw rate coefficients for the same reasons as have been mentioned for the $\dot\alpha$-pitch rate terms.

Furthermore it is assumed, that thrust has no effects on the aerodynamic coefficients and no "geometric" corrections as for the longitudinal model are necessary. This implies, that time histories from the flight path reconstruction directly can be used for identification of the coefficients appearing in the submodels. This was done in the same way as for the longitudinal model by means of regression analyses for each test point indicated in figure 9. After this the resulting data were integrated into a complete model valid for the flight envelope of interest. Hereby also for the complete model the linear structure, as postulated for the submodel, was maintained. However, the aerodynamic parameters are modelled in the same way as has been done for the longitudinal model viz. as a function of angle of attack, incorporating effects due to Mach and configuration changes.

The implementation of the complete lateral model within the a priori model structure did not give rise to any difficulties. In fact it appeared that the final model was more simple than adopted in the a priori model.

6. POM Results

As already has been indicated in section 4 the ATG and POM flight test data have been processed in the same way as the test data for the mathematical modelling. After the NSM data processing, the ATG data were not further processed

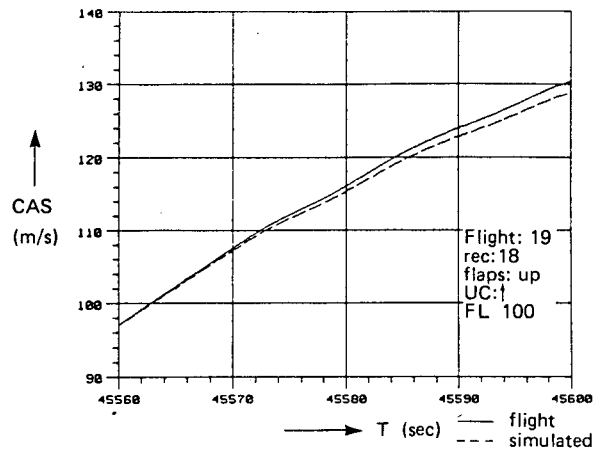

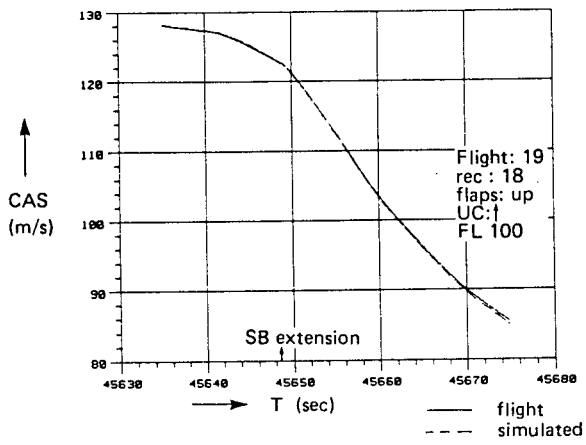

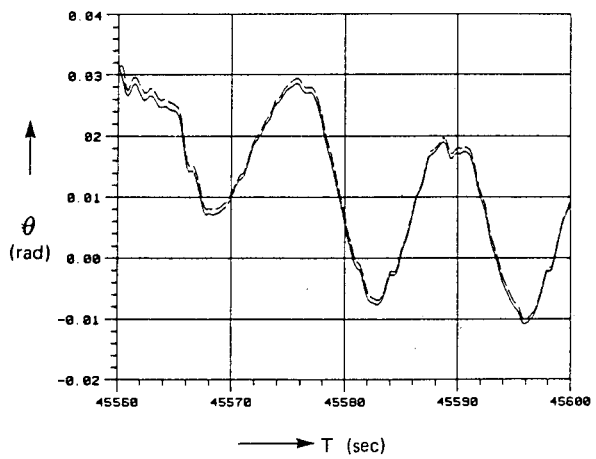

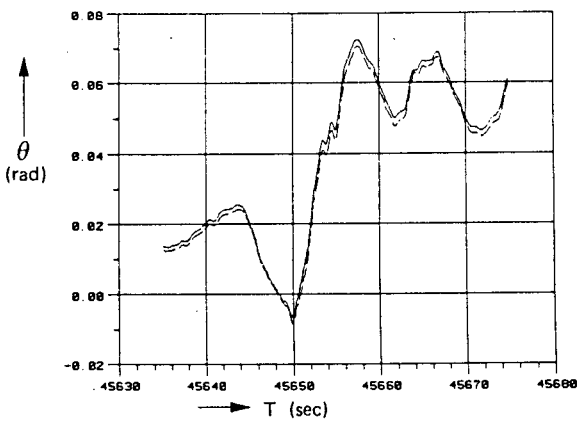

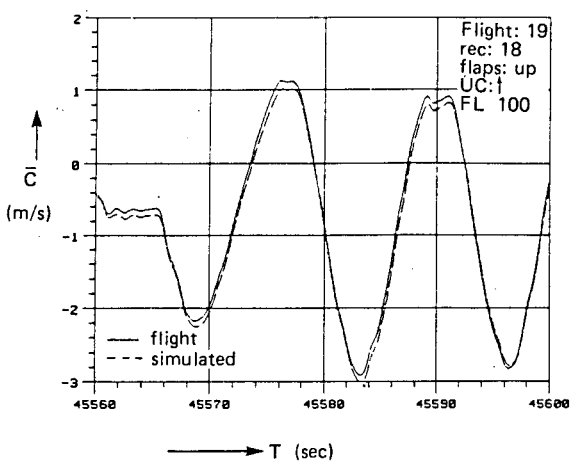

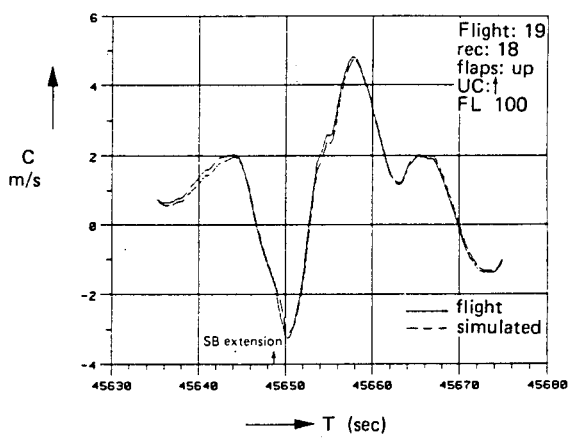

Fig. 12 Level flight acceleration

Fig. 13 Level flight deceleration

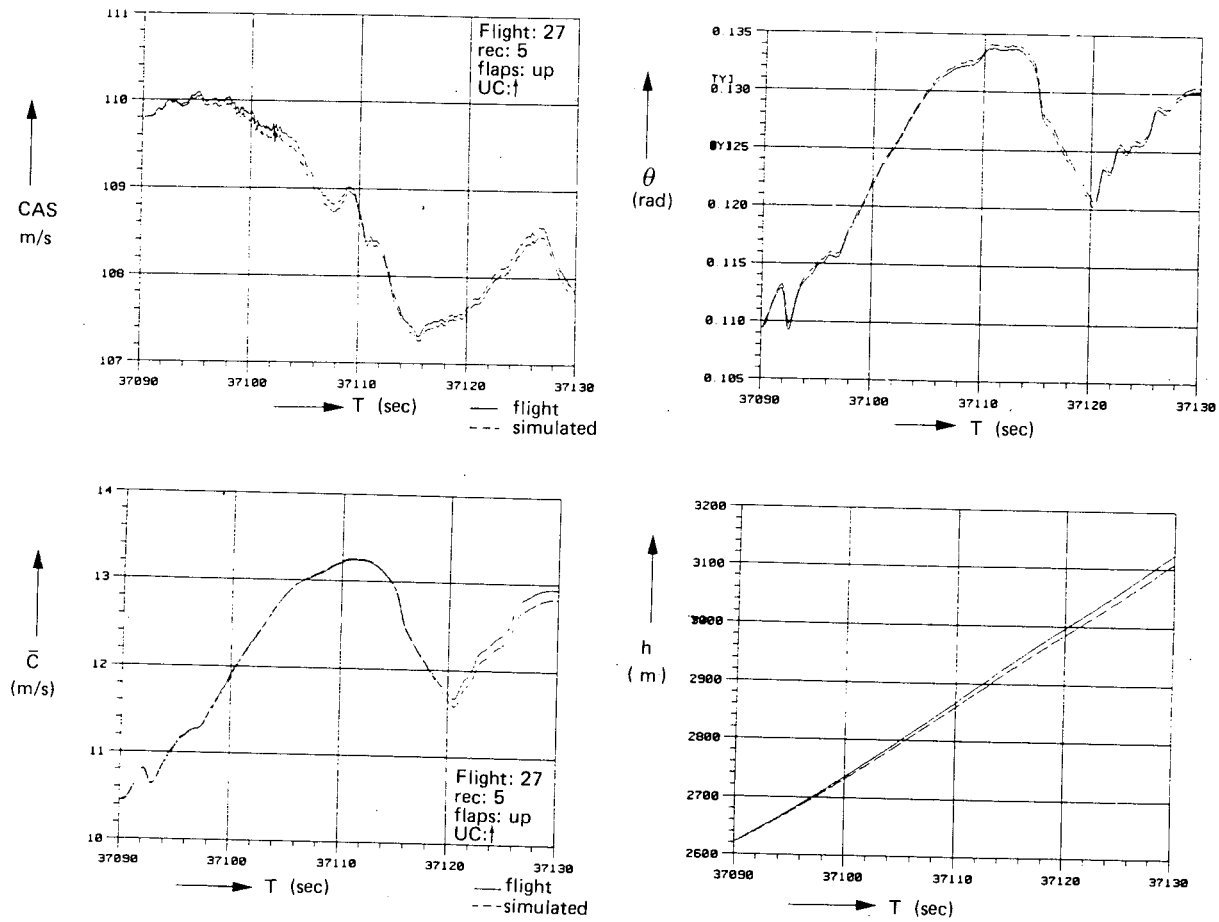

Fig. 14 All engine climb

as is indicated in figure 6. Because the reconstruction of the flight path on the ground is different in nature from the one required in free air, these cases have been dealt with separately. As a result of this also two sets of parameters were defined viz. one set of ground parameters and one set of air parameters. From these sets the variables could be selected, specified by the Simulator manuafacturer (CAE), for a particular ATG manoeuvre. The ATG recordings were visually checked and selected on a graphics terminal. After this the data were converted to TH COPY format, put on magnetic tape and sent to CAE. CAE has standard procedures available to make high resolution plots of the data in a form directly suitable for the FAA evaluation.

The POM data required by the FAA are a specific selection from the ATG test data. The flight recordings necessary for the proof of match creation were sent to DUT. Here the mass properties and initial atmospheric parameters, present at the start of a flight test manoeuvre, were adopted in the simulation programme. Because practical experience shows, that the initial conditions of the flight test manoeuvre and the computed initial condition of the simulation do not coincide exactly, small offsets in control surfaces were used to compensate for the bias. After this, the input signal of the flight test was employed to drive the simulation programme with the submodels of interest included. The resulting model responses then could directly be compared with the flight test time histories. Hereby it must be mentioned, that with respect to the angle of attack and sideslip angle the reconstructed values of the flight test data are considered in the comparison with the simulation results. This in contrast with what usually is done, viz. a comparison with the corrected measured vane angles.

Obviously criteria are required to accept or reject a certain model response. To fulfill phase II requirements in reference 1, for the requested POM tests, tolerances are defined for a number of specific parameters representative for that test. Using reference 1, it appeared that the POM data fell within these tolerances.

After the POM data were generated they were put on magnetic tape and sent to the simulator manufacturer.

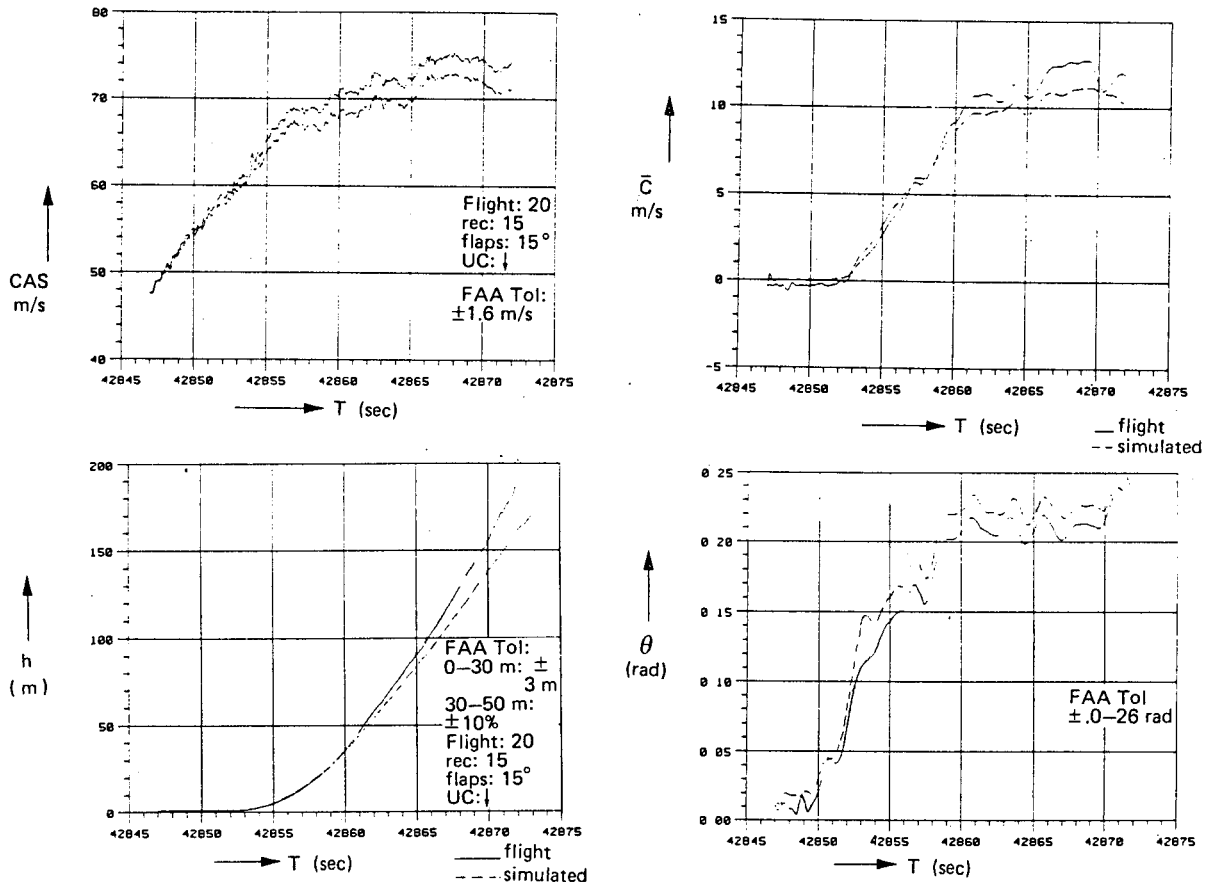

Fig. 15 Normal take-off

As an example in figures 12 to 15 time histories are presented from the POM data base. Characteristic parameters are shown of a level flight acceleration and deceleration, an all-engine partial climb and a normal take-off. Furthermore in figures 16 and 17 characteristic motions are depicted viz. the short period and dutch roll. In the figures also the simulation responses are depicted (dotted lines) as a result of the flight test measured input signals. As can be noticed a good agreement is achieved. Where appropriate the tolerances are indicated on the plots as defined by the FAA.

7. Concluding remarks

Ground based flight simulation as a training tool becomes more and more important in todays aviation. However, as a result of this the requirements with respect to the fidelity have been increased. Obviously also the proof of this fidelity is essential. In particular for small and older aircraft, however, the flight test data base is marginal with respect to the present demands of for instance a Phase II approved simulator. This situation arose when a Phase II approved simulator was required for the Cessna Citation 500 of RLS. Therefore a flight test programme was carried out with an accurate instrumentation system. Employing dynamic flight test techniques and advanced computer data processing and parameter identification techniques, it was possible to generate the mathematical models and data base of the Citation 500 in a relatively short period of time. The models were implemented in a 6 DOF engineering simulation. Using this simulation, it was possible to generate a proof of match, where a comparison was made between the flight test measured responses and the simulation responses using flight recorded input signals. From this it could be concluded, that the identified mathematical models were adequate representations of the actual aircraft characteristics (Ref. 9, 10, 11).

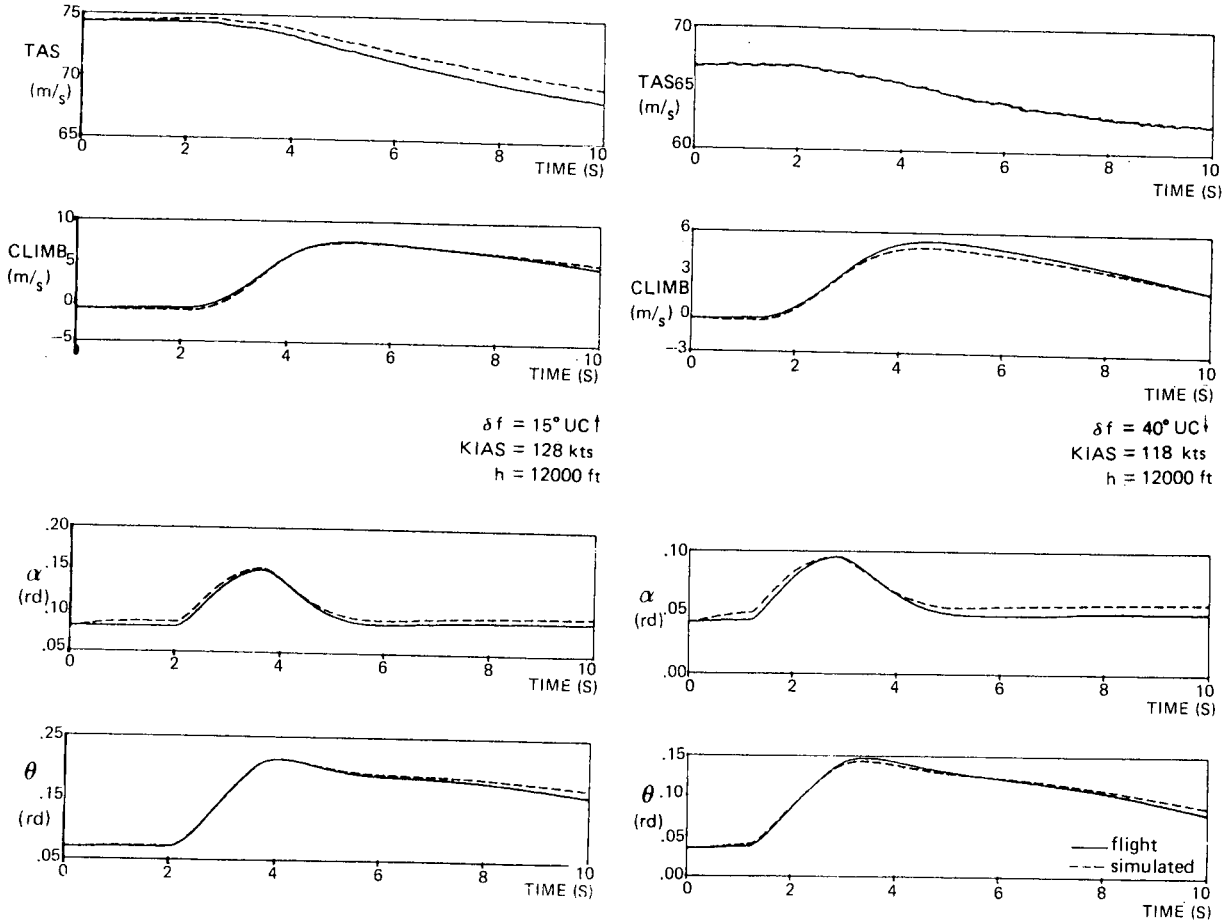

Fig. 16 Short period dynamics
FAA tol: 10% of period
.02 in damping

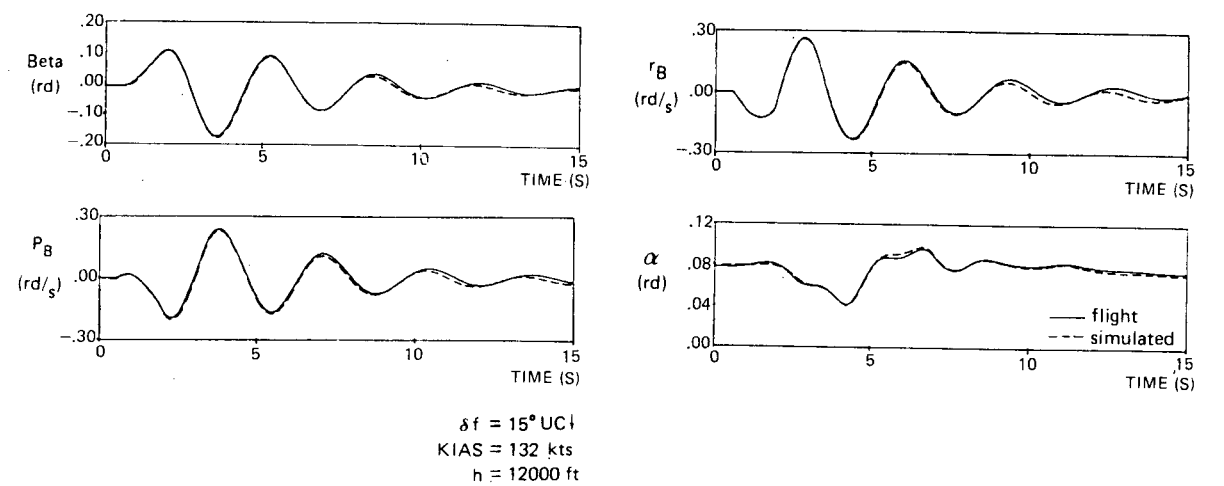

Fig. 17 Dutch roll dynamics (yaw damper off)
FAA tol: 10% of period
.02 in damping

8. References

1. Anon
   Airplane simulator and visual system evaluation.
   FAA Advisory Circular 120-40A, 1983

2. Anon
   Cessna Citation Maintenance Manual.
   Chapter 6, Dimensions and Areas.
   Cessna Aircraft Company

3. Breeman, J.H., Simons, J.L.
   Evaluation of a method to extract performance data from dynamic manoeuvres for a jet transport aircraft.
   NLR MP 78021 U, 1978

4. Anon
   Cessna Citation Operating Manual.
   Cessna Aircraft Company

5. Anon
   Citation 500 aircraft pilot test procedures for FAA Phase II ATG manoeuvres.
   CAE Electronics Ltd. Montreal, Canada
   Revision 1: January 1987

6. Wilt, M. v.d.
   Flight path reconstruction of symmetric unsteady flights.
   NLR TR 76133 U, 1976

7. Mulder, J.A., Jonkers, H.L., Horsten, J.J., Breeman, J.H., Simons, J.L.
   Analysis of aircraft performance, stability and control measurements.
   AGARD lecture series no. 104 on parameter identification, 1979

8. Nieuwpoort, A.M.H., Breeman, J.H., Erkelens, L.J.J., Geest, P.J. v.d.
   Correlation between flight simulation and processing of flight tests based on inertial measurements.
   NLR MP 85058 U, 1985

9. Baarspul, M., Mulder, J.A., Nieuwpoort, A.M.H., Breeman, J.H.
   Mathematical model identification for flight simulation, based on flight and taxi tests.
   DUT Report LR-550, April 1988.

10. Mulder, J.A., Baarspul, M., Breeman, J.H., Nieuwpoort, A.M.H., Verbraak, J.P.T., Steeman, P.S.J.M.
    Determination of the mathematical model for the new Dutch Government Civil Aviation School flight simulator.
    SPTE paper, 18th Annual Symposium, Amsterdam

11. Mulder, J.A.
    Aircraft flight control system identification.
    8th IFAC-IFORS Symposium on Identification and System Parameter Estimation.
    Beijing, China, August 1988.

FLIGHT DECK DEVELOPMENT AND THE ENGINEERING PILOT

H. Benedictus

Royal Dutch Airlines

1. Becoming an engineering-pilot

Once upon a time there was a young man who was crazy about aeroplanes. So nobody was really surprised when he in 1957 had himself registered to become a student in Aeronautical Engineering at Delft University of Technology. He was just one of the 80 new enthusiastic aviation freaks.
Some years later he and his observing friends and relatives were surprised: on behalf of the Delft University professor Van der Maas gave him permission to fly small aeroplanes!
April 24, 1961 he made his first solo-flight in a Piper Cup, taking of from Zestienhoven, the airport of Rotterdam.
Surprise, however, became happy amazement when he got the unique chance to attend the Rijksluchtvaartschool in Eelde, the pilots training school for the 'big' world of flying.
It has to be admitted, it was not a normal chain of events. One had to comply with a number of conditions: adequate progress with respect to the study in aeronautics, more than average medical fitness, demonstrated piloting skills.
And he had to be active in a defined graduation area: the potential candidate had to be a 'pupil' of professor Gerlach, heading for graduation in 'Stability and Control'. And that was not easy. That required courage, patience, loyalty, understanding, insight and intelligence. Because it was not easy to follow professor Gerlach when he was proving on the blackboard that one of the gust-derivatives, according to the simplified method of calculation, is:

$$C_{m_{\alpha_g}} = \left(C_{N_{w_\alpha}} \cdot \frac{x_{cg}-x_w}{\bar{c}} - C_{T_{w_\alpha}} \cdot \frac{z_{cg}-z_w}{\bar{c}}\right) \cdot \frac{x_{cg}-x_w}{\bar{c}}$$

$$+ C_{N_{h_\alpha}} \cdot \left(1-\frac{d\varepsilon}{d\alpha}\right) \cdot \left(\frac{V_h}{V}\right)^2 \cdot \frac{S_h}{S} \cdot \left(\frac{x_{cg}-x_h}{\bar{c}}\right)^2$$

There is no reason for the reader to become scared. This is the first and the last equation or formula in this chapter. It is true, the road through the Stability and Control landscape was covered with integrals and derivatives, but on entering the real life I was almost unable to find and use them, which is a shame.
As a consequence there was no argument for me to produce them for this article.

Coming back from Eelde in 1964, professor Gerlach coached me towards the finish-line through a couple of graduation subjects which were related to flight testing.
One of them, as an example, was the determination of the aerodynamic coefficients of the wing of the Fokker S 12, an aircraft owned by Delft University of Technology for research purposes, see Fig. 1.

Receiving the diploma on the in harmony chosen graduation date was not easy. The pure scientist is not used to take into account factors such as the aircraft's nuts and bolts problems and the ever so important influence of meteorological conditions on a test flight.
It became evident that the word 'delay' is very common in the world of aviation. I have no idea who was most relieved on July 9th, 1965, when the goal was achieved and the roads of professor Gerlach and me were going to split, see Fig. 2.

2. Engineering pilot with KLM Royal Dutch Airlines

After a planned participation of 4 years in the Fokker F28 certification flight test program for the Dutch Airworthiness Authority, the RLD, KLM Royal Dutch Airlines opened its doors. KLM, totally right, abides the principle that an engineering pilot is to be a line-pilot to start with.
Later it will be considered whether the specific pilot is qualified for a side activity, when the company needs participation in a project or assistance in a department.
After two years of DC-8 line-flying I was asked to join the 'Training Department' in order to critically re-write the DC-8 flight techniques. After having successfully completed this task, the vice-president of Flight Operations arranged a transition to the 'Flight Technical Department'.
This department comprises the sub-departments 'Aircraft Operating Procedures', 'Aircraft Performance' and 'Fuel Management', 'Flight Support Services' (Flight Handling, Communications, ATC, Meteo) and 'Navigation Documentation'.
'Aircraft Operating Procedures' mainly consists of 'typebureaus' responsible for the flight-technical support of the applicable fleet. A typebureau also puts the Aircraft Operations Manual together. When a new aircraft type is introduced in the company, a typebureau is therefore installed just over a year before the new type enters service.

It may be obvious that the engineers, working in the 'Flight Technical' area have to be assisted by technical pilots, as on many areas operational experience and knowledge is needed.
When I joined 'Flight Technical' I got involved in subjects as the introduction of cat II/III lower weather minima, standardization of abnormal and emergency procedures for all cockpits, participation in the initial development of new flightdeck systems, such as 'Flight Warning Systems' and 'Electronic Flight Instrument Systems' (EFIS).
All these activities lead to the participation in various bodies and organizations, such as the Airlines Electronic Engineering Committee (AEEC, related to ARINC), Society of Automotive Engineers (SAE), IATA, ICAO, etc.

After a couple of years I was transferred to a staffoffice in 'Flight Technical, Specification Projects'.
I was then flying the Boeing 747.

3. Specification Projects

Fortunately it is history that the manufacturer determines what is good for the user, see Fig. 3.
The real world proved that finally nobody gets the desired credit.
The technical experts need the inputs from the future user in the design phase, to incorporate his wishes.
The user, on the other hand, has to stay in touch with the manufacturers to balance operational planning with the latest technological developments.
For this necessary cooperation and coordination there are fortunately various possibilities. I already mentioned organizations like ARNINC, AEEC and SAE. In these organizations airlines meet with airframe- and equipment-manufacturers through sub-committees, dedicated to certain new developments.
Today's main subjects are Satellite communication, Datalink, Collision Avoidance, Global Positioning System, Integrated modular avionics, High speed databus and Electronic library system.
Next to these organized activities, there are also a lot of direct informal contacts between user and manufacturer. Airlines are invited for 'brainstorming sessions', product evaluation and participation in preliminary test programmes.
A typical example is the development of the Collision Avoidance System. The equipment manufacturers who participated in this program needed the airlines

badly. Prototype systems had to be installed in line-flying aircraft to obtain operational experience. Evaluation and observer programs were set up, where a great number of pilots with different engineering background were invited to see, fly and criticize the system.
At the same time the airframe manufacturers installed the system in their engineering simulators and invited airline engineers and technical pilots to tackle the problems related to the specific flight deck.
KLM's 'Specification Project Department' participated by attending the meetings, flying the observer seat on United and Northwest TCAS evaluation flights and joining the equipment manufacturers in there demonstration flights.

With respect to all these activities the 'Specification Projects' bureau was set up, to take care of these and other tasks, which do not belong to any of the other bureaus in the 'Flight Technical Department'.
It will be obvious that close cooperation with the other departments is of utmost importance, very often even unavoidable, such as in the introduction period of a new aircraft type, when the new typebureau has to 'take over' from the 'Specification Projects' bureau.

4. Flight deck development

The way in which airframe manufacturers took care of flight deck design went through an evolution.
In the beginning there was one design. The manufacturer was responsible, the airline had no choice.
Maybe there was no need to be involved, the flightdeck was simple and straight forward, see Fig. 4.
But when the aircraft became bigger, faster and operated in an ever widening operational environment, the flight deck became more complicated. Airlines approached the manufacturers with special requests and with typical requirements.
In this second phase, flight decks started to differ per individual airline. Very soon both manufacturer and airline realized that this was a situation which had to be avoided. The manufacturer had to deal with the related engineering, production and certification workload.

The airline had to pay the bill of a more expensive customized flight deck, faced more problems in the exchange of spare-parts and was hindered when trying to sell a rather unique aircraft.
As a consequence, in present time the airframe manufacturer takes the initiative to establish flight deck working groups as soon as a new project is started.
The manufacturer invites a large group of potential customers to participate.
Of course the group does not have to start from scratch. The manufacturer is responsible for a basic proposal, based upon a number of fixed starting criteria, such as flight deck size, number of flight deck seats, number of engines, basic system-characteristics and applicable display-technology status.

As a typical example we will follow the Boeing 747-400 flight deck development.

5. Boeing 747-400 flight deck

5.1. B747 Block Change

In 1985 it became clear that Boeing was going to procedure an updated became of the existing B747-200/300. Driving factors were the airlines needs for more range and better fuel economy. Furthermore there were possibilities to update the various technologies in the B747. The first B747's date from the sixties and the state of the art has changed tremendously in the meantime.
At the beginning of the eighties a new technological development for the flightdeck was initiated with the introduction of aircraft such as the Airbus A310 and the Boeing 757 and 767.

Digital computers and Cathode Ray Tubes (CRT's) found a permanent place in the cockpit. This development was irreversibly continued when newer aircraft like the Fokker 100 and the Airbus A320 were designed.

Boeing presented the successor to the existing B747 types as the 'B747 Block Change', see Fig. 5.
Boeing proposed to use the cockpit design of the Boeing 757 and 767 in an adapted form. Boeing argued that this approach would reduce engineering costs, certification problems and flight testing. Commonality with B757 and B767 would also serve those airlines already operating these models.

However, a large number of potential customers, particularly in Europe, KLM included, came with a counterproposal.
They objected to this technological 'backwardness' in an aircraft with an average life of around twenty years.
Their proposal was based upon the introduction of the latest technology:
new displays and improved display system architecture.
The alternate flightdeck layout would finally result in a number of advantages:

- at least 50 kgs. weight reduction;
- increased reliability;
- identical interchangeable displays;
- identical interface units;
- reduction in the total number of line-replaceable units;
- improvement of flight- and dispatch-redundancy.

After a couple of meetings Boeing agreed to the alternate proposal.

5.2. New standard B747-400 flight deck

When this basic agreement was reached, Boeing continued to meet with the airlines involved on a regular basis. The starting position was set, and an enormous amount of detailed discussions would follow.

Together with the flight deck layout-related items, see Fig. 6, the airlines had put together a long list of requirements.
These included items like:

- standby electrical power requirements;
- circuitbreaker location (flight deck or electronic equipment bay);
- fuel quantity accuracy;
- weight and balance measurement and indication;
- windshear protection.

Let us stay with the layout-aspects, and start with the display system.

5.3. Integrated Display Systems (IDS)

The layout was established: Primary Flight Display (PFD) in front of the pilots, Navigation Display (ND) inside next to the PFD, the engines and Systems Displays on the center panel in an over/under arrangement. By the way, Boeing uses the

terminology Engine Indicating and Crew Alerting System displays (EICAS displays) for the engines and systems (CRT's).

This layout of six identical displays opened the door towards the already mentioned redundancy, required by the airlines.
To achieve the maximum, in flight and for ground dispatch, the following design criteria were added:
- all displays should have identical software;
- there should be three totally identical electronic interface units;
- all data should go to each display;
- capabilities for in flight source and display switching should be provided.

These requirements defined the 747-400 IDS architecture, see Fig. 7.

With the basic architecture set, Boeing was then leading the airline participants through a lengthy iterative process of defining the display synoptics. Proposals for the EFIS (PFD and ND) and EICAS displays were sent to the participating airlines. The initial discussions were based on paperwork only. However, very soon the need arose to study the dynamic characteristics of a specific display. Fortunately Boeing was able to provide an engineering simulator. Many briefings, simulator sessions and de-briefings followed.

5.4. Some EFIS features

The navigation display did not cause too many heartburning. The experience obtained with the A310 and the B757/767 and the wish from the airlines to maintain commonality whenever possible, quickly lead to the synoptics used at present. The most commonly used ND display mode is the map mode, in which the Flight Management System (FMS) presents the actual aircraft position relative to the programmed route and other selected data such as airports, waypoints and radio beacons, see Fig. 8.

Discussions focused on problems which could relatively easy be solved, such as:
- maximum selectable range: 640 nm was chosen for this long range aircraft;
- back-view possibilities: solved by adding the select possibility to bring the aircraft symbol to the center of the display;
- ADF and VOR bearing info: switches were added enabling the pilot to present the required bearing information on the display, with relevant information about what was selected in the lower corners of the ND.

Definition of the PFD-symbology took considerably more effort, see Fig. 9. Typical discussion areas were autoflight mode annunciation, presentation of all air data in the display (airspeed, altitude and vertical speed) and presentation of heading information on the bottom of the display (a consequence of the side by side EFIS arrangement).

Evaluation of the airspeed presentation was supposed to be easy. Various airlines were able to use their experience with respect to the presentation of airspeed on a vertical tape in the PFD. This did, however, not prevent long working sessions on this subject! The two hot items were speed tape orientation and rolling digits. With respect to the orientation, it was amazing to find that human factors opinions were split on the question whether the low speed values should be at the top or at the bottom of the speed tape.
Third parties like NASA, FAA, SAE got involved. Simulator evaluations were executed, which, however, did not lead to a consensus.
But the pilots wished to incorporate the speed trend vector, the arrow alongside the speedscale where the point is situated at the speed which would be reached in the next 10 seconds. The trend vector appeared to be the key to the solution of the orientation problem. Most pilots concluded that the high numbers should be up with a trend vector in use, leading to a required upward pointing vector in case of an accelerating aircraft. Problem solved!

Parallel to these discussions, the question had to be answered whether the presentation of the actual speed via rolling digits in the airspeed tape was a display improvement. When there was no unanimous agreement within the airlines fight deck working group, the final decision was made by the Boeing test pilots: the Boeing standard speed tape would have rolling digits.

5.5. EICAS features

Boeing 747-400 EICAS, comprising the two displays on the center panel, see Fig. 10, is basically intended to:

- give the flight crew engine primary and secondary information;
- provide caution and warning features;
- give the crew information about the technical status of the aircraft as related to the dispatchability of the aircraft;
- present memo messages reminding the flight crew about certain system selections, such as parking brakes set.

The left part of the upper display is used for the display of primary engine data. The right part is normally blank, as the alerting part of EICAS will display any fault message on that part, when applicable.
The lower display is intended for supplementary information. Secondary engine data will be displayed during engine start, system synoptics will be displayed during engine start, system synoptics will be selected by the crew when considered convenient for the flight execution (e.g. doors page) or helpful for a specific procedure (e.g. presentation of the fuel system when selections are made). For these purposes a display select panel is installed in the glareshield panel.

For our B747-400 Flight Deck Working Group, the workload which came out of the EICAS related subjects was almost comparable to EFIS.
Understandable, because here also there was the controversy between the inheritance of B757/767 technology, aimed for by Boeing, and the pressure from the airlines to use the latest technology. System synoptics are available now, but were not part of Boeings initial proposal. They were not considered as 'need to have' and denied as additional 'nice to have' because of the unacceptable engineering workload. Combined airline's pressure was necessary.
The struggle for the feature, that a system synoptic is presented automatically when a caution or warning is triggered for that system, was lost.

In some aircraft, checklists are presented on the displays. It is possible to incorporate the 'normal' checklist in the system. The advantages do not balance the disadvantages:
a) every airline has a different checklist approach;
b) it is a fact that many changes are made;
c) it is not easy to close the loop, resulting in 'getting lost'-situations during checklist interruptions.

The situations is different however for the 'emergency' checklist. Automatic emergency checklist presentation was developed for and applied in aircraft like the Airbus A130 and the Fokker 100.
The system is well accepted by the pilots who fly these aircraft. The airlines did not achieve implementation in the B747-400.

The last discussion item concerning EICAS to be mentioned is the presentation of engine data.

For aircraft like the B747-200/300 and the DC-10 research was already done with respect to the optimum presentation of engine data: round dial or vertical tape. KLM asked the National Aerospace Laboratory NLR to assist. An extensive simulation study was done, during which 18 flight crew members flew the two possibilities. Conclusions were in favour of the vertical tape instruments, mainly because engine failures were noted more quickly on vertical tape instruments, than on circular instruments.
As a consequence vertical tape instruments were implemented on KLM's B747's and DC-10's.
The many years of line experience did not prove otherwise, flight crews are responding positively.
No wonder that KLM's input for the B747-400 engine data presentation called for tapes. Boeing also provided possibilities to evaluate both presentations in their engineering simulator.
The subject engineering pilots probably responded from their own experiences on previous types and their company policies: there was no consensus, some preferred the tape, while others stayed with the round dials.
At present everybody is faced with the beauty of computer flexibility. It is a fact that on the one hand many problems can be solved by calling: 'That is just a matter of software!'
On the other hand aviation is also faced with related problem areas: software control, software handling, validity checking, reliability and redundancy.
AEEC has assigned a special working group to tackle these problems. Anyway, engine data presentation was a problem which was going to be solved through the magic of software: Boeing offered both and made it 'pin-selectable' or selectable per individual user.

5.6. Caution and warning features

Around 1978 the Committee S 7 of the Society of Automotive Engineering (SAE) responsible for flight deck layout, panels and controls, prepared a document aimed to take care of proper management of all flight deck alerts: the Flight Deck Alerting System.
An important step was to define levels of alert:

- emergency level 3, requiring immediate corrective action by the crew;
- caution level 2, requiring immediate crew awareness and future compensatory action;
- advisory level 1, requiring crew awareness;
- information level 0.

Centralised crew alerting was proposed through a master aural attention sound , an optional master visual alert, a master warning and master caution lights. Through the use of the attention sound and the related displayed messages the number of dedicated flight deck warning sounds, such as horns, bells, rattles and beepers had to be reduced to a SAE recommended maximum of four.
In addition to the attention getters an explanatory message should be given on a display.
Other features of the system had to be the selection of the priority (important messages first) and flight phase adaption (suppression of failures during certain critical phases of flight).

First aircraft to have flight alerting systems installed were Airbus A130 and B747/757, however with certain differences.
Here again Boeing was following the B757/767 when defining the B747-400.

Basically the B747-400 meets the SAE recommendations:

- the number of aurals is reduced to four, which are:
  1. the fire bell for any fire warning;
  2. a two tone siren as the attention for level 3 warnings (cabin altitude, autopilot disconnect, configuration warning and overspeed warning);
  3. the level 2 caution attention which is a beeper and
  4. the chime, drawing the crew's attention to an incoming call with additional information about the source of the call on the audio select panel.
- master warning and caution lights in the glareshield, in front of the pilots;
- a message, indicating the failure, is presented on the upper EICAS display, warnings in red, cautions and advisories in amber. The message guides the crew directly to the appropriate page in the emergency checklist;
- flight phase inhibition is implemented, though limited to the take off phase, see Fig. 11.

It needs no clarification that take offs at high grossweights with related high take off speeds are flight critical manoeuvres. Proper guidance in case of any failure during the take off phase is very important.
Therefore it was not an easy task to define the take off inhibit schedule . Is 80 kts the correct speed value to initiate the caution inhibits? Is 400 feet above the ground not too low an altitude to re-initiate suppressed cautions?
Besides, some people had a hard time to accept the engine fire warning bell inhibit at all!

Nevertheless, the introduction of the flight deck alerting systems is an important step towards safer flight deck procedures.

5.7. Navigation

The introduction of inertial navigation systems was an important step towards navigation, basically independent from ground based systems. The inertial systems are already used in the 'old' B747's and in the DC-10 RNAV area navigation system. The next step was the Flight Management System (FMS), with the first applications in the A310 and B757/767.
FMS computers do not only take care of lateral (waypoint to waypoint) navigation but, through incorporation of engine data, aircraft characteristics and performance data, vertical guidance is also provided. Although roughly identical, differences did exist between the Boeing 'brown' and Airbus 'gray' system, named after the basic flight deck colours as used by the two manufacturers.
It was the task of the flight deck working group to define a system for the B747-400 by 'mixing' the brown and gray systems in a way acceptable to all parties. It was further the task to improve the final system, learning from the shortcomings of the existing systems and incorporating the latest technology improvements.

Boeing immediately realized that there was not sufficient engineering time to meet the long list of airline demands in one step and proposed a baseline definition with a future update package, to be implemented a few years after the first flight.
Typical 'B-package' items are:
- GPS and MLS position update;
- crew alertness monitor;

- flight planning capabilities, enabling the crew to 'build' a new flight plan;
- ACARS data link system interface;
- safe altitude presentation, such as minimum enroute and minimum sector altitudes;
- flight plan printing;
- multiple alternate selection;
- fueling panel interface for fuel loading purposes.

Most of the customers were pleased with the way the lateral navigation part of the FMS worked.
Quickly agreement was reached on a number of improvement items. The vertical navigation part, on the B747-400, basically available from 400 feet to final approach, was subject to criticism and more improvement was wanted, especially for the descent part.
It is a fact that the air traffic control system is not yet able to handle FMS equipped aircraft to its full capabilities. Descent clearances and ATC limitations are too often not in agreement with the vertical FMS plan. But experiences showed that vertical descent path problems were also caused by FMS limitations. As an example, FMS did not demonstrate the required flexibility to handle wind-changes, commanded heading changes, altitude interventions and speed interventions.
In addition pilots had problems to understand and follow the FMS on its way down, making it sometimes difficult to properly interfere when the actual flight path was considered to be incorrect. Actions of the manufacturer were aimed to improve the related control laws. Further vertical navigation attention items were:

- FMC derived take off speeds;
- automatic derate to climb thrust after take off;
- improved autothrottle operation during go-around;
- descent energy prediction circles, showing descent capabilities on the navigation display, both for the clean and 'dirty' configuration;
- altitude baro setting alert, commanding pilots action when crossing through transition-altitude or -level.

A last general remark

When FMS was designed, the pilot's interface was a Control Display Unit (CDU), an alpha-numeric keyboard with connected display. Later it was realized that such a CDU is a good tool to be used for other functions as well. In order to save flight deck space, weight and spare parts, the Multipurpose CDU (MCDU) was introduced, see Fig. 12.
The MCDU is basically identical to the 'old' FMS CDU, but it has the possibility to interface with a couple of functions, selected by means of the MENU function key and the applicable line-select key.
Additional functions on the B747-400 MCDU are:

- IRS NAV, permitting direct IRS navigation in case of FMC failure;
- alternate nav. radio tuning, an addition to automatic FMS nav. radio tuning;
- alternate EFIS/EICAS controls, to be used in case of an applicable control panel failure;
- interface with the CMC maintenance computer;
- interface with the ACARS Data link system.

5.8. Autoflight

It was a logical choice for Boeing to maintain the B747-300 triplex autoflight system philosophy also for B747-400.
The airlines agreed, but it was necessary though to consider a number of changes.
On request of the airlines Boeing studied:

a) Cruise Autopilot Redundancy

At present in climb, cruise and descent one autopilot is in command. Single failure or inadvertent disconnect results in a no-autopilot situation. This was considered undesirable by the airlines for a long range, two-crew aircraft;

After doing research, Boeing declared that the above item was all but not achievable and regarded warning, related to failure or disconnect, adequate for the necessary pilot awareness.

b) Control wheel Steering (CWS)

The only Boeing aircraft type with a CWS mode, in which mode autopilot lateral and vertical inputs are made through the control column, is the B737. Half of the airlines, participating in the flight deck working group, was in favour of implementation of CWS in the B747-400 as well.
When Boeing research showed the impact on price and complexity, the issue was withdrawn from the agenda.

c) Autoland Roll-out Guidance

There was unanimous agreement that the B747-400 autoland capabilities had to be extended towards the so-called Cat III B limits: a decision height of 20 feet above the runway with a minimum visibility of 75 meters.
Nosewheel steering was incorporated in the localizer guided directional channel, which makes it possible to have the autopilot engaged down to taxi speed on the runway.

The interface with the pilots, the Mode Control Panel (MCP), installed in the glareshield panel, is an improved version of the B757/767 panel, see Fig. 13.

6. Some conclusive remarks

- The purpose of this chapter is to provide some background information on the procedures which are followed when a new flight deck has to be developed. The Boeing 747-400 is used as a typical example.
- The reader may get the impression that the confrontation between manufacturers and airlines around a new flight deck definition is a continuous battle. Fortunately this is not the case. It is true that in this article Boeing was playing the role of the bad guy, but this was only necessary to set the scene.
  Every other airline will agree that Boeing was and is a good discussion partner and uses the airlines inputs to achieve a safe, economic and user-friendly product.
  It is however unavoidable that opinions and approaches differ ever so often because of the differences in operational philosophy, commonality considerations, economical aspects, etc.

- The first meeting of the B747-400 flight deck working group was in April 1985. The last meeting was in March 1989, when TCAS implementation was discussed. There were many meetings in between. It is therefore necessary to emphasize that this article only covers a fraction of the many discussions.
- It is a fact that in meetings all over the world the inputs of Netherlands participants are always highly appreciated.
  The Delft University of Technology is well known and is the source of the skill of engineering people from the Netherlands. I sincerely hope that this will be proudly noted by a departing professor Gerlach.
- I personally want to thank professor Gerlach for his friendly and solid contribution to the scientific basis which now allows me to be part of the beautiful working environment, described in this article, see Fig. 14.

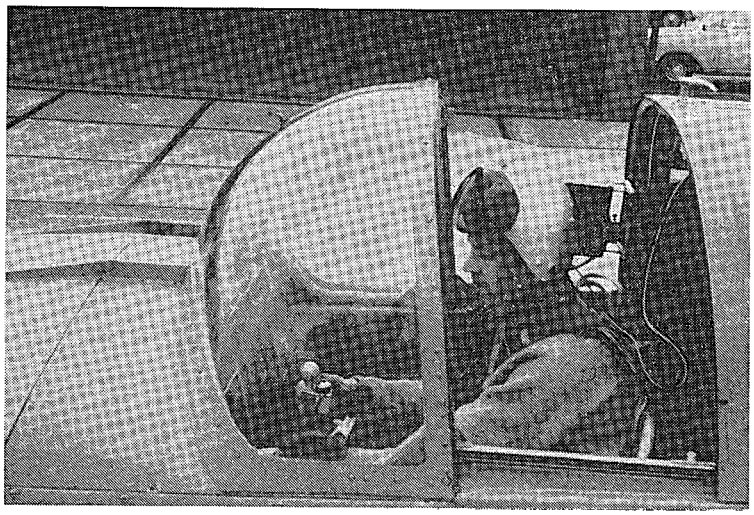

Fig. 1. The Fokker S12 flight deck

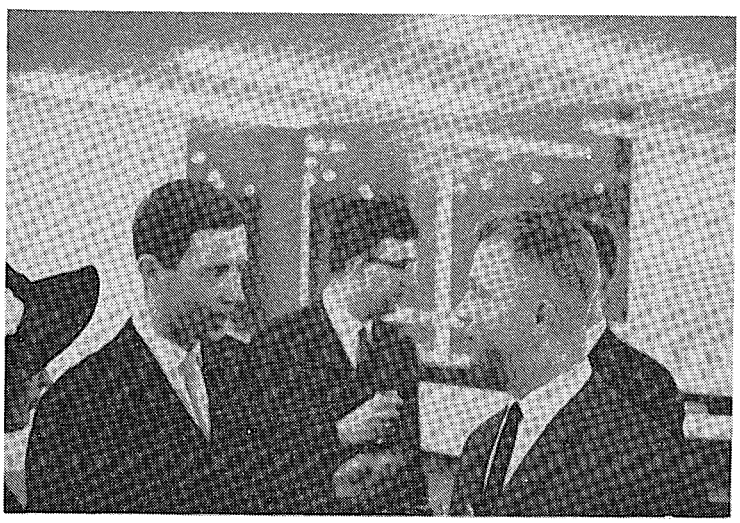

Fig. 2. Graduation day

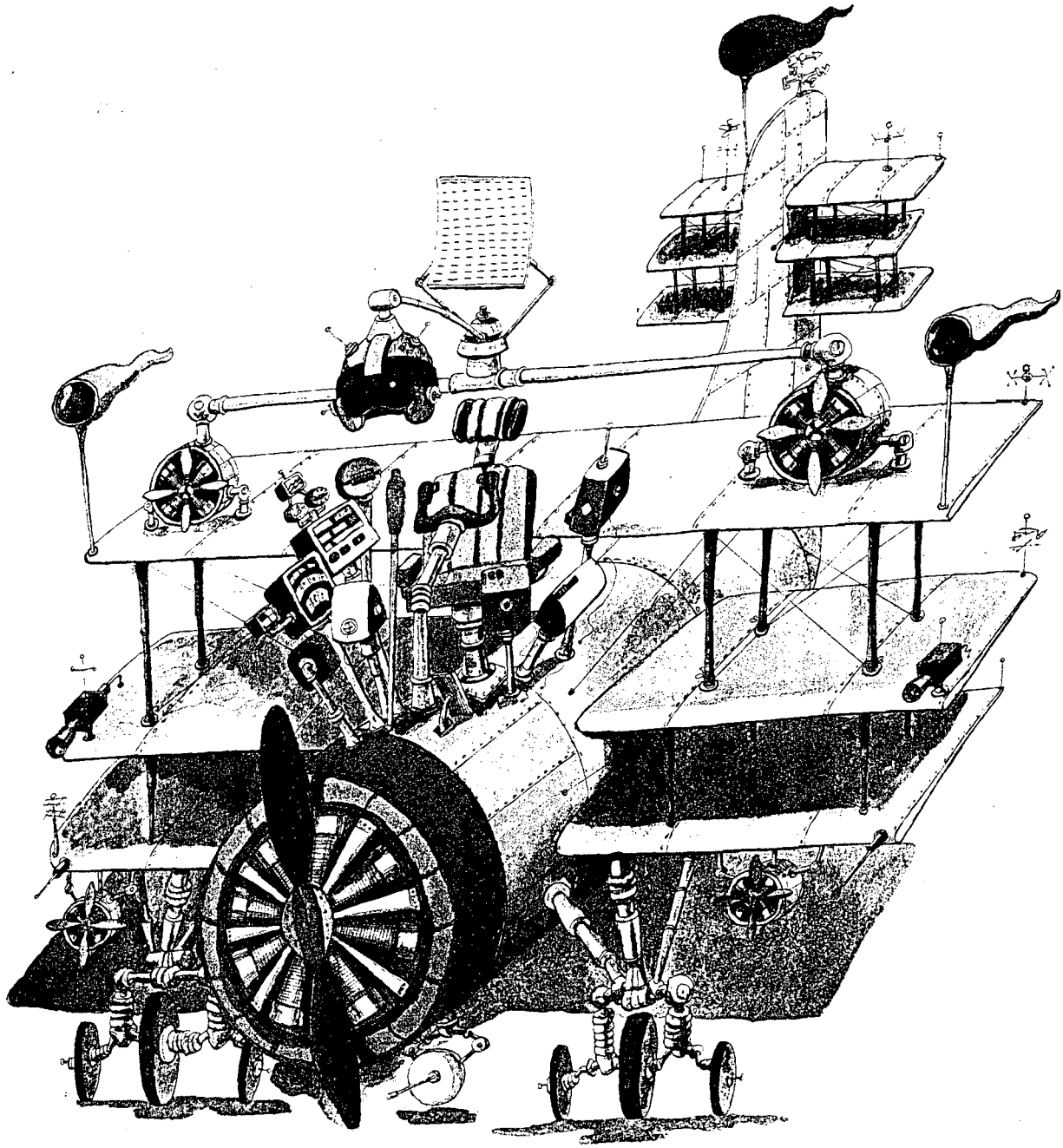

Fig. 3. Coordination between manufacturer and user is needed.

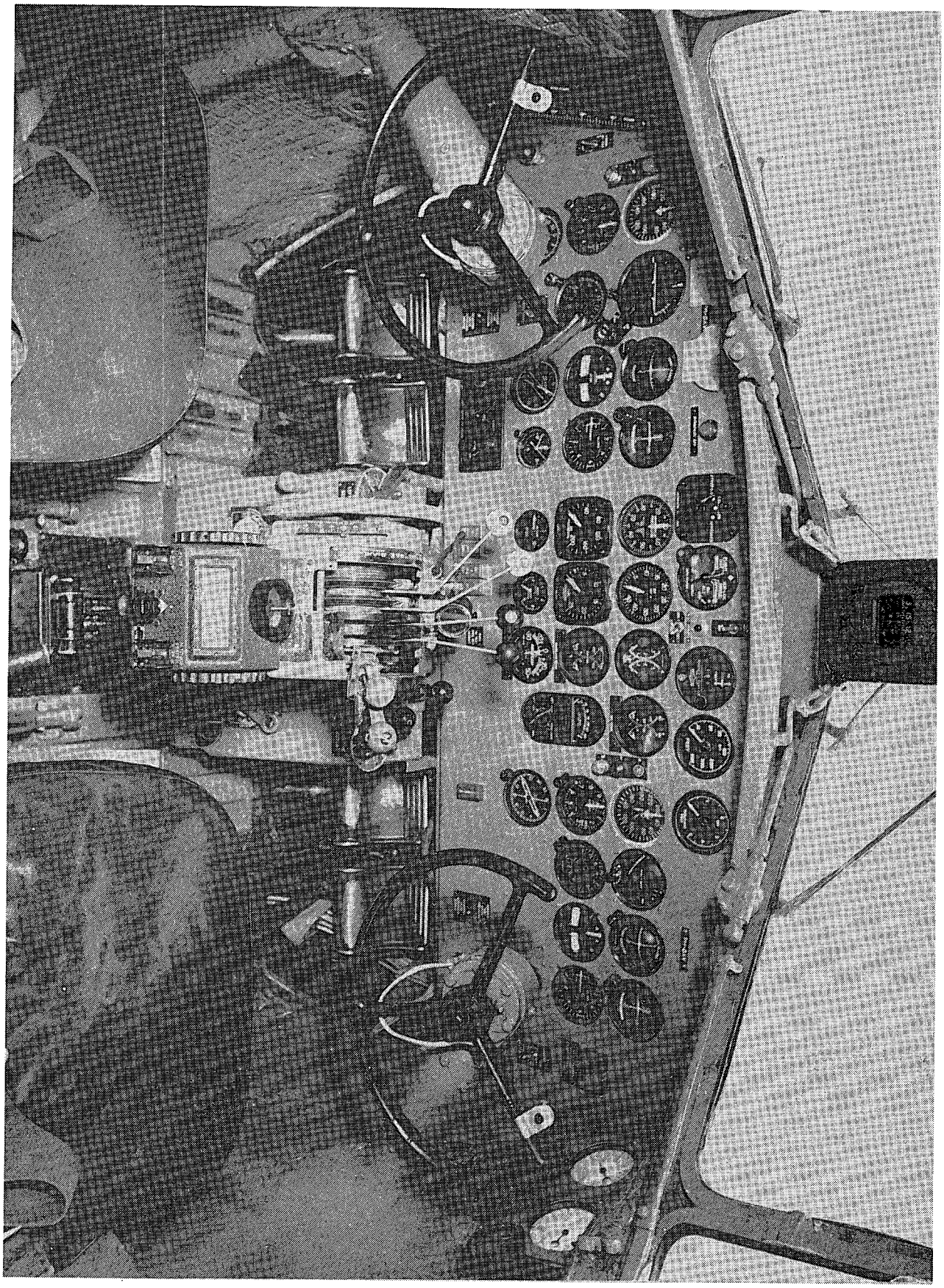

Fig. 4. DC 3 Flightdeck

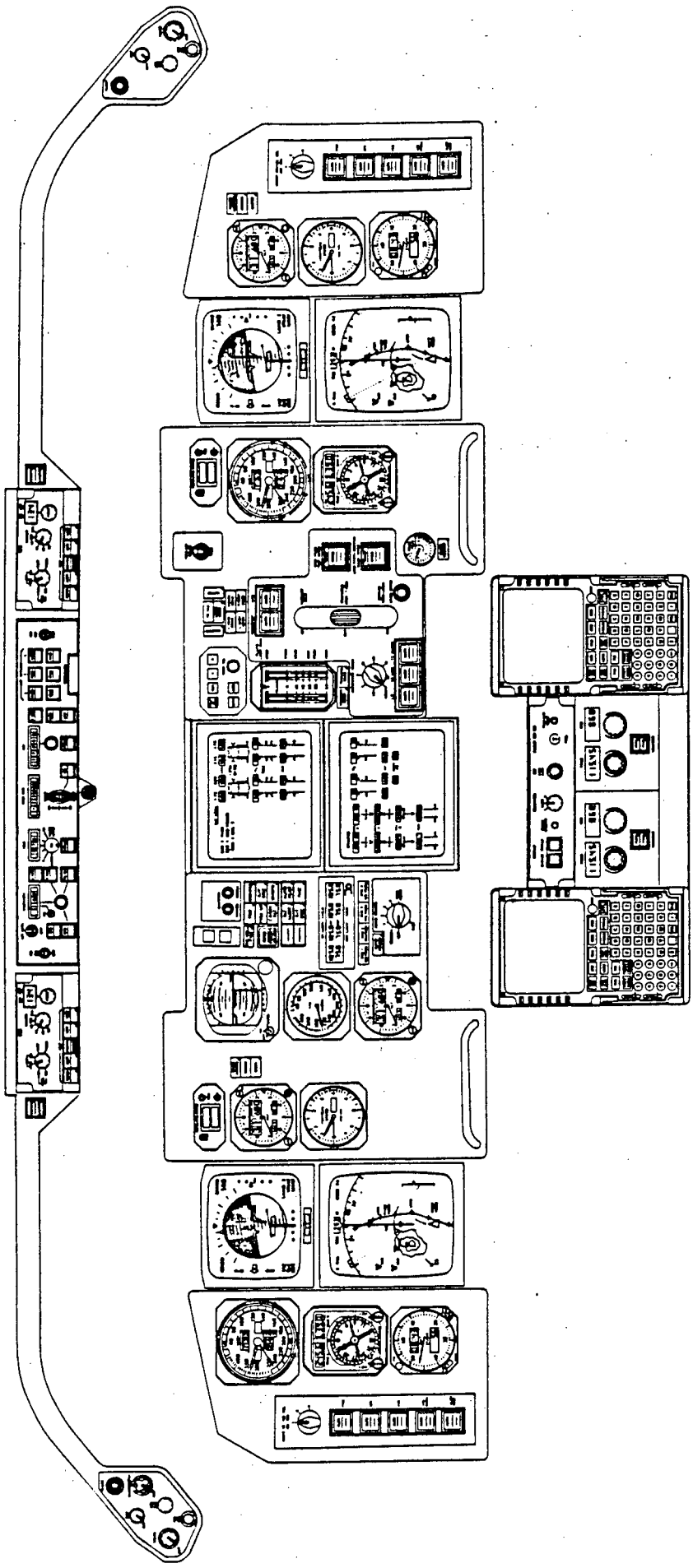

Fig. 5. Boeing 747 'Block Change'.

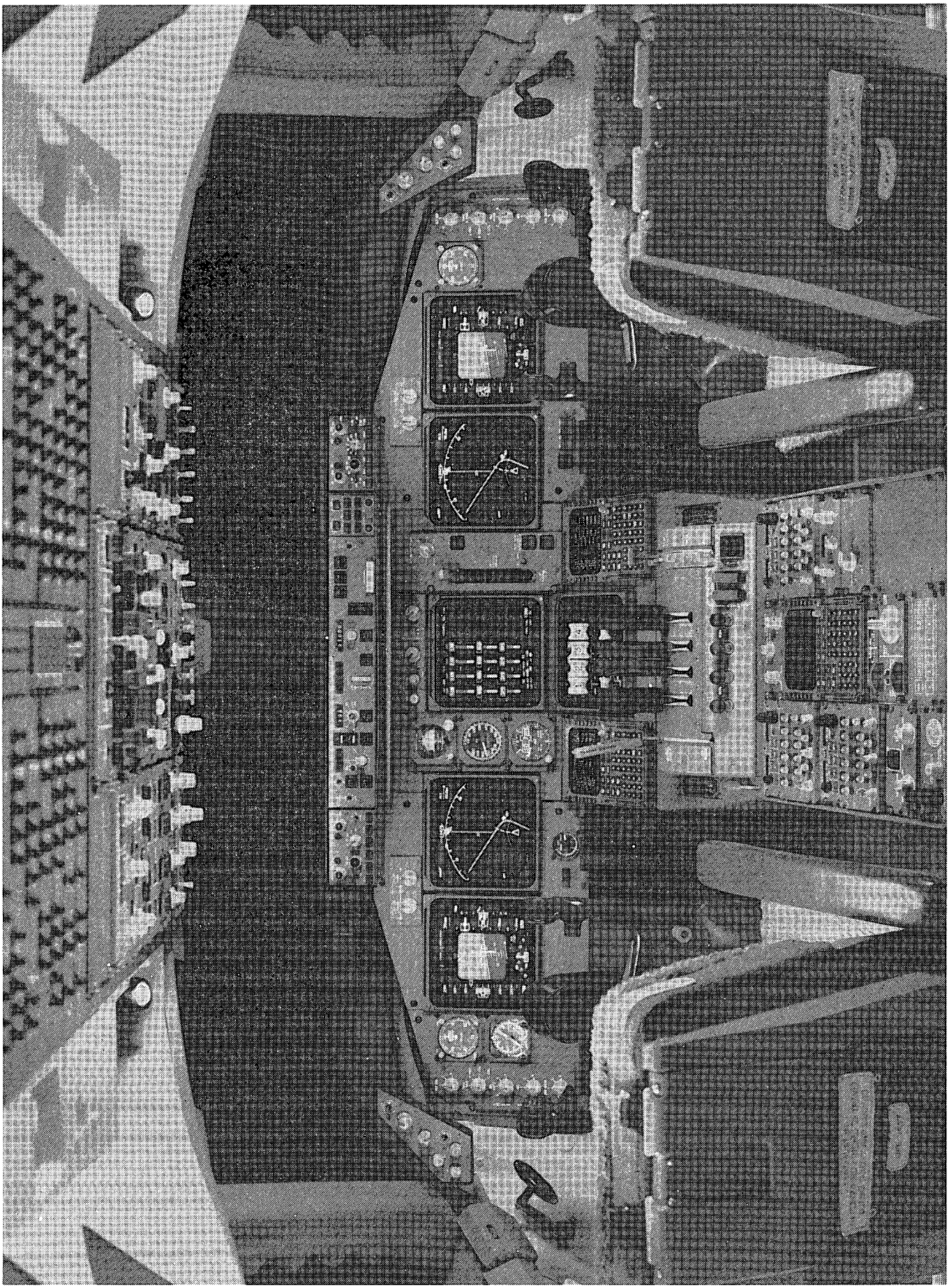

Fig. 6. Boeing 747-400 Flight deck.

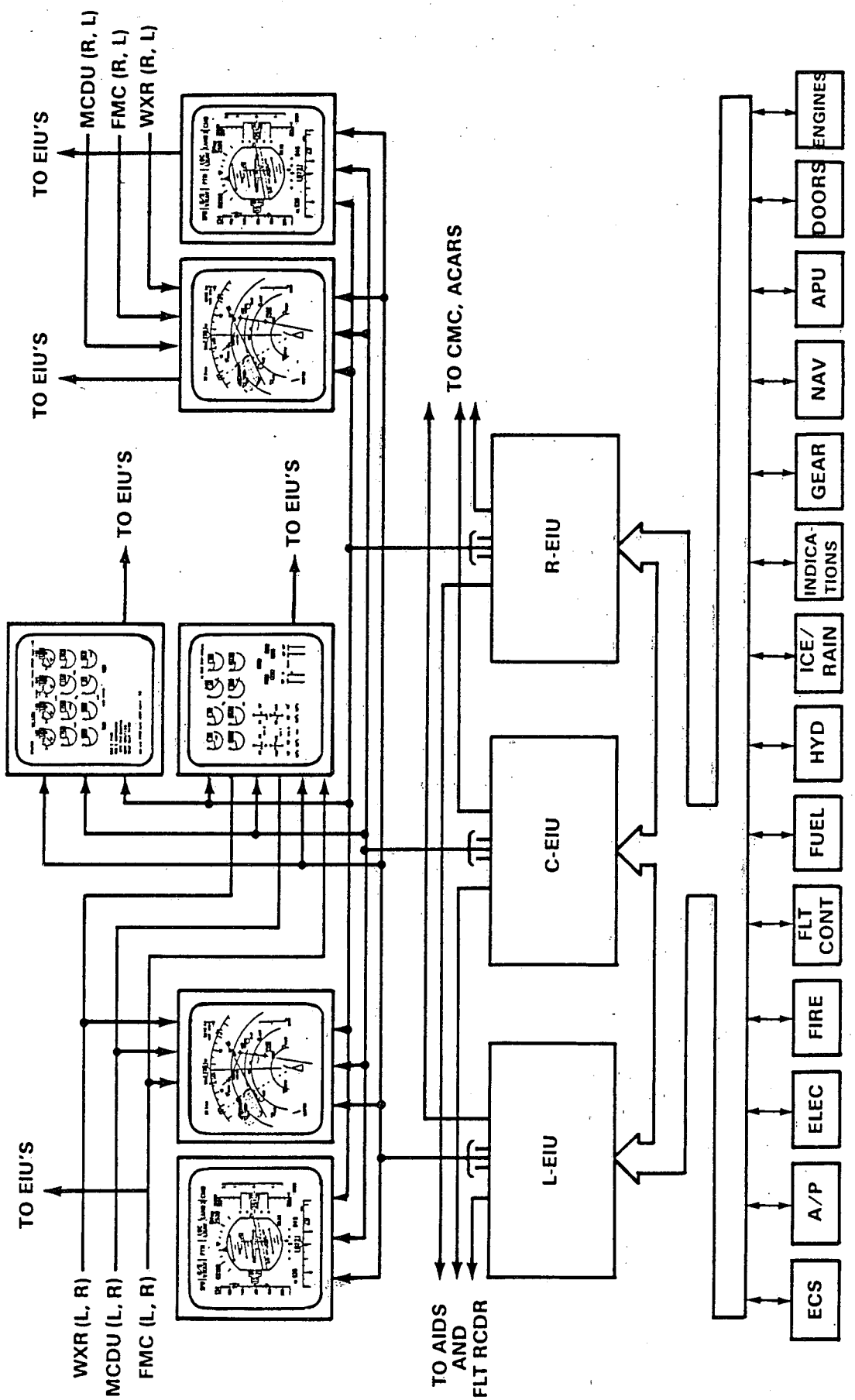

Fig. 7. IDS Architecture.

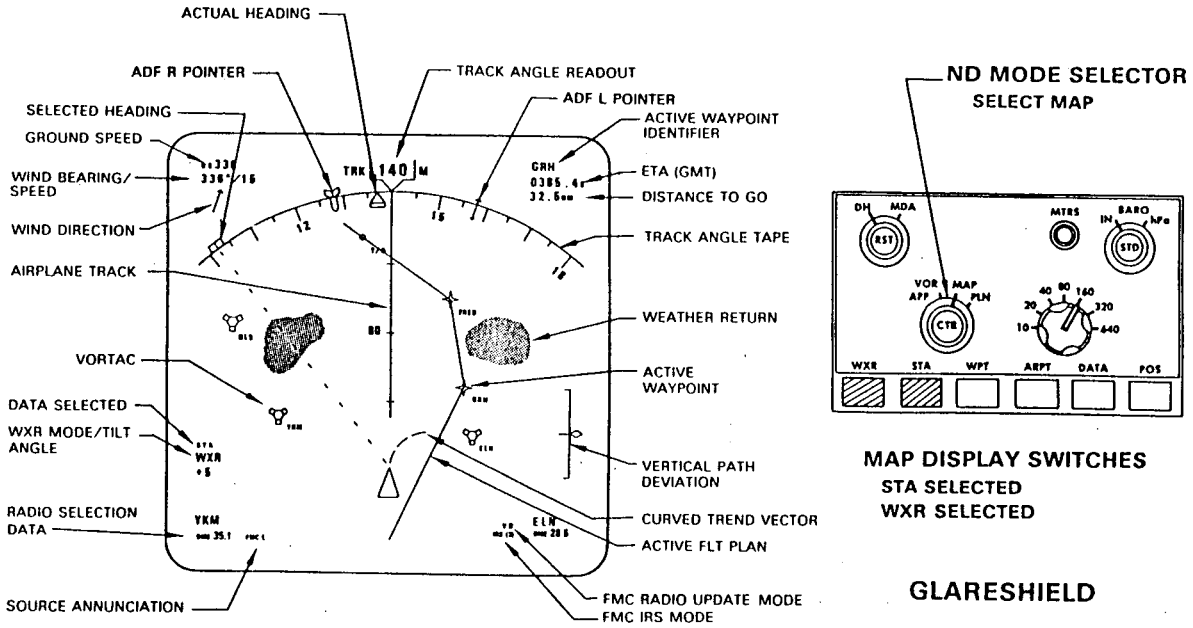

Fig. 8. Navigation Display, map mode.

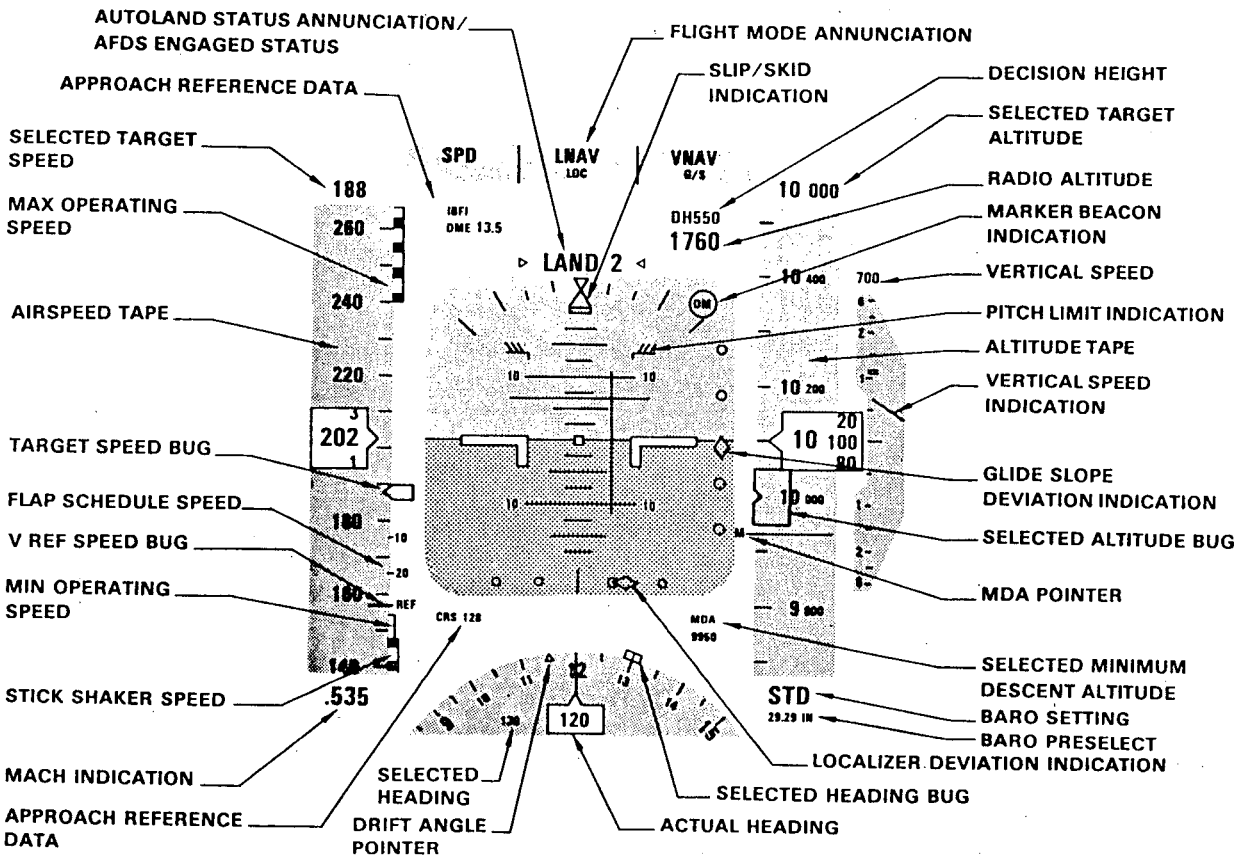

Fig. 9. Primary flight display.

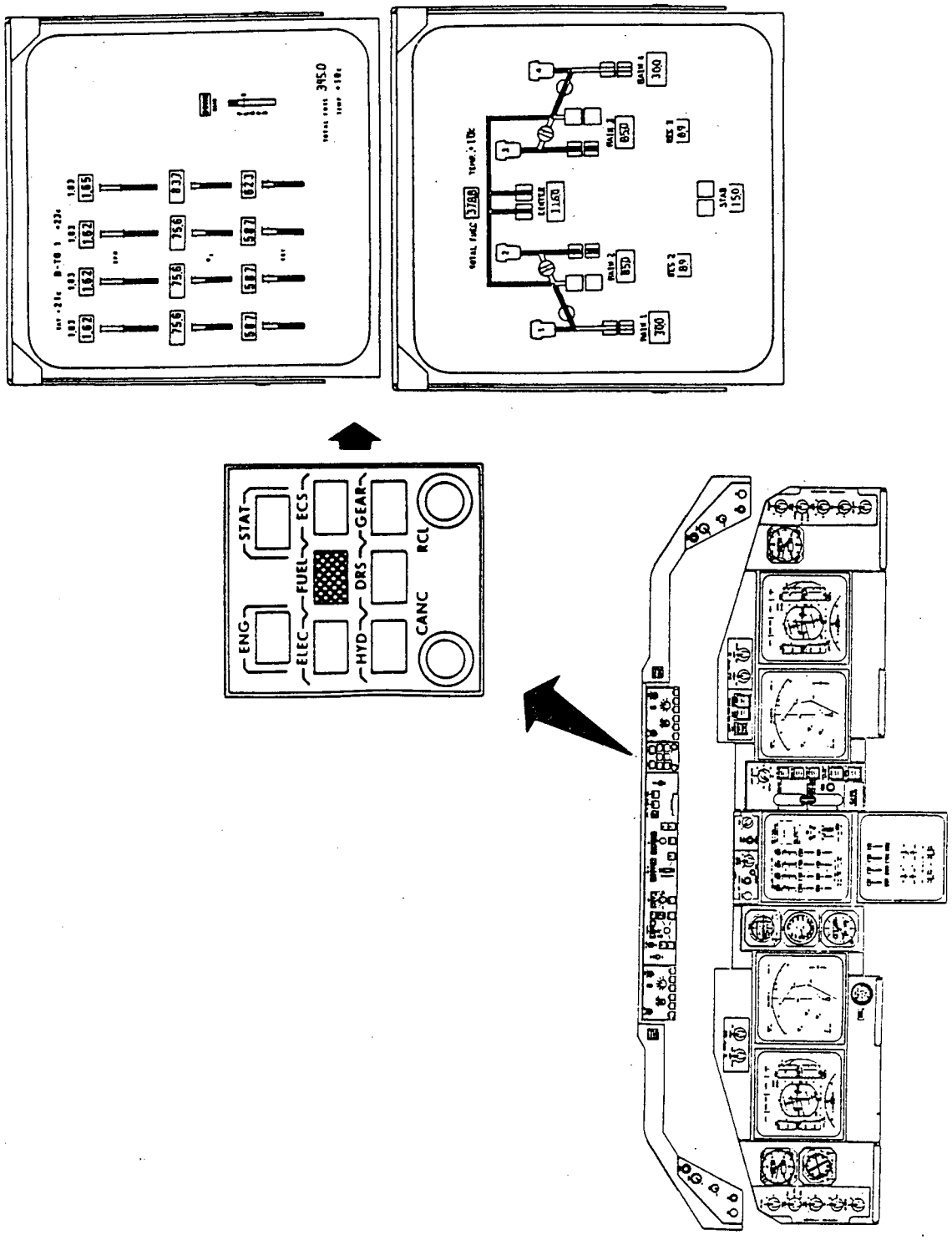

Fig. 10. EICAS control panel and display.

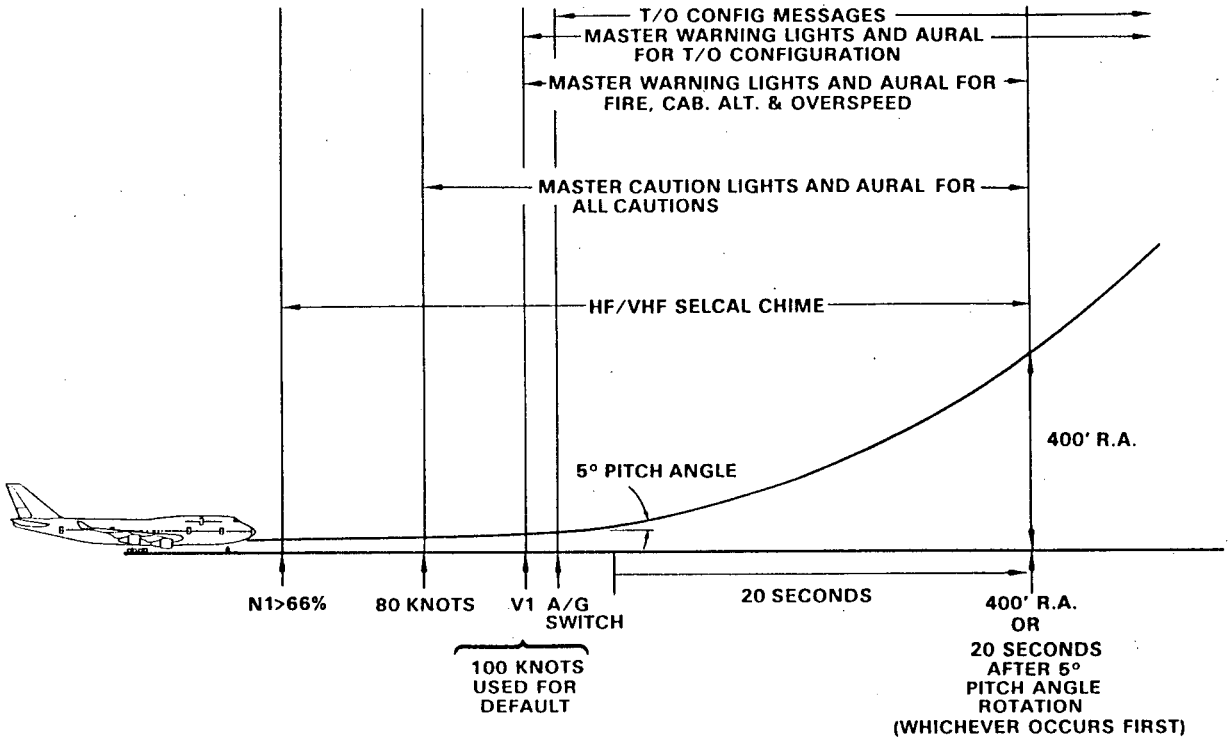

Fig. 11. Take off inhibit.

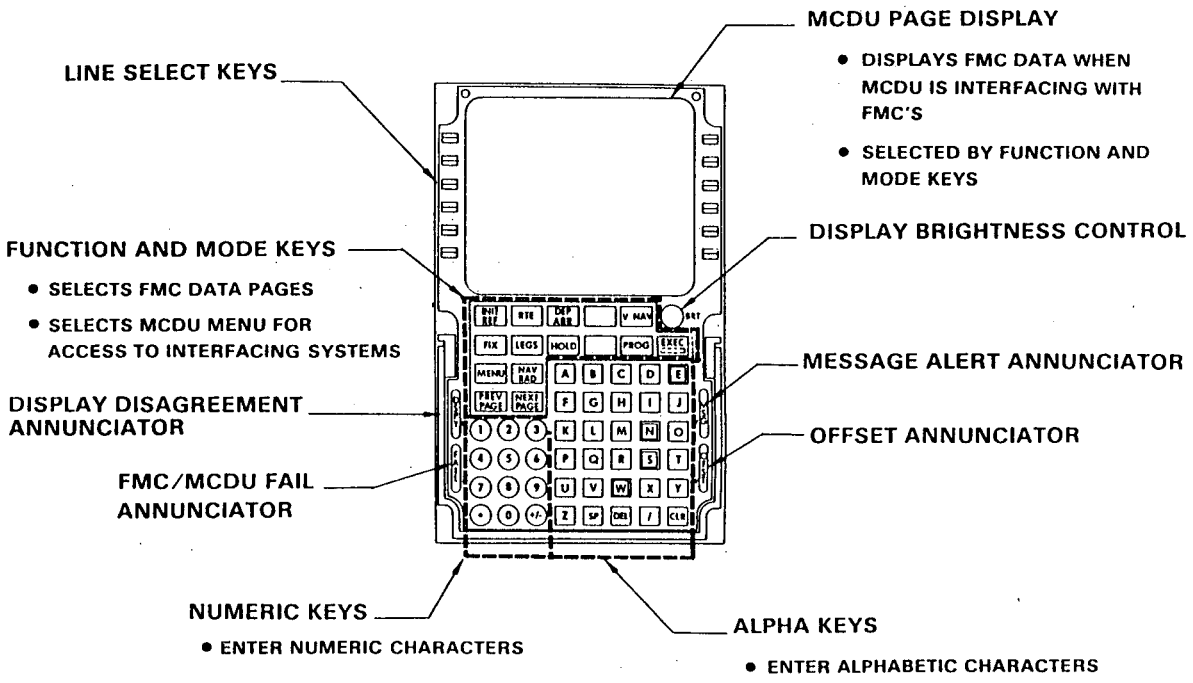

Fig. 12. Multipurpose Control Display Unit.

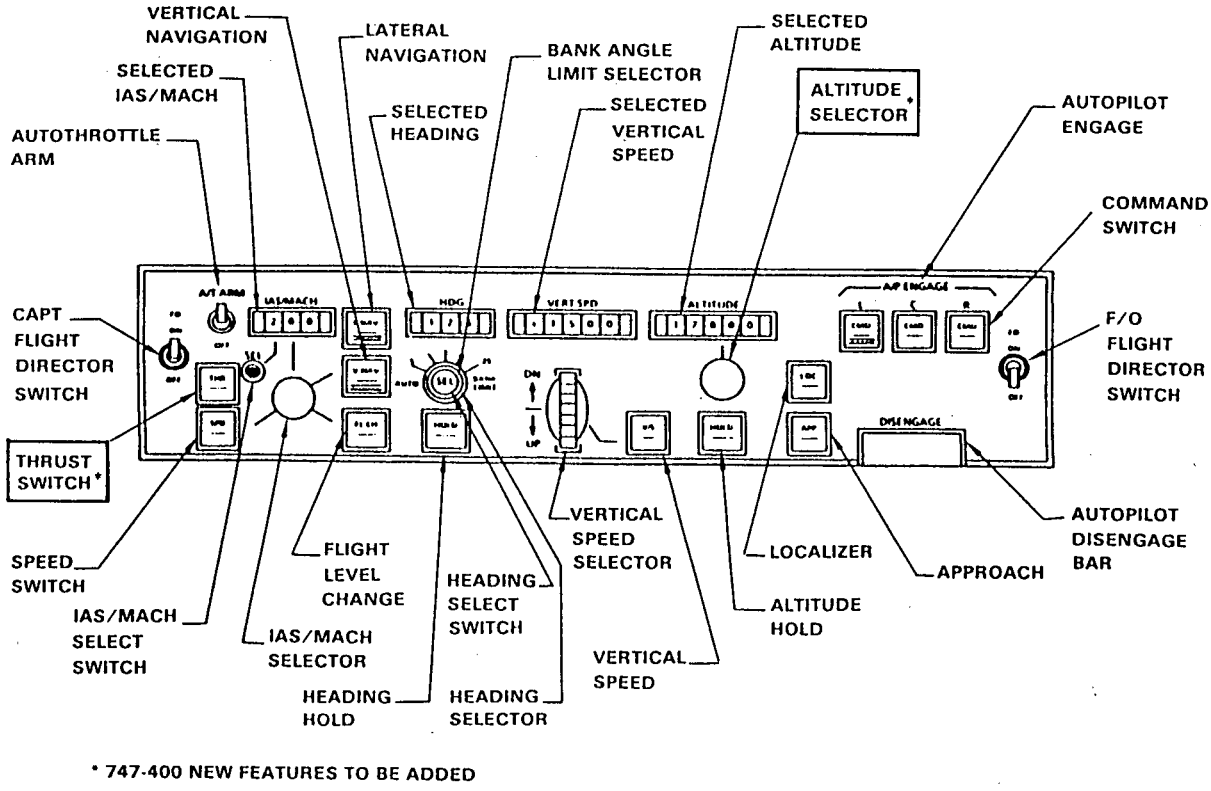

Fig. 13. Autoflight Mode Control Panel.

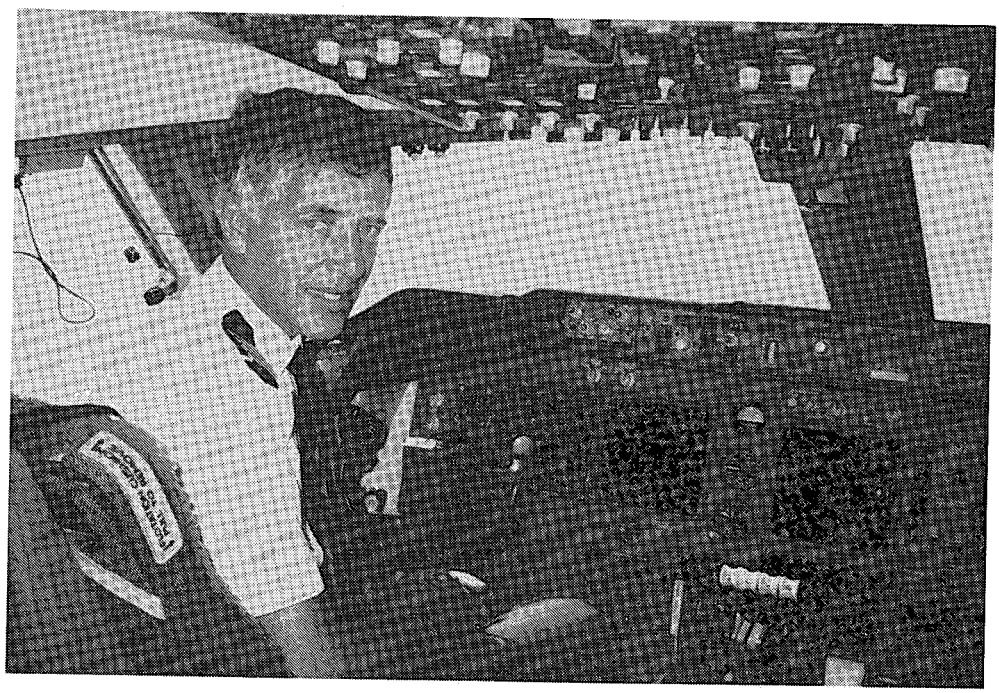

Fig. 14. Me and the B747-400.

SEMI PASSIVE ATTITUDE STABILIZATION FOR A GEODETIC SATELLITE

P.Ph. van den Broek

Delft University of Technology

Summary.

In this paper a stabilization concept for a geodetic satellite is described. In view of the pointing requirements passive gravity gradient stabilization could be applied. For thermal control it would be useful to to rotate the satellite about its vertical axis. It is proposed to eliminate the resulting gyroscopic cross coupling effect by employing a counter rotating flywheel. The paper describes the system, some of the critical aspects and the reliability of the total system.

1. Introduction.

In the early days of spaceflight a considerable number of artificial satellites were attitude stabilized by passive stabilization. In this type of stabilization natural effects on the satellite were used to maintain the satellite in a more or less fixed attitude (refs. 1-4). These effects comprise natural, external torques and gyroscopic effects. One appropriate natural torque was increased by proper shaping of the satellite, or the satellite was given a rotation about one principal axis, whereas the other torques were minimized. This stabilization had no, or very few, moving parts and therefore it was very simple and reliable. On the other hand, the natural torques are relatively weak as compared to some of the disturbances, which limited the accuracy of the attitude. As the reliability of active systems have increased tremendously over the years,and as the pointing accuracy requirements became more and more demanding, passive stabilization is not often used in current satellites. Still for applications where a low pointing accuracy is sufficient and reliability and simplicity are important it may be worthwhile to consider passive stabilization.

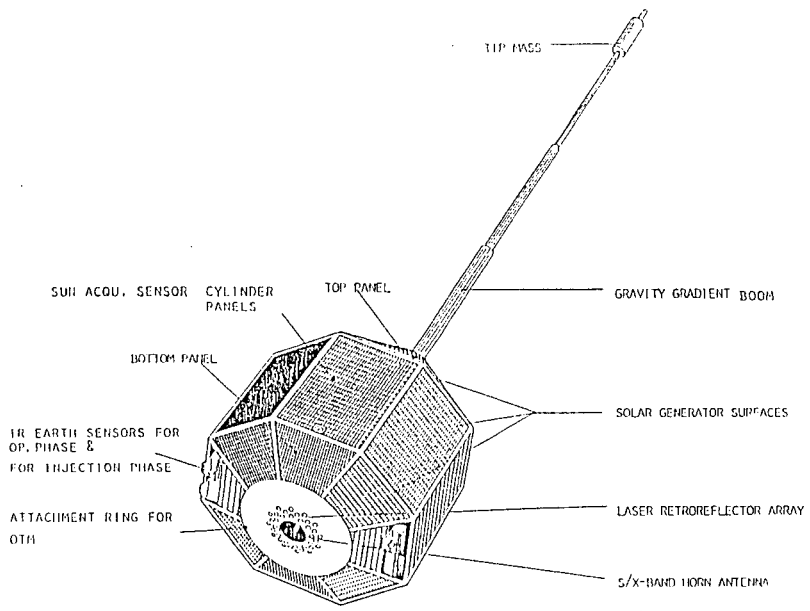

Fig. 1. The POPSAT satellite.

In this paper a possible application of passive gravity gradient stabilization for the proposed geodetic satellite POPSAT (fig. 1) is discussed. This concept of a geodetic satellite (ref. 7), studied by ESA from 1983 to 1987, has now been stopped and replaced by ARISTOTELES geopotential fields mission. Nevertheless some interesting results for a non-classical variant of the gravity gradient stabilization will be presented. The requirements for the attitude are quite moderate, so that passive stabilization is very well feasible. However, for thermal control of the spacecraft it would be useful to rotate the satellite. As

the direction of the vertical axis should be fixed, the satellite would have to rotate about this vertical axis. Such a rotation would introduce severe gyroscopic effects. To eliminate these effects it is proposed in this paper to equip the satellite with a counter rotating flywheel.

In section 2 of this paper some aspects of passive stabilization, and in particular of gravity gradient stabilization will be presented. In section 3 a global description of the POPSAT satellite will be given. The stabilization concept for the POPSAT satellite will be explained in section 4 and some additional comments will be given in section 5.

2. Passive attitude stabilization

Passive attitude stabilization comprises those stabilization techniques, in which the attitude is fixed to a certain accuracy by natural effects. This is in contrast to active systems, where the attitude is fixed by a closed loop system, comprising sensors, actuators and a controller. One class of passive stabilization concepts employs natural torques.

In general, torques on a satellite may be due to four different causes, (refs. 1,2) viz.

1) the earth's magnetic field,
2) aerodynamic forces,
3) gravity gradient effects, and
4) solar radiation pressure.

In passive stabilization the torque resulting from one of these causes is maximized, by proper shaping of the satellite, whereas the other torques, then acting as disturbances, are minimized. As an example, if the torque due to aerodynamic forces is selected as stabilizing torque, the satellite might be equipped with a vane, analogous to the tail of an arrow. Thus the longitudinal axis of the spacecraft tends to be aligned with the velocity vector. It may be noted that the restoring torque is generated in a natural way, determined by the shape of the satellite and without any moving parts. This is characteristic for all types of passive stabilization and therefore passive stabilization is very reliable. It must be admitted however, that in addition to the restoring torque, which yields the static stability, also some damping is required, to damp the oscillatory motions. Those damping mechanisms are in general fairly simple in construction, so that they do not reduce the total systems reliability. Because of this, passive systems may be good candidates for long duration missions.

However, a few factors reduce the applicability of passive systems. One of these is the attitude accuracy that can be realized. In the equilibrium state, the restoring torque is equal in magnitude to the disturbing torque. If the restoring torque per unit attitude deviation is small, compared to the disturbances, then large deviations will occur. The external torques depend on the altitude of the orbit (refs. 1,4). In general, it may be stated, that in low and medium altitude orbits ($h < 20.000$ km) the forces due to solar radiation pressure are very small, and consequently, the resulting torque per unit attitude deviation is small. This eliminates solar radiation pressure as a viable option. In a low orbit, ($h < 500$ km) the aerodynamic effects are considerable. As such aerodynamic torques could be used, if the

stabilized attitude (one axis parallel to the velocity vector) is useful. However, in a low orbit the aerodynamic drag also affects the orbit considerably, in the sense that it reduces the lifetime of the satellite. Then the most significant benefit of a passive system, being the reliability, is of less importance. Because of these limitations only magnetic effects and the gravity have been applied for passive stabilization. Magnetic stabilization aligns one satellite axis parallel to the local magnetic field vector, comparable to the alignment of a magnetic compass. The gradient of the gravity tends to align one satellite axis parallel to the local vertical. As in many satellite missions it is required that one side of the vehicle is pointing to the earth, gravity gradient stabilization is an interesting option. Therefore, the gravity gradient torque will be discussed in some detail. However, it will be pointed out, that the restoring torque is rather small, and therefore it is not applicable if a high pointing accuracy is required.

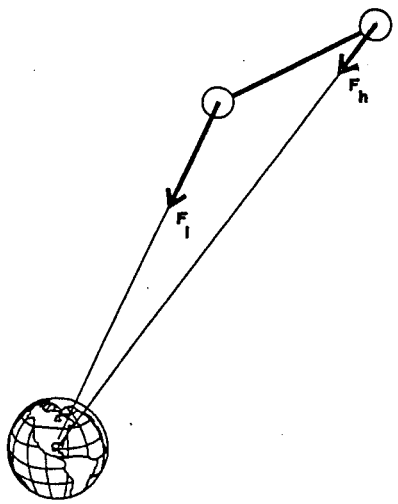

Fig. 2. Forces causing the gravity gradient torque.

The gravity gradient torque is caused by the fact that the gravity force decreases if the distance to the center of the earth increases. If a dumbbell shaped satellite is considered, consisting of two equal masses (see fig. 2), then the gravity force F_l on the lower mass is larger than the force F_h on the higher mass. The resulting force keeps the satellite in its orbit around the earth. The difference between the forces F_h and F_l, both in magnitude and in direction, yields a torque, that tends to align the connecting rod between the masses parallel to the local vertical. For an arbitrarily shaped satellite the components of the

torque along the principal axes of the satellite may be given by (ref. 2):

$$T_{gg} = 3\,\Omega_0^2\, U_R \times \bar{I} \cdot U_R \qquad (2\text{-}1)$$

where Ω_0 = orbital frequency
= $2\pi/T$, T = orbital period,
U_R = unit vector along the local vertical, and
$\bar{I}$ = inertia tensor

If the torque is expressed in components along the principal axes, the inertia tensor is:

$$\bar{I} = \begin{bmatrix} I_x & 0 & 0 \\ 0 & I_y & 0 \\ 0 & 0 & I_z \end{bmatrix}$$

The differences in forces due to the gravity gradient are very small, and thus the resulting torques are small as well. This is confirmed by the expressions (2-1), where the orbital frequency Ω_0 is of the order of 10^{-3} or less.

Another type of stabilization, which can be considered as passive stabilization, is spin stabilization (refs. 1,2). This is based on the fact, that the angular momentum vector of a rotating body is constant in inertial space if the external torques are zero. In its simples form this is achieved by rotating a satellite about its principle axis with the largest moment of inertia. Usually such a satellite is shaped more or less rotationally symmetric about the rotation axis. If the external torques are zero, this axis will maintain its direction in inertial space. In terrestial applications this principle is used in directional gyros and artificial horizons in aircraft. However, if the external torques are non zero the satellite axis will drift away from its initial direction. The motion of the angular momentum vector is given by the expression (ref.2):

$$T = \frac{dB}{dt} = \frac{\partial B}{\partial t} + \Omega \times B \qquad (2\text{-}2)$$

In this expression $\frac{dB}{dt}$ is the derivative of B relative to an inertially fixed reference frame. The derivative $\frac{\partial B}{\partial t}$ is the rate of change of the components of B relative to a reference frame, that itself rotates with an angular velocity Ω. For spinning satellites the rotating frame is often selected with one axis parallel to the momentum vector B. If

furthermore the magnitude of the rotation rate and thus the magnitude of the angular momentum vector is constant then $\frac{\partial B}{\partial t} = 0$, and Ω is the angular drift of the momentum vector. Expression (2-2) shows that for a given disturbing torque T the drift rate Ω may be reduced by increasing the angular momentum B. This may be realized by increasing the rotation rate of the satellite. On the other hand, if a non zero drift is required, for instance to rotate the angular momentum vector to a predetermined attitude, expression (2-2) shows, that a torque

$$T = \Omega \times B \qquad (2\text{-}3)$$

has to be applied.

Because of its simplicity spin stabilization has widely been applied. Drawbacks are that the spin rate has to be maintained between certain limits, and that the spin axis drift has to be corrected from time to time. These phenomena require some (active) control in the system. It may be applied with relatively large intervals, so that the system is passive most of the time.

3. The POPSAT satellite

The POPSAT system was a geodetic satellite-based system, that was proposed for realization in the mid 1990's (ref. 7). As stated before, the project has been abandoned in 1987. The system was conceived for two main purposes:

1. To position points on the earth surface with respect to the center of mass to an accuracy of less better $\pm$ 10 cm and relative to each other with an accuracy of better than $\pm$ 5 cm.
2. To monitor the earth's rotation rate or its revolution time to an accuracy of better than 0.5 ms and the spin axis motion to an accuracy of better than $\pm$ 10 cm on a continuous basis for averaging intervals of one day.

The system would comprise a space segment and a number of ground stations. The space segment (fig. 1) consists of one satellite in a high inclination orbit at an altitude of 7000 km. For the determination of the orbital and geodetic parameters and the point positioning precise and frequent tracking is required. To this end the satellite is equipped with a Microwave Tracking System (MTS). This would provide an all-day, all-weather range and range-rate measuring capability, delivering range measurements to ground stations with random errors less than 10 cm, as well as range-rate measurements. In addition to this system the satellite would carry a retro reflector array to enable tracking by laser ground stations. This laser tracking system could be used only during favorable weather conditions to contribute to the calibration of the microwave tracking system.

The orbit of the satellite is defined as the trajectory of the satellite's center of mass. The range measurements are measured to the appropriate instrumentation equipment, viz. the microwave antenna or the laser reflector. In view of the accuracy of the range measurements and

the fact that the equipment and the mass center are separated over some distance, the attitude of the satellite is important. This leads to the requirement that the antenna pointing accuracy has to be within 3 degrees of nadir and it should be known to within ± 1 degree accuracy. This means for the attitude of the spacecraft, that the antenna axis should be aligned within 3 degrees from the local vertical, thus the attitude control requirements are rather moderate and the stabilization could be accomplished by means of the gravity gradient. The stabilization may be supported by active control with magnetic coils, e.g. for initial attitude aquisition and damping of librational oscillations.

The tracking data from sixteen dedicated MTS-tracking stations are used to reconstruct the orbit and geodetic parameters and for point positioning. These are performed with a common software program. The equations of motion for the satellite contain dynamic gravitational and non-gravitational force field models. Forces which have measurable effects on the POPSAT orbit are earth gravitation, direct lunar and solar attraction, earth and ocean tides, as well as solar, albedo, earth radiation and photonic thrust. Earth gravitation effects will be refined by establishing a dedicated POPSAT gravity model during the initial mission phase. For the non-gravitational surface force, modelling has been adopted for the POPSAT system.

One of the effects to be included in the model is the photonic thrust, caused by temperature differences on the outer skin of the spacecraft. To take into account these effects the surface temperature should be measured at 5 minutes intervals at about 50 nodes on the spacecraft shell. The need for modelling these temperature effects and the equipment for skin temperature measurements could be eliminated if a uniform temperature distribution over the spacecraft skin could be realized. A simple way to achieve this is to rotate the satellite with a constant speed. This would mean for POPSAT that the satellite should be spinning about its antenna axis, as the direction of this axis should remain pointing to nadir. However, this reference direction rotates in inertial space with a low speed of one revolution per orbital period. It will be shown that the gravity gradient torques are by far insufficient to maintain the antenna axis vertical, due to the gyroscopic cross coupling effects. In the remaining part of this paper a method will be discussed, which should eliminate these effects. Thus a stabilization system, based on the gravity gradient will be combined with the benefits of a rotating spacecraft to realize a uniform temperature distribution.

4. POPSAT gravity gradient stabilization.

4.1. Satellite data.

As indicated in the preceding section, the attitude requirements for POPSAT are rather modest: Earth pointing with an accuracy of 3 degrees. In principle this could be achieved using gravity gradient stabilization. To minimize temperature differences on the outer skin it would be useful to rotate the satellite about its vertical axis.

To implement the gravity gradient stabilization the satellite is configured as depicted in fig. 1. It consists of a main body and a stabilizing mass, attached to an extendible boom. From eq. 2-1 it can be seen, that the stabilizing torques depend on the moments of inertia. For the following discussion it will be assumed, that the moments of inertia of the POPSAT satellite about the nominally horizontal axes are equal:

$$I_x = I_y = 2050 \text{ kgm}^2 \qquad (4\text{-}1)$$

whereas the moment of inertia about the nominally vertical axis is

$$I_z = 315 \text{ kgm}^2 \qquad (4\text{-}2)$$

As mentioned in section 3, the orbital altitude is h= 7000 km. The orbital period of a satellite in such an orbit is

$$T = 4 \text{ hr } 16 \text{ m}$$

and the orbital frequency is

$$\Omega_0 = 4.08\ 10^{-4} \text{ s}^{-1} \qquad (4\text{-}3)$$

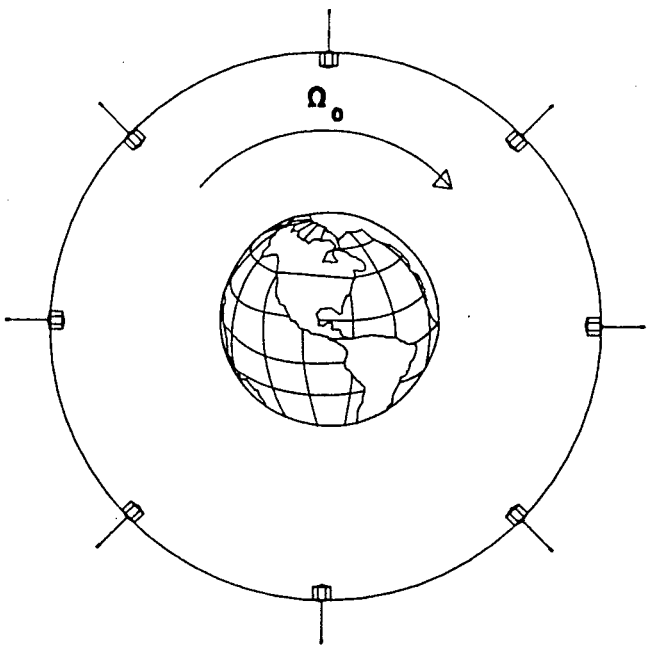

Fig. 3. The motion of the satellite in its orbit.

Usually the attitude of a satellite is defined as the attitude of a body fixed axes frame with respect to a reference frame. In this paper the possibilities of rotating the satellite about its vertical axis is considered, while the attitude angle about the vertical axis is not relevant. As a matter of fact only the attitude of the microwave antenna with respect to the local vertical is important. Therefore the attitude of the antenna axis is defined using a satellite axes frame, which does not rotate with the satellite. The Z_s-axis coincides with the nominally vertical antenna axis of the satellite, positive in the downward direction. The X_s-axis is normal to the Z_s-axis and is parallel to the orbital plane, positive in the direction of the velocity vector, and the Y_s-axis completes the right handed axes frame. Consequently, the yaw angle ψ of this frame is zero by definition.

The motion of the satellite in its orbit is depicted in fig 3. This shows that the satellite is rotating in inertial space at the low speed of 1 revolution per orbit. If the satellite maintains a constant attitude with respect to the local vertical reference frame the angular velocity vector Ω of the satellite frame, resolved in components along this frame, is for small attitude angles ϕ and θ (see fig.4):

$$\Omega = \begin{bmatrix} 0 \\ -\Omega_0 \\ \Omega_0 \, \phi \end{bmatrix} \qquad (4\text{-}4)$$

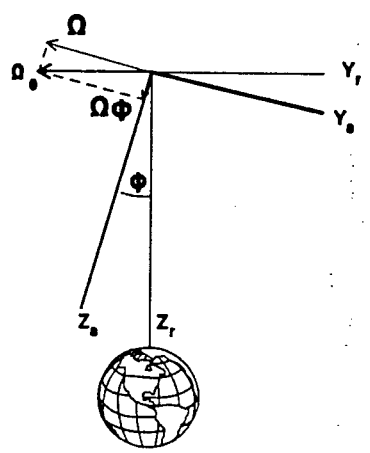

Fig. 4. The angular velocity vector of the satellite frame

and the angular momentum vector is (see fig. 5):

$$B = \begin{bmatrix} 0 \\ -\Omega_0 I_y \\ \Omega_0 I_z \phi \end{bmatrix}$$

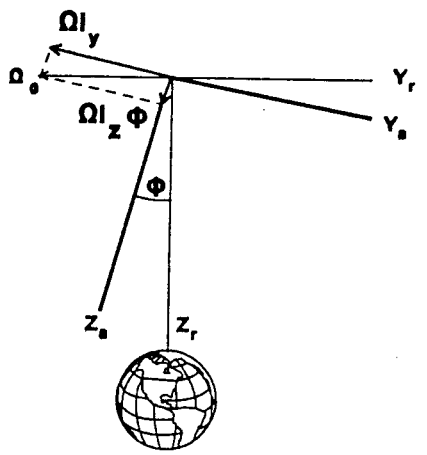

Fig. 5. The angular momentum of the non rotating satellite.

If the satellite is rotating about the Z_s-axis, with a speed of ω_z, defined as the speed of the satellite with respect to the satellite axis frame, the angular velocity vector Ω_0 remains unchanged, but the angular momentum vector becomes (fig. 6):

$$B = \begin{bmatrix} 0 \\ -\Omega_0 I_y \\ (\omega + \Omega_0 \phi) I_z \end{bmatrix} \qquad (4\text{-}5)$$

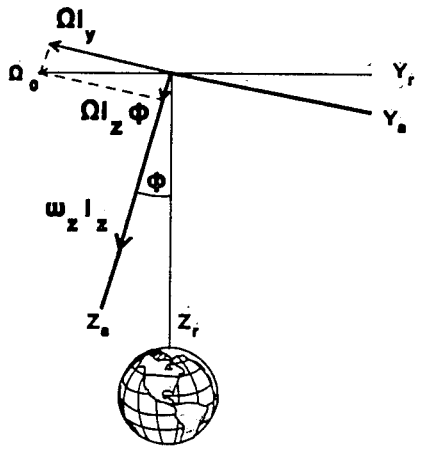

Fig. 6. The angular momentum of the rotating satellite.

4.2. Uncompensated satellite rotation.

The gravity gradient torque, acting on the satellite, may be calculated using the data given in (4-1) through (4-3). If the attitude deviates by a small angle ϕ about the X_s-axis and a small angle θ about the Y_s-axis, it can be found from eq. (2-1) that:

$$T_{gg} = \begin{bmatrix} -8.66\ 10^{-4} \\ -8.66\ 10^{-4} \\ 0 \end{bmatrix} \qquad (4\text{-}6)$$

where the attitude deviations are measured in radians.
Although this torque is quite small (the maximum attitude deviations should be less than 3 degrees = 0.052 rad), it may be applied for attitude stabilization, provided that the disturbances are still smaller than the maximum achievable gravity gradient torque.

It follows from eq. (2-3) that, to maintain a fixed attitude of the satellite with respect to the rotating local vertical frame, an external torque has to be applied (see fig.7).

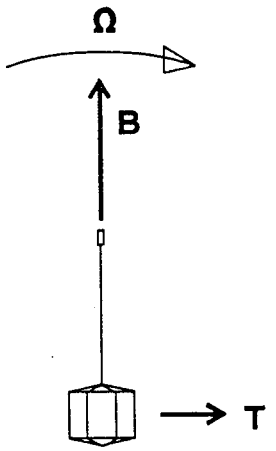

Fig. 7. The torque required to rotate the angular momentum.

Substituting (4-4) and (4-5) in (2-3), and taking (4-3) for the angular velocity of the satellite frame the required torque can be expressed by:

$$T_r = \begin{bmatrix} -0.129\ \omega_z + 2.89\ 10^{-4}\phi \\ 0 \\ 0 \end{bmatrix} \qquad (4\text{-}7)$$

If only unmodified gravity gradient stabilization is applied, this torque has to be generated by the stabilizing gravity gradient torque T_{gg}, given by (4-6). Equating (4-6) and (4-7) yields a relation between the rotation speed and the attitude deviations in the equilibrium state:

$$-8.66\ 10^{-4}\ \phi = -0.129\ \omega_z + 2.89\ 10^{-4}\phi$$

$$-8.66\ 10^{-4}\ \theta = 0$$

which gives the equilibrium attitude of the antenna axis.

$$\phi = 0.112\ 10^{3}\ \omega_z$$

$$\theta = 0$$

Taking into account that the maximum allowed attitude deviation is 3 degrees = 0.052 rad. the maximum rotation speed of the satellite would be:

$$\omega_z = 4.64\ 10^{-4}\ s^{-1} = 1.14\ \Omega_0$$

This is about the same speed as the orbital frequency. This speed will be insufficient for adequate thermal control. However, if the satellite rotates at a much higher speed, e.g. two or three orders of magnitude, the required stabilizing torques will be proportionally larger. In principle, such torques might be realized by reconfiguring the satellite (e.g. a much longer boom to increase the difference between the moments of inertia), but that possibility will not be discussed in this paper. A faster rotating satellite will behave like a spin stabilized satellite. To some extent its motion will be disturbed by gravity gradient torques, but its rotation axis will remain basically fixed in inertial space.

4.3. Gyroscopic compensation.

Unmodified gravity gradient stabilization cannot be applied to the rotating satellite due to the gyroscopic stiffness of the rotating body. This effect can be eliminated by providing the satellite with a counter rotating flywheel. The spin axis of this wheel should be parallel to the Z_s-axis of the satellite and the rotation direction should be opposite to the rotation of the satellite itself.The wheel speed should be such that, in the nominal attitude, the component of its angular momentum along the Z_s-axis is equal (but opposite) to the component of the angular momentum of the satellite itself along the same axis. The component of the angular momentum along the Z_s-axis, due to the satellite rotation is $I_z\omega_z$. The component due to the wheel is $I_w\omega_w$. Thus the wheel speed should be:

$$\omega_w = -\frac{I_z}{I_w}\,\omega_z \qquad (4\text{-}8)$$

The effect of this compensating wheel can be explained in two ways. The first way is somewhat mathematically oriented, the second is more physically oriented.

The angular momentum of the satellite system, including the wheel, is the sum of the angular momentum of the satellite itself and that of the wheel. The contribution of the satellite is given by (4-5), analogous the contribution of the wheel may be given by:

$$B_w = \begin{bmatrix} 0 \\ -\Omega_0 I_{w,y} \\ (\omega_w + \Omega_0 \phi) I_w \end{bmatrix}$$

so that the total angular momentum vector becomes (fig. 8):

$$B_t = \begin{bmatrix} 0 \\ -\Omega_0 (I_y + I_{w,y}) \\ (\omega_z + \Omega_0 \phi) I_z + (\omega_w + \Omega_0 \phi) I_w \end{bmatrix}$$

In this expression $I_{w,y}$ is the moment of inertia of the wheel about an axis normal to the spin axis.

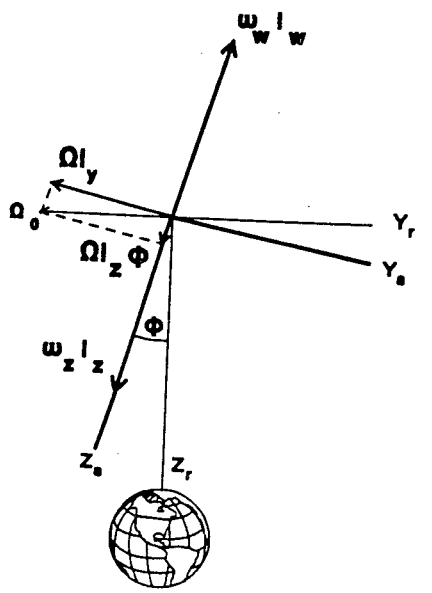

Fig. 8. The angular momentum of the compensated satellite.

Substitution of (4-8) yields:

$$B_t = \begin{bmatrix} 0 \\ -\Omega_0 (I_y + I_{w,y}) \\ \Omega_0 (I_z + I_w) \phi \end{bmatrix} \approx \begin{bmatrix} 0 \\ -\Omega_0 I_y \\ \Omega_o I_z \end{bmatrix} \quad (4\text{-}9)$$

For simplicity, it has been assumed here that $I_{w,y} << I_y$ and $I_w << I_z$, or alternatively, that the contribution of the wheel is included in I_y and I_z. From the second form of (4-9) it can be concluded that the angular momentum of the compensated rotating satellite is equal to the angular momentum of the non-spinning satellite.

Once again, the torque required to keep the satellite in a fixed attitude with respect to the rotating local frame follows from (2-3). Substitution of (4-4) and (4-9) yields:

$$T_r = \begin{bmatrix} 2.89\ 10^{-4}\phi \\ 0 \\ 0 \end{bmatrix}$$

This expression shows, that in this case, a torque proportion to the roll angle ϕ is required to maintain this roll angle. This torque requirement is due to gyroscopic effects. If this torque is not applied the satellite will tend to reduce its roll angle. It may be noted that the gyroscopic effect amplify the restoring torque due to the gravity gradient. If the roll angle ϕ and the pitch angle θ are zero, no torque is required and then the satellite assumes its equilibrium attitude.

The effect of the compensating wheel can also be explained in a more physical way.

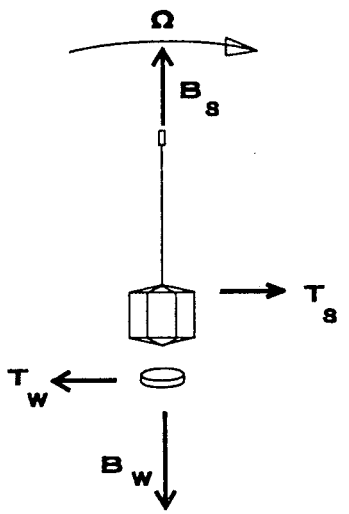

Fig. 9. The gyroscopic interaction between satellite and wheel

For the satellite to maintain its required attitude a torque has to be applied (see e.(2-3)). If a wheel is added, it can be shown in an analogous way, that a torque has to be applied to this wheel as well to keep its rotation axis parallel to the Z_s-axis of the satellite (see fig. 9). The angular momentum of the wheel is chosen equal in magnitude but opposite to the angular momentum of the satellite, so that the torque required for the wheel is equal and opposite to the torque required by the satellite. By connecting the wheel and the satellite the torque on the satellite is provided by the wheel and conversely, according to Newton's third law, the reaction torque from the satellite is provided to the wheel.

In the preceding discussion it has been shown, that a combination of gravity gradient stabilization for attitude stabilization and rotation of the satellite about the local vertical for thermal control is in principle feasible. This concept is based on the fact, that the angular momentum of the satellite is compensated by a counter rotating flywheel. If, however, this compensation is insufficient, i.e. when the wheel speed does not match the satellite speed sufficiently, then attitude deviation may be expected. From the discussion, presented in section 4.2, it may be expected, that the satellite speed should not deviate more than about one revolution per orbit from the nominal value, determined by the relation (4-8). Therefore it will be necessary to determine the required wheel speed and the corresponding satellite speed very accurately. Subsequently the wheel speed and the satellite speed should be controlled very accurately.

The counter rotating wheel compensates for the gyroscopic effects, but the motion as a gravity gradient stabilized satellite will not be affected. Due to disturbances the satellite may perform slow oscillations about the X_s-axis and about the Y_s-axis. It may also be necessary to provide a additional system to damp these librational motions.

5. Additional control.

In this section some remarks and suggestions will be made on the additional control for the satellite speed, the wheel speed and the libration damping. In this paper no extensive discussion will be given, but merely some suggestions that may be developed into feasible concepts. In this area more research will be needed.

5.1. Rotation speed control.

One requirement for the stabilization is, that the wheel speed and the satellite rotation speed are controlled very accurately. The absolute value of the speeds will not be very critical, but the ratio should be equal to the ratio given by (4-8) with a high accuracy. The angular velocity of the satellite frame Ω_0 is rather small and consequently attitude errors due to gyroscopic effects will build up slowly. Therefore it is expected that relatively short term deviations of one of

the speeds is not very harmful, as long the value averaged over e.g. one orbital period is correct.

To control the satellite rotation speed and the wheel speed these variables have to be measured. The wheel speed can be measured with the required accuracy by counting revolutions over a sufficiently long period of time. In particular, if a direct current drive motor is used, the commutation pulses may very well be counted. By controlling the power to the drive motor the wheel speed can be adjusted if necessary. An alternate wheel speed control might be the application of a synchronous drive motor. Based on such reasoning it is assumed that the wheel speed, at least with respect to the satellite, can be kept at an appropriate value with sufficient accuracy.

The measurement and control of the satellite rotation rate may be somewhat more complicated. It might be feasible to measure the speed employing a gyroscope. In that case a ring laser gyro could be preferred, as the reliability of a mechanical gyro may be insufficient. As also in this case the average speed over a longer period is sufficient, the revolutions of the satellite may be counted. This can be performed, employing a slit type sun sensor or possibly a magnetometer.

If the rotation speed is not correct, it has to be adjusted, while the wheel speed has to be kept constant. As a matter of fact, the angular momentum of the satellite along the Z_s-axis is not zero, so that angular momentum has to be added to or removed from the satellite-wheel system. This can only be realized by generating an external torque along the Z_s-axis.

Conversely, if at a certain time the angular momentum is correct, a deviation can only build up from external torques. The possible causes for disturbing torques are listed in section 2. Out of these, only the magnetic field of the earth may cause a reduction in satellite speed, by generating eddy currents or magnetic hysteresis in the rotating satellite. As obviously the magnetic field is strong enough to reduce the speed, is can also be employed to increase the speed. To this end the satellite has to be equipped with magnetic coils in one plane, parallel to the Z_s-axis or two coils, mutually perpendicular and parallel to the Z_s-axis. To switch these coils in the proper sequence the direction of the external magnetic field has to be measured, so that the satellite has to be in equipped with a magnetometer.

Thus far it has been assumed that the required rotation speeds are known, or alternatively that if the wheel speed is kept at a fixed value, the corresponding satellite speed is known. In view of the required accuracy it will probably not be possible to determine the values pre-flight. Therefore, the required values have to be determined in flight, during the initial phase after injection into orbit. The procedure could be as follows.

Initially the satellite rotation is reduced to zero and the Z_s-axis is aligned with the local vertical. This is in fact a standard procedure

for any gravity gradient stabilized satellite and it may be performed using magnetic coils and the magnetometer. Next, the wheel speed is set to and maintained at an appropriate value, that may be equal to the operational value. Then, the resulting satellite rotation speed is measured. The ratio between the wheel speed and the satellite speed is to be maintained throughout the satellites operational lifetime.

In this procedure it is assumed that the satellite speed is constant during the measurement of this speed. If the speed is measured by counting revolutions during e.g. one orbital period, it is assumed that braking effects due to the earth magnetic field are negligible. If this condition is not met, a not quite correct value will be determined but, hopefully, the error will be sufficiently small to reach an acceptable gravity gradient stabilization. From observations, to be made on the subsequent satellite motion, the error may be determined and corrected.

It should be emphasized, that in this section only suggestions have been made that might have been developed into a working system. In particular for the procedure for the required satellite speed determination and control further studies and simulations would have been needed. Due to the cancellation of the project the required details on the actual satellite will not be available.

5.2. Libration damping

Due to the elimination of the gyroscopic cross coupling effects the satellite will move like a conventional, non spinning gravity gradient stabilized satellite. If no additional measures are taken such a satellite may perform slow oscillations about the X_s-axis and the Y_s-axis. It may be necessary to damp those librational motions to meet the attitude requirements.

For conventional gravity gradient satellites mechanical devices may be used to dissipate excess energy of the libration in a passive way. For the spinning satellite such a solution may be difficult to develop. Therefore, it is suggested to damp the librations using the magnetic field of the earth and one or more magnetic coils in the satellite. In order to damp the motion the attitude and preferably the attitude rate has to be measured. As the motions are very slow, (the frequency is of the same order of magnitude as the orbital frequency), and considering the relatively high rotation speed of the satellite about the Z_s axis, it will not be possible to measure the attitude rate about the horizontal axes with respect to the local vertical reference frame. So, the attitude angles ϕ and θ have to be measured, and using an observer or state reconstructing filter the attitude rates may be determined. The attitude angles about the horizontal axes can be measured by horizon sensors. These would be required also for the conventional POPSAT satellite. As the satellite is spinning, it might be possible to use one sensor for both attitude angles or two sensors may be used giving additional redundancy. Also it may be feasible to use static, non scanning sensors, using the satellite rotation to generate the scan.

Once the characteristics of the libration are determined, appropriate torques have to be generated to effectuate the damping. The torques that can be generated are limited due to the fact that no torque can be generated about the local magnetic field vector. If three mutually perpendicular magnetic coils are used, it may be possible to generate the most effective torque, taking into account the indicated limitation. However, it may very well be sufficient to use only one coil, normal to the Z_s-axis for damping. This would eliminate the need to switch the other coils in phase with the satellite rotation.

From this discussion it may become clear that the libration damping is a rather complex process, for which the feasibility will have to be demonstrated with further analysis and simulations. However, it should be kept in mind that active libration damping for a conventional POPSAT satellite may be complex as well.

6. Reliability

The stabilization of the rotating satellite by the gravity gradient appears to result in a rather complex system. It comprises a spinning flywheel, a subsystem to control the wheel speed and a subsystem to control the satellite speed, both at a high accuracy, and a system for the damping of the librational motion of the satellite. The question arises, wether the reliability of the total system is not reduced to an unacceptable level. In discussing the answer to this question, the total system may be partitioned into two parts, viz.:

1. The subsystem related to the gravity gradient stabilization as such, irrespective of the rotation of the satellite, and
2. The subsystem related to the compensation of the angular momentum of the rotating satellite.

The first mentioned subsystem is in fact the libration damping system. This system consist of horizon sensors, control electronics and magnetic coils. Nowadays the reliability of electronic components is very high, so that it may be assumed that a sufficient total system reliability may be expected. On the other hand, if the damping system fails during the operational phase of the satellite, the pointing accuracy will be reduced, but still a useful stabilization system may be expected. In general, moving mechanical parts may be considered less reliable than fixed parts, due to wearing effects. If in a rotating satellite horizon sensors without moving parts can be used, the reliability of the damping system might even be estimated as somewhat higher than a non rotating satellite, as in that case (mechanical) scanning sensors may be necessary.

In the conventional POPSAT concept, libration damping by a magnetic system, employing horizon sensors, was proposed. Rotating the satellite would not reduce the system reliability as far as libration damping is concerned.

The second subsystem, related to the satellite rotation comprises the flywheel and the speed control systems. Both the wheel speed measurement and control system and the satellite rotation speed control system

consist of non mechanical components, if the wheel drive motor is considered as not being part of the speed control system. In view of the reliability of electronic components, it may be assumed that these systems do not reduce the reliability significantly.

The most critical component may be the flywheel and its drive system. If mechanical bearings (ball bearings) are used, wearing may occur and a reduction in reliability may be expected. If, however, a wheel with a relatively large moment of inertia is employed, the wheel speed will be correspondingly lower according to (4-8). This may increase the reliability. It may also be possible to employ magnetic bearings, thus eliminating mechanical contact between the wheel and the satellite. This could increase the reliability as well.

An important factor in addition to the reliability are the consequences of a failure. Now, if the flywheel would fail, that means, if it would stop rotating, then also the satellite would come to a complete stop, as far as the rotation about the Z_s-axis is concerned. Due to the satellite speed control the net angular momentum about the Z_s-axis is kept at zero at a very high accuracy. This will remain in the event, that the wheel would stop. As a matter of fact the braking process is an internal exchange of angular momentum between the wheel and the satellite, so that no rotations of the satellite about the horizontal axes will be introduced. From that event on the satellite would behave as a conventional, non rotating gravity gradient stabilized satellite. The benefits of the rotation would be lost and the total satellite system performance would be reduced, but still a useful satellite would remain.

Summarizing, it may be stated that the total system reliability may be reduced to some, likely small, extent as compared to a conventional system. But in case of failure still a useful system would survive.

7. Conclusions.

In this paper a system has been described which combines gravity gradient stabilization to point the antenna axis of a microwave tracking system parallel to the local vertical and satellite rotation about the vertical axis for thermal control purposes. It has been shown that simple gravity gradient stabilization is by far insufficient to compensate for the gyroscopic effects of the rotation. Therefore it has been proposed to provide the satellite with a counter rotating flywheel. The speed of this wheel and the rotation speed of the satellite have to be controlled with a very high accuracy. Concepts for the accurate determination of the required values of these variables and the possibilities for control have been described. Additionally, a suggestion for the damping of the natural motions of the gravity gradient satellite have been given. Finally the reliability of the total system has been discussed.

These discussions show that the proposed concept may be expected to be feasible and that the total system reliability would be comparable to the conventional gravity gradient stabilization.

8. References

1. O.H. Gerlach — Attitude Stabilization and Control of Earth Satellites. Report VTH-122. 1965

2. E. Slagmuylders, P.Ph. van den Broek — Passieve Standstabilisatie van Satellieten. Rapport VTH-176. 1975

3. R.H. Cronin, T.R. Kane — Gravitational Stabilization of a Two-body Satellite. Journal of Spacecraft and Rockets, Vol.10 no.5, May 1973

4. N. Ives — Passive and Semi Passive Attitude Control of an Earth Satellite. ESRO-TM.35. 1966

5. L.E. Wiggins — Relative Magnitudes of the Space-environment Torques on a Satellite. AIAA Journal 2.

6. W. Hughes — Environmental Torques on a Satellite. ESRO-TM-28. 1966

7. POPSAT, A Candidate Satellite System for Solid Earth Applications and Sciences. Preliminary Feasibility Study, Final Report Vol.1. ESA contract no. 5309/83/F/CG/SC. November 1983

VISUAL-VESTIBULAR INTERACTION IN PILOT'S PERCEPTION OF AIRCRAFT OR SIMULATOR MOTION

R.J.A.W. Hosman
J.C. van der Vaart

Delft University of Technology

ABSTRACT.

The importance of man's vestibular organs in perceiving cockpit motion in an aircraft or a simulator is nowadays hardly questioned, as witnessed by the present widespread use of six-degrees-of-freedom motion systems for flight simulators. Still more advantage could be gained from the use of moving base simulators.

In order to illustrate this, the paper reviews research on control behaviour and performance of subjects in target following and disturbance tasks. By using results of work by the authors and by others, the importance of peripheral visual and vestibular motion perception in tasks that require inner-loop stabilization, is emphasized. Results of stimulus response experiments, especially designed to gather insight in central and peripheral visual and vestibular perception of motion are summarized and used to explain findings of tracking experiments.

It is concluded that peripheral visual and cockpit motion cues are of paramount importance in actual or simulated manual aircraft control and that, in simulation, the compensation for simulator motion system dynamics, computing time-delays and motion control laws deserve much more attention.

1. INTRODUCTION.

The influence of motion cues on pilot's control behaviour in manual flight control and therefore also in flight simulation are considered much more important than some twenty years ago. As a consequence present day training flight simulators are equipped with six degree of freedom motion systems and the requirements on motion simulation for Phase I, II and III simulators are laid down in the regulations. Due to the subsequent development of visual display systems flight simulation has become a well matured technique with wide applications in pilot training and aerospace research and development.

However, flight simulation in itself will always have certain limitations, mainly in the field of time delays and motion simulation. Because of these limitations manual control of the simulated aircraft is considered a more demanding task then flying of the real aircraft. The present-day shortcomings of flight simulation should not be overemphasized but the authors feel that some further improvement is possible if more is known about the process of perceiving (simulated) aircraft motions.

In manual flight attitude stabilization is the inner loop of aircraft control. Since aircraft are higher order systems, it follows from elementary principles of control theory that for attitude stabilization not only attitude but also angular rate information should be available to the pilot to establish stability.

Experimental research indicate that in many situations, inner loop attitude stabilization may, after some training and at the cost of some mental effort, be attained by using central (or foveal) visual information only, for instance from flight instruments. However, experiments also indicate that the information mediated by peripheral vision and by the vestibular system is much more appropriate for inner loop stabilization. By these modalities, man perceives much more directly the rate of change - first time derivative - of aircraft motion variables.

A long series experiments performed at the Faculty of Aerospace Engineering of the Delft University of Technology yielded a better understanding of the contribution of the visual- and vestibular system to the pilot's perception of aircraft rotary motions. It is evident now that improvements in the motion perception process and the consequential improvements in tracking performance due to peripheral visual and vestibular motion cues results mainly from a faster perception process.

The research summarized in Chapter 2 is concerned with control behaviour and performance of subjects in target following and disturbance compensation tracking tasks. These tasks mainly require short term stabilization and error compensation, the disturbance compensation in fact is a pure stabilization task. In these experiments peripheral field displays and cockpit motion improved tracking performance and changed dynamic behaviour of the pilots if compared to the no-motion case with flight instruments only.

Chapters 3 and 4 are devoted to experiments more specifically aimed at the perception process in these control tasks, i.e. perception of attitude and angular rate by vision (Chapter 3) and perception of aircraft cockpit motion by way of the vestibular system (Chapter 4).

Chapter 5 summarizes the results of these and related experiments by others. Implications of the experimental findings for human vehicle control behaviour and flight simulation are indicated.

2. THE INFLUENCE OF VISUAL AND VESTIBULAR MOTION PERCEPTION ON MAN VEHICLE CONTROL.

A large number of investigations on the influence of motion perception on man-vehicle control were published during the last twenty years [6, 11, 12, 13, 15, 17, 19]. Most of these feature the use of moving base aircraft or car simulators. The amount of experimental data is impressive but results are difficult to compare, firstly due to a wide variety in simulated vehicle dynamics and simulator moving base dynamics, next, due to differences in the type of motion to be controlled. Some experiments are on lineair motion, others on rotational motion.

In addition, two different types of tracking tasks may be distinguished. It is well known that in disturbance compensation tasks and target following tasks, see Fig. 2.1, cockpit motion has a completely different effect on subject's control behaviour [6, 12], although performance improves in either case.

Apart from these there may be differences in the visual displays and in the error scores to be minimized by subjects. Moreover subjects may range from naïve non-pilots in one experiment to experienced professional pilots in another.

In spite of these mayor and minor differences in experimental apparatus and set-up, it is now well established that vestibular motion cues and peripheral visual cues have a beneficial effect on subject's performance (more accurate tracking) and that they do change subject's control behaviour.

The influence of motion perception on tracking performance and control behaviour will be illustrated by results of roll tracking tasks only, since these tasks are most extensively documented. In these tasks, there are three major sources of information to the subject for perceiving aircraft roll motion.

- central visual information on the artificial horizon (central display)
- peripheral visual information from the outside world and
- cockpit roll motion as perceived by the vestibular system.

Examples of experiments featuring one or more of these sources of motion information can be found in the references [6, 11, 12, 13, 15, 17, 19]. Peripheral visual stimuli were used in several research programs [6, 15]. They were presented to subjects by vertically moving checkerboard or horizontal stripes patterns on two TV monitors, see Fig. 2.2. In some cases cockpit motion is "displayed" to subjects with a certain time-delay due to the dynamic characteristics of the simulator motion system. For compensatory tracking experiments, it is essential that motion cues presented by the visual displays and the motion system are accurately synchronized.

Before considering a number of results into more detail, it may be worthwhile to mention that a general conclusion to be drawn from all experiments is, that peripheral field displays and cockpit motion have a similar influence on tracking performance and control behaviour when added to a central display. This holds for disturbance tasks and for following tasks alike. In both cases changes in performance and subject's dynamic behaviour are, as a rule, larger due to cockpit motion than due to peripheral visual cues.

For a more detailed analysis, the results of compensatory tracking tasks by the present authors [6] are now considered. A disturbance task and

a target following task were done with a double integrator (K/s^2) as the controlled element. Disturbance tasks were run with all (7) combinations of the central display (C), peripheral displays (P) and cockpit motion (M), target following tasks were, by necessity, only run with combinations of displays featuring the central display (C, CP, CM, CPM). Since simulator and controlled element dynamics, visual displays and the general experimental set-up and procedures remained unchanged in these experiments, they offer a sound basis of comparison for the effect of several motion cues for the two types of control tasks.

Fig. 2.3 shows the tracking error standard deviation as a function of display condition. The trend of these data corresponds very well with performance data of others.

In order to express measured control behaviour by a small number of parameters, the quasi lineair human operator model by McRuer [14] was used to match the data:

$$H_p(s) = K_p \cdot \frac{1 + T_L s}{1 + T_I s} \cdot e^{-\tau_e s} \qquad (2.1)$$

In eq. (2.1) K_p is the controller gain and T_I and T_L are human operator lag and lead terms respectively. The effective time-delay τ_e accounts for all time delays in perception, mental processing and control output generation. In addition, two more parameters i.e. the crossover frequency ω_c and phase margin ϕ_m were calculated from the measured data. Crossover frequency is the frequency where the gain of the open loop frequency response $H_p(\omega).H_c(\omega)$ crosses unity, see Fig. 2.4. Phase margin is defined as the phase angle $\phi(\omega_c)$ of $H_p(\omega).H_c(\omega)$ at ω_c, augmented with 180°:

$$\phi_m = 180 + \phi_{H_p.H_c}(\omega_c) \qquad (2.2)$$

A high crossover frequency is an indication of a high controller gain over a large frequency range, which is desirable for accurate disturbance compensation. However, there is a limit on the magnitude of controller gain, set by the requirement for closed loop stability. Phase margin is a measure for the stability of the man machine system. After training, well motivated subjects choose as high a controller gain as they feel to be compatible with a comfortable phase margin. For a detailed analysis, the reader is referred to Sheridan and Ferell [16].

Addition of the peripheral visual displays and/or cockpit motion affects the dynamic behaviour of the subjects differently in disturbance tasks when compared to target following tasks, see Fig. 2.5 and [6, 12].

In disturbance tasks, effective time delay τ_e is seen to decrease. This enables subjects to increase the gain K_p, thereby increasing the crossover

frequency ω_c, while they appear to be able to maintain an approximately constant phase margin ϕ_m, see Fig. 2.5 and Table 2.2.1.

In the target following task the subjects use the additional information from the peripheral field displays and cockpit motion quite differently. Here subjects use the additional rate information to increase the time lead constant T_L while they decrease the static gain K_p. The result is an increase in phase lead in the low frequency range ($\omega < 3$ rad/sec), see Fig. 2.5. Control bandwidth, as characterized by ω_c is approximately constant, but phase margins increase, see Table 2.2.1.

The different effect of peripheral field displays and cockpit motion on control behaviour in target following tasks compared with disturbance tasks is also reported in [6, 12]. For a detailed analysis the reader is referred to Van der Vaart and Hosman [18].

Work by others on the influence of additional rate information as supplied by peripheral vision and cockpit motion [6, 11, 12, 13, 15, 17, 19] shows at least qualitatively similar effects. Quantitatively, however, changes in performance and control behaviour differ considerably among experiments. It will be shown in Chapter 5 that some of these differences can be explained by differences in the dynamics of the controlled systems.

Disturbance task.

Display condition	ω_c rad/sec	ϕ_m degree	K_p	T_L sec	T_I sec	τ_e sec	σ_ϕ degree
C	3.18	14	1.3	0.53	0.1	0.24	1.94
P	3.16	15	1.3	0.50	0.1	0.23	2.67
CP	3.55	15	1.3	0.55	0.1	0.24	1.64
M	4.64	21	2.7	0.30	0.1	0.13	0.99
CM	4.76	19	2.6	0.30	0.1	0.14	0.79
PM	4.89	19	2.6	0.30	0.1	0.13	1.00
CPM	5.03	18	2.6	0.30	0.1	0.14	0.70

Following task.

C	2.26	15	0.55	1.	0.1	0.35	2.23
CP	2.24	35	0.15	4.	0.1	0.35	1.63
CM	2.23	39	0.09	6.	0.1	0.35	1.32
CPM	1.66	56	0.08	6.	0.1	0.35	1.26

Table 2.1.: Crossover frequency, phase margin, quasi-lineair pilot model parameters and tracking performance from the tracking experiment[6].

3. THE PERCEPTION OF VEHICLE MOTION FROM CENTRAL AND PERIPHERAL FIELD DISPLAYS.

The following two chapters summarize findings of stimulus-response type experiments in which the displays and simulator were exactly the same as those of the tracking experiments of Chapter 2. These tests were especially designed to gather data on the visual perception process involved in the tracking experiments reviewed in Chapter 2.

Experiment

Speed and accuracy of visual motion perception were investigated by presenting discrete, constant values of roll attitude and roll rate. Roll attitude was presented on the central artificial horizon display (denoted by C). In roll rate experiments, stimuli were either displayed on the artificial horizon (C), on the peripheral field displays (P) or simultaneously on both display types (CP). Since the peripheral field displays have a continuous checkerboard pattern, they do not yield any cues on roll attitude.

After observing a single stimulus during a preset exposition time, subjects were required to make an estimate of stimulus magnitude (roll angle in attitude estimation, angular rate in rate estimation experiments). Stimulus magnitudes ranged from minus to plus 30 degrees with increments of 3 degrees for roll angle estimation. For roll rate experiments the range of the stimuli was ± 25 deg/sec, the increments being 2.5 deg/sec. On the keyboard a single key corresponded to the increments of 3 degrees of roll angle or 2.5 deg/sec of roll rate. The keyboard included 10 keys for clockwise rotations, 10 keys for counter clockwise rotation and a zero key, see Fig. 3.1.

An experimental run contained 100 stimuli which were presented at fixed intervals, stimulus magnitudes were presented in random order and stimulus presentation was preceded by an audio tone in the subject's head phone, see Fig. 3.2. Immediately after a keyboard response, the remaining error (error roll angle or error roll rate depending on the experimental task) was shown on the displays, giving subjects immediate knowledge of the result. A correct response made the displayed angle return to zero in the roll attitude perception task. In the roll rate experiments a correct answer would "freeze" the displays.

Stimulus exposition time could be varied and was set at a constant value prior to each run.
During a run perception errors and response times RT were recorded. After each run mean and standard deviations of these variables and a score parameter $S_c = \sigma^2_{e_{n_2}} / \sigma^2_{e_{n_1}}$ were computed.

Three subjects, university staff members and qualified jet transport pilots, volunteered in the experiment. Their instructions were firstly to respond as accurately and secondly as quickly as possible to the presented stimuli. All experimental conditions (5 for roll attitude and 15 for roll rate) were replicated 5 times for each subject. For a full description of the experiment the reader is referred to [7,8].

Results

In Fig. 3.3, it can be seen that if compared by the error score as defined above, roll attitude is perceived more accurately and within a much shorter exposure time than roll rate. In addition it is evident that a given accuracy for roll rate perception can be obtained in a shorter exposure time from the peripheral displays than from the central display.

Response times as a function of exposure time, are shown in Fig. 3.4. For the central display only, roll attitude response time is around 0.1 sec faster than roll rate response time. Roll rate perception from the peripheral displays shows a response time 0.06 sec shorter than the for the case of central display only. Roll rate perception from the central and peripheral displays combined shows scores approximately equal to the ones from peripheral displays although with slightly longer response times.

4. VESTIBULAR MOTION PERCEPTION.

In the Introduction, the important role of man's vestibular organ in inner loop attitude stabilization tasks was already mentioned. The present chapter summarizes the main dynamic characteristics of the vestibular system as far as its function for angular motion perception is concerned. The second part of this chapter reviews two stimulus response experiments which included cockpit motion.

Strictly speaking, the only physical input quantity to be sensed by the vestibular semi-circular canals, is angular acceleration. The output of this organ may be expressed in change in output neural firing rate, or more general as motion sensed by a human subject. Physically, the semi-circular canal organs have the dynamics of a heavily damped second order system. Input angular acceleration and motion as sensed by man would then be related by the transfer function:

$$H(s) = \frac{K}{(1+\tau_1 s)\ (1+\tau_2 s)} \qquad (4.1)$$

where K is a static gain, τ_1 = 10 sec and τ_2 = 0.005 sec for man, see van Egmond[2].

In the frequency range typical for human motion, the frequency response of the output of this system features a phase lag of approximately 90 degrees relative to the angular acceleration input. In frequency response, angular rate has exactly 90 degrees of phase lag relative to angular acceleration. It would be grossly incorrect to infer from this that the semi-circular canals can be considered as rate-sensors, but it may safely be said that the vestibular output due to most every day motions is correlated with input rate.

From neuro-physiological research, it is known that due to the differentiating action of certain sensory cells in the vestibular organs, an additional lead term should be introduced into the transfer function numerator:

$$H(s) = \frac{K \cdot (1+\tau_3 s)}{(1+\tau_1 s) \cdot (1+\tau_2 s)} \qquad (4.2)$$

where for man $\tau_3 = 0.11$ sec.

The lead time constant τ_3 was evaluated by Fernandez and Goldberg [3,5] for the squirrel monkey. From measurements of thresholds for angular motion perception in a flight simulator a similar lead term τ_3 with the above mentioned value was determined by the authors [5].

The influence of the lead term on vestibular system model output is readily demonstrated by a numerical example. The step response of a second order system, simulating roll motion aircraft dynamics, see Fig. 4.1, was taken as the input to the semicircular canal dynamics according to equation (4.2). It can be seen from Fig. 4.2 that the vestibular output is advanced in time relative to the rate signal by 150 msec, suggesting an important advantage of vestibular motion perception when compared to visual motion perception.

Experiment.

Second order system step responses as the one shown in Fig. 4.1 were used as stimuli in a stimulus response experiment using the same Delft University flight simulator as in the tracking tasks reviewed in Chapter 2 with exactly the same visual displays as in the former experiments. Subjects were asked to estimate the final roll angle magnitude by pressing the appropriate key on the keyboard also mentioned in the preceding chapter. The experiment was designed to investigate the temporal advantages due to cockpit motion and peripheral displays. Therefore in case of the display condition comprised the central display, subjects should be prevented from waiting till the final value of the step was reached. Subjects were trained to optimize their response between accuracy and speed such that for all display conditions the same subject strategy would be used.

Just as in the other stimulus response experiments, response magnitude was subtracted from the input magnitude immediately after the subject's response. The second order system was, after subject's response, made to respond to this difference - or error - signal. After a transient motion, steady state response showed the error magnitude, see Fig. 4.3. In this way correct responses would return the simulator and the artificial horizon to zero roll angle. After an incorrect subject response the error was displayed during a few seconds, after which the roll angle was reset to zero before the next presentation.

Due to simulator limitations, step inputs were limited to ± 12 degrees, with increments of 2 degrees. This range was made to correspond with ± 6 keys on the keyboard, a single key corresponding with the stimulus increment of 2 degrees.

The natural frequency of the second order system was $\omega_0 = 2$ rad/sec, the damping ratio was $\zeta = 0.7$. Stimulus magnitudes were presented in random order. During a single run, 65 stimuli were presented. The same seven display conditions as in the disturbance tracking tasks were used. Observation errors and response times were recorded. Two subjects, university staff members who also participated in the experiments described in Chapter 2 and 3, volunteered in the experiment. A full description of this experimental work is given in [9].

Results

Table 4.1 shows means and standard deviations of step response perception error and response times for 2 subjects and 5 replications, for the seven display conditions. From the mean response times, which are all under 1.3 sec, it can be seen that subjects are quite able to decide on the magnitude of the final value, well before the final, steady-state value is reached. Peripheral displays shorten response time by 0.06 sec. and cockpit motion causes the response times to decrease by 0.21 sec. relative to the central display only condition. These changes were found to be significant ($p < 0.01$). Perception accuracy is only slightly improved by cockpit motion and appears to be hardly influenced by any of the other changes in display condition.

Display condition	$\bar{\bar{RT}}$ sec	σ_{RT} sec	$\bar{\bar{\Delta\phi}}$ degrees	$\sigma_{\Delta\phi}$ degrees
C	1.163	0.162	0.15	1.34
P	1.098	0.174	0.32	1.39
CP	1.127	0.178	0.03	1.34
M	0.948	0.191	-0.06	1.19
CM	0.992	0.231	0.02	1.22
PM	0.905	0.173	0.16	1.26
CPM	0.940	0.212	0.09	1.25

Table 4.1: Mean response time and perception error as a function of display condition.

Thus the experimental results confirmed the above mentioned finding that the vestibular system needs a shorter time to perceive motion than the visual system. The outcome of the experiment did not exactly fit to the model based computations. Three reasons can be given for this:
- the parameters of the semi-circular canal transfer function are estimates and not necessarily exactly correct
- the computed Δt of 150 msec is based on the difference between the vestibular model output and the stimulus rate ignoring the time-lag due to the visual angular rate perception
- cockpit motion stimuli may appear much stronger to subjects, which may influence response behaviour.

The influence of vestibular motion perception on the time needed to estimate the step magnitude depends on the dynamic characteristics of the system involved. This can be demonstrated by computing the time advance Δt See Fig. 4.4. Although there is a frequency range where this lead time is nearly constant, the lead of the vestibular output is seen to increase when the natural frequency ω_0 of the second order system decreases.

In order to evaluate if the influence of the contribution of the vestibular output on pilot's motion perception is as strong as suggested by Fig. 4.4, especially at low natural frequencies ($\omega_0 < 1$ rad/sec), the experiment was extended. By using a second order system with different

natural frequency to generate step response outputs, the response times of the subjects could be expected to change depending on display condition: central- or peripheral visual and/or vestibular stimulation. Thus it was expected that the relation between the time advance Δt and the natural frequency ω_0 could be evaluated experimentally.

From Fig. 4.4 it is clear that the natural frequency range of the second order system between 0.5 and 2 rad/sec is the most interesting due the increase of Δt with decreasing ω_0. For the details of these measurements see (10).

In Fig. 4.5 the time advance Δt as defined above is plotted together with the differences of the response times to the stimuli presented by the central display RT_C and cockpit motion RT_M for the three second order systems. Clearly the experimentally determined differences are larger than the model based time advance Δt. However, a sharp increase of $RT_C - RT_M$ with decreasing natural frequency ω_0 is found.

In van de Grind [4] it is shown that some time delay occurs in visual motion perception due to the fact that the stimulus has to pass the motion detector field on the retina before the associated neural circuit can generate an output. Time delays from 50 msec up to 2 sec depending on stimulus velocity are reported. This is confirmed by the stimulus response experiment, described in Chapter 3, where subjects had to estimate roll rate from the central display. It was shown that roll rate stimuli had to be exposed to the subjects for 100 to 200 msec before the roll rate could be perceived. In addition it has been found that the response time for roll rate perception is approximately 100 msec longer than for roll attitude perception. McRuer 14 described tracking experiments with first and second order dynamic characteristics. Based on these data it is assumed that the central visual system needs an additional 150 msec to perceive rate information. In Fig. 4.5 this time interval is added to the computed time advance Δt. The resulting line corresponds well with the values of $RT_C - RT_M$ found experimentally.

Thus based on the model predictions and the experimental results it may be concluded that vestibular motion perception leads the central visual or foveal motion perception with an amount of time which depends on the characteristics of the motion signal to be perceived.

5. DISCUSSION AND CONCLUSIONS.

From the results of the experiments described in Chapters 3 and 4, the basic differences in the perception characteristics of the visual and vestibular system for vehicle control can be summarized as follows.

- The time needed to perceive roll attitude from a central display is shorter than that to perceive its first time derivative, roll rate.
- Roll rate is perceived faster from the peripheral field displays than from the central display at equal accuracies.
- Due to the dynamic characteristics of the semi-circular canals of the vestibular system the output is advanced in time relative the rate signal. This time advance increases with decreasing bandwidth of the motion signal to be perceived.

Some classic, well documented results from visual tracking tasks with a central display only can be explained by the above distinctions between roll angle and roll rate perception. It has long been known [14] that measured transfer functions for subjects controlling a single, respectively a double integrator, can well be approximated by:

$$H_{p_1}(s) = K_p . e^{-\tau_1 s} \qquad (5.1)$$

$$H_{p_2}(s) = K_p . s . e^{-\tau_2 s} \qquad (5.2)$$

where $\tau_1 = 0.24$ sec, $\tau_2 = 0.38$ sec.

Evidently, see eq. (5.1), a subject controlling a single integrator, will primarily observe the presented error signal itself, whereas a subject controlling a double integrator, see eq. (5.2), will observe the time derivative of the error signal as the principal variable. Bearing in mind the difference between continuous tracking and stimulus response type observation tasks, together with the approximative nature of eqs. (5.1) and (5.2), the difference in experimentally obtained time constants $\tau_2 - \tau_1 = 0.14$ sec can well be explained by the response times for rate perception, which were found to be about 0.10 sec longer than for attitude perception in Chapter 3.

Disturbance task

The shorter perception time of roll rate due to the addition of peripheral visual cues and vestibular cues provides the subject with the ability to decrease the time delay τ_e as expressed in eq. (3.1) when performing a disturbance tracking task. This smaller time delay is used to increase the crossover frequency ω_c at a constant value of the phase margin ϕ_m.

The decrease of the effective time delay τ_e as measured in disturbance tracking tasks due to the addition of peripheral visual cues (0.03 sec) and vestibular cues (0.10 sec), see Table 2.1, corresponds with the shorter response times in the stimulus response experiments due to the same changes in display condition (peripheral cues 0.03 sec and vestibular cues 0,17 sec). See Chapter 3 and 4. Thus changes in time-delay in the tracking task can be attributed to changes in the perception process.

It stands to reason that if cockpit motion in a tracking task is delayed, the advantage of the early rate perception by the vestibular system will decline and eventually vanish. Hence the subject's control performance will decrease and the standard deviation of the controlled variable will increase. Results of an experiment on the influence of delayed cockpit motion on roll tracking performance by Levison [13] are shown in Fig. 5.1.

Taking the error standard deviations from Table 2.1 for the disturbance task and the response times of Table 4.1 for the corresponding display conditions, a plot similar to that of Fig. 5.1 can be made, see Fig. 5.2. Results of three conditions of the disturbance task (P, M and PM) deviate from the other conditions since, due to inaccurate roll attitude information to the subjects (no central display), tracking performance is not quite comparable with the other conditions.

Target following task

In the target following task subjects appear not to be able to speed up the perception process when peripheral visual or vestibular cues are added to the central visual cues. In contrast with the disturbance task, the peripheral visual and vestibular cues in target following tasks are not directly related to the first time derivative of the controlled variable, the roll error signal e_ϕ. See Fig. 2.1. In target following tasks subjects use the peripheral visual and vestibular feedback cues to increase the lead time constant T_L in the model of eq. (3.1), thereby increasing the phase margin ϕ_m while crossover frequency ω_c remains constant, see [18]. Again the influence of cockpit motion on changes in performance and dynamic behaviour is stronger than the influence of the peripheral field displays.

Concluding remarks

In this paper, the paramount importance of peripheral visual and especially vestibular information for inner-loop aircraft attitude stabilization was illustrated by results of tracking experiments. The emphasis on inner-loop control and vestibular feedback was not meant to imply that vision of the outside world scene is not important for certain other aspects of man-vehicle control such as orientation, navigation and trajectory control.

The summarized results of stimulus-response experiments indicate that the advantages from peripheral visual (outside world displays) and vestibular (cockpit motion) information are mainly due to the shorter perception times of these modalities when compared to central vision (primary flight display). The experimental results show that for larger aircraft (lower natural frequencies) cockpit motion provides the pilot with more time advance Δt than smaller aircraft.

In order to take full advantage of these systems, simulation time delays have to be minimized. Although the time advantage to be gained by cockpit motion is small when expressed in seconds, human performance and control behaviour are dramatically changed. It is therefore essential that the possible advantages to be obtained by costly flight simulator motion systems and visual displays are not nullified by delays caused by digital computer software and hardware [1].

6. REFERENCES.

1. Baarspul, M., Hosman, R.J.A.W. and Vaart, J.C.van der. Some fundamentals of simulator cockpit motion generation. Proceedings of the International Conference on "Advances in Flight Simulation Visual and Motion Systems". Royal Aeronautical Society, London, April 29-May 1,1986.
2. Egmond, A.A.J. van, Groen, J.J. and Jonkees, L.B.W. The function of the vestibular organ. Practica-Oto-Laryngologica, Vol. XIV, Supplement 2, S.Karger, Basel, New York, 1952.
3. Fernandez, C. and Goldberg, J.M. Physiology of peripheral neurons innervating semi circular canals of the squirel monkey, III. Variations among units in their discharge properties, Journal of Neurophysiology, Vol. XXXIV, No. 4, 1971.

4. Grind, W.A. van de, Koenderink, J.J. and Doorn, A.J. van. The distribution of human motion detector properties in monocular visual field. Vision Research, Vol. 26, No 5, pp 797-810, 1986.
5. Hosman, R.J.A.W. and Vaart, J.C. van der. Vestibular models and thresholds of motion perception. Results of tests in a flight simulator. Delft University of Technology, Department of Aerospace Engineering, Report LR-265, 1978.
6. Hosman, R.J.A.W. and Vaart, J.C. van der. Effects of vestibular and visual motion perception on task performance. Acta Psychologica 48 (1981) 271-287.
7. Hosman, R.J.A.W. and Vaart, J.C. van der. Accuracy of visually perceived roll angle and roll rate using an artificial horizon and peripheral displays. Delft University of Technology, Department of Aerospace Engineering, Report LR-393, 1983.
8. Hosman, R.J.A.W. and Vaart, J.C. van der. Perception of roll rate from artificial horizon and peripheral displays. Delft University of Technology, Department of Aerospace Engineering, Report LR-403, 1983.
9. Hosman, R.J.A.W. and Vaart, J.C. van der. Accuracy of system step response roll magnitude estimation from central and peripheral visual displays and simulator cockpit motion. Proceedings of the Twentieth Annual Conference on Manual Control. NASA Conference Publication 2341, 1984.
10. Hosman, R.J.A.W., Roggekamp, R.P.G.M. and Vaart, J.C. van der. Contribution of vestibular system output to motion perception. Proceedings of the Twenty-third Annual Conference on Manual Control. Massachusetts Institute of Technology, Cambridge MA, June 1988, to be published.
11. Junker A.M. and Replogle, C.R. Motion effects on the human operator in a roll axis tracking task. Aviation, Space and Environmental Medicine, 46: 819-822, 1975.
12. Levison, W.H. A model for pilot use of roll axis motion cues in steady-state tracking tasks. Bolt Beranek and Newman Inc. Report No. 3808, Cambridge, Mass, 1978.
13. Levison, W.H., Lancroft, R.E. and Junker, A.M. Effects of simulation delays on performance and learning in a roll-axis task. Fifteenth Annual Conference on Manual Control. AFFDL TR 79-3134, 1979.
14. McRuer, D.T., Graham, D., Krendel, E.S. and Reisener, W. Human Pilot Dynamics in Compensatory Systems. Theory, Models, and Experiments with Controlled Element and Forcing Function Variations. AFFDL-TR-65-15, Wright Patterson AFB, OHIO, 1965.
15. Moriarty, D.T., Junker, A.M. and Price, D.R. Roll axis tracking improvement resulting from peripheral visionmotion cues. Twelfth Annual Conference on Manual Control, NASA TM-X-73, 170, 1973.
16. Sheridan, Th. B. and Ferell, W.R. Man-Machine Systems: Information, Control and Decision. Models of Human Performance. MIT Press, Cambridge Massachusetts, 1974.
17. Stapleford, R.L., Peters, R.A. and Alex, F.R. Experiments and a model for pilot dynamics with visual and motion inputs. NASA CR-1325, 1966.
18. Vaart, J.C. van der and R.J.A.W. Hosman. Compensatory tracking in disturbance tasks and target following tasks. The influence of cockpit motion on performance and control behaviour. Delft University of Technology, Faculty of Aerospace Engineering, Report LR-511, 1987.
19. Zacharias, G.L. and Young, L.R. Influence of combined visual and vestibular cues on human perception and control of horizontal rotation. Exp. Brain Res. (1981)41: 159-171.

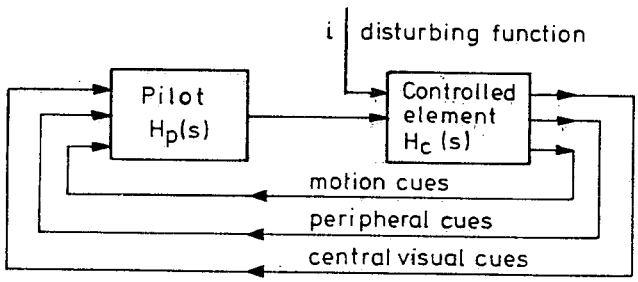

a. Disturbance task

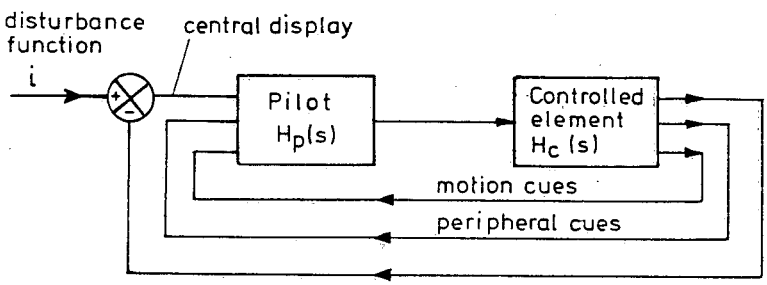

b. Target following task

2.1 Block diagrams of the human controller and controlled element.
a. Disturbance task: all cues closely related.
b. Target following task: error displayed on central display not directly related to other cues.

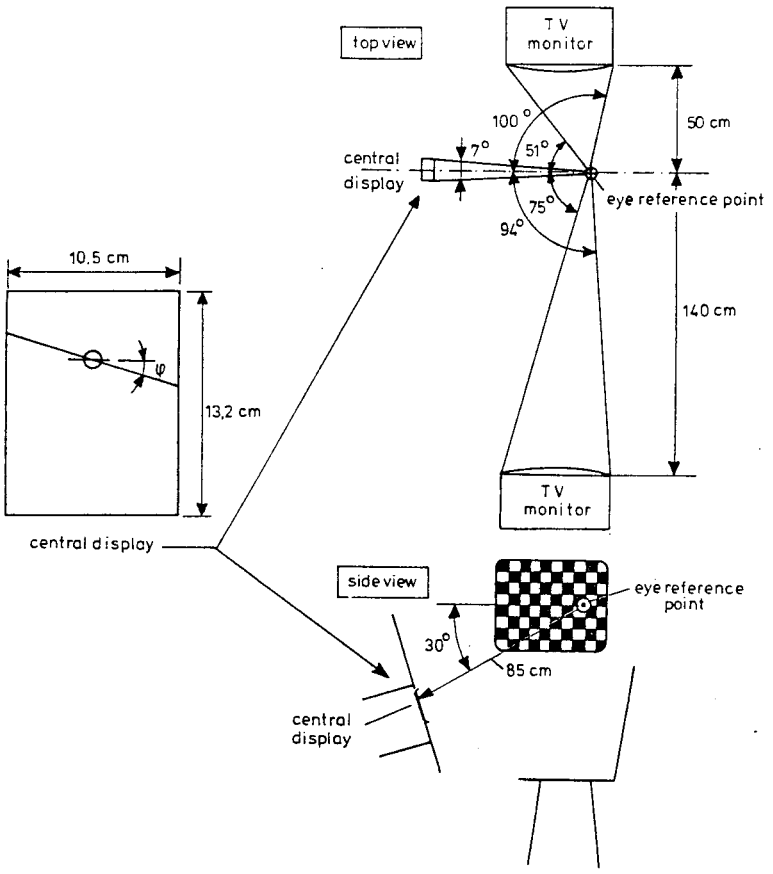

2.2 Position of central and peripheral displays relative to the subject's eye reference point.

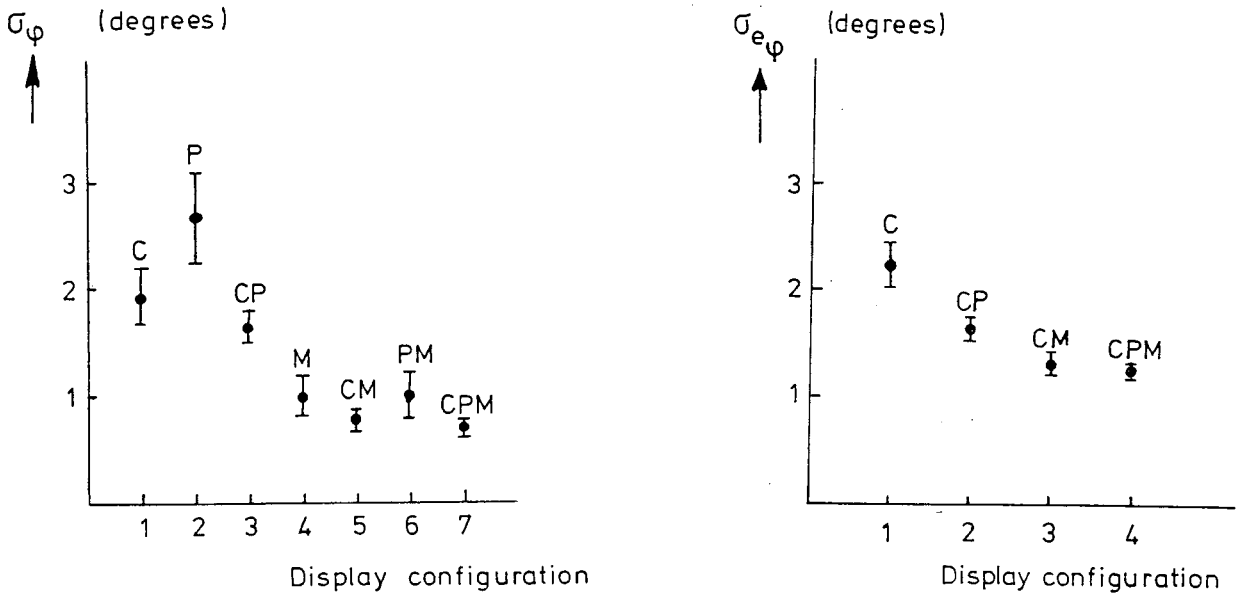

a. Disturbance task

b. Target following task

2.3 Tracking error standard deviation as a function of display configuration for disturbance and target following task.

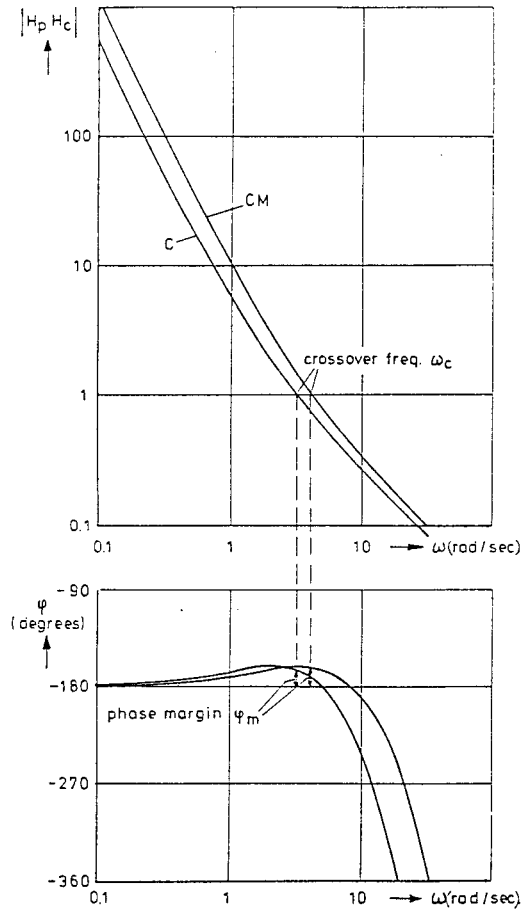

2.4 Examples of the open loop describingfunction $H_p(\omega).H_c(\omega)$, the crossover frequency ω_c and the phase margin ϕ_m.

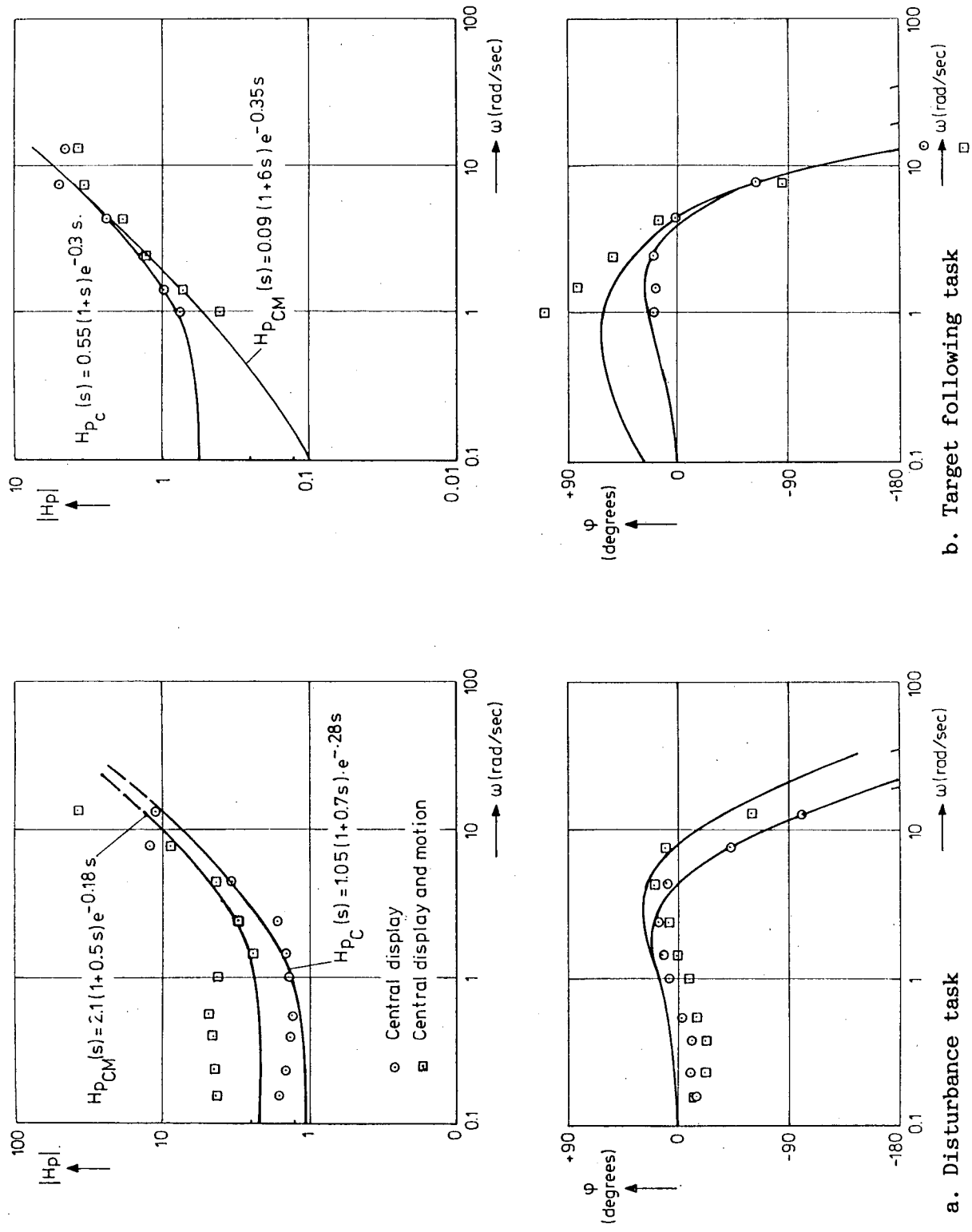

2.5 Examples of the gain and phase of the measured human controller describingfunctions in the disturbance and target following task.

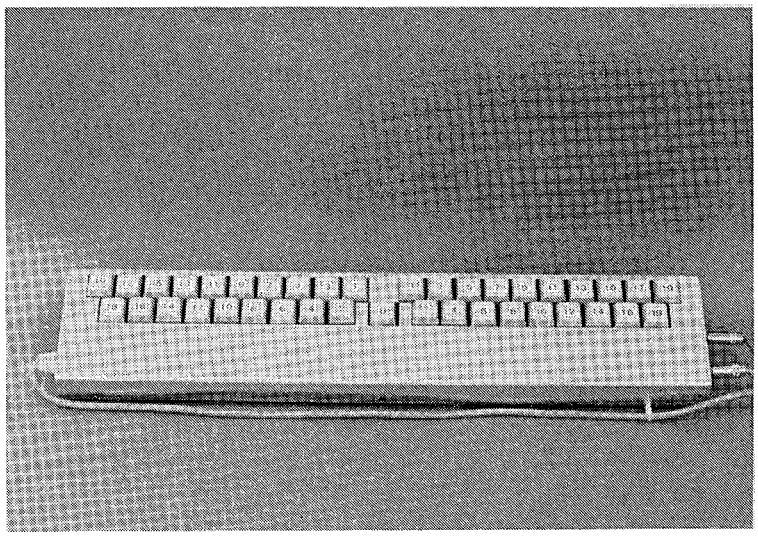

3.1 Digital keyboard.

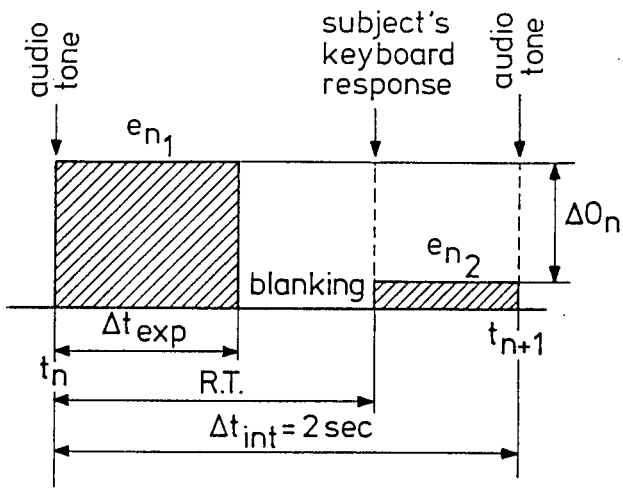

3.2 Sequence of one interval of a test run.

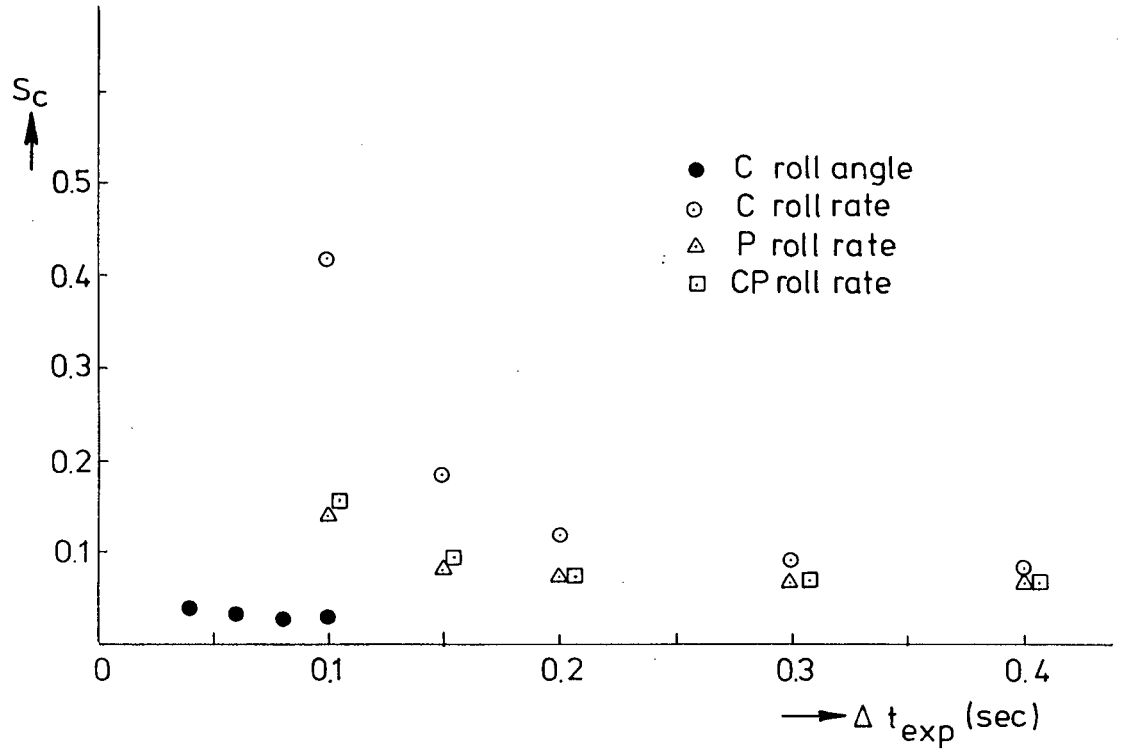

3.3 Score parameter S_c for roll attitude and roll rate estimation as a function of exposure time and display configuration.

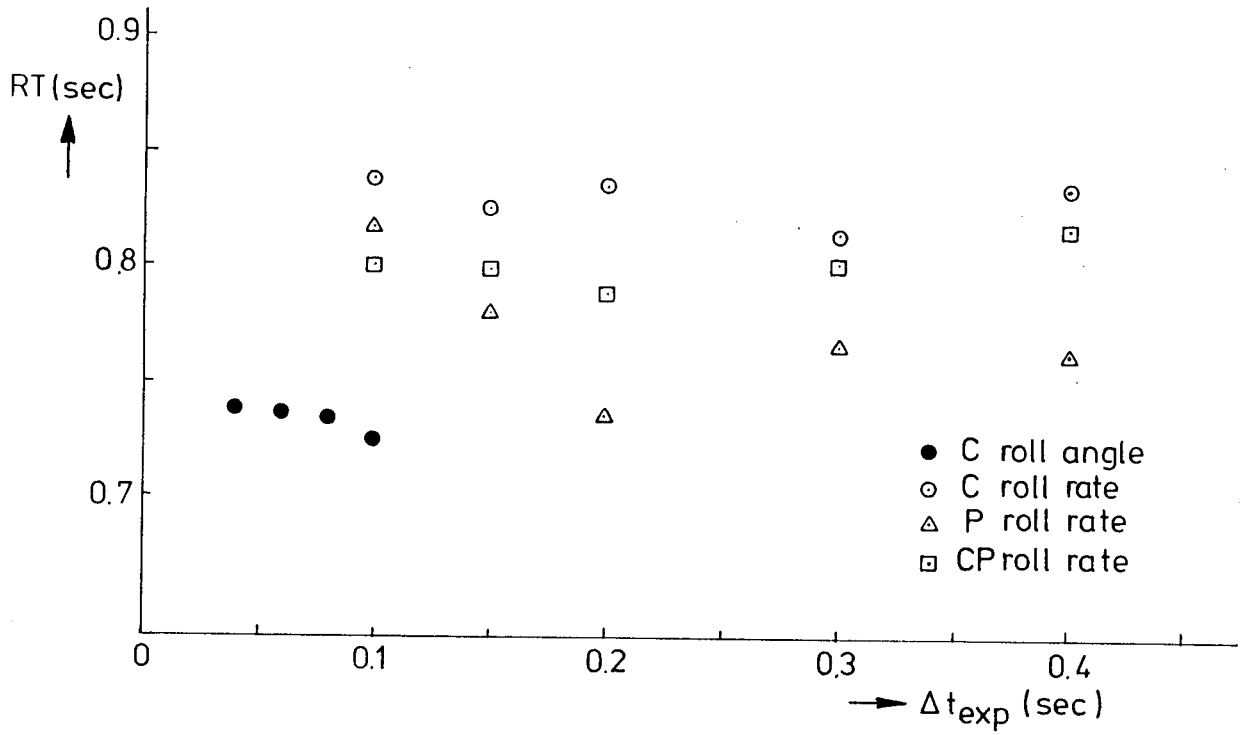

3.4 Response time to roll attitude and roll rate stimuli as a function of exposure time and display configuration.

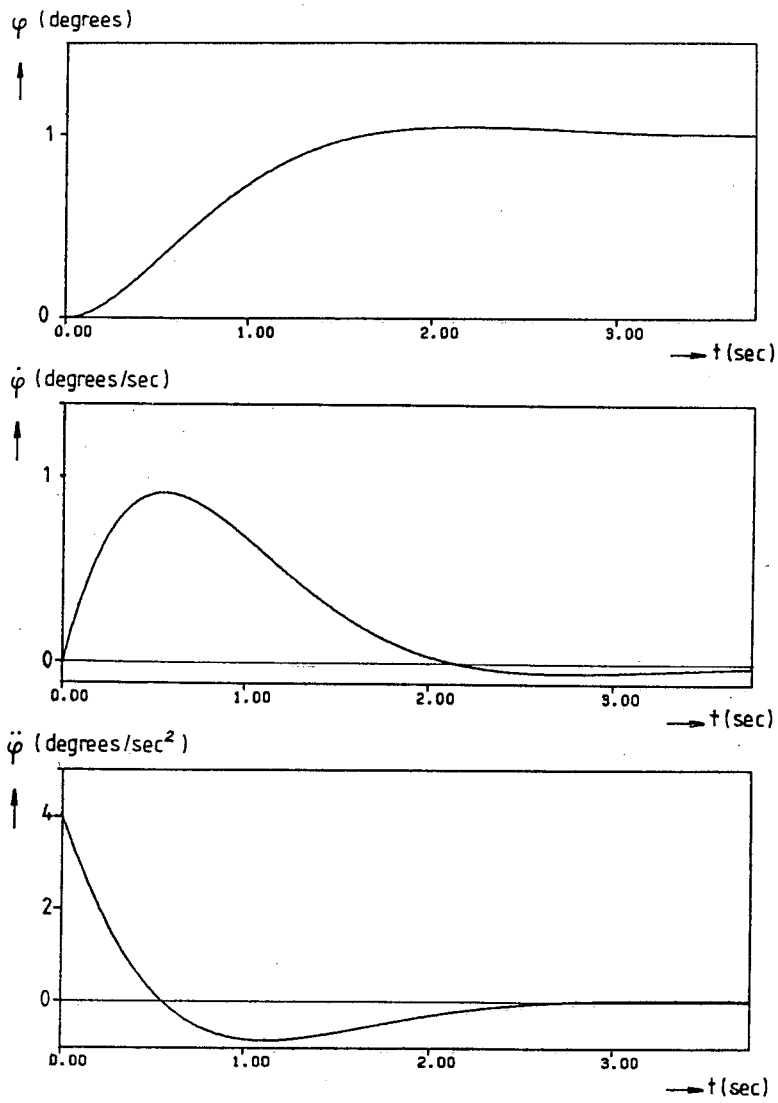

4.1 Attitude, rate and acceleration of a second order system step response

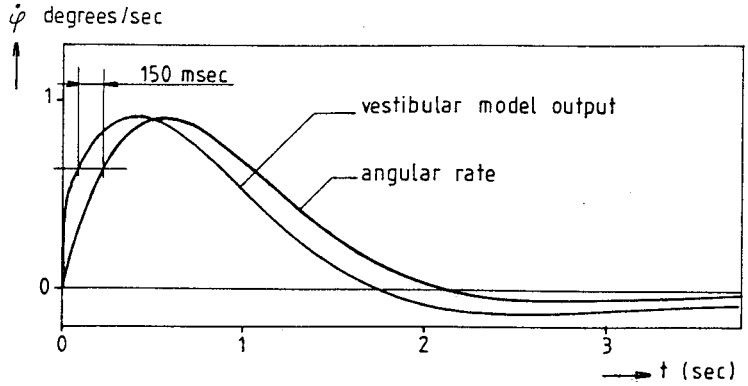

4.2 Angular rate output of a second order system step response and the calculated semi-circular canal output according to eq. (4.2).

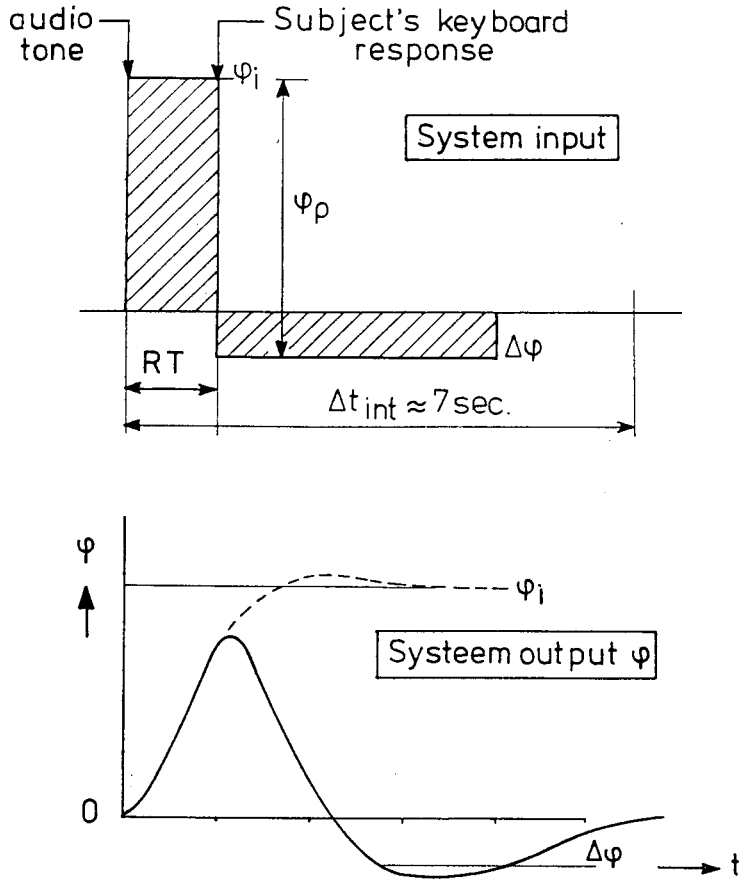

4.3 Sequence of one interval of a test run.

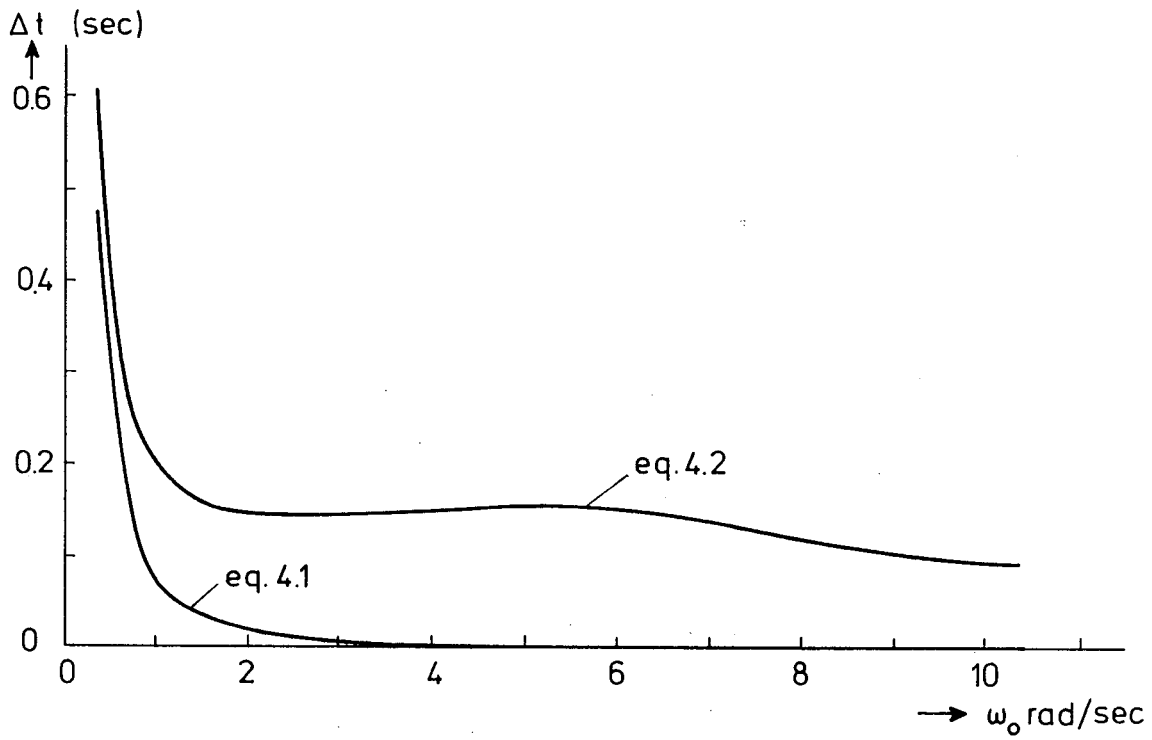

4.4 The time advance Δt of the semi-circular canal output relative to the roll rate signal as a function of the natural frequency ω_0 of the second order system.

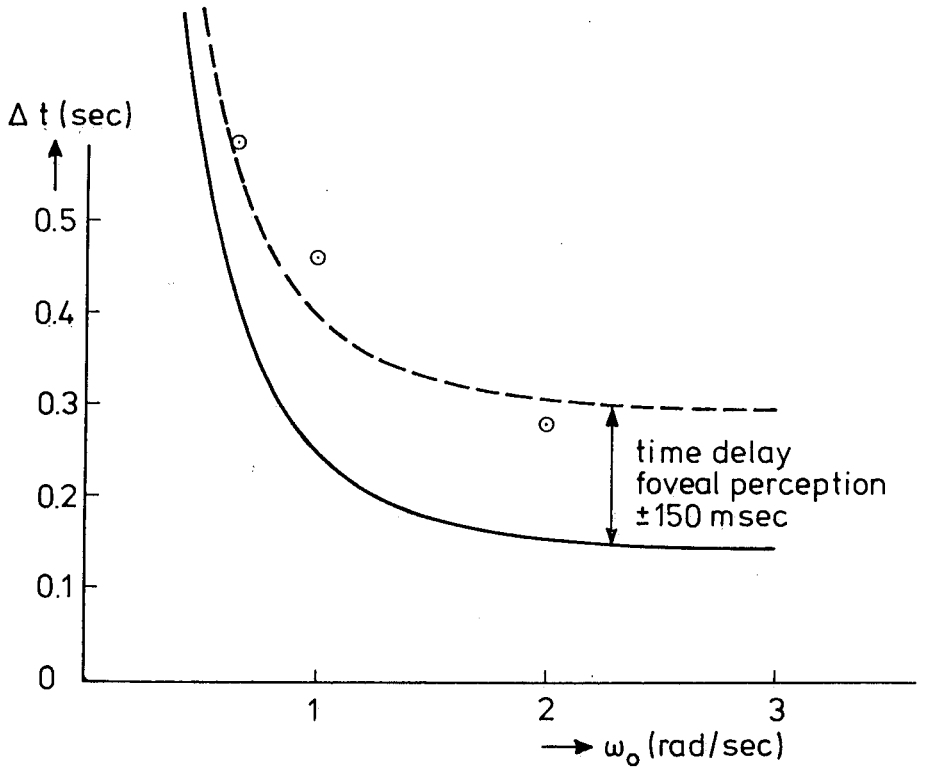

4.5 The response time difference RT_C - RT_M compared to the time advance Δt and the time delay due to foveal motion perception.

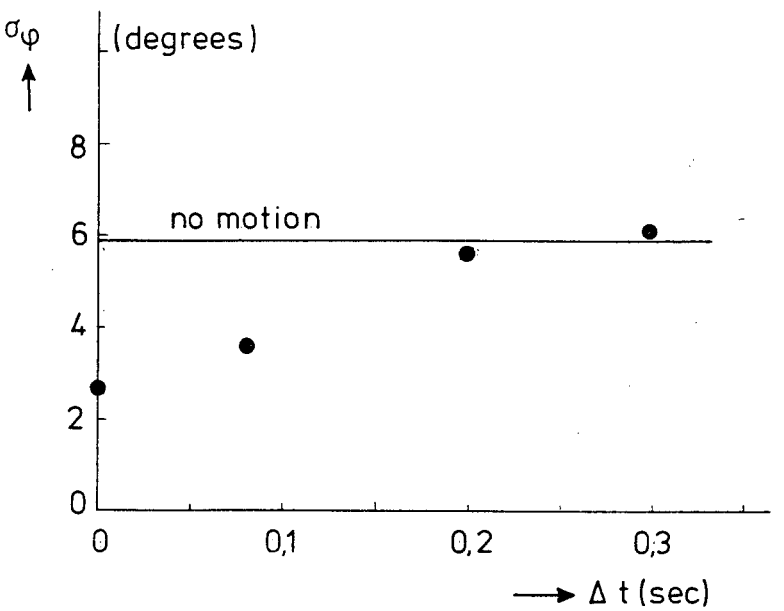

5.1 Root mean square of the roll angle in a roll tracking task as a function of simulator motion time delay Δt compared with the no motion performance, taken from Ref. 13.

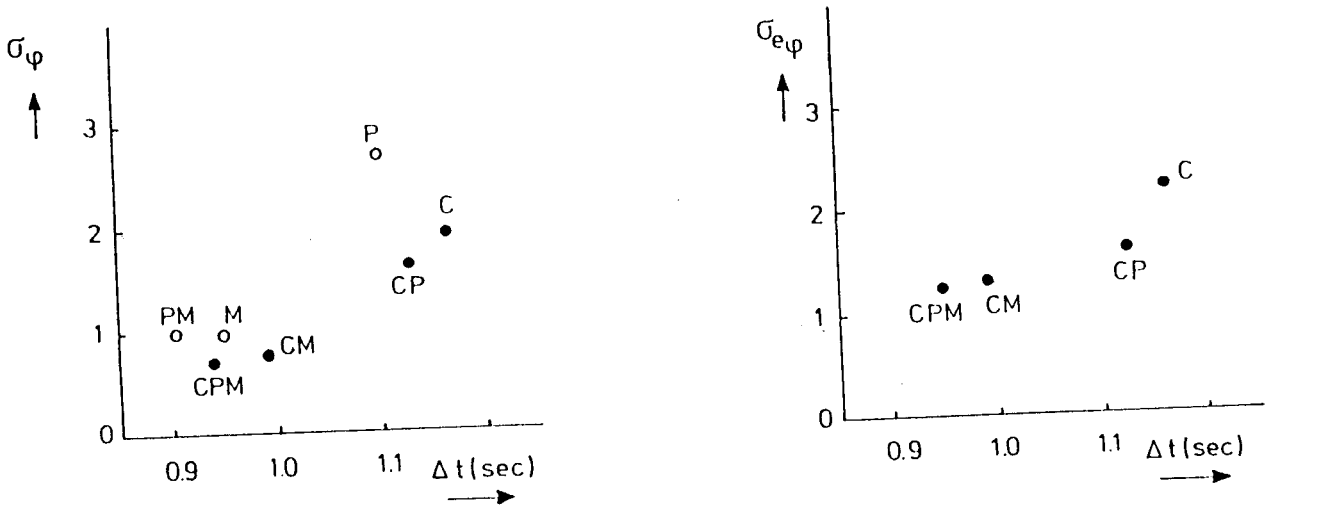

a. Disturbance task

b. Target following task

5.2 Tracking performance in the disturbance and target following tracking task from Fig. 2.3, as a function of the response time RT from table 4.1, for the same display conditions. Open symbols: no central display.

PARAMETER ESTIMATION FOR STOCHASTIC SYSTEMS

P.J.G. Loos

Royal Dutch Airlines

ABSTRACT

This report reviews briefly a parameter estimation program for stochastic systems (MLPEFSS) which was developed as part of the final examination at the Department for Aeronautical Engineering. The program employs a Gauss-Newton optimization of a Maximum Likelihood criterion to estimate the unknown parameters appearing in a linear, time invariant state space description of a stochastic system.

The state space description for dynamic systems and the definition of statistical estimators are first discussed. Then the filter-error method is presented in a form well suited for computer implementation. This method combines a non-stationary Kalman filter with an output-error parameter estimation technique thus accounting for both process noise (unmeasured stochastic input signals) and measurement noise.

Next the problem of optimizing the non-linear likelihood function resulting from the filter-error method with respect to the unknown parameters is discussed. The Hooke and Jeeve direct search method and the second order Gauss-Newton optimization algorithm are treated in more detail.

Finally the results of one of the test cases which were used to validate the Maximum Likelihood Parameter Estimation program For Stochastic Systems (MLPEFSS) are given.

CONTENTS

NOMENCLATURE

SYMBOLS

$\underline{\underline{A}}$ constant matrix,
system matrix

$\underline{\underline{B}}$ constant matrix,
input matrix deterministic signals

$\underline{\underline{C}}$ constant matrix,
state observation matrix

$\underline{\underline{D}}$ input observation matrix

$\underline{\underline{E}}$ output matrix stochastic signals

$\underline{f}[.]$	vector valued function
$\underline{\underline{G}}$	input matrix stochastic signals
$\underline{g}[.]$	vector valued function
$\underline{h}[.]$	vector valued function
$\underline{h}$	arbitrary p dimensional vector
i	integer
$J(.)$	cost criterion
j	row number in matrix
$\underline{\underline{K}}_p$	Kalman filter gain matrix (time update step)
$\underline{\underline{K}}(t_i)$	Kalman filter gain matrix (measurement update step)
k	column number in matrix, iteration
$\underline{m}$	mean vector
m	number of deterministic input signals
N	number of time samples
n	number of state variables
$\underline{\underline{P}}$	covariance matrix
$P(.)$	element of the unknown parameter vector $\underline{\xi}$
$p(.)$	probability density function
r	number of measured output variables
ΔT	sample time
t	time
$\underline{U}_N$	sequence of N deterministic input vectors $(\underline{u}_1, \underline{u}_2, \ldots, \underline{u}_N)$
$\underline{u}$	deterministic input signal vector
$\underline{\underline{V}}_{\underline{v}}$	covariance matrix measurement noise
$\underline{\underline{V}}_{\underline{w}}$	covariance matrix process noise
$\underline{\underline{V}}_{\underline{wv}}$	covariance matrix process and measurement noise
$\underline{v}$	measurement noise
$\underline{\underline{W}}$	weighting matrix, variance of error signal
$\underline{w}$	stochastic input signal vector (= process noise)
$\underline{X}[.]$	vector valued function
$\underline{X}_N$	sequence of N measured state vectors $(\underline{x}_1, \underline{x}_2, \ldots, \underline{x}_N)$
$\underline{x}$	state vector
$\underline{Y}_N$	sequence of N measured output vectors $(\underline{y}_1, \underline{y}_2, \ldots, \underline{y}_N)$
$\underline{y}$	measured output vector

GREEK SYMBOLS

$\underline{\underline{\Gamma}}$	input transition matrix (discrete time)
$\partial/\partial x$	partial derivative with respect to x
$\partial^2/\partial x^2$	second order partial derivative with respect to x
δ_{ij}	Kronecker delta
ε	real positive number
$\underline{\underline{\Phi}}$	state transition matrix (discrete time)
$\underline{\underline{\Phi}}(t, t_0)$	state transition matrix (continuous time)
$\underline{\xi}$	unknown parameter vector

SUBSCRIPTS

0	initial condition, nominal
i	discrete time index
j	discrete time index
$\underline{u}$	deterministic input
$\underline{v}$	measurements
$\underline{w}$	stochastic input
=	matrix
_	vector

SUPERSCRIPTS

.	derivative with respect to time
"	second order derivative with respect to time
^	estimated or optimal according to mentioned criterion

MATHEMATICAL NOTATION

$\arg\max_x$	value of x that maximizes a given function
$\arg\min_x$	value of x that minimizes a given function
cov	covariance
E	expectation
exp	exponential
ln	natural logarithm
tr	trace
Π	series product
π	pi (=3.1459...)
Σ	series summation
*	transpose
|	conditioned on
|.|	absolute value, determinant
∞	infinity
$\nabla_{\underline{x}}$	gradient with respect to vector $\underline{x}$
$\nabla^2_{\underline{x}}$	second order gradient with respect to vector $\underline{x}$

ACRONYMS

MAP	Maximum A Posteriori
MIMO	Multiple Input, Multiple Output
ML	Maximum Likelihood
MLPEFSS	Maximum Likelihood Parameter Estimation program For Stochastic Systems

I INTRODUCTION

To describe the stability and control characteristics of an aircraft a mathematical model is often used [Ref. 1] . To this end an aircraft can be considered as a multivariable system. Originating from Modern System Theory the state space description shows to be an excellent mathematical way to describe multivariable dynamic systems [Ref. 2] . The equations used in this description are

$$\dot{\underline{x}}(t) = \underline{f}[\underline{x}(t),\underline{u}(t),\underline{w}(t),t] \quad , \quad \underline{x}(t_0) = \underline{x}_0 \tag{I.1}$$

$$\underline{y}(t) = \underline{g}[\underline{x}(t),\underline{u}(t),\underline{v}(t),t] \tag{I.2}$$

The variable $\underline{x}(t)$ is called the state vector of the system and consists of n state variables. The input vector $\underline{u}(t)$ contains the m deterministic input variables whereas $\underline{w}(t)$ represents the stochastic input variables (process noise) . $\underline{y}(t)$ is the output vector with the r measured output signals and $\underline{v}(t)$ represents the measurement noise.
The functions $\underline{f}[.]$ and $\underline{g}[.]$ can be expressed as a mathematical formula which is defined by its form and the numerical values of the constants in it. The latter contain the so-called stability and control derivatives [Ref. 3] .

Determination of these aircraft stability and control derivatives is often one of the main objectives of aircraft flight tests. This can be seen as an inverse problem (deriving a mathematical model that fits measured data) which is the subject of the System Identification Theory [Ref. 4] .
In general this identification process can be separated into first determining the general form of the model (model identification step) and thereafter determining the parameters appearing in this model (parameter estimation step) .

Aircraft system identification projects are very expensive due to the flight tests, costly data acquisition systems and computer usage involved. Therefore methods which reduce flight test and computer time are of constant interest. The introduction of digital computers was a major improvement in this respect enabling the use of statistical parameter estimation algorithms to deduce derivatives from non-stationary flights [Ref. 5] .

The remainder of this report reviews briefly the design of a parameter estimation computer program with the following characteristics :

- -applicable to general dynamic systems represented with the linear, time invariant state space description
- -interactive building and changing of the model equations
- -statistical parameter estimation approach (maximum likelihood method)
- -suited to handle random input signals (process noise) and measurement noise
- -interactive numerical optimization of the likelihood function

The program is applicable to a wide range of parameter estimation problems. Applied to the field of aircraft model identification the above given characteristics give rise to the following favourable qualities.
The state space description allows processing of flight data obtained with non-stationary flight test maneuvers. The use of non-stationary flight test

techniques results in a considerable reduction of the flight test time required.
The flexibility to change the model equations interactively provides the possibility to examine the influence of different model forms (i.e. the model identification step) .
A statistical approach to the parameter estimation problem opens the way to use a digital computer to extract the unknown parameters in an efficient manner. The statistical estimators also provide an indication of the accuracy of the resulting estimates.
Atmospheric turbulence can be considered as a random input signal. The possibility to estimate parameters from flight tests under turbulent atmospheric conditions offers several benefits. The flight test program execution is less dependent on weather conditions thus releasing the test aircraft and data acquisition systems earlier for other projects. The response of the aircraft to atmospheric turbulence is determined directly and not as an extension of calm air stability and control characteristics. Sometimes it is not realistic to expect or even possible to execute calm air flight tests (terrain following) or the only available measurements are obtained during turbulence. Further it is a feasibility check for applications that require real-time and on-line parameter estimation algorithms (adaptive control, on-line quick look) . These on-line algorithms obviously have to be able to extract stability and control derivatives from measurements under turbulent flight conditions. The latter algorithms are however not the subject of this report. Another interesting application is the investigation of atmospheric turbulence. To this end the parameter estimation program is used not only to estimate the unknown stability and control derivatives of the aircraft but also the parameters which describe the structure of the atmospheric turbulence encountered.
Interactive minimization of the likelihood function (which is in general highly non-linear) makes the employment of engineering insight and judgement possible. This can give an enormous reduction in required computer time.

II SYSTEM DESCRIPTION

There are many ways to describe the input-output relation of a dynamic system in a mathematical way. For multivariable or so-called MIMO (= multiple input, multiple output) systems the state space description introduced by Zadeh and Desoer [Ref. 6] is commonly used. More conventional methods which describe such systems with impuls responses or transfer functions lack the compactness and insight given by the state space description. As an extra advantage the computations associated with the state space description of a system are easily implemented on a digital computer.
The state equation in differential form (II.1)

$$\dot{\underline{x}}(t) = \underline{f}[\underline{x}(t),\underline{u}(t),\underline{w}(t),t] \qquad \text{(II.1)}$$

and the output equation (II.2)

$$\underline{y}(t) = \underline{g}[\underline{x}(t),\underline{u}(t),\underline{v}(t),t] \qquad \text{(II.2)}$$

cover a wide class of dynamic systems. The program discussed in this report applies only to systems which are time invariant and which are adequately

described by a first order (linear) approximation of (II.1) and (II.2). For time invariant systems the functions $\underline{f}$ and $\underline{g}$ are not explicitly dependent on the variable t. A linear approximation of $\underline{f}$ and $\underline{g}$ to describe a system is possible when small perturbations from a nominal input signal, nominal state trajectory and the associated nominal output signal are considered. The linear differential state equation and output equation follow from a truncated Taylor expansion of (II.1) and (II.2) around these nominal signals. This results in

$$\dot{\underline{x}}(t) = \underline{\underline{A}}\underline{x}(t) + \underline{\underline{B}}\underline{u}(t) + \underline{\underline{G}}\underline{w}(t) \qquad \text{(II.3)}$$

and

$$\underline{y}(t) = \underline{\underline{C}}\underline{x}(t) + \underline{\underline{D}}\underline{u}(t) + \underline{\underline{E}}\underline{v}(t) \qquad \text{(II.4)}$$

where $\underline{u}(t)$, $\underline{x}(t)$ and $\underline{y}(t)$ denote the small perturbations from the nominal signals.

The above given equations apply to continuous time systems. For discrete time systems equivalent formulas exist. A combination of a continuous time differential state equation and a discrete time output equation is required when describing a continuous time system from which measurements are taken at discrete time intervals. This results in the following mixed state space description

$$\dot{\underline{x}}(t) = \underline{\underline{A}}\underline{x}(t) + \underline{\underline{B}}\underline{u}(t) + \underline{\underline{G}}\underline{w}(t) \qquad \text{(II.5)}$$

$$\underline{y}(i) = \underline{\underline{C}}\underline{x}(i) + \underline{\underline{D}}\underline{u}(i) + \underline{\underline{E}}\underline{v}(i) \qquad \text{(II.6)}$$

For implementation on a digital computer the solution of the linear differential state equation can be evaluated at equidistant time points. Choosing the period time ΔT between the consecutive time points small enough so that $\underline{u}(t)$ and $\underline{w}(t)$ can be considered constant over the time interval $(t, t+\Delta T)$ yields the following explicit solution

$$\underline{x}(t+\Delta T) = e^{\underline{\underline{A}}\Delta T}\underline{x}(t) + \int_{t_0}^{t} e^{\underline{\underline{A}}(t-\tau)}\underline{\underline{B}}\underline{u}(\tau)d\tau + \int_{t_0}^{t} e^{\underline{\underline{A}}(t-\tau)}\underline{\underline{G}}\underline{w}(\tau)d\tau$$

or when denoted with transition matrices

$$\underline{x}(t+\Delta T) = \underline{\underline{\Phi}}\underline{x}(t) + \underline{\underline{\Gamma}}_{\underline{u}}\underline{u}(t) + \underline{\underline{\Gamma}}_{\underline{w}}\underline{w}(t) \qquad \text{(II.7)}$$

Determination of the matrix exponential $e^{\underline{\underline{A}}\Delta T}$ can be done using the series expansion

$$e^{\underline{\underline{A}}\Delta T} = \sum_{i=0}^{\infty} \frac{\Delta T^i}{i!} \underline{\underline{A}}^i$$

Although this expansion converges for all real square matrices $\underline{\underline{A}}$ a normalized series expansion is used in the present work to speed up convergence and prevent a loss of accuracy [Ref. 7] . In this normalized

evaluation of the matrix exponential $e^{\underline{\underline{A}}\Delta T}$ the matrix $\underline{\underline{A}}$ is divided by 2^n such that the largest eigenvalue of the resulting matrix smaller is than ΔT^{-1}. The convergence of the series expansion of the exponential of the resulting matrix is then assured within a fixed number of terms. The program described in this report uses by default 20 terms but this number can be changed by the user. The resulting matrix exponential is squared up n times to yield the required matrix exponential $e^{\underline{\underline{A}}\Delta T}$.

III SYSTEM IDENTIFICATION TECHNIQUES

In terms of System Theory the goal of system identification is to obtain an input-output relation. Identification of a system based solely on the observed input and output signals without any further specification of its characteristics (so called black box approach) poses however an insolvable problem. First nothing can be said in this case about the repeatability of the system response to an identical input signal (time dependent characteristics of the system). Furthermore the response of the system to a specific input signal cannot be predicted from the responses to different input signals unless some internal coherency within the system is assumed.

Fortunately the black box approach is seldom necessary. From knowledge of the basic physical processes governing the behaviour of the system additional information can be deduced. Casting this information into a mathematical form appropriate to the objectives of the analyst and the system identification technique used is called the model identification step.
Dependent on the available knowledge and information the model identification step yields a mathematical description of the system with more or less numerical values lacking. Determination of these values from experimental data is called parameter identification.

A first attempt to the parameter identification step is solving the set of model equations for the unknown parameters using measured data. Finding a unique solution to this set of equations is however very unlikely. Firstly the mathematical description is an approximation of the real system and secondly the measured data is noise corrupted. Therefore the measured data will not be consistent with the mathematical model for any value of the parameter vector.

From the foregoing it is clear that on the one hand an a priori model is needed to extend the measured data to an input-output relation while on the other hand this model will be inconsistent with the measured data. To solve this dilemma the notion of an assumed model is used. This assumed model includes the essential characteristics of the system which are needed to solve the problem at hand but it is recognized that this model is not exact. Engineering judgement is used in the model identification step to determine the essential characteristics of the system and to assure that the assumed model describes the real system closely enough with respect to these characteristics.

For the parameters which remain to be determined in the assumed model there exists no correct numerical value due to the imperfectness of the model structure. It is however possible to determine the parameter values which makes the model the "best" representation of the essential characteristics of the real system. This determination is called parameter estimation and it includes a definition of the "best" representation.

IV STATISTICAL ESTIMATORS

An estimator is used to determine a numerical value for the set of unknown parameters which appear in the mathematical description of a system from the results of an experiment. Denoting the set of unknown parameters as the vector $\underline{\xi}$ the estimator can be defined with a function

$$\hat{\underline{\xi}} = \underline{h}(\underline{Y}_N, \underline{U}_N)$$

The results of the experiment $\underline{Y}_N$ depend on the deterministic input signal $\underline{U}_N$ applied to the system, the value of the parameter vector $\underline{\xi}$ and the stochastic signals $\underline{v}$ and $\underline{w}$. The latter vectors represent respectively the measurement noise and process noise which are present during the execution of the experiment. $\underline{Y}_N$ and $\underline{U}_N$ are sequences of measured output respectively input variables, i.e.

$$\underline{Y}_N = (\underline{y}_1, \underline{y}_2, \ldots, \underline{y}_N) \qquad \text{and} \qquad \underline{U}_N = (\underline{u}_1, \underline{u}_2, \ldots, \underline{u}_N)$$

In the notation used before $\underline{Y}_N$ can be written as

$$\underline{Y}_N = \underline{g}[\underline{X}_N(\underline{U}_N, \underline{w}, \underline{\xi}) \ , \ \underline{U}_N \ , \ \underline{v} \ , \ \underline{\xi}]$$

Due to the stochastic components $\underline{v}$ and $\underline{w}$ the result of the experiment $\underline{Y}_N$ is a random variable. From the definition of an estimator it follows that also the estimate $\hat{\underline{\xi}}$ of the parameter vector $\underline{\xi}$ a random variable is.

Basically there are two different methods (the deterministic approach and the statistical approach) to derive the function $\underline{h}[.]$ to yield an effective estimator
In the statistical approach the estimator is defined by specifying the function $\underline{h}[.]$ using the statistical properties of the stochastic variables involved with the parameter estimation problem. For this method the probability density function of the process noise $p_{\underline{w}}(\underline{w})$ and the measurement noise $p_{\underline{v}}(\underline{v})$ have to be known.

In the deterministic approach, which will not be used in the present work, the definition of the estimator is not based on statistical information but on heuristic reasoning. In practice however the computational schemes involved with a deterministic approach often resemble very much the computations required to determine the estimates resulting from a statistical approach.

The statistical estimators used in the program discussed are the so-called Maximum Likelihood estimator (ML) and Maximum A Posteriori estimator

(MAP) . For a given mathematical system description and with the knowledge of the probability density functions $p_{\underline{w}}(\underline{w})$ and $p_{\underline{v}}(\underline{v})$ the probability density function of the measured variables can be determined. This probability density function depends on the unknown parameter vector $\underline{\xi}$ as these parameters appear in the mathematical system description. This dependence will be accentuated by denoting

$$p(\underline{Y}_N) = p(\underline{Y}_N, \underline{\xi})$$

The maximum likelihood estimate of the unknown parameters can now be defined as the vector $\hat{\underline{\xi}}_{ML}$ that maximizes the value of the probability density function of the measurements for the observed data $\underline{Y}_N$, i.e.

$$\hat{\underline{\xi}}_{ML} = \arg \max_{\underline{\xi}} p(\underline{Y}_N, \underline{\xi}) \qquad \text{(IV.1)}$$

In words the maximum likelihood estimator yields the value $\hat{\underline{\xi}}_{ML}$ for the unknown parameters which makes the observed data $\underline{Y}_N$ most probable.

One drawback of the maximum likelihood estimator is that it is not capable to incorporate a priori knowledge about the values of the unknown parameters in the estimate. This information is often available from other or previous experiments or it can result from engineering judgement. This a priori information can be used by assigning a probability density function $p(\underline{\xi})$ to the unknown parameter vector $\underline{\xi}$ even though the vector $\underline{\xi}$ is not random. This method of specifying a probability density function as a measure of reliability or confidence in a certain value for a deterministic variable stems from the field of Information Theory [Ref. 8] . A statistical estimator which combines the a priori information contained in $p(\underline{\xi})$ and the information obtained with the experiment is the Maximum A Posteriori estimator. This MAP estimator is defined by

$$\hat{\underline{\xi}}_{MAP} = \arg \max_{\underline{\xi}} p(\underline{\xi}|\underline{Y}_N)$$

With Bayes rule this can be rewritten as

$$\hat{\underline{\xi}}_{MAP} = \arg \max_{\underline{\xi}} p(\underline{\xi}|\underline{Y}_N) = \arg \max_{\underline{\xi}} \frac{p(\underline{Y}_N|\underline{\xi})\, p(\underline{\xi})}{p(\underline{Y}_N)}$$

Here $p(\underline{Y}_N)$ is a marginal probability density function which is independent of $\underline{\xi}$ and therefore the MAP estimate can be determined with

$$\hat{\underline{\xi}}_{MAP} = \arg \max_{\underline{\xi}} p(\underline{Y}_N|\underline{\xi})p(\underline{\xi})$$

It can be shown for both the Maximum Likelihood estimator and the Maximum A Posteriori that they are asymptotically unbiased and efficient.

V FILTER ERROR METHOD

The result of combining the state space description with the statistical ML or MAP estimator depends on the stochastic characteristics of the system identification problem at hand. When both process noise and measurement noise are present the state variables cannot be determined in a deterministic way. Therefore a stochastic determination of the state variables has to be used, based on the assumed system description and on statistical assumptions regarding the process and measurement noise. The combination of a statistical state estimator and a parameter estimator is called the filter error method.

The Kalman filter [Ref. 9] is a well-known state estimator, which is well suited for implementation on a digital computer when only additive Gaussian noise is considered. To derive the Kalman filter it is naturally to convert the mixed continuous/discrete form of the assumed model (II.5 and II.6) into a pure discrete form since all practical applications are programmed on a digital computer. This leads to

$$\underline{x}(t_i) = \underline{\underline{\Phi}}\underline{x}(t_{i-1}) + \underline{\underline{\Gamma}}_{\underline{u}}\underline{u}(t_{i-1}) + \underline{\underline{\Gamma}}_{\underline{w}}\underline{w}(t_{i-1}) \qquad (V.1)$$

$$\underline{y}(t_i) = \underline{\underline{C}}\underline{x}(t_i) + \underline{\underline{D}}\underline{u}(t_i) + \underline{v}(t_i) \qquad (V.2)$$

The state estimation problem is to find the best estimate $\underline{\hat{x}}(t_i)$ for $\underline{x}(t_i)$ based on the measurements $\underline{Y}_N$. For $N < i$ this is called a prediction problem and for $N > i$ a smoothing problem. The filtering problem ($N = i$) is of interest in the present context.

The best estimate of the state can be defined by a statistical criterion (e.g. maximum likelihood estimator, maximum a posteriori estimator) . For state estimation the most appropriate statistical estimator is the MAP estimator which uses the conditional probability density function $p_{\underline{x}}(\underline{x}(t_i) \mid \underline{Y}_i)$ or

$$p_{\underline{x}}(\underline{x}(t_i) \mid \underline{y}(t_i), \underline{y}(t_{i-1}), \underline{y}(t_{i-2}), \ldots, \underline{y}(t_1)) \qquad (V.3)$$

The computational excellence of a Kalman filter comes forward when a recursive expression for (V.3) is derived [Ref. 10] . This recursion starts with a known Gaussian distribution of the state variables at time $t = t_{i-1}$ based on the measurements $\underline{Y}_{i-1}$ and characterized by

$$E[\underline{x}(t_{i-1}) \mid \underline{Y}_{i-1}] = \underline{\hat{x}}(t_{i-1} \mid \underline{Y}_{i-1})$$

$$\mathrm{cov}[\underline{x}(t_{i-1}) \mid \underline{Y}_{i-1}] = \underline{\underline{P}}(t_{i-1} \mid \underline{Y}_{i-1})$$

From this the conditional probability density function

$$p_{\underline{x}}(\underline{x}(t_i) \mid \underline{Y}_i) \qquad (V.4)$$

has to be determined to find the best estimate of the state variables and to provide a starting point for the next recursion.

$$(\underline{\underline{A}} + \underline{\underline{B}}\underline{\underline{C}}\underline{\underline{B}}^*)^{-1}\underline{\underline{B}}\underline{\underline{C}} = \underline{\underline{A}}^{-1}\underline{\underline{B}}(\underline{\underline{C}}^{-1} + \underline{\underline{B}}^*\underline{\underline{A}}^{-1}\underline{\underline{B}})^{-1}$$

results in

$$\hat{\underline{x}}(t_i|\underline{Y}_i) = \hat{\underline{x}}(t_i|\underline{Y}_{i-1}) + \underline{\underline{P}}(t_i|\underline{Y}_{i-1})\underline{\underline{C}}^*\{\underline{\underline{V}}_{\underline{v}} + \underline{\underline{C}}\underline{\underline{P}}(t_i|\underline{Y}_{i-1})\underline{\underline{C}}^*\}^{-1} \cdot$$

$$\cdot \{\underline{y}(t_i) - \underline{\underline{C}}\hat{\underline{x}}(t_i|\underline{Y}_{i-1}) - \underline{\underline{D}}\underline{u}(t_i)\}$$

The covariance of the estimate $\hat{\underline{x}}(t_i|\underline{Y}_i)$ (which is a minimum variance estimate for the problem as stated) is given by

$$\underline{\underline{P}}(t_i|\underline{Y}_i) = \underline{\underline{P}}(t_i|\underline{Y}_{i-1}) +$$

$$- \underline{\underline{P}}(t_i|\underline{Y}_{i-1})\underline{\underline{C}}^*\{\underline{\underline{V}}_{\underline{v}} + \underline{\underline{C}}\underline{\underline{P}}(t_i|\underline{Y}_{i-1})\underline{\underline{C}}^*\}^{-1}\underline{\underline{C}}\underline{\underline{P}}(t_i|\underline{Y}_{i-1})$$

The recursive algorithm derived needs a starting value for the mean and covariance of the state variables. An obvious choice is to specify the initial state $\underline{x}_0$ and a measure of confidence in this value $\underline{\underline{P}}_0$ as the starting values for the state estimation problem.
To highlight the computational simplicity of the recursive Kalman filter algorithm (which was likely obscured in the derivation above) the main formulas, used in a practical application are summarized below. The assumptions (model and statistics) , initial conditions ,time update and measurement update formulas are given for the case of correlation between system and observation noise. This extension [Ref. 11] was omitted in the foregoing derivation for clarity.

Assumed model

$$\underline{x}(t_i) = \underline{\underline{\Phi}}\underline{x}(t_{i-1}) + \underline{\underline{\Gamma}}_{\underline{u}}\underline{u}(t_{i-1}) + \underline{\underline{\Gamma}}_{\underline{w}}\underline{w}(t_{i-1})$$

$$\underline{y}(t_i) = \underline{\underline{C}}\underline{x}(t_i) + \underline{\underline{D}}\underline{u}(t_i) + \underline{v}(t_i)$$

Assumed statistics

$$E[\underline{w}(t_i)] = \underline{0} \quad , \quad E[\underline{v}(t_i)] = \underline{0}$$

$$E[\underline{w}(t_i)\underline{w}^*(t_j)] = \underline{\underline{V}}_{\underline{w}}\delta_{ij}$$

$$E[\underline{v}(t_i)\underline{v}^*(t_j)] = \underline{\underline{V}}_{\underline{v}}\delta_{ij}$$

$$E[\underline{w}(t_i)\underline{v}(t_j)] = \underline{\underline{V}}_{\underline{wv}}\delta_{ij}$$

Starting values

$$\hat{\underline{x}}(t_0|\underline{Y}_0) = \underline{x}_0$$

$$\underline{\underline{P}}(t_0|\underline{Y}_0) = \underline{\underline{P}}_0$$

Time update step

$$\hat{\underline{x}}(t_i|\underline{Y}_{i-1}) = \underline{\underline{\Phi}}\hat{\underline{x}}(t_{i-1}|\underline{Y}_{i-1}) + \underline{\underline{\Gamma}}_{\underline{u}}\underline{u}(t_{i-1}) +$$

$$+ \underline{\underline{K}}_p\{\underline{y}(t_{i-1}) - \hat{\underline{y}}(t_{i-1}|\underline{Y}_{i-1})\}$$

$$\underline{\underline{K}}_p = \underline{\underline{\Gamma}}_w \underline{\underline{V}}_{wv} \underline{\underline{V}}_v^{-1}$$

$$\hat{\underline{y}}(t_{i-1}|\underline{Y}_{i-1}) = \underline{\underline{C}}\hat{\underline{x}}(t_{i-1}|\underline{Y}_{i-1}) + \underline{\underline{D}}\underline{u}(t_{i-1})$$

$$\underline{\underline{P}}(t_i|\underline{Y}_{i-1}) = [\underline{\underline{\Phi}} - \underline{\underline{K}}_p\underline{\underline{C}}]\underline{\underline{P}}(t_{i-1}|\underline{Y}_{i-1})[\underline{\underline{\Phi}} - \underline{\underline{K}}_p\underline{\underline{C}}]^* +$$

$$+ \underline{\underline{\Gamma}}_w \underline{\underline{V}}_w \underline{\underline{\Gamma}}_w^* - \underline{\underline{K}}_p \underline{\underline{V}}_v \underline{\underline{K}}_p^*$$

Measurement update

$$\hat{\underline{x}}(t_i|\underline{Y}_i) = \hat{\underline{x}}(t_i|\underline{Y}_{i-1}) + \underline{\underline{K}}(t_i)\{\underline{y}(t_i) - \hat{\underline{y}}(t_i|\underline{Y}_{i-1})\}$$

$$\hat{\underline{y}}(t_i|\underline{Y}_{i-1}) = E[\underline{y}(t_i|\underline{Y}_{i-1})] = \underline{\underline{C}}\hat{\underline{x}}(t_i|\underline{Y}_{i-1}) + \underline{\underline{D}}\underline{u}(t_i)$$

$$\underline{\underline{K}}(t_i) = \underline{\underline{P}}(t_i|\underline{Y}_{i-1})\underline{\underline{C}}^*\{\underline{\underline{V}}_v + \underline{\underline{C}}\underline{\underline{P}}(t_i|\underline{Y}_{i-1})\underline{\underline{C}}^*\}^{-1}$$

$$\underline{\underline{P}}(t_i|\underline{Y}_i) = \underline{\underline{P}}(t_i|\underline{Y}_{i-1}) - \underline{\underline{K}}(t_i)\underline{\underline{C}}\underline{\underline{P}}(t_i|\underline{Y}_{i-1})$$

The estimates $\hat{\underline{x}}(t_i|\underline{Y}_i)$ and $\underline{\underline{P}}(t_i|\underline{Y}_i)$ determined in the measurement update step serve as new starting values for the next recursion.

The derived state estimator (non-stationary Kalman filter) accounts for the stochastic character of the state variables. Now a statistical estimator is required to define the "best" model representation and to find the corresponding estimates for the unknown parameters.
Bayes rule can be used in order to derive a maximum likelihood estimator for the parameters which is consistent with the recursive appearance of the Kalman filter [Ref. 12] . This gives

$$p(\underline{Y}_N \,,\, \underline{\xi}) = p(\underline{y}(t_N) \mid \underline{Y}_{N-1}, \underline{\xi}) \,.\, p(\underline{Y}_{N-1} \,,\, \underline{\xi})$$

which results in

$$p(\underline{Y}_N \,,\, \underline{\xi}) = \prod_{i=1}^{N} p(\underline{y}(t_i) \mid \underline{Y}_{i-1}, \underline{\xi}) \qquad (V.10)$$

The Gaussian distribution $p(\underline{y}(t_i) \mid \underline{Y}_{i-1}, \underline{\xi})$ follows directly from the Kalman filter algorithm. The mean and covariance are given by

$$E[\underline{y}(t_i \mid \underline{Y}_{i-1}, \underline{\xi})] = \underline{\underline{C}}\hat{\underline{x}}(t_i \mid \underline{Y}_{i-1}, \underline{\xi}) + \underline{\underline{D}}\underline{u}(t_i)$$

$$\mathrm{cov}[\underline{y}(t_i \mid \underline{Y}_{i-1}, \underline{\xi})] = \underline{\underline{C}}\underline{\underline{P}}(t_i|\underline{Y}_{i-1})\underline{\underline{C}}^* + \underline{\underline{V}}_v$$

Substitution in (V.10) results in the following probability density function

$$p(\underline{Y}_N , \underline{\Xi}) = \prod_{i=1}^{N} |2\pi[\underline{\underline{C}}\underline{\underline{P}}(t_i|\underline{Y}_{i-1})\underline{\underline{C}}^* + \underline{\underline{V}}_{\underline{\underline{V}}}]|^{-1/2} .$$

$$\exp[-1/2\{\underline{y}(t_i) - \underline{\underline{C}}\hat{\underline{x}}(t_i|\underline{Y}_{i-1},\underline{\Xi}) - \underline{\underline{D}}\underline{u}(t_i)\}^* . [\underline{\underline{C}}\underline{\underline{P}}(t_i|\underline{Y}_{i-1})\underline{\underline{C}}^* + \underline{\underline{V}}_{\underline{\underline{V}}}]^{-1} .$$

$$. \{\underline{y}(t_i) - \underline{\underline{C}}\hat{\underline{x}}(t_i|\underline{Y}_{i-1},\underline{\Xi}) - \underline{\underline{D}}\underline{u}(t_i)\}] \qquad (V.11)$$

Thus a maximum likelihood estimate for the system parameters is found by maximizing (V.11) with respect to $\underline{\Xi}$. Equivalently the negative of the logarithm of (V.11) can be minimized, deleting irrelevant constant terms this cost function becomes then

$$J_{ML}(\underline{\Xi}) = \sum_{i=1}^{N} (\{\underline{y}(t_i) - \underline{\underline{C}}\hat{\underline{x}}(t_i|\underline{Y}_{i-1},\underline{\Xi}) - \underline{\underline{D}}\underline{u}(t_i)\}^* . [\underline{\underline{C}}\underline{\underline{P}}(t_i|\underline{Y}_{i-1})\underline{\underline{C}}^* + \underline{\underline{V}}_{\underline{\underline{V}}}]^{-1}$$

$$. \{\underline{y}(t_i) - \underline{\underline{C}}\hat{\underline{x}}(t_i|\underline{Y}_{i-1},\underline{\Xi}) - \underline{\underline{D}}\underline{u}(t_i)\} +$$

$$+ \ln|\underline{\underline{C}}\underline{\underline{P}}(t_i|\underline{Y}_{i-1})\underline{\underline{C}}^* + \underline{\underline{V}}_{\underline{\underline{V}}}|) \qquad (V.12)$$

A MAP estimate for the parameters of the system is obtained by maximizing the conditional probability density function $p_{\underline{\Xi}}(\underline{\Xi} \mid \underline{Y}_N)$, this results in an additional term in the cost criterion

$$J_{MAP}(\underline{\Xi}) = J_{ML}(\underline{\Xi}) + (\underline{\Xi} - \underline{m}_{\underline{\Xi}})^* \underline{\underline{P}}_{\underline{\underline{\Xi}}}^{-1}(\underline{\Xi} - \underline{m}_{\underline{\Xi}}) + \ln|\underline{\underline{P}}_{\underline{\underline{\Xi}}}|$$

where $\underline{m}_{\underline{\Xi}}$ and $\underline{\underline{P}}_{\underline{\underline{\Xi}}}$ are the mean and covariance of the (Gaussian assumed) a priori distribution of the system parameters.

The state estimation algorithm and cost criteria derived above provide the means to determine an estimate of the parameters for a system with stochastic state variables.

VI NUMERICAL OPTIMIZATION METHODS

The previous shows that the statistical approach to the parameter estimation problem results in a cost criterion which has to be minimized. A solution in closed form is seldom available for this minimization problem. Therefore a numerical algorithm has to be used to determine the best value of the parameter vector.
Many optimization algorithms have been developed which can be used to find the minimum of a cost function [Ref. 13] . For the general problem however there exists no robust and efficient algorithm, that is an algorithm which always finds the minimum within acceptable accuracy and time. Successful application of a parameter estimation program thus greatly depends on the implemented optimization strategy.

The optimization problem at hand involves a cost function $J(\underline{\Xi})$ with the p dimensional vector valued argument $\underline{\Xi}$. Geometrically the cost function

can be seen as a $p+1$ dimensional hypersurface. The global minimum of this hypersurface has to be determined. It is defined as the point $\hat{\underline{\xi}}$ in the vector space for which

$$J(\hat{\underline{\xi}}) \leq J(\underline{\xi}) \quad \text{for all} \quad \underline{\xi}$$

holds. In general the existence and uniqueness of this minimum cannot be proved when the concept of an assumed model is used for the parameter estimation problem. Using a plausible assumed model justifies however a search for the global minimum in the cost function $J(\underline{\xi})$.

A cause for problems are local minima. $\tilde{\underline{\xi}}$ is defined as a local minimum of the function $J(\underline{\xi})$ when there exists an $\varepsilon > 0$ such that

$$J(\tilde{\underline{\xi}}) \leq J(\tilde{\underline{\xi}} + \underline{h}) \quad \text{for all} \quad \underline{h} \quad \text{with} \quad |\underline{h}| < \varepsilon$$

From the definitions it follows that the global minimum is also a local minimum while the reverse is not true. Most optimization algorithms search for a local minimum in the cost function. It is however very difficult to determine whether the local minimum found with the algorithm also satisfies the condition for the global minimum.

The cost function for the filter-error method is highly non-linear in the parameters $\underline{\xi}$. To find the extremes of non-linear multi-dimensional cost functions many iterative algorithms have been developed. These algorithms generate a sequence of values $\underline{\xi}_k$ given a starting value $\underline{\xi}_0$ which converges to the minimum of the cost function. There are however many problems associated with such an iterative scheme. First a starting value $\underline{\xi}_0$ has to be determined then, while employing an algorithm to compute $\underline{\xi}_{k+1}$ from $\underline{\xi}_k$, the convergence of the algorithm has to be evaluated. When the algorithm has converged to a point in the parameter space it has to be decided whether a minimum has been found or the algorithm has stalled at an arbitrary point. When the former is true then it is still possible that it is a local minimum, the latter indicates a failure of the optimization algorithm for the problem at hand.

The iterative nature of the algorithms requires specification of the step direction and step length in the parameter space to update the parameters. Three methods can be discerned dependent on the highest order of the derivative of the cost function which is used to determine the step direction and step length. Zero order methods do not use explicitly the derivative of the cost function, they are also called direct search methods. First order methods or gradient methods use the first order derivative of the cost function. The higher computational costs, associated with the determination of the derivative is often justified by a more rapid convergence. Higher order methods are usually restricted to second order methods to prevent the computational effort from becoming disproportionate.

Direct search methods

The simplest direct search method consists of evaluating the cost function at a number of points which are chosen randomly or systematically within the parameter space. The simplicity of this method is only surpassed by its inefficiency. The information about the shape of the cost function, obtained

with the function evaluations, is completely discarded in the search for the minimum.

More intelligent direct search methods use exploratory moves to look for directions in the parameter space along which the cost function decreases. Once such a direction is found it is used in a so-called pattern move. Thus the search is directed to the minimum by the local behaviour of the cost function which is determined by exploratory moves. Various implementations of these intelligent direct search methods exist. They may differ in the tactics used to determine pattern directions, the step length of the pattern move and the way they proceed when the information contained in the pattern direction has lost its usefulness.

The parameter estimation program which resulted from the present work comprises two direct search algorithms. The first one is a simple method which determines the cost function value at equidistant points in the parameter space. This method is well suited to investigate the shape of the cost function. The second is an iterative pattern search method due to Hooke and Jeeves [Ref. 14] . The algorithm starts with exploratory moves. From the initial estimate $\underline{\xi}_0$ which is called a base point, a step is made in turn along each coordinate direction (Fig. 1) . If the cost function decreases then the new coordinate is retained. Otherwise a negative step is tried which is either retained when the cost function decreases or retracted. When all coordinate directions have been explored a point in the parameter space is found which is called the present base point $\underline{\xi}_1$. Now a pattern move is made from this present base point. This consists of a step with direction and distance equal to the difference between the present and the previous base point. From the new point, found after the pattern move, exploratory steps are made which are retained when the cost function decreases relative to the present base point $\underline{\xi}_1$ and retracted otherwise. Again a new present base point $\underline{\xi}_2$ is found when all coordinate directions have been explored and the described procedure can be repeated. This procedure continues until no new present base point can be found indicating that the pattern move has lost its value. A new pattern direction can be found by exploratory moves around the latest found present base point $\underline{\xi}_k$. If this fails to produce a new base point then the present base point is either close to the minimum or the exploratory step sizes are too big. Reduction of the exploratory step size until a specified limit is reached concludes the algorithm.

Gradient methods

These methods use the gradient or first order derivative of the cost function with respect to the unknown parameters to determine the step direction of the parameter update. The gradient of the cost function is a vector in the p dimensional parameter space which points tangent to the iso-criterion surface defined by $J(\underline{\xi})$ = constant. Geometrically it is a vector which points in a direction opposite to the direction of steepest descent. The maximum decrease of the cost function resulting from a step in the parameter space with infinitesimal but given length is achieved in the direction of steepest decent. Using this information, contained in the gradient of the cost function, can quicken the iterative search for the minimum.

Gradient methods have however some drawbacks. The gradient is a local property of the iso-criterion hypersurfaces. Therefore, although providing the steepest direction of the hypersurface in a given point of the parameter

space, the gradient can point far from the global minimum. This deficiency of the gradient methods is closely related with the sensitivity to scaling of the parameters.
Close to the minimum another problem is encountered when no special measures with respect to the step length of the parameter update are taken. The algorithms tend to stall when approaching a local minimum as the norm of the gradient vector decreases. One way to solve this problem is to use a one-dimensional line search which however complicates the optimization algorithm due to the extra iterative search required.
The first order derivative of the cost function has to be determined for the gradient methods. Programming of an analytically derived expression for the first order derivative yields the most accurate results with a minimum of computational effort. This approach is however cumbersome and error prone. Numerical differentiation can yield an approximation of the derivative without these problems. This method employs central or one sided differences using only cost function evaluations to determine the derivative. Major drawbacks are the number of function evaluations required and the problem of accuracy which is mainly determined by the choice of the magnitude of the differences.
The parameter estimation program discussed here contains a steepest descent gradient method using an analytically determined first order derivative. Optionally a one-dimensional line search can be combined with this method.

Second order methods

These methods are based on a second order Taylor expansion of the cost function around a given point $\underline{\xi}_k$ in the parameter space

$$J(\underline{\xi}) = J(\underline{\xi}_k) + \left.\frac{\partial J}{\partial \underline{\xi}^*}\right|_{\underline{\xi}=\underline{\xi}_k} (\underline{\xi} - \underline{\xi}_k) + \frac{1}{2} (\underline{\xi} - \underline{\xi}_k)^* \left.\frac{\partial^2 J}{\partial \underline{\xi} \partial \underline{\xi}^*}\right|_{\underline{\xi}=\underline{\xi}_k} (\underline{\xi} - \underline{\xi}_k)$$

The hypersurface defined in the p+1 dimensional space by this approximate cost function is a hyperparaboloid. It is completely determined by the value, the first order derivative and the second order derivative of the cost function in an arbitrary point $\underline{\xi}_k$. The second order derivative is a matrix, also called the Hesse matrix.
The Newton-Raphson optimization algorithm uses this approximation in an iterative search for the minimum of the cost function. The cost function value and the first and second order derivatives in a given starting point $\underline{\xi}_k$ are required. With this information the hyperparaboloid which best approximates the hypersurface of the cost function around $\underline{\xi}_k$ is determined. The minimum of this hyperparaboloid is used as the starting point for the next iteration. The minimum can be found by equating the gradient of the Taylor expansion to zero, this yields

$$\left.\frac{\partial J}{\partial \underline{\xi}}\right|_{\underline{\xi}=\underline{\xi}_k} + \left.\frac{\partial^2 J}{\partial \underline{\xi} \partial \underline{\xi}^*}\right|_{\underline{\xi}=\underline{\xi}_k} (\underline{\xi} - \underline{\xi}_k) = \underline{0}$$

which has the solution

$$\underline{\xi}_{k+1} = \underline{\xi}_k - \left\{ \frac{\partial^2 J}{\partial \underline{\xi} \partial \underline{\xi}^*} \right|_{\underline{\xi}=\underline{\xi}_k} \Bigg\}^{-1} \left. \frac{\partial J}{\partial \underline{\xi}} \right|_{\underline{\xi}=\underline{\xi}_k}$$

In this new starting point $\underline{\xi}_{k+1}$ the cost function value and the first and second order gradient are determined for the next iteration.
For a cost function which is quadratic in the parameters the minimum is found in one step. In the region close to a local minimum of an arbitrary cost function (where the second order derivative is positive definite) the convergence of the Newton-Raphson method is outstanding. Further from the minimum the positive definiteness of the second order derivative is not assured leading to bad convergence or even divergence. These problems can be circumvented by using a start-up optimization algorithm with an assured (but possibly slow) convergence until the forementioned region is reached. Compared with gradient methods, the Newton-Raphson method is not sensitive to scaling of the parameters. Thus the performance is not degraded for cost functions with long narrow shaped valleys. Main disadvantage of the method is the necessity to determine and invert the second order derivative or Hesse matrix. The associated computational costs can be balanced however with the one-dimensional line search algorithm which is not necessary in the Newton-Raphson algorithm.

For quadratic cost functions belonging to the general class of cost functions

$$J(\underline{\xi}) = \sum_{i=1}^{N} 1/2 \{ [\underline{f}(\underline{\xi},..)]^* \underline{\underline{W}} [\underline{f}(\underline{\xi},..)] + \ln|\underline{\underline{W}}^{-1}| \}$$

(compare with the cost functions derived for the filter error method) an approximation of the second order derivative is possible. The following holds for the first order derivative

$$\nabla_{\underline{\xi}} J(\underline{\xi}) = \sum_{i=1}^{N} \{ \nabla_{\underline{\xi}} [\underline{f}(\underline{\xi},..)^*] \underline{\underline{W}} \underline{f}(\underline{\xi},..) + 1/2 \underline{f}(\underline{\xi},..)^* \nabla_{\underline{\xi}} \underline{\underline{W}} \underline{f}(\underline{\xi},..) +$$

$$+ 1/2 |\underline{\underline{W}}| \nabla_{\underline{\xi}} [|\underline{\underline{W}}^{-1}|] \}$$

The second order gradient $\nabla^2_{\underline{\xi}} J(\underline{\xi})$ can be expressed with the so called Hesse matrix

$$\nabla^2_{\underline{\xi}} J(\underline{\xi}) = \begin{bmatrix} \partial^2/\partial\xi_1\partial\xi_1 & \partial^2/\partial\xi_1\partial\xi_2 & \cdots & \partial^2/\partial\xi_1\partial\xi_p \\ \partial^2/\partial\xi_2\partial\xi_1 & \partial^2/\partial\xi_2\partial\xi_2 & \cdots & \partial^2/\partial\xi_2\partial\xi_p \\ \vdots & \vdots & & \vdots \\ \partial^2/\partial\xi_p\partial\xi_1 & \partial^2/\partial\xi_p\partial\xi_2 & \cdots & \partial^2/\partial\xi_p\partial\xi_p \end{bmatrix} \cdot J(\underline{\xi})$$

For the elements $\partial^2/\partial\xi_j\partial\xi_k\ [J(\underline{\xi})]$ of this Hesse matrix the following expression can be derived

$$\partial^2/\partial\xi_j\partial\xi_k\ [J(\underline{\xi})] = \sum_{i=1}^{N} (\partial^2/\partial\xi_j\partial\xi_k[\underline{f}(\underline{\xi},..)]^* \underline{\underline{W}}\ \underline{f}(\underline{\xi},..) +$$

$$+ \partial/\partial\xi_j[\underline{f}(\underline{\xi},..)^*]\ \partial/\partial\xi_k[\underline{\underline{W}}]\ \underline{f}(\underline{\xi},..) +$$

$$+ \partial/\partial\xi_j[\underline{f}(\underline{\xi},..)^*]\ \underline{\underline{W}}\ \partial/\partial\xi_k[\underline{f}(\underline{\xi},..)] +$$

$$+ \partial/\partial\xi_k[\underline{f}(\underline{\xi},..)^*]\ \partial/\partial\xi_j[\underline{\underline{W}}]\ \underline{f}(\underline{\xi},..) +$$

$$+ 1/2\ \underline{f}(\underline{\xi},..)^*\ \partial^2/\partial\xi_j\partial\xi_k[\underline{\underline{W}}]\ \underline{f}(\underline{\xi},..) +$$

$$+ 1/2\ \partial/\partial\xi_k[|\underline{\underline{W}}|\ \partial/\partial\xi_j\{|\underline{\underline{W}}^{-1}|\}]) \qquad (VI.1)$$

A good approximation of this Hesse matrix is the Fisher information matrix which elements are defined by the expectation of VI.1 . The expectation of the error signal $E[f(\underline{\xi},..)]$ approaches zero near the minimum of the cost function. The second order moment of the error signal $E[f(\underline{\xi},..)f(\underline{\xi},..)^*]$ is equal to $\underline{\underline{W}}^{-1}$, the inverse of the weighting matrix $\underline{\underline{W}}$. The following applies then for the elements of the Fisher information matrix

$$E[\partial^2/\partial\xi_j\partial\xi_k\ [J(\underline{\xi})]] = \sum_{i=1}^{N} \partial/\partial\xi_j[\underline{f}(\underline{\xi},..)^*]\ \underline{\underline{W}}\ \partial/\partial\xi_k[\underline{f}(\underline{\xi},..)] +$$

$$+ 1/2\ E[\underline{f}(\underline{\xi},..)^*\ \partial^2/\partial\xi_j\partial\xi_k[\underline{\underline{W}}]\ \underline{f}(\underline{\xi},..)] +$$

$$+ 1/2\ \partial/\partial\xi_k[|\underline{\underline{W}}|\ \partial/\partial\xi_j\{|\underline{\underline{W}}^{-1}|\}]$$

Rewriting this using

$$\underline{f}(\underline{\xi},..)^*\ \partial^2/\partial\xi_j\partial\xi_k[\underline{\underline{W}}]\ \underline{f}(\underline{\xi},..) = tr(\partial^2/\partial\xi_j\partial\xi_k[\underline{\underline{W}}]\ \underline{f}(\underline{\xi},..)\ \underline{f}(\underline{\xi},..)^*)$$

and

$$\partial/\partial\xi_k[|\underline{\underline{W}}|\ \partial/\partial\xi_j\{|\underline{\underline{W}}^{-1}|\}] = tr(\partial/\partial\xi_k[\underline{\underline{W}}]\ \partial/\partial\xi_j[\underline{\underline{W}}^{-1}] +$$

$$+ \underline{\underline{W}}\ \partial^2/\partial\xi_j\partial\xi_k[\underline{\underline{W}}^{-1}])$$

yields

$$\partial^2/\partial\xi_j\partial\xi_k\ [J(\underline{\xi})] \approx \sum_{i=1}^{N} \partial/\partial\xi_j[\underline{f}(\underline{\xi},..)^*]\ \underline{\underline{W}}\ \partial/\partial\xi_k[\underline{f}(\underline{\xi},..)] +$$

$$+ \tfrac{1}{2}\,\mathrm{tr}(\partial^2/\partial\xi_j\partial\xi_k[\underline{\underline{W}}]\;\underline{\underline{W}}^{-1} + \partial/\partial\xi_k[\underline{\underline{W}}]\;\partial/\partial\xi_j[\underline{\underline{W}}^{-1}] +$$

$$+ \underline{\underline{W}}\;\partial^2/\partial\xi_j\partial\xi_k[\underline{\underline{W}}^{-1}])$$

This finally results in the following expression for the elements of the Fisher information matrix

$$\partial^2/\partial\xi_j\partial\xi_k\,[J(\underline{\xi})] \approx \sum_{i=1}^{N} \partial/\partial\xi_j[\underline{f}(\underline{\xi},..)^*]\;\underline{\underline{W}}\;\partial/\partial\xi_k[\underline{f}(\underline{\xi},..)] +$$

$$+ \tfrac{1}{2}\,\mathrm{tr}(\partial/\partial\xi_j[\underline{\underline{W}}]\;\underline{\underline{W}}^{-1}\;\partial/\partial\xi_k[\underline{\underline{W}}]\;\underline{\underline{W}}^{-1}) \qquad \text{(VI.2)}$$

The derived approximation of the second order derivative or Hesse matrix requires only the determination of first order derivatives. The second order optimization algorithm which uses expression (VI.2) to approximate the second order gradient is called the Gauss-Newton method. This method possesses the same excellent performance as the Newton-Raphson method near the minimum of the cost function where the assumptions made are valid. Further from the minimum the Gauss-Newton can be expected to perform better because (VI.2) assures a positive definite second order gradient. As mentioned before the Newton-Raphson method can diverge in these regions due to a non-positive definite Hesse matrix.

It follows that in order to minimize the cost function resulting from the filter error method with a second order Gauss-Newton optimization algorithm the first order derivatives

$$\partial/\partial\xi_j[\underline{f}(\underline{\xi},..)] \qquad \text{and} \qquad \partial/\partial\xi_j[\underline{\underline{W}}]$$

are required. With

$$\underline{f}(\underline{\xi},..) = \underline{y}(t_i) - \hat{\underline{y}}(t_i|\underline{Y}_{i-1}) = \underline{y}(t_i) - \underline{\underline{H}}\hat{\underline{x}}(t_i|\underline{Y}_{i-1}) - \underline{\underline{D}}\underline{u}(t_i)$$

and

$$\underline{\underline{W}} = [\,\underline{\underline{H}}\underline{\underline{P}}(t_i|\underline{Y}_{i-1})\underline{\underline{H}}^* + \underline{\underline{V}}_{\underline{\underline{V}}}\,]^{-1}$$

Determination of these first order derivatives involves the determination of the derivatives of the Kalman filter matrices. The necessary computations require a punctilious but straightforward application of the rules for differentiation and is omitted here.

VII THE PROGRAM MLPEFSS

Solving a system identification problem with a statistical estimator is an endless task without the use of digital computers. Also the iterative numerical optimization of the cost function compels the use of a digital computer. To this end the derivations of the mathematical descriptions and algorithms were aimed at an implementation on a digital computer. The Maximum Likelihood Parameter Estimation program For Stochastic Systems (MLPEFSS) that resulted employs the state space description to describe the

assumed model which can include both measurement noise and process noise. The filter-error method is used in combination with the maximum likelihood estimator to obtain the "best" representation of the system. The cost function optimization section of the program includes a grid like direct search method and the Hooke & Jeeves direct search method, the steepest descent gradient method and the second order Gauss-Newton method. The user of the program can choose the desired optimization method interactively thus directing the optimization process.

To verify the working of the complete program it was decided to test it on several parameter estimation problems using simulated data. The results of one test case is given here. A simulation of a second order system with a spring stiffness 10 N/m and a damping coefficient 1 Ns/m was employed to generate the simulated data (Fig. 2) . Both the measurement noise and process noise were obtained using a pseudo random generator with near Gaussian and near white signal characteristics.
The deterministic input signal was a block type signal with amplitude 1 N and a period of 4 s . This deterministic input signal is plotted in Fig. 3a with an additive process noise signal. The mean and standard deviation of the process noise are 0 respectively 0.05 . The simulation yielded the measured variables Y(1) and Y(2) given in Fig. 3b-c . Measurement noise with a mean value 0 and standard deviation 0.01 was added.
The spring stiffness and damping coefficient were considered as unknown parameters. Within the framework of a statistical parameter estimation method the estimate of a parameter is a random variable and the result of the estimation method is a sample of this random variable. Therefore 9 different simulations were made (using different stochastic signals) which resulted in the parameter estimates presented in Fig. 3d-e .
Combining the results yields the following values for the estimates of the spring stiffness P(1) and the damping coefficient P(2)

	True value	Estimate	Standard deviation
P(1)	10.00	10.01	0.078
P(2)	1.00	1.03	0.033

Based on the satisfactory results of all test cases it could be stated that the program performs well for the task it was designed for.

The next step, which has not yet been carried out, is to use the program on real parameter estimation problems. Compared with the simulated test cases used to validate the program MLPEFSS, the application to real system identification problems is much more complicated. It wil involve the determination of the assumed model structure (model identification) , the design of a data acquisition system and the design of an (optimized) control input signal.
Some improvements of the program MLPEFSS are still possible. At the moment the program is suited for linear, time invariant dynamic systems. Incorporation of an Extended Kalman filter is a way to make the program MLPEFSS applicable to non-linear dynamic systems. Further the Gauss-Newton optimization algorithm can be improved by using a rank-deficient matrix inversion method for the Fisher information matrix. This method prevents a large parameter update step when the measurements contain little or no information regarding this parameter, thus improving the convergence.

VIII REFERENCES

[1] Etkin B. — Dynamics of Flight
John Wiley & Sons , New York , 1959

[2] Kwakernaak H.
Sivan R. — Linear Optimal Control Systems
John Wiley & Sons , New York , 1972

[3] Gerlach O.H. — Lecture Notes on Airplane Stability and Control
Part I & II
Report LR-384-I & II
Delft University of Technology,
Department of Aerospace Engineering, 1983

[4] Eykhoff P. — System Identification, Parameter and State Estimation
John Wiley & Sons , London , 1974

[5] Gerlach O.H. — The Determination of Stability Derivatives and Performance Characteristics from Dynamic Manoeuvres
AGARD CP-85 , Flight Test Techniques
paper 16 , 1971

[6] Zadeh L.A.
Desoer C.A. — Linear System Theory : The State Space Approach
McGraw-Hill , New York , 1963

[7] Moler C.
Van Loan C. — Nineteen Dubious Ways to Compute the Exponential of a Matrix
SIAM Review , vol 20 , no 4 , 1978

[8] Reza F.M. — An Introduction to Information Theory
McGraw-Hill , New York , 1961

[9] Leondes C.T.
(editor) — Theory and Application of Kalman Filtering
AGARDOgraph 139 , 1970

[10] Bierman G.J. — Factorization Methods for Discrete Sequential Estimation
Academic Press , New York , 1977

[11] Sage A.P.
Melsa J.L — Estimation Theory with Applications to Communications and Control
McGraw-Hill , New York , 1971

[12] Maine R.E.
Illif K.W. — Identification of Dynamic Systems
AGARDOgraph 300 , 1985

[13] Murray W. — Numerical Methods for Unconstrained Optimization
Academic Press , London , 1972

[14] Hooke R.
Jeeves T.A. — Direct Search Solution of Numerical and Statistical Problems
J.Ass.comput.Mach. , vol 8 , 1961

Hooke & Jeeve
Direct search method

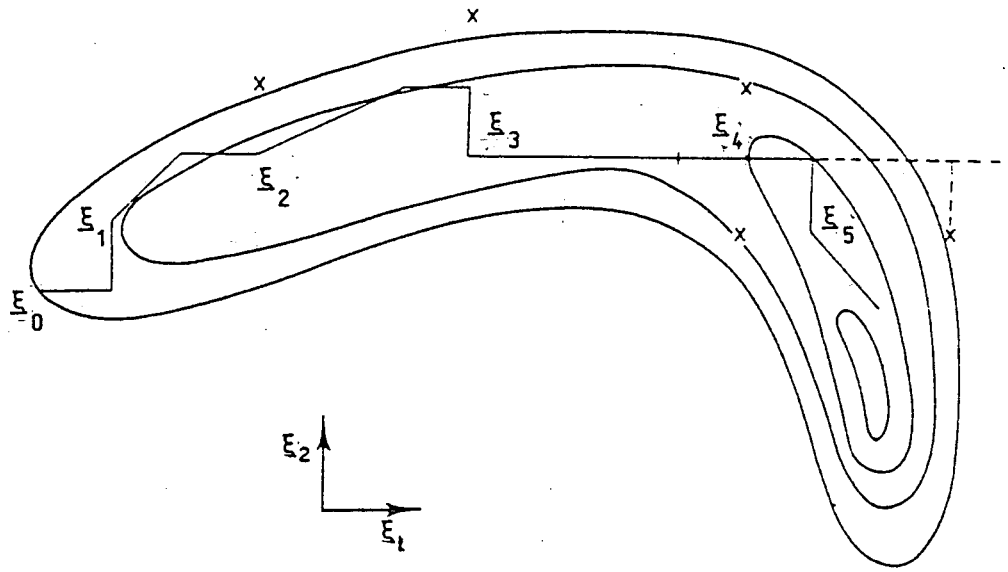

Fig. 1

Damped mass-spring system

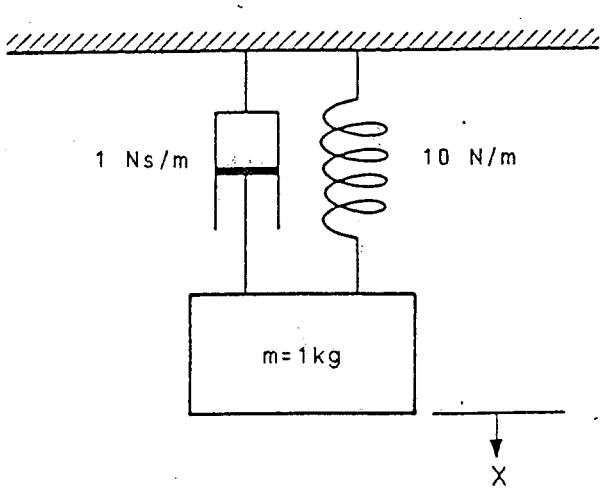

Fig. 2

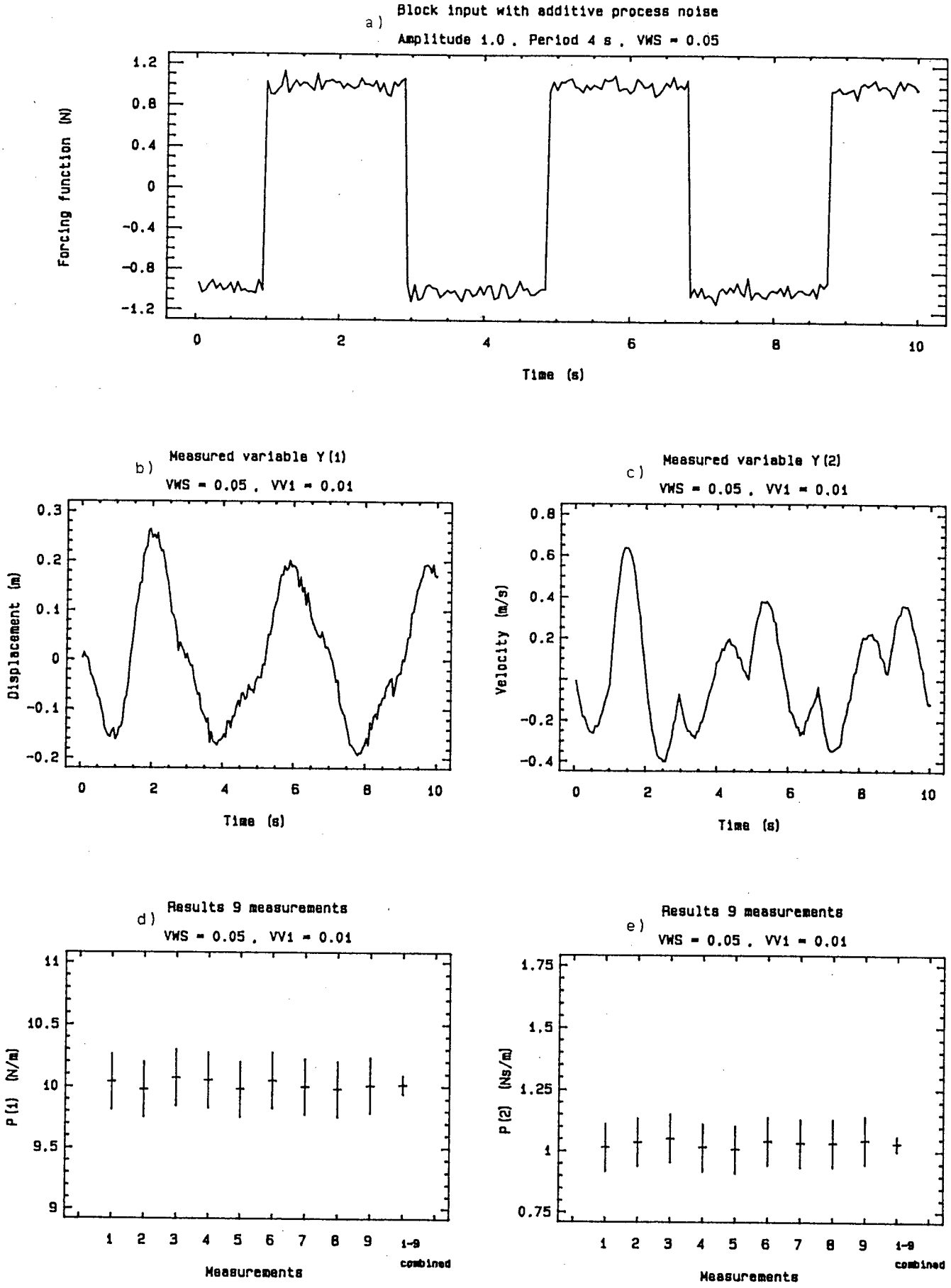
a)
Block input with additive process noise
Amplitude 1.0 . Period 4 s . VWS = 0.05
Forcing function (N)
Time (s)
b)
Measured variable Y(1)
VWS = 0.05 . VV1 = 0.01
Displacement (m)
Time (s)
c)
Measured variable Y(2)
VWS = 0.05 . VV1 = 0.01
Velocity (m/s)
Time (s)
d)
Results 9 measurements
VWS = 0.05 . VV1 = 0.01
P(1) (N/m)
Measurements
1-9 combined
e)
Results 9 measurements
VWS = 0.05 . VV1 = 0.01
P(2) (Ns/m)
Measurements
1-9 combined

Fig. 3

OPTIMAL INPUTS FOR AIRCRAFT PARAMETER ESTIMATION

J.A. Mulder

Delft University of Technology

Summary

The accuracy of aircraft stability- and control derivatives as estimated from dynamic response measurements depends on the form of the time histories of the control inputs. After selecting a suitable criterion and imposing constraints on either the aircraft's state or the control inputs it is possible to optimize the form of these time histories. A new method for control input optimization is proposed in the present paper. The new method avoids some disadvantages of earlier methods and was succesfully applied in the design of longitudinal and lateral flighttest manoeuvres.

OPTIMAL INPUTS FOR AIRCRAFT PARAMETER ESTIMATION

Aircraft stability- and control derivatives, i.e. the parameters in linear models of external aerodynamic forces and moments, can be estimated from measurements of dynamic flighttest manoeuvres. These manoeuvres are the responses on small longitudinal or lateral control inputs such that the validity of the linear aerodynamic models is not violated. Other types of parameters, defining the aircraft's inertial characteristics such as mass, center of gravity, moments and products of inertia are usually derived from measurements on the ground, or from a numerical integration over the spatial volumes of the structural components of the aircraft.

The accuracy of the estimated stability- and control derivatives depends not only on the characteristics of the flighttest instrumentation system but also on the form of the control input time histories. In the present work, attention is focussed on the optimization of aircraft control inputs for the estimation of stability and control derivatives. Starting with the work of Nahi, Ref. 16, the problem of calculating optimal input signals for the estimation of parameters in dynamical systems from response measurements was subsequently studied by several authors. Surveys of available literature are given in Refs. 5 and 7. In the field of dynamic flight testing, Gerlach in Ref. 3 appears to be the first who explicitly recognized the influence of the form of input signals on the accuracy of stability- and control derivatives estimated from dynamic flight test measurements. He proposed a qualitative method for the determination of 'optimal' frequencies in scalar input signals to linear second order systems, see also Ref. 4.

The significance of the work of Nahi stems for the idea to use a norm of Fisher's information matrix (M) as a criterion (J) for the optimization of input signals. The inverse of Fisher's information matrix (M^{-1}), may be interpreted as a 'universal' lower bound on parameter estimation accuracies, called the Cramér-Rao lower bound (CRLB); see Ref. 15. The idea to base the optimization of input signals on a norm of the information matrix results in input signals which have a general significance, in the sense of being independent of the algorithm used to estimated the parameters.

In principle, any scalar norm of M could be used as a criterion for the optimization of input signals. Only the following three norms, however, are frequently mentioned in the literature, see Ref. 5:

a) $J = \text{tr } M$

By maximizing tr M, the trace of the information matrix, no attention is given to the condition of the information matrix. This means that the optimized input signals will not necessarily lead to good or even acceptable parameter estimation accuracies, since the latter are related to the Cramér-Rao lower bound. In spite of this rather unfavourable characteristic the criterion was used by several authors, for reasons of computational efficiency; e.g. Refs. 16 and 19.

b) $J = \ln \det M$

Input signals based on maximization of ln det M are called 'D-optimal'. These input signals minimize the volume of the one-sigma ellipsoid of the Gaussian multidimensional probability density function of parameter estimation errors, as explained in Ref. 5.

c) $J = \text{tr } M^{-1}$

The resulting input signals are called 'A-optimal', see Ref. 12, and minimize the sum of the variances of the parameter estimation errors, i.e. the diagonal elements of the Cramér-Rao lower bound.

Important contributions to the theory of optimal input signals were made by Mehra, Refs. 10, 11 and 12. Based on the work of Kiefer and Wolfowitz in Ref. 9, and Kiefer, Ref. 8, Mehra proposes algorithms for the design of scalar and multidimensional input signals in the frequency domain as well as in the time domain.

Algorithms for the optimization of input signals in the frequency domain are efficient with respect to computation time; Ref. 10. Furthermore, the underlying optimization problem can be shown to be convex. In this context, convexity refers to the form of the object function or criterion for which the extreme must be located. Convexity is an attractive property, as it implies one global extreme rather than several or even many local extremes. The result of the optimization is a line spectrum, which can in a rather heuristic way be used to compose an input signal in the time domain; see also Ref. 5.

The frequency domain algorithms depend on the assumption of stationarity of the system response. Consequently, the system must be asymptotically stable. Furthermore, the assumption of stationarity means in practice, that the length of the resulting input signals in the time domain must be at least several times the largest characteristic period of the system. This would lead to rather long, and therefore time-consuming flight test manoeuvres.

In the time domain, the optimization of input signals can be formulated in terms of a nonlinear optimal control problem; see Refs. 5 and 11. Nonlinear optimal control problems are notoriously difficult to solve; Ref. 2. Furthermore, in actual implementations it may be important to apply constraints on the input signal in the frequency domain. A typical example is the limitation of the input signal bandwith as imposed by the finite sample rate of the instrumentation system. It is difficult to take account of such constraints in the frequency domain when the factual optimization is performed in the time domain.

A new method for optimizing input signals is proposed in the present paper. The method circumvents some of the problems just mentioned. The basic idea is to represent input signals by a linear combination of a finite number of members of a set of orthonormal functions. In doing so, input signals are described by a finite number of parameters. These parameters may subsequently be optimized. In the following Sections, the method is discussed in detail. The new method is succesfully applied to the problem of optimizing a two dimensional lateral aircraft control input signal in Ref. 13.

A so-called circularity problem arises as a result of the optimized input signals being dependent on the parameters in the system model. Consequently, these parameters have to be known before the optimization process can be carried out. However, estimation of these parameters would obviously not be required if they were already known. A possible procedure to address the circularity problem would consist of the implementation of a sequence of optimized input signals. The first input signal would be based on some a priori estimates of the system parameters. Each following input signal would be based on parameter values as deduced from measured responses on a preceding input signal. Such an iterative procedure raises the interesting and yet unsolved question whether, and if so under which conditions, it would converge.

In dynamic flight testing it is often possible to determine fairly accurate a priori estimates of stability- and control derivatives from aerodynamic calculations or windtunnel measurements. This means that the circularity problem is generally not of great practical importance.

In the present paper the new method for the optimization of input signals is described in detail. It is shown, that optimal input signals may be derived as the solution of a nonlinear optimization problem. Starting with the general case of nonlinear systems, it is shown that in the case of linear systems, the necessary computations can be carried out much more efficiently.

1 Representation of multidimensional input signals

In the following, let $\underline{u}(t)$ denote an s dimensional input signal with components $u_\ell(t)$, $\ell = 1(1)\ s$:

$$\underline{u}(t) = \text{col}\,[u_1(t),\ \ldots,\ u_\ell(t),\ \ldots,\ u_s(t)]. \qquad t \in [t_o,\ t_1] \tag{1}$$

The crux of the present method for the optimization of input signals lies in the introduction of certain constraints on form and energy of each of the components of the multidimensional input signal $\underline{u}(t)$ in the time interval $[t_o, t_1]$. The constraints on form are the consequence of an approximation of the components u_ℓ of $\underline{u}$ by means of a weighted sum of a finite number of p orthonormal functions $\psi_k(t)$, $k = 1(1)\ p$, according to:

$$u_\ell(t) = \sum_{k=1}^{p} \beta_{k\ell}\ \psi_k(t) \tag{2}$$

in which $\beta_{k\ell}$, $k = 1(1)\ p$, denote a set of weighting factors. The functions $\psi_k(t)$ are assumed to be orthonormal on $[t_o, t_1]$, as defined by:

$$\int_{t_o}^{t_1} \psi_k(t)\ \psi_n(t)\ dt = \delta_{kn}$$

where δ_{kn} denotes the Kronecker delta. The shape of the orthonormal functions $\psi_k(t)$ has still to be defined in more detail later on.
The energy of the different components $u_\ell(t)$ of $\underline{u}(t)$ in the time interval $[t_o,t_1]$ is constrained to a set of fixed and a priori selected values.
The energy E_ℓ of the component $u_\ell(t)$ in $[t_o,t_1]$ can be written as:

$$E_\ell = \int_{t_o}^{t_1} u_\ell^2(t)\, dt = \int_{t_o}^{t_1} \{ \sum_{k=1}^{p} \beta_{k\ell}\, \psi_k(t)\}^2\, dt$$

$$= \sum_{k=1}^{p} \sum_{n=1}^{p} \beta_{k\ell}\, \beta_{n\ell} \int_{t_o}^{t_1} \psi_k(t)\, \psi_n(t)\, dt = \sum_{k=1}^{p} (\beta_{k\ell})^2 \qquad (3)$$

Eq. (3) is in fact, a particular form of Parseval's theorem, Ref. 1. It follows from (3) that for given energy E_ℓ in the time interval $[t_o,t_1]$, the component $u_\ell(t)$ can be represented by a point P_ℓ on a hypersphere in p dimensional euclidian space with radius $R_\ell = \sqrt{E_\ell}$. The position of P_ℓ on the sphere can be expressed not only in Cartesian or rectangular, but also in spherical coordinates. The rationale behind the introduction here of spherical coordinates will become clear in Section 2 below. The relations between the rectangular coordinates $\beta_{k\ell}$ and the corresponding spherical coordinates $\phi_{j\ell}$ of P_ℓ can be written as:

$$\beta_{1\ell} = R_\ell \sin \varphi_{1\ell}, \qquad (4a)$$

$$\beta_{k\ell} = R_\ell \prod_{j=1}^{k-1} \cos \phi_{j\ell} \sin \varphi_{k\ell}, \qquad \text{for } k = 2(1)\ p-1, \qquad (4b)$$

$$\beta_{p\ell} = R_\ell \prod_{j=1}^{p-1} \cos \phi_{j\ell}, \qquad (4c)$$

as depicted in Fig. 1 for the case p = 3. The form of the relations (4) depends on the particular definition of the spherical coordinates, which is not unique. The present definition, however, results in the simplest algorithms for the analytical expressions of the matrix derivatives, to be derived later in Section 4.

It will be convenient to define the vectors:

$$\underline{\beta}_\ell = \text{col}\,[\beta_{1\ell}, \ldots, \beta_{p\ell}], \qquad \text{for } \ell = 1(1)\ s,$$

where p is the number of individual orthogonal components in u_ℓ and s is the dimension of u, i.e. the number of input signals considered together.

The elements of each vector $\underline{\beta}_\ell$ are the weighting factors in a representation (2) of the corresponding component of u_ℓ of the input vector $\underline{u}$. Next, the elements of all the vectors $\underline{\beta}_\ell$ are arranged in one column, in the form of a new vector $\underline{\beta}$, (5), with elements β_i. If q denotes the dimension of this new vector $\underline{\beta}$, then q = sp, since $\underline{\beta}$ contains s vectors $\underline{\beta}_\ell$ of dimension p each. Consequently, in (5), i ranges from 1 to q:

$$\underline{\beta} = \begin{bmatrix} \underline{\beta}_1 \\ \vdots \\ \underline{\beta}_\ell \\ \vdots \\ \underline{\beta}_s \end{bmatrix} = \begin{bmatrix} \beta_1 \\ \vdots \\ \beta_i \\ \vdots \\ \beta_q \end{bmatrix} \tag{5}$$

The vector $\underline{\beta}$ contains the weighting factors in the representations of all components of $\underline{u}$.

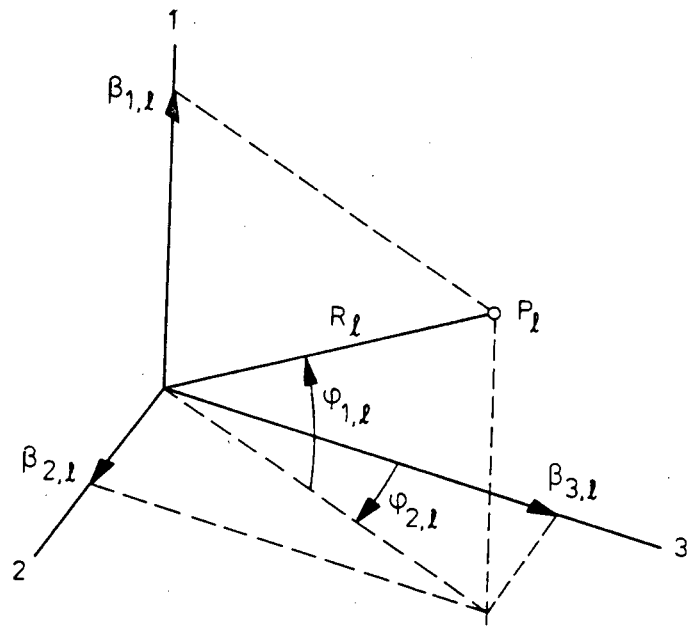

Fig. 1: Rectangular and spherical coordinates of P_ℓ in p dimensional Euclidean space representing u_ℓ with energy $E_\ell = R_\ell^2$ in $[t_o, t_1]$.

Next, a set of q so-called elementary input signals is introduced. An elementary input signal is an s-dimensional vector, indicated by $\underline{e}_i$, and defined as follows:

$$\underline{e}_1(t) = \begin{bmatrix} \psi_1(t) \\ 0 \\ \vdots \\ 0 \end{bmatrix} \Big\updownarrow s \quad , \quad \underline{e}_2(t) = \begin{bmatrix} \psi_2(t) \\ 0 \\ \vdots \\ 0 \end{bmatrix} \quad , \ \ldots , \quad \underline{e}_p(t) = \begin{bmatrix} \psi_p(t) \\ 0 \\ \vdots \\ 0 \end{bmatrix} \quad ,$$

(6)

$$\underline{e}_{p+1}(t) = \begin{bmatrix} 0 \\ \psi_1(t) \\ 0 \\ \cdot \\ \cdot \\ \cdot \\ 0 \end{bmatrix} \quad , \ \ldots , \quad \underline{e}_i(t) = \begin{bmatrix} 0 \\ \cdot \\ 0 \\ \psi_k(t) \\ \cdot \\ \cdot \\ 0 \end{bmatrix} \Big\updownarrow \ell \quad , \ \ldots , \quad \underline{e}_q(t) = \begin{bmatrix} 0 \\ \cdot \\ 0 \\ \cdot \\ \cdot \\ \cdot \\ \psi_p(t) \end{bmatrix} \quad ,$$

where k = 1(1) p and ℓ = 1(1) s.

It may be deduced from (6) that $i = (\ell-1).p + k$, which implies that $i = 1(1)\ q$. The set of elementary input signals can be interpreted as the columns of a matrix D(t), as shown in Fig. 2 for the case that $s = 2$ and $p = 4$.

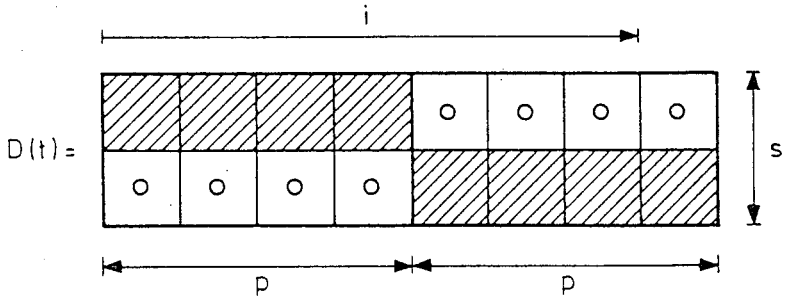

Fig. 2: Definition of matrix D(t) pf a 2-dimensional input signal (s=2) consisting of 4 orthonormal functions (p=4). Shaded areas denote nonzero elements; i refers to a particular column of D(t), i.e. the elementary input signal $\underline{e}_i(t)$.

The advantage of these elementary input signals is, that they allow $\underline{u}(t)$ to be written in the following compact form:

$$\underline{u}(t) = D(t)\ .\ \underline{\beta} = \sum_{i=1}^{q} \beta_i\ \underline{e}_i(t), \qquad (7)$$

in which $\underline{\beta}$ denotes the vector of weighting factors as defined in (5).

In principle, any set of functions orthonormal on $[t_o,t_1]$ could be used in (1-2). If the set is 'complete' then any continuous function on $[t_o,t_1]$ can be approximated 'to any desired degree of accuracy' by increasing the total number of orthonormal functions, i.e. the value of p; Ref. 1. This means that for $p \to \infty$, optimized input signals of the form (2) will be independent of the particular class of orthonormal functions used. In practice, for reasons discussed in the following Sections, p is limited to finite and relatively small values. In that case, it must be expected that the form of the optimized input signals will be influenced by the set of orthonormal functions used in (2). For example, in

Ref. 21, a set of orthonormal functions is described which consists of positive and negative steps to +1 and -1 respectively. Application of these so-called Walsh functions, see Fig. 3, would result in input signals consisting of a finite number of positive and negative steps of varying magnitudes*.

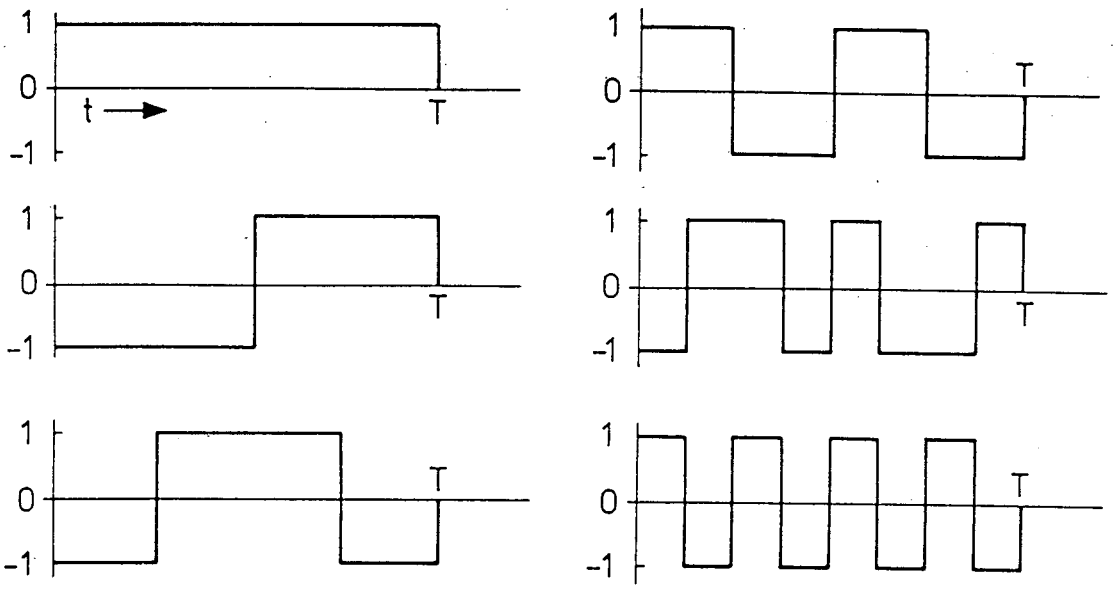

Fig. 3: Orthonormal Walsh functions in the time interval [0,T].

In the present work, it was decided to make use of sets of orthonormal sinusoidal or sin functions. One advantage of this decision is that each sin function is - although loosely - related to a particular frequency, which makes it possible to 'influence' the frequency contents of the optimized input signals by excluding particular terms from (2). This might be desirable for reasons mentioned below. The following two sets of sin functions may readily be shown to be orthonormal over the time interval $[t_o, t_1]$:

set 1:

$$\psi_k(t) = \sqrt{\frac{2}{T}} \sin \omega_k t, \qquad (8)$$

---

* Input signals of this kind are considered to be less suitable for actual implementation in flight. However, for excitation of for instance the pharmaco-kinetic system described in Ref. 20, such input signals would be very practical.

$$\omega_k = k\,\omega_{o_1}, \qquad \omega_{o_1} = \frac{2\pi}{T},$$

set 2:

$$\psi_k(t) = \sqrt{\frac{2}{T}} \sin \omega_k t, \tag{9}$$

$$\omega_k = k\,\omega_{o_2}, \qquad \omega_{o_2} = \frac{\pi}{T},$$

in which $k = 1(1)\ p$, $t \in [t_o, t_1]$, and $T = t_1 - t_o$. The sin functions of set 1 and set 2 are depicted in Fig. 4 and Fig. 5 respectively. It is noted that any input signal which is composed of set 1 or set 2 functions will be zero at $t = t_o$ and $t = t_1$. This is another advantage of using sin functions for the design of aircraft control input signals: since in flight these input signals will be superimposed on the corresponding trim values, the resulting time histories of control surface deflections will be free of unwanted discontinuities.

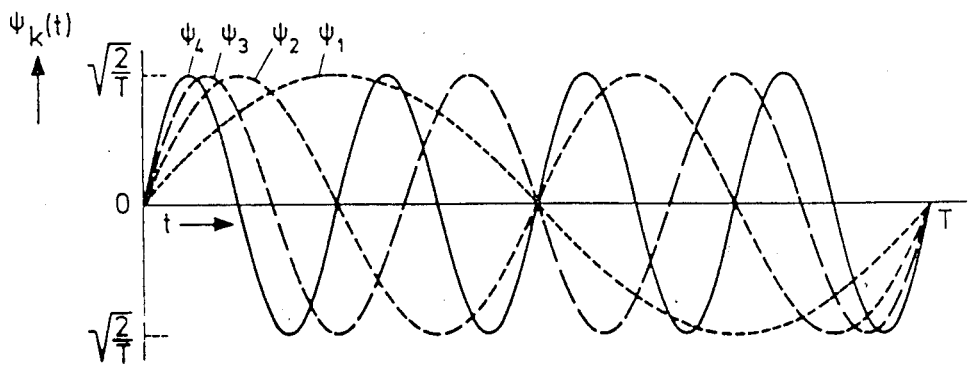

Fig. 4: Orthonormal sin functions of set 1, (8), in the time interval [0,T].

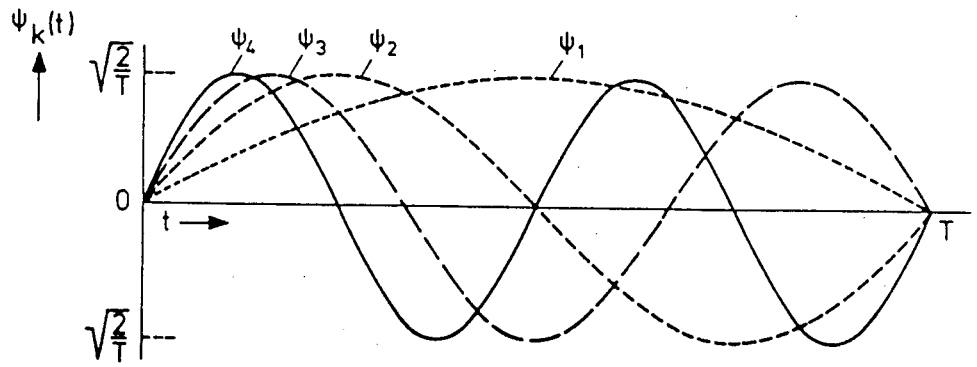

Fig. 5: Orthonormal sin functions of set 2, (9), in the time interval [0,T].

Set 1 consists of functions having k periods in $[t_o,t_1]$, set 2 consists of functions having k half periods in $[t_o,t_1]$.

Sets of only sin functions are not complete. It is possible to define a complete set of orthonormal functions by adding a constant and cosin functions to the sin functions of set 1. The resulting set of functions is indicated as set 3; see Fig. 6:

set 3:

$$\psi_o(t) = \frac{1}{T}, \qquad (10)$$

$$\psi_{1_k}(t) = \sqrt{\frac{2}{T}} \sin \omega_k t,$$

$$\psi_{2_k}(t) = \sqrt{\frac{2}{T}} \cos \omega_k t,$$

$$\omega_k = k\,\omega_{o_1},\ \omega_{o_1} = \frac{2\pi}{T},$$

in which again k = 1(1) p, $t \in [t_o,t_1]$ and $T = t_1 - t_o$.

In the present context, functions of set 3 are of theoretical interest only. Input signals based on these functions will in general not be zero at t_o and t_1.

However, their performance may be compared to the performance of input signals consisting of set 1 of set 2 functions. This allows evaluation of the penalty imposed by the non-completeness of these latter sets of orthonormal functions.

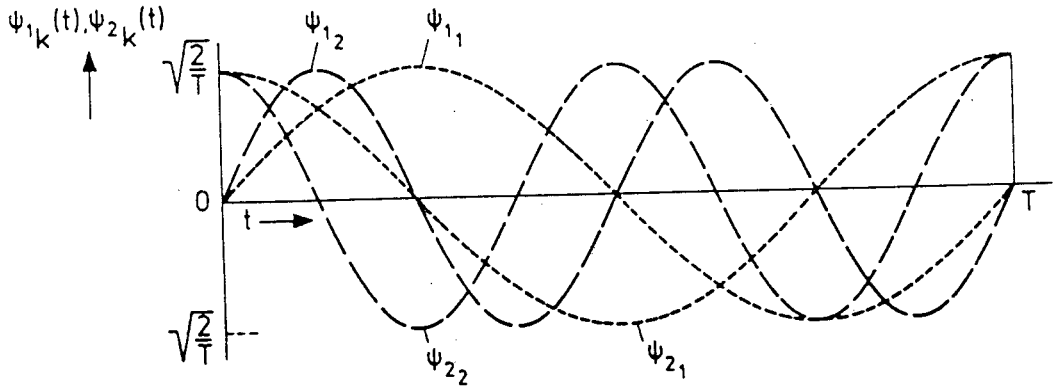

Fig. 6: Orthonormal functions of set 3, (10), in the time interval [0,T].

As mentioned above, ω_k in (8), (9) and (10) is loosely related to the frequency contents of the particular function. As k becomes larger, the power of the corresponding sin or cosin function in a power spectral density plot is concentrated more closely around ω_k. This fact may be used by the designer, to limit the frequency contents of input signals. It is possible, for instance, to take account of the finite bandwidth of the presampling filters in the measurement system. Another possibility is to design input signals such that undesirable characteristic modes are not excited. A typical example of such characteristic modes could be the high frequency structural modes of flexible aircraft.

2 Input signal optimization for nonlinear system parameter estimation

In the present Section it is shown that the design of multidimensional input signals for nonlinear system parameter estimation may be formulated in terms of a nonlinear optimization problem. The nonlinear systems considered are of the following form:

$$\dot{\underline{x}}(t) = \underline{f}(\underline{\theta}, \underline{x}(t), \underline{u}(t)) \tag{11}$$

in which $\underline{x}$ denotes an n-dimensional state vector, $\underline{u}$ an s-dimensional input signal and $\underline{\theta}$ a vector of r system parameters for which it is assumed that a set of approximate a priori values is known. Furthermore, $\underline{f}$ denotes a real valued vector function of dimension n. Each of its components is assumed to be continuous, such that its partial derivatives with respect to $\underline{\theta}$, $\underline{x}$ and $\underline{u}$ exist. The system is observed at discrete instants of time $t_i \in [t_o, t_1]$, i = 1(1) N, according to the following nonlinear observation model:

$$\underline{y}(i) = \underline{h}(\underline{\theta}, \underline{x}(i), \underline{u}(i)) \tag{12}$$

in which $\underline{y}$ denotes an m-dimensional vector of observations at $t = t_i$. The usual assumption is made, that observation measurement errors are adequately represented by additive stationary Gaussian sequences of stochastic variables, which are assumed to have zero mean values and to be uncorrelated in time. However, measurement errors pertaining to the same instant of time are not assumed to be uncorrelated. This leads to the following measurement model:

$$\begin{aligned} &\underline{y}_m(i) = \underline{y}(i) + \underline{v}(i), \\ &E\{\underline{v}(i)\} = \underline{0}, \\ &E\{\underline{v}(i)\ \underline{v}^T(j)\} = V_{vv} \cdot \delta_{ij}, \end{aligned} \tag{13}$$

for i,j = 1(1) N.

The input signal, $\underline{u}(t)$, is also sampled at discrete instants of time. The corresponding measurement errors are assumed to be small enough to be negligible. This situation is considered to be quite representative for the case of flight tests, where control surface deflections can indeed be measured with high accuracy.

The system model (11) is restricted to be deterministic. In the present context this implies that the actual measurements are made in a stable atmosphere, where turbulence is negligible. Furthermore, stochastic contributions to the aerodynamic forces and aerodynamic moments, as generated for instance in the

boundary layer, are also neglected. In general these stochastic contributions are very small, except in those flight regimes where appreciable flow separation occurs.

With the assumptions made above, the solution of the system differential equations may, for given values of the initial state vector $\underline{x}_o = \underline{x}(t_o)$ and the parameter vector $\underline{\theta}$, be calculated according to:

$$\underline{x}(t) = \underline{x}_o + \int_{t_o}^{t} \underline{f}(\underline{\theta}, \underline{x}(t), \underline{u}(t))\, dt. \qquad (14)$$

The maximum likelihood (ML) estimate of $\underline{\theta}$ corresponds to the global maximum of the logarithm of the likelihood function ln L of the observation measurements, see Ref. 15. For a given input signal time history $\underline{u}(t)$ in the time interval $[t_o, t_1]$, this likelihood function depends not only on the parameter vector $\underline{\theta}$, but in addition on $\underline{x}_o$ and on the elements of the variance matrix of measurement errors V_{vv}. The dimensions of the parameter vector $\underline{\theta}$ and the initial vector $\underline{x}_o$ are r and n respectively. In the most general case, the total number of nonidentical elements in the symmetrical covariance matrix V_{vv} of observation measurement errors is $\frac{1}{2}$ m (m + 1), if this matrix is assumed to be nondiagonal. In cases where $\underline{x}_o$ and V_{vv} are unknown, they must be estimated in addition to $\underline{\theta}$. The solution of the ML estimation problem then involves locating the global maximum in the r + n + $\frac{1}{2}$ m (m + 1) dimensional space of $\underline{\theta}$, $\underline{x}_o$ and the upper triangular elements of V_{vv}. The elements of V_{vv}^{-1} rather than of V_{vv} are chosen here as the unknowns to be estimated. This has the effect of simplifying the analytical expressions of the partial first- and second order derivatives below. For notational convenience, the upper triangular elements of V_{vv}^{-1} are arranged in a new parameter vector $\underline{n}$ of dimension $\frac{1}{2}$ m (m +1).

An important aspect of ML estimation theory is the possibility to calculate a covariance matrix of estimated parameters. Such a covariance matrix is also derived for the parameters mentioned above of the present estimation problem. For notational convenience, all these estimated parameters are gathered into one vector of dimension r + n + $\frac{1}{2}$ m (m + 1) which is called the augmented parameter vector $\underline{\theta}_a$. The augmented parameter vector $\underline{\theta}_a$ may be partitioned as follows:

$$\underline{\theta}_a = \begin{bmatrix} \underline{\theta} \\ -- \\ \underline{x}_o \\ -- \\ \underline{\eta} \end{bmatrix} .$$

In correspondence with this partitioning, it is possible to partition the 'augmented' covariance matrix $V_{\theta_a\theta_a}$ of the estimated parameters:

$$V_{\theta_a\theta_a} = \begin{bmatrix} V_{\theta\theta} & V_{\theta x_o} & V_{\theta\eta} \\ V_{x_o\theta} & V_{x_o x_o} & V_{x_o\eta} \\ V_{\eta\theta} & V_{\eta x_o} & V_{\eta\eta} \end{bmatrix} \qquad (15)$$

The important role of Fisher's information matrix in ML estimation theory stems from the fact that its inverse, $C_{\theta_a\theta_a}$, called the Cramér-Rao lower bound (CRLB), constitutes an asymptotic limit for $V_{\theta_a\theta_a}$ as N goes to infinity, Ref. 15:

$$\lim_{N \to \infty} V_{\theta_a\theta_a} = M^{-1}_{\theta_a\theta_a} = C_{\theta_a\theta_a} .$$

The information matrix $M_{\theta_a\theta_a}$ is a positive, semi-definite and symmetrical matrix which can be partitioned as:

$$M_{\theta_a\theta_a} = \begin{bmatrix} M_{\theta\theta} & M_{\theta x_o} & M_{\theta\eta} \\ M_{x_o\theta} & M_{x_o x_o} & M_{x_o\eta} \\ M_{\eta\theta} & M_{\eta x_o} & M_{\eta\eta} \end{bmatrix}$$

in which the blocks $M_{\theta\eta}$, $M_{\eta\theta}$, $M_{x_o\eta}$ and $M_{\eta x_o}$ can be shown to contain only elements equal to zero, see Ref. 14:

$$M_{\theta_a\theta_a} = \begin{bmatrix} M_{\theta\theta} & M_{\theta x_o} & 0 \\ M_{x_o\theta} & M_{x_o x_o} & 0 \\ 0 & 0 & M_{\eta\eta} \end{bmatrix} \qquad (16)$$

The CRLB, $C_{\theta_a\theta_a}$, being the inverse of $M_{\theta_a\theta_a}$, is structurally identical to $M_{\theta_a\theta_a}$ in the sense that it contains the same off-diagonal blocks with zero elements. This can easily be proven by showing that the matrix product $M_{\theta_a\theta_a} \cdot C_{\theta_a\theta_a}$ is equal to the unity matrix. $C_{\theta_a\theta_a}$ may be written as:

$$C_{\theta_a\theta_a} = \begin{bmatrix} \begin{bmatrix} M_{\theta\theta} & M_{\theta x_o} \\ M_{x_o\theta} & M_{x_o x_o} \end{bmatrix}^{-1} & \begin{matrix} 0 \\ 0 \end{matrix} \\ \begin{matrix} 0 & 0 \end{matrix} & M_{\eta\eta}^{-1} \end{bmatrix} .$$

Maximum likelihood estimates are asymptotically efficient, so:

$$\lim_{N \to \infty} \begin{bmatrix} V_{\theta\theta} & V_{\theta x_o} \\ V_{x_o\theta} & V_{x_o x_o} \end{bmatrix} = \begin{bmatrix} M_{\theta\theta} & M_{\theta x_o} \\ M_{x_o\theta} & M_{x_o x_o} \end{bmatrix}^{-1},$$

$$\lim_{N \to \infty} V_{\eta\eta} = M_{\eta\eta}^{-1},$$

$$\lim_{N \to \infty} V_{\theta\eta} = \lim_{N \to \infty} V_{\eta\theta} = 0,$$

$$\lim_{N \to \infty} V_{x_o\eta} = \lim_{N \to \infty} V_{\eta x_o} = 0.$$

Consequently, asymptotically for $N \to \infty$, the elements of $\hat{\underline{\eta}}$ are not correlated with the elements of either $\hat{\underline{\theta}}$ or $\hat{\underline{x}}_o$.

The upperdiagonal block of $M_{\theta_a\theta_a}$ in (16) represents the combined information matrix of the parameter vector $\underline{\theta}$ and the vector of initial conditions $\underline{x}_o$. For simplicity, this matrix is indicated in the following as:

$$M = \begin{bmatrix} M_{\theta\theta} & M_{\theta x_o} \\ M_{x_o\theta} & M_{x_o x_o} \end{bmatrix} . \qquad (17)$$

With (17), it is now possible to write $M_{\theta_a\theta_a}$ and $C_{\theta_a\theta_a}$ as follows:

$$M_{\theta_a\theta_a} = \begin{bmatrix} M & 0 \\ 0 & M_{\eta\eta} \end{bmatrix}, \tag{18}$$

$$C_{\theta_a\theta_a} = \begin{bmatrix} M^{-1} & 0 \\ 0 & M_{\eta\eta}^{-1} \end{bmatrix}. \tag{19}$$

Three matrix norms for the optimization of inputsignals, as defined above, may now be applied to (18) and (19). The resulting criteria can be written as follows:

a) $J = \text{tr } M_{\theta_a\theta_a} = \text{tr } M + \text{tr } M_{\eta\eta}$,

b) $J = \ell n \det M_{\theta_a\theta_a} = \ell n (\det M \cdot \det M_{\eta\eta}) = \ell n \det M + \ell n \det M_{\eta\eta}$,

c) $J = \text{tr } M_{\theta_a\theta_a}^{-1} = \text{tr } C_{\theta_a\theta_a} = \text{tr } M^{-1} + \text{tr } M_{\eta\eta}^{-1}$.

The elements of M depend on the time histories of the components of the multi-dimensional input signal $\underline{u}(t)$, $t \in [t_o, t_1]$. The elements of $M_{\eta\eta}$, however, may be shown to be fully independent of these time histories. This independence leads to constant terms in the three above criteria. Obviously, the optimized input signals will be independent of these constant terms, which therefore may as well be omitted. This results in the following simplified criteria:

a) $J = \text{tr } M$,

b) $J = \ell n \det M$,

c) $J = \text{tr } M^{-1}$.

In the present work, the problem of optimizing input signals with respect to these simplified criteria is formulated in terms of a parameter optimization problem. This leads to conceptually very simple algorithms which are described below.

Let J denote the value of any one of the above criteria for the optimization of input signals. The information matrix M and consequently each of the criteria J depends on the form and energy of the input signals. If these input signals are represented in terms of orthonormal functions as described in Section 1, Eq. (2):

$$u_\ell(t) = \sum_{k=1}^{p} \beta_{k\ell}\, \psi_k(t), \qquad \ell = 1(1)\ s,$$

then J becomes a scalar function with the q = sp weighting factors $\beta_{k\ell}$ as arguments:

$$J = J(\underline{\beta}) = J(\underline{\beta}_1, \ \ldots, \ \underline{\beta}_\ell, \ \ldots, \ \underline{\beta}_s), \tag{20}$$

where:

$$\underline{\beta}_\ell = \text{col}\ [\beta_{1\ell}, \ \beta_{2\ell}, \ \ldots, \ \beta_{p\ell}].$$

According to Section 1, the components of the s-dimensional input signal with prescribed energies E_ℓ, $\ell = 1(1)\ s$, can also be represented as s points P_ℓ on hyperspheres in a p dimensional space with radii $R_\ell = \sqrt{E_\ell}$. Let $\underline{\phi}_\ell$ denote the vector of spherical coordinates of one of these points P_ℓ, as defined in (4) and Fig. 1:

$$\underline{\phi}_\ell = \text{col}\ [\phi_{1\ell}, \ \phi_{2\ell}, \ \ldots, \ \phi_{p-1,\ell}],$$

then J in (20) can be written in a alternative form with a smaller number - viz. s(p-1) - of spherical coordinates as arguments:

$$J = J(\underline{\phi}_1, \ \ldots, \ \underline{\phi}_\ell, \ \ldots, \ \underline{\phi}_s). \tag{21}$$

The correspondence between (20) and (21) is that both relations define J as a function of a finite number of arguments or parameters. In principle, therefore,

both of these relations allow the formulation of the optimization problem of input signals in terms of a parameter optimization problem. The solution of such a parameter optimization problem involves locating the global extreme of one of the above criteria J in the space of the elements of
$\underline{\beta}_\ell$ or $\underline{\phi}_\ell$, $\ell = 1(1)\ s$.

It is well known, however, that in order to arrive at meaningful results, it is essential to take account constraints on the input signal $\underline{u}(t)$ or the state vector $\underline{x}(t)$, $t \in [t_o, t_1]$, or on both $\underline{u}(t)$ and $\underline{x}(t)$; see e.g. Refs. 5 and 16.

These constraints may be 'hard' constraints, restricting amplitudes or energies to given boundaries, usually imposed by physical limitations, or they may be 'soft' constraints, taking the form of penalty functions in the optimization algorithms.

In the context of dynamic flight tests, hard constraints on the amplitudes of input signals, imposed by physical limitations of control surface deflections, or on aircraft state variables with respect to the permissible flight envelope, are usually not of immediate practical interest. The reason is, that actually implemented control surface deflections and resulting state variable excursions are usually kept inside much smaller boundaries in order to ensure an 'adequate' description of aerodynamic forces and moments by means of linearized models.

In practice it is difficult, if not impossible, to determine beforehand where these latter, more restrictive boundaries should lie. It is even more difficult to say whether they should be in the form of amplitude or energy constraints, on input signals, on state variables, or on both.

In the majority of cases where no discontinuous aerodynamic phenomena occur during the execution of a dynamic flight test manoeuvre, amplitude constraints on either input signals or state variables seem to be not very appropriate to ensure the validity of linearized aerodynamic models. The reason is, that the accuracy of such linearized models will in most cases deteriorate only fairly gradually if such amplitude constraints should be violated.

It appears that dynamic flight test manoeuvres may best be optimized by imposing energy constraints on either input signals or state variables or on both. It follows from the arguments given above, that the rationale behind such constraints is not very exact. Also it seems rather indifferent whether these constraints are put on the input signals or on the state variables. In view of this, energy constraints on the input signals were applied in the present work. This decision led to very simple and efficient algorithms as described below.

Returning to the functional relationships in (20) and (21), the crucial difference between the two expressions is, that the former represents an optimization problem to which a set of constraints must still be added, while the latter represents an inherently unconstrained optimization problem. This unconstrained optimization problem leads to optimized input signal components $u_\ell(t)$ of prescribed energy E_ℓ each.

Unconstrained optimization problems are, in general, much easier to solve than optimization problems where 'hard' or 'soft' constraints must be taken into account. The possibility to formulate the input signal optimization problem in terms of an unconstrained parameter optimization problem, has in fact been the rationale behind the transformation of Cartesian to spherical coordinates in Section 1.
In principle, a variety of algorithms may be applied to solve such optimization problems; e.g. ref. 18. If, partial derivatives of J with respect to its arguments $\underline{\phi}_1$, ..., $\underline{\phi}_s$, are not available, it is possible to apply one of the direct search types of optimization methods, for instance Powell's algorithm, Ref. 17. These algoritms depent only on the value of J for given values of the arguments in (21).

It is noted here, that each evaluation of the function J in (21), requires the numerical solution of the system differential equations in (11), as well as the solution of the set of so-called sensitivity differential equations for the calculation of the information matrix; see Ref. 15. Actual input signal optimizations could consequently turn out to need excessive amounts of computer time. However, in the next Section, it is shown that in the case of linear system and observation models, the repeated solution of system- and sensitivity equations evaluation can be avoided.

3 Input signal optimization for linear system parameter estimation

The method, described in the previous Section for the calculation of optimal input signals for nonlinear system parameter estimation, is now applied to the more restricted case of linear system parameter estimation. The systems considered are of the following form:

$$\dot{\underline{x}}(t) = F(\underline{\theta}) \cdot \underline{x}(t) + G(\underline{\theta}) \cdot \underline{u}(t), \tag{22}$$

in which as before $\underline{x}$ denotes an n-dimensional state vector, $\underline{u}$ an s-dimensional input signal and $\underline{\theta}$ a vector of the r parameters which are to be estimated. $F(\underline{\theta})$ and $G(\underline{\theta})$ denote constant matrices of appropriate dimensions. At N discrete instants of time $t_i \in [t_o, t_1]$, i = 1(1) N, the system is observed according to the following model:

$$\begin{aligned} \underline{y}(i) &= H(\underline{\theta}) \cdot \underline{x}(i) + J(\underline{\theta}) \cdot \underline{u}(i), \\ \underline{y}_m(i) &= \underline{y}(i) + \underline{v}(i) \end{aligned} \tag{23}$$

in which $\underline{y}$ denotes an m-dimensional observation vector, $H(\underline{\theta})$ and $J(\underline{\theta})$ denote constant matrices of appropriate dimensions, and $\underline{y}_m$ denotes the measurement of $\underline{y}$. The measurement noise $\underline{v}(i)$ is assumed to be zero mean, uncorrelated in time and Gaussian as in (13). It is assumed again, that $\underline{u}(t)$ is known exactly and that (22) is deterministic, i.e. the system is not subjected to unmeasurable stochastic inputs.

The performance criterion for input signals is again a scalar norm J of M, the joint information matrix of $\underline{\theta}$ and $\underline{x}_o$:

$$M = \begin{bmatrix} M_{\theta\theta} & M_{\theta x_o} \\ M_{x_o\theta} & M_{x_o x_o} \end{bmatrix}. \tag{24}$$

The general expression for M for the case of nonlinear systems, is still valid in the present case of linear systems. In this expression, M is described in terms of so-called sensitivity matrices S(t). The elements of these sensitivity matrices are partial derivatives, representing the 'sensitivity' of the

components of the observation vector $\underline{y}$ with respect to the components of the parameter vector $\underline{\theta}$ and the vector of initial conditions $\underline{x}_o$. The information matrix M for observation measurements at discrete instants of time t_i can be written as:

$$M = \sum_{i=1}^{N} S^T(i)\, V_{vv}^{-1}\, S(i), \tag{25}$$

in which i refers to the discrete time instant t_i and V_{vv} represents the not necessarily diagonal covariance matrix of the vector $\underline{v}(i)$ of observation measurement errors. The matrix S(i) in (25) represents the sensitivity matrix S at the discrete sampling time t_i.

The sensitivity matrix S(t) can be partitioned as follows:

$$S(t) = [S_\theta(t) \qquad S_{x_o}(t)] \tag{26}$$

The partial derivatives of the components $\underline{y}$ with respect to the components of $\underline{\theta}$ are contained in the matrix $S_\theta(t)$, while the partial derivatives of the components of $\underline{y}$ with respect to the components of $\underline{x}_o$ are contained in the matrix $S_{x_o}(t)$. The matrices $S_\theta(t)$ and $S_{x_o}(t)$ of partial derivatives in (26) may be computed as follows. First $S_\theta(t)$ is partitioned in terms of column vectors :

$$S_\theta(t) = [\underline{y}_{\theta_1}(t) \qquad \underline{y}_{\theta_2}(t) \qquad .... \qquad \underline{y}_{\theta_r}(t)],$$

where the i-th column vector $\underline{y}_{\theta_i}(t)$ is defined as $\dfrac{\partial \underline{y}(t)}{\partial \theta_i}$.

Next, the partial derivatives of the matrices of the system and observation model in (22) and (23) respectively, with respect to the component θ_j of $\underline{\theta}$, are defined as:

$$F_{\theta_j}(\underline{\theta}) = \frac{\partial F(\underline{\theta})}{\partial \theta_j}, \qquad G_{\theta_j}(\underline{\theta}) = \frac{\partial G(\underline{\theta})}{\partial \theta_j},$$

$$H_{\theta_j}(\underline{\theta}) = \frac{\partial H(\underline{\theta})}{\partial \theta_j}, \qquad J_{\theta_j}(\underline{\theta}) = \frac{\partial J(\underline{\theta})}{\partial \theta_j},$$

where $j = 1(1)\ r$.

It is to be noted that these matrix partial derivatives are constant for a given parameter vector $\underline{\theta}$, i.e. independent of the state vector $\underline{x}(t)$ and the input signal $\underline{u}(t)$. In a similar way, the partial derivatives of the state vector $\underline{x}$ with respect to the components θ_j of $\underline{\theta}$ are defined as:

$$\underline{x}_{\theta_j}(t) = \frac{\partial \underline{x}(t)}{\partial \theta_j}.$$

These vectors of partial derivatives vary as a function of time depending on $\underline{x}_o$ and $\underline{u}(t)$. This follows directly from the particular form of the sensitivity differential equations used to calculate these vectors of partial derivatives; see Ref. 15. The sensitivity equations are readily derived from (22) by partially differentiating both sides of this equation with respect to θ_j, and subsequently changing the order of the differentiation with respect to θ_j and t, for which it must be assumed that $\underline{x}$ is analytic; see Ref. 1. The resulting sensitivity equations of $\underline{x}_\theta(t)$ are constant, linear and of the following form:

$$\dot{\underline{x}}_{\theta_j}(t) = F(\underline{\theta}) \cdot \underline{x}_{\theta_j}(t) + F_{\theta_j}(\underline{\theta}) \cdot \underline{x}(t) + G_{\theta_j}(\underline{\theta}) \cdot \underline{u}(t), \qquad (27)$$

with initial conditions:

$$\underline{x}_{\theta_j}(t_o) = \underline{0},$$

where $j = 1(1)\ r$.

The vectors of partial derivatives $\underline{y}_{\theta_j}(t)$ are calculated with the following relation, resulting from partial differentiation of both sides of (23) with respect to θ_j. The resulting relation is:

$$\underline{y}_{\theta_j}(i) = H(\underline{\theta}) \cdot \underline{x}_{\theta_j}(i) + H_{\theta_j}(\underline{\theta}) \cdot \underline{x}(i) + J_{\theta_j}(\underline{\theta}) \cdot \underline{u}(i), \qquad (28)$$

where $j = 1(1)\ r$, and i refers to the discrete sample times $t_i \in [t_o, t_1]$.

The second matrix of partial derivatives in S(t) is $S_{x_o}(t)$, see (2). In a similar way as $S_\theta(t)$ above, $S_{x_o}(t)$ may also be partioned in terms of column vectors according to:

$$S_{x_o}(t) = [\underline{y}_{x_{o_1}}(t) \quad \underline{y}_{x_{o_2}}(t) \quad \ldots\ldots \quad \underline{y}_{x_{o_n}}(t)]$$

Next, analogous to $\underline{x}_{\theta_j}(t)$ above, the partial derivatives of the state vector $\underline{x}(t)$ with respect to the components x_{o_j} of the initial state $\underline{x}_o$, j = 1(1) n, are defined as:

$$\underline{x}_{x_{o_j}}(t) = \frac{\partial \underline{x}(t)}{\partial x_{o_j}} .$$

The vectors of partial derivatives $\underline{x}_{x_{o_j}}(t)$ may also be calculated with a set of sensitivity differential equations, in a similar way as the vectors $\underline{x}_{\theta_j}(t)$ above. These sensitivity equations are derived by partially differentiating both sides of (22) with respect to x_{o_j}, and subsequently changing the order of differentiation with respect to x_{o_j} and with respect to time of the term in the left hand side. The resulting sensitivity equations of $\underline{x}_{x_{o_j}}(t)$ are of the following form:

$$\dot{\underline{x}}_{x_{o_j}}(t) = F(\underline{\theta}) \cdot \underline{x}_{x_{o_j}}(t) \qquad (29)$$

with initial conditions:

$$\underline{x}_{x_o}(t_o) = I,$$

where j = 1(1) n.

It is noted, that these sensitivity equations are constant and linear, similar to the sensitivity equations in (27).

Finally, partial differentiation of both sides of (23) with respect ot x_{o_j} results in the following relation for the vectors of partial derivatives $\underline{y}_{x_{o_j}}(t)$:

$$\underline{y}_{x_{o_j}}(i) = H(\underline{\theta}) \cdot \underline{x}_{x_{o_j}}(i) \qquad (30)$$

where j = 1(1) n, and i refers again to the discrete sample times t_i $[t_o, t_1]$.

By solving the sensitivity differential equations in (27) and (29), and subsequently applying the relations (29) and (30), it is now possible to compute the vectors of partial derivatives in the matrices $S_\theta(i)$ and $S_{x_o}(i)$, i = 1(1) N. Subsequently, these matrices are used to compose the sensitivity matrices S(i) according to (26). Finally, the information matrix M of $\underline{\theta}$ and $\underline{x}_o$ is computed with (25).

It is noted, that the solution of the system differential equations (22) is needed for the solution of the sensitivity differential equations (27) in which $\underline{x}(t)$ appears as a forcing function.

In a way, completed analogous to the nonlinear case discussed in Section 2, it is possible again to formulate the problem of optimizing input signals $u_\ell(t)$, ℓ = 1(1) s of given energy E_ℓ in $[t_o, t_1]$, in terms of an unconstrained nonlinear parameter optimization problem. The problem is to calculate the global extreme of the criterion J with respect to its arguments, the elements of the vectors $\underline{\phi}_1, \ldots, \underline{\phi}_\ell, \ldots, \underline{\phi}_s$ of spherical coordinates, Eq. (21):

$$J = J(\underline{\phi}_1, \ldots, \underline{\phi}_\ell, \ldots, \underline{\phi}_s).$$

As mentioned before, input signal optimizations may be time consuming since every function evaluation requires the solution of the system and sensitivity differential equations, (22), (27) and (29). In the present case of linear system models, however, it is possible to compute a set of co-called elementary information matrices instead. Each of these matrices corresponds to a particular

elementary input signal as defined in (6). The information matrix M can be shown to be a linear combination of these elementary information matrices.

According to (7), the s-dimensional input signal $\underline{u}(t)$ can be written as Eq. (7):

$$\underline{u}(t) = \sum_{i=1}^{q} \beta_i \cdot \underline{e}_i(t),$$

in which $\underline{e}_i$ denotes an elementary input signal as defined in (6), and $q = sp$, p denoting the selected number of orthonormal functions; see Section 1.

According to (26), the sensitivity matrix $S(t)$ is composed of a sensitivity matrix $S_\theta(t)$ for the parameter vector $\underline{\theta}$ and a sensitivity matrix $A_{x_o}(t)$ for the initial condition $\underline{x}_o$.
As discussed above, the sensitivity matrices $S_\theta(i)$ at the discrete sample times $t_i \in [t_o, t_1]$ are derived from the solution of the system differential equations (22) and the sensitivity differential equations (27). The solution of these differential equations is the response to a given initial condition $\underline{x}_o$ and given input signal $\underline{u}(t)$, $t \in [t_o, t_1]$. It is readily ascertained that (22) and (27) represent a set of nonhomogeneous linear ordinary differential equations. This means that the solution of these differential equations is in fact a superposition of the response of the homogeneous equations to the initial condition $\underline{x}_o$, and the response of the nonhomogeneous equations to the forcing function $\underline{u}(t)$ with zero initial condition.

In the present method for the optimization of input signals, the following considerations are the rationale for assuming the initial state $\underline{x}_o$ to be equal to zero. In the optimization of input signals for dynamic flight tests, the system differential equations (22) describe dynamic excursions of the aircraft from a given nominal stationary flight condition. This nominal flight condition is, therefore, characterized by the condition $\underline{x}(t) = 0$. It would be rather inconvenient for the pilot to require that the aircraft should be in a particular initial condition $\underline{x}_o \neq 0$ at the start of a flight test manoeuvre at time $t = t_o$. Furthermore, if the time interval needed to arrive at that particular initial condition, say $[t_{-1}, t_o]$, were added to the original time interval $[t_o, t_1]$ of the flight test manoeuvre, it would also be possible to

exploit the longer time interval $[t_{-1},t_1]$ for the optimization of an input signal for a zero initial condition at time $t = t_{-1}$. With respect to the most efficient use of available flight test time, clearly the performance of the resulting input signal in the time interval $[t_{-1},t_1]$ should be compared to the performance of an input signal in the time segment $[t_{-1},t_o]$ resulting in a prescribed initial condition $\underline{x}_o \neq 0$ at time $t = t_o$, followed by an optimized input signal for this non-zero initial condition in the time interval $[t_o,t_1]$.

It is obvious that the performance of the optimal input signal in the time interval $[t_{-1},t_1]$ will be at least as good as the performance of the two-segment input signal in the same time interval. It can be concluded, therefore, that the design of optimal manoeuvres may be based on the assumption that the initial conditions of the aircraft are equal to zero.

This implies, that the solution of the differential equations (22) and (1-27) to be considered here, is identical to only one of the possible responses mentioned above, i.e. the response of the nonhomogeneous equations to the forcing function $\underline{u}(t)$ with zero initial condition.

According to (7), the forcing function or input signal $\underline{u}(t)$ is composed of linear combinations of elementary input signals $\underline{e}_i(t)$. Due to the linearity of the nonhomogeneous differential equations (22) and (27), the response to $\underline{u}(t)$ is in fact identical to a superposition of 'elementary responses' to elementary input signals $\underline{e}_i(t)$. This allows the 'total' sensitivity matrix $S_\theta(t)$ to be written as follows:

$$S_\theta(t) = \sum_{i=1}^{q} \beta_i \cdot S_\theta(t,i), \qquad (31)$$

in which i refers to the elementary input signal $\underline{e}_i(t)$. The matrices $S_\theta(t,i)$ are, for obvious reasons, called here elementary sensitivity matrices. Turning now to the sensitivity matrix S(t) in (26) it should be remarked that $\underline{x}_o$, although assumed zero in the manoeuvre optimization process, still has to be estimated from the actual flight test data. Keeping this in mind, S(t) may be written as:

$$S(t) = \left[\sum_{i=1}^{q} \beta_i \, . \, S_\theta(t,i) \qquad S_{x_o}(t) \right]. \tag{32}$$

This expression for the sensitivity matrix may be substituted in Eq. (25) for the information matrix M of the parameter vector $\underline{\theta}$ and the vector of initial conditions $\underline{x}_o$. The result is:

$$M = \sum_{k=1}^{N} S^T(k) \, . \, V_{vv}^{-1} \, . \, S(k) =$$

$$= \sum_{k=1}^{N} \begin{bmatrix} \sum_{i=1}^{q} \beta_i \, . \, S_\theta^T(k,i) \\ \\ \\ S_{x_o}^T(k) \end{bmatrix} . \, V_{vv}^{-1} \, . \left[\sum_{i=1}^{q} \beta_i \, . \, S_\theta(k,i) \quad S_{x_o}(k) \right] =$$

$$= \begin{bmatrix} \sum_{i=1}^{q} \sum_{j=1}^{q} \beta_i \beta_j . \sum_{k=1}^{N} S_\theta^T(k,i) . V_{vv}^{-1} . S_\theta(k,j) & \sum_{i=1}^{q} \beta_i . \sum_{k=1}^{N} S_\theta^T(k,i) . V_{vv}^{-1} . S_{x_o}(k) \\ \\ \sum_{i=1}^{q} \beta_i . \sum_{k=1}^{N} S_{x_o}^T(k) . V_{vv}^{-1} . S_\theta(k,i) & \sum_{k=1}^{N} S_{x_o}^t(k) . V_{vv}^{-1} . S_{x_o}(k) \end{bmatrix},$$

in which k = 1(1) N refers to the discrete sample times $t_k \in [t_o, t_1]$. Next, <u>elementary information matrices</u> are introduced as:

$$M_{\theta\theta}(i,j) = \sum_{k=1}^{N} S_\theta^T(k,i) \, . \, V_{vv}^{-1} \, . \, S_\theta(k,j),$$

$$M_{\theta x_o}(i) = \sum_{k=1}^{N} S_\theta^T(k,i) \, . \, V_{vv}^{-1} \, . \, S_{x_o}(k), \tag{33}$$

$$M_{x_o\theta}(i) = \sum_{k=1}^{N} S_{x_o}^T(k) \, . \, V_{vv}^{-1} \, . \, S_\theta(k,i).$$

The information matrix M above can be expressed in terms of these elementary information matrices:

$$= \begin{bmatrix} \sum_{i=1}^{q} \sum_{j=1}^{q} \beta_i \beta_j \cdot M_{\theta\theta}(i,j) & \sum_{i=1}^{q} \beta_i \cdot M_{\theta x_o}(i) \\ \sum_{i=1}^{q} \beta_i \cdot M_{x_o \theta}(i) & M_{x_o x_o} \end{bmatrix} . \qquad (34)$$

It is noted, that the elementary information matrices introduced in (33) are not information matrices in the sense of Fisher since - in general - they are not symmetric. It follows from (33) that:

$$M_{\theta\theta}(i,j) = M_{\theta\theta}^{T}(i,j), \qquad (35)$$

and:

$$M_{\theta x_o}(i) = M_{x_o \theta}^{T}(i). \qquad (36)$$

For the computation of the elementary information matrices in (33), the input signal $\underline{u}(t)$, i.e. the values of the parameters β_i in (7), may be yet unknown. This means, that these elementary information matrices may be computed prior to the actual optimization of the object function, i.e. the criterion in (25). It should be noted, that the asymmetry relations (35) and (36) may be employed to reduce the total number of different elementary information matrices to be computed.

The information matrix M in (34) can be calculated from these elementary information matrices for any set of values of the parameters β_i, i.e. any input signal $\underline{u}(t)$ of the general form (7). Accordingly, the elementary information matrices are computed only once for a given set of elementary input signals $\underline{e}_i(t)$.

In cases, as the present one, where direct search methods are applied for the optimization of the object function, it is not uncommon that the function has to be evaluated in a 'very large' number of points in the space of its arguments. In those cases, the calculation of M with (34) rather than via a direct solution of the system and sensitivity differential equations and application of the general expression for M in (25), will result in a considerable reduction of the computation time needed for the optimization of J.

4 Application of the method of Newton and Raphson

Experience gained in the course of the present work with Powell's direct search method, Ref. 17, showed that convergence became progressively slower as the total number of spherical coordinates in (21) increased. This limited the number of arguments for practical purposes to approximately 20.

A very attractive characteristic of Newton-Raphson methods, Ref. 18, is that the sequence of steps to a (local) extreme may be given a simple geometrical interpretation. Furthermore, the original method may readily be modified in order to assure convergence in cases of large numbers of arguments; see e.g. Refs. 6 and 20.

The slightly disappointing performance of Powell's direct search method and the attractive properties of Newton-Raphson methods led to the application of these latter methods to the present problem of input signal optimization.

For application of Newton-Raphson methods it is convenient to introduce a new vector $\underline{\phi}$ of spherical coordinates which contains all vectors $\underline{\phi}_\ell$, $\ell = 1(1)\ s$, in (21), s denoting again the dimension of the input signal $\underline{u}(t)$. As explained earlier in Section 2, each vector $\underline{\phi}_\ell$ is of the same dimension p-1. This means that the new vector $\underline{\phi}$ is of dimension s(p-1). $\underline{\phi}$ can be defined similarly to $\underline{\beta}$, see (5), as:

$$\underline{\phi} = \begin{bmatrix} \underline{\phi}_1 \\ \vdots \\ \underline{\phi}_\ell \\ \vdots \\ \underline{\phi}_s \end{bmatrix} \tag{37}$$

Starting from a given approximation $\underline{\phi}(i)$ of $\underline{\phi}_{stat}$ at which J attains a stationary and therefore extreme value, the Newton-Raphson method of calculating a closer approximation $\underline{\phi}(i+1)$ is:

$$\underline{\phi}(i+1) = \underline{\phi}(i) - \left[\frac{\partial^2 J}{\partial \underline{\phi}\ \partial \underline{\phi}^T}\right]^{-1} \cdot \frac{\partial J}{\partial \underline{\phi}}\ , \tag{38}$$

assuming, that the Hessian matrix $\frac{\partial^2 J}{\partial \underline{\phi}\ \partial \underline{\phi}^T}$ is either positive- or negative definite.

The Newton-Raphson method requires calculation of the first and second order partial derivatives of J, with respect to its arguments, the elements of $\underline{\phi}$/ It is possible to derive analytical expressions for these derivatives for the following three cases, see Ref. 14:

a) $J = \text{tr } M$,

b) $J = \ell n \det M$,

c) $J = \text{tr } M^{-1}$.

Only the elementary information matrices $M_{\theta\theta}(i,j)$, $M_{\theta x_o}(i)$ and $M_{x_o\theta}(i)$ appear in these analytical expressions. This leads to significant savings in computing time, as the elementary information matrices are calculated only once for a given set of elementary input signals, see Section 3.

The original Newton-Raphson method (32) may be modified, in order to assure convergence in cases where the Hessian matrix is ill-conditioned; see Ref. 20.

The Newton-Raphson method was applied to the optimization of rudder and aileron input signals in Ref. 13. The results showed, that the algorithm would quickly converge to an extreme, even in cases with a number of arguments as large as 62 (s = 2, p = 32).

5 Conclusions

It was shown that multidimensional input signals for parameter estimation of nonlinear and linear dynamical systems can be represented in terms of sets of orthonormal functions. Input signals described in this way may be optimized with respect to one of several criteria based on Fisher's information matrix, by solving a nonlinear optimization problem.

Linear dynamical systems excited by input signals as described above, allow a more efficient computation of the information matrix if a set of so-called elementary information matrices is computed and stored beforehand.

6 References

1. G. Arfken, 'Mathematical methods for physicists', second edition, Academic Press, 1970.

2. S.E. Dreyfus, 'Dynamic programming and the calculus of variations', Academic Press, 1965.

3. O.H. Gerlach, 'Analyse van een mogelijke methode voor het meten van prestaties en stabiliteits- en besturingseigenschappen van een vliegtuig in niet-stationaire, symmetrische vluchten (Analysis of a possible method for the measurement of performance and stability and control characteristics in non-steady symmetrical flight)', Report VTH-117, Delft University of Technology, Department of Aerospace Engineering, November 1964.

4. O.H. Gerlach, 'The determination of stability derivatives and performance characteristics from dynamic maneuvers',AGARD Conference Proceedings No. 85, Toulouse, 1971, Report VTH-163, Delft University of Technology, Department of Aerospace Engineering, 1971.

5. G.C. Goodwin, R.L. Payne, 'Dynamic System Identification: Experiment Design and Data Analysis', Academic Press, 1977.

6. N.K. Gupta, R.K. Mehra, 'Computational aspects of maximum likelihood estimation and reduction in sensitivity function calculations', IEEE Transactions on Automatic Control, Vol. AC-19, No. 6, December 1974.

7. R. Kalaba, K. Spingarn, 'Control, Identification, and Input Optimization', Mathematical Concepts and Methods in Science and Engineering, Vol. 25, Plenum Press, 1982.

8. J. Kiefer, 'Optimum Designs in Regression Problems, II', Ann. Math. Stat., Vol. 32, 1961.

9. J. Kiefer, J. Wolfowitz, 'The equivalence of two extremum problems', Canadian J. Math., Vol. 12, 1960.

10. R.K. Mehra, 'Frequency-domain synthesis of optimal inputs for multi input - multi output (mimo) systems with process noise', Decision and Control Conference, Phoenix, Arizona, 1974-1.

11. R.K. Mehra, 'Time-domain synthesis of optimal inputs for system identification', Decision and Control Conference, Phoenix, Arizona, 1974-2

12. R.K. Mehra, N.K. Gupta, 'Status of input design for aircraft parameter identification', AGARD Conference Proceedings No. 172 on 'Methods for Aircraft State and Parameter Identification', Hampton, Virginia, November 1974.

13. J.A. Mulder, 'Aircraft control input optimization for aerodynamic derivative estimation in dynamic manoeuvres', 7th IFAC symposium on 'Identification and System Parameter Estimation', York, UK, July 1985.

14. J.A. Mulder, 'Design and evaluation of dynamic flight test manoeuvres', Report LR-497, Delft University of Technology, Delft, The Netherlands, October, 1986.

15. N.E. Nahi, 'Estimation theory and Applications', John Wiley and Sons, 1969.

16. N.E. Nahi, 'Optimal inputs for parameter estimation in dynamic systems with white observation noise', Joint Automatic Control Conference, pp. 506-513, 1969.

17. M.J.D. Powell, 'An efficient method for finding the minimum of a function of several variables without calculating derivations', Computer Journal, Vol. 7, pp. 155-162, 1964.

18. R. Schmidt, 'Advances in Nonlinear parameter optimization', Lecture Notes in Control and Information Sciences, Springer-Verlag, 1982.

19. G. Schulz, 'Entwurf optimaler Eingangssignale für die System identifizierung', Forschungsbericht FB 76-40, DFVLR, Institut für Dynamik der Flugsysteme, Oberpfaffenhofen, 1976.

20. P. Sonneveld, J.A. Mulder, 'Development and identification of a multi compartment model for the distribution of adriamycin in the rat', Journal of Pharmacokinetics and Biopharmacentrics, Vol. 9, pp. 577-601, 1981.

21. D.A. Swick, 'Walsh function generation', IEEE Transactions on Information Theory, IT-15, p. 167, 1969.

MATHEMATICAL MODELLING OF FLIGHT IN TURBULENCE & WINDSHEAR

M. Baarspul

Delft University of Technology

Summary

A method is described to generate 'patchy' atmospheric turbulence and windshear for pilot-in-the-loop, real-time flight simulation. The turbulence model generates five uncorrelated, non-Gaussian turbulence velocities, which disturb the forces and moments in the equations of motion of the airplane.
The wind speed and direction, for the real-time simulation of windshear, are modelled by expressions matched to experimental data.
Some examples of thunderstorm shears and microbursts are presented.

Introduction

The application of turbulence and windshear in piloted flight simulation may be used for several purposes, e.g.:

- To serve as a general distracting element to increase the pilot's overall workload.
- To represent the actual disturbances acting on the aircraft in real flight, in order to investigate pilot-aircraft performance.

In the first application, simple filtering of Gaussian white noise is a possible solution, as the accuracy requirements on the simulated turbulence are rather low. However, as greater reliance is placed on the flight simulator, the accurate reproduction of turbulence and windshear becomes more important. Atmospheric turbulence is, in contrast with other elements of flight simulation like aircraft motion due to control inputs, not deterministic but stochastic by nature. So, the mathematical model, describing the turbulence velocity components, is based on statistical methods like power spectra and probability distributions.

Measurements of actual turbulence velocities have shown that atmospheric turbulence is a non-Gaussian process which poses a serious problem on its simulation. The so-called 'patchy' characteristics of atmospheric turbulence exhibit local regions of higher energy concentrations separated by relatively calm periods, which cause deviations from the Gaussian distribution function. The non-Gaussian characteristics will be described in the following by two parameters: 'Kurtosis', K, and a "patchiness parameter", R.

Fig. 1 shows the Gaussian and a possible non-Gaussian distribution function which are distinguished by the value of the Kurtosis, K, defined as[13]:

$$K = \frac{m_4}{(m_2)^2}$$

where:

m_2 is the second order central moment, known as the variance, σ^2;

m_4 is the fourth order central moment, which takes the value

$- m_4 = 3\sigma^4$ - (resulting in K = 3, see below) in a Gaussian process.

The second parameter, which describes the 'patchiness' in atmospheric turbulence, is the parameter 'R', to be defined below. The patchy characteristics may cause sudden large deviations in aircraft attitude, which

demand pilot corrective actions. In particular in training and research simulation with the pilot-in-the-loop, patchy atmospheric turbulence is essential for pilot acceptance.

The complete patchy turbulence simulation is obtained, using five turbulence velocities as inputs to the mathematical model of the airplane, see Fig. 2. The generation of each of these turbulence velocities consists of three independent white noise sources, feeding three linear filters, as shown in Fig. 3. The filter outputs a(t), b(t) and c(t) are mixed such, as to obtain the desired patchy characteristic of the turbulence velocity. The longitudinal turbulence velocity $u_{g_{sym}}$ and vertical velocity $w_{g_{sym}}$ in Fig. 3. determine the symmetric airplane motions due to atmospheric turbulence[7]. The lateral turbulence velocity v_g and the turbulence velocities $u_{g_{asym}}$ and $w_{g_{asym}}$ in Fig. 3 determine the asymmetric airplane motions due to atmospheric turbulence[8].

The actual generation of each of these five stochastic turbulence velocities employs the product of two independent Gaussian processes, shaped by linear filters to acquire the power spectra of the turbulence velocities, according to Dryden[4]. Turbulence velocities as a result of the multiplication, however, are more severely non-Gaussian than indicated by experimental data[15,16]. Therefore, a third independent Gaussian process, linearly filtered also to obtain the Dryden power spectrum, is added to create a wide variety of possible patchy characteristics[13].

The following describes the mathematical formulation for the generation of each of the five turbulence velocities.

1. The longitudinal turbulence velocity $u_{g_{sym}}$:

The spectral equation for the longitudinal turbulence velocity, according to Dryden, reads[7]:

$$\Phi_{u_g u_g}(\omega) = \frac{2}{\pi} \sigma_{u_g}^2 \frac{L_{u_g}}{V} \frac{1}{1 + \omega^2 \left(\frac{L_{u_g}}{V}\right)^2} \qquad (1)$$

where: $\sigma_{u_g}^2$ is the variance of the longitudinal turbulence velocity and L_{u_g} is the scale length of this velocity. Fig. 4 shows the standard deviation of the

longitudinal turbulence velocity for different atmospheric conditions as a function of altitude. Fig. 5 shows the scale length as a function of altitude for the same atmospheric conditions[1]. The auto-power spectral densities of the filter outputs $a_1(t)$, $b_1(t)$ and $c_1(t)$, see Fig. 3, as derived in[13], read:

$$\Phi_{a_1a_1}(\omega) = \frac{2}{\pi}\sigma_{u_1}\frac{L_{u_g}}{V}(R+1)\frac{1}{1+\left(\frac{L_{u_g}}{V}\right)^2(R+1)^2\omega^2} \tag{2}$$

$$\Phi_{b_1b_1}(\omega) = \frac{2}{\pi}\sigma_{u_1}\frac{L_{u_g}}{V}\frac{(R+1)}{R}\frac{1}{1+\left(\frac{L_{u_g}}{V}\right)^2\left(\frac{R+1}{R}\right)^2\omega^2} \tag{3}$$

$$\Phi_{c_1c_1}(\omega) = \frac{2}{\pi}\sigma_{c_1}^2\frac{L_{u_g}}{V}\frac{1}{1+\left(\frac{L_{u_g}}{V}\right)^2\omega^2} \tag{4}$$

The patchiness parameter R in the equations (2) and (3) is defined as the ratio between the cutoff frequencies of the filters with transfer functions $H_{a_1}(j\omega)$ and $H_{b_1}(j\omega)$[13], see below. Values applied for R in the simulation of patchy turbulence range from zero to one. With decreasing R, the average patch length increases. Figs. 6 and 7 show the effect of the parameter R on the longitudinal turbulence velocity $u_{g_{sym}}$.

The filter transfer functions $H_{a_1}(j\omega)$, $H_{b_1}(j\omega)$ and $H_{c_1}(j\omega)$, see Fig. 3, completely determine the shapes of the power spectral densities $\Phi_{aa}(\omega)$, $\Phi_{bb}(\omega)$ and $\Phi_{cc}(\omega)$, according to the following equations[13]:

$$\begin{aligned}\Phi_{aa}(\omega) &= |H_{a_1}(j\omega)|^2 \cdot \Phi_{oo}(\omega)_1\\ \Phi_{bb}(\omega) &= |H_{b_1}(j\omega)|^2 \cdot \Phi_{oo}(\omega)_2\\ \Phi_{cc}(\omega) &= |H_{c_1}(j\omega)|^2 \cdot \Phi_{oo}(\omega)_3\end{aligned} \tag{5}$$

where $\Phi_{oo}(\omega)_1$, $\Phi_{oo}(\omega)_2$, and $\Phi_{oo}(\omega)_3$ are the input auto-power spectra of independent Gaussian white noise signals, having the constant values of K_a^2, K_b^2 and K_c^2 respectively.

Substituting the expressions (2), (3) and (4) in (5) gives the expressions for the filter transfer functions[13]:

$$H_{a_1}(j\omega) = \frac{1}{K_a}\sqrt{\left[\frac{2}{\pi}\,\sigma_{u_1}\,\frac{L_{u_g}}{V}\,(R+1)\right]}\;\frac{1}{1 + \frac{L_{u_g}}{V}\,(R+1)\,j\omega} \tag{6}$$

$$H_{b_1}(j\omega) = \frac{1}{K_b}\sqrt{\left[\frac{2}{\pi}\,\sigma_{u_1}\,\frac{L_{u_g}}{V}\,\frac{(R+1)}{R}\right]}\;\frac{1}{1 + \frac{L_{u_g}}{V}\,\frac{(R+1)}{R}\,j\omega} \tag{7}$$

$$H_{c_1}(j\omega) = \frac{1}{K_c}\,\sigma_{c_1}\sqrt{\left[\frac{2}{\pi}\,\frac{L_{u_g}}{V}\right]}\;\frac{1}{1 + \frac{L_{u_g}}{V}\,j\omega} \tag{8}$$

In the equations (6), (7) and (8) the following relations yield:

$$\sigma_{u_1} = \sigma_{a_1}\;\sigma_{b_1}\,, \text{ where } \sigma_{a_1} = \sigma_{b_1}$$

$$\sigma_{u_g}^2 = \sigma_{u_1}^2 + \sigma_{c_1}^2 = \sigma_{a_1}^2 \cdot \sigma_{b_1}^2 + \sigma_{c_1}^2 \tag{9}$$

The parameter Q is defined as the ratio of the standard deviations of the processes $u_1(t)$ and $c_1(t)$, see Fig. 3:

$$Q = \frac{\sigma_{a_1}\,\sigma_{b_1}}{\sigma_{c_1}} = \frac{\sigma_{u_1}}{\sigma_{c_1}} \tag{10}$$

From equations (9), it follows for σ_{u_1} and σ_{c_1}:

$$\sigma_{u_1} = \frac{Q \cdot \sigma_{u_g}}{\sqrt{(1 + Q^2)}} \quad \text{and} \quad \sigma_{c_1} = \frac{\sigma_{u_g}}{\sqrt{(1 + Q^2)}}\,. \tag{11}$$

The Kurtosis K of the probability distribution of the turbulence velocity $u_{g_{sym}}$ is completely determined by the parameter Q:

$$K = \frac{9Q^4 + 6Q^2 + 3}{(1 + Q^2)^2} \quad , \tag{12}$$

where Q ranges from zero to infinity. The Gaussian probability distribution (K=3) is obtained for Q = 0. The modified Bessel distribution (K=9) results for Q = ∞.

2. The vertical turbulence velocity $w_{g_{sym}}$:

The spectral equation for the vertical turbulence velocity, according to Dryden, reads[7]:

$$\Phi_{w_g w_g}(\omega) = \frac{1}{\pi} \sigma_{w_g}^2 \frac{L_{w_g}}{V} \frac{1 + 3\omega^2 \left(\frac{L_{w_g}}{V}\right)^2}{\left(1 + \omega^2 \left[\frac{L_{w_g}}{V}\right]^2\right)^2} \tag{13}$$

where $\sigma_{w_g}^2$ and L_{w_g} are the variance and the scale length of the vertical turbulence velocity, respectively, see Figs. 8 and 9, which present the standard deviation and the scale length of the vertical turbulence velocity as a function of altitude for different atmospheric conditions. The auto-power spectral densities of the filter outputs $a_2(t)$, $b_2(t)$ and $c_2(t)$, see Fig. 3, as derived in[13], read:

$$\Phi_{a_2 a_2}(\omega) = \frac{2}{\pi} \sigma_{u_2} \frac{L_{w_g}}{V} \frac{(R+1)}{R} \frac{1}{1 + \left(\frac{L_{w_g}}{V}\right)^2 \left(\frac{R+1}{R}\right)^2 \omega^2} \tag{14}$$

$$\Phi_{b_2 b_2}(\omega) = \frac{1}{\pi} \sigma_{u_2} \frac{L_{w_g}}{V} (R+1) \frac{(1-R) + (3+R)(R+1)^2 \left(\frac{L_{w_g}}{V}\right)^2 \omega^2}{\left[1 + \left(\frac{L_{w_g}}{V}\right)^2 (R+1)^2 \omega^2\right]^2} \tag{15}$$

$$\Phi_{c_2c_2}(\omega) = \frac{1}{\pi}\,\sigma_{c_2}^2\,\frac{L_{w_g}}{V}\,\frac{1 + 3\,(\frac{L_{w_g}}{V})^2\,\omega^2}{[1 + (\frac{L_{w_g}}{V})^2\,\omega^2]^2} \qquad (16)$$

Substituting the expressions (14), (15) and (16) in the equations (5), results in the expressions for the filter transfer functions:

$$H_{a_2}(j\omega) = \frac{1}{K_a}\sqrt{[\frac{2}{\pi}\,\sigma_{u_2}\,\frac{L_{w_g}}{V}\,\frac{(R+1)}{R}]}\,\frac{1}{1 + \frac{(R+1)}{R}\,\frac{L_{w_g}}{V}\,j\omega} \qquad (17)$$

$$H_{b_2}(j\omega) = \frac{1}{K_b}\sqrt{[\frac{1}{\pi}\,\sigma_{u_2}\,\frac{L_{w_g}}{V}\,(R+1)]}\,\frac{\sqrt{(1-R) + (R+1)\,\sqrt{(3+R)}\,\frac{L_{w_g}}{V}\,j\omega}}{[1 + (R+1)\,\frac{L_{w_g}}{V}\,j\omega]^2} \qquad (18)$$

$$H_{c_2}(j\omega) = \frac{1}{K_c}\,\sigma_{c_2}\,\sqrt{[\frac{1}{\pi}\,\frac{L_{w_g}}{V}]}\,\frac{1 + \sqrt{3}\,\frac{L_{w_g}}{V}\,j\omega}{(1 + \frac{L_{w_g}}{V}\,j\omega)^2} \qquad (19)$$

The values of σ_{u_2} and σ_{c_2} follow from equation (11). However, in this equation σ_{u_g} should now be replaced by σ_{w_g}.

3. The lateral turbulence velocity v_g:

The spectral equation for the lateral turbulence velocity, according to Dryden, is identical to the spectral equation for the vertical turbulence velocity $w_{g_{sym}}$ [8]. So, the derivation of the auto-power spectral densities of the filter outputs $a_3(t)$, $b_3(t)$ and $c_3(t)$, see Fig. 3, are identical to the expressions (14), (15) and (16), provided that the index w_g is replaced by v_g and the subscript 2 by 3. Summarizing the expressions for the filter transfer functions for the generation of the lateral turbulence velocity:

$$H_{a_3}(j\omega) = \frac{1}{K_a}\sqrt{\left[\frac{2}{\pi}\,\sigma_{u_3}\,\frac{L_{v_g}}{V}\,\frac{(R+1)}{R}\right]}\,\frac{1}{1 + \frac{(R+1)}{R}\,\frac{L_{v_g}}{V}\,j\omega} \tag{20}$$

$$H_{b_3}(j\omega) = \frac{1}{K_b}\sqrt{\left[\frac{1}{\pi}\,\sigma_{u_3}\,\frac{L_{v_g}}{V}\,(R+1)\right]}\,\frac{\sqrt{(1-R) + (R+1)\sqrt{(3+R)}\,\frac{L_{v_g}}{V}\,j\omega}}{\left[1 + (R+1)\,\frac{L_{v_g}}{V}\,j\omega\right]^2} \tag{21}$$

$$H_{c_3}(j\omega) = \frac{1}{K_c}\,\sigma_{c_3}\sqrt{\left[\frac{1}{\pi}\,\frac{L_{w_g}}{V}\right]}\,\frac{1 + \sqrt{3}\,\frac{L_{v_g}}{V}\,j\omega}{\left(1 + \frac{L_{v_g}}{V}\,j\omega\right)^2} \tag{22}$$

The values of σ_{u_3} and σ_{c_3} again follow from equation (11). However, in this case σ_{u_g} is replaced by σ_{v_g}.

4. The longitudinal turbulence velocity $\hat{u}_{g_{asym}}$, where $\hat{u}_g = \frac{u_g}{V}$:

The expression for the effective one-dimensional power spectral density function of the longitudinal turbulence velocity $\hat{u}_{g_{asym}}$, as derived in[8], reads:

$$I_{\hat{u}_g}(\Omega_x L_g, B) = \frac{\overline{\hat{u}_g^2}}{\pi}\int_0^\infty h^2\left(\Omega_y \frac{b}{2}\right)\,\frac{1 + \Omega_x^2 L_g^2 + 4\Omega_y^2 L_g^2}{(1 + \Omega_x^2 L_g^2 + \Omega_y^2 L_g^2)^{5/2}}\,d(\Omega_y L_g) \tag{23}$$

This function is approximated by the following general expression[8]:

$$I_{\hat{u}_g}(\Omega_x L_g, B) = I_{\hat{u}_g}(0,B)\,\frac{1 + \tau_3^2\,\Omega_x^2\,L_g^2}{(1 + \tau_1^2\,\Omega_x^2\,L_g^2)\,(1 + \tau_2^2\,\Omega_x^2\,L_g^2)}\,, \tag{24}$$

where: $B = \frac{b}{2L_g}$ and $L_g = L_{u_g}$.

$\hat{I}_{u_g}(0,B)$ is presented as a function of B in Fig. 10 and Fig. 11 presents τ_1, τ_2 and τ_3 as functions of B. Table 1 presents the numerical values of these variables.

Using the same method as for the derivation of the filter transferfunctions for $u_{g_{sym}}$ and $w_{g_{sym}}$, the filter transferfunctions for the generation of $\hat{u}_{g_{asym}}$ read[14], see Fig. 3:

$$H_{a_4}(j\omega) = \frac{1}{K_a}\sqrt{C}\,\frac{1}{1 + A \cdot j\omega} \tag{25}$$

$$H_{b_4}(j\omega) = \frac{1}{K_b}\sqrt{F}\,\frac{B + E \cdot j\omega}{(1 + D\cdot j\omega)(1 + G\cdot j\omega)} \tag{26}$$

$$H_{c_4}(j\omega) = \frac{1}{K_c}\sqrt{H}\,\frac{1 + L \cdot j\omega}{(1 + M\cdot j\omega)(1 + N\cdot j\omega)} \tag{27}$$

The constants A up to and including N in the above transfer functions read:

$$A = \frac{L_{u_g}}{V} \cdot \frac{R+1}{R} \cdot \tau_1$$

$$B = [\tau_1 (R+1) - \tau_2 R]^{\frac{1}{2}} \cdot [1 + \alpha R (\tau_1 - \tau_2)]^{\frac{1}{2}}$$

$$C = \frac{Q}{\sqrt{(1 + Q^2)}}\left[\frac{2}{\pi}\hat{I}_{u_g}(0,B)(\alpha + \beta)\right]^{\frac{1}{2}} \frac{L_{u_g}}{V}\frac{R+1}{R}\tau_1 ,$$

where: $\alpha = \dfrac{\tau_1^2 - \tau_3^2}{\tau_1(\tau_1^2 - \tau_2^2)}$ and $\beta = \dfrac{\tau_2^2 - \tau_3^2}{\tau_2(\tau_2^2 - \tau_1^2)}$

$$D = \frac{L_{u_g}}{V}(R+1)\tau_1$$

$$E = \frac{L_{u_g}}{V}(R+1)\left[\tau_1 \tau_3^2 + \beta R \tau_1^2 \tau_2(\tau_1 - \tau_2)\right]^{\frac{1}{2}}$$

$$F = \frac{Q}{\sqrt{(1 + Q^2)}} \cdot \left[\frac{2}{\pi} \cdot \frac{\hat{I}_{u_g}(0,B)}{(\alpha + \beta)}\right]^{\frac{1}{2}} \cdot \frac{L_{u_g}}{V} \cdot \frac{\tau_1(R+1)}{[\tau_1(R+1) - \tau_2 R]^2}$$

$$G = \frac{L_{u_g}}{V} \frac{\tau_1 \tau_2 (R+1)}{\tau_1 (R+1) - \tau_2 R}$$

$$H = \frac{1}{1 + Q^2} \hat{I}_{u_g} (0,B)$$

$$L = \frac{L_{u_g}}{V} \cdot \tau_3 \quad ; \quad M = \frac{L_{u_g}}{V} \cdot \tau_1 \quad ; \quad N = \frac{L_{u_g}}{V} \cdot \tau_2$$

5. The vertical turbulence velocity $\alpha_{g_{asym}}$, where $\alpha_g = \frac{w_g}{V}$:

The expression for the effective one-dimensional power spectral density function of the vertical turbulence velocity $\alpha_{g_{asym}}$ reads[8]:

$$I_{\alpha_g} (\Omega_x L_g, B) = \frac{3}{\pi} \overline{\alpha_g^2} \int_0^\infty h^2 (\Omega_y \frac{b}{2}) \cdot \frac{\Omega_x^2 L_g^2 + \Omega_y^2 L_g^2}{(1 + \Omega_x^2 L_g^2 + \Omega_y^2 L_g^2)^{5/2}} d(\Omega_y L_g) \tag{28}$$

This function is, like $\hat{I}_{u_g} (\Omega_x L_g, B)$, approximated by the following expression[8]:

$$I_{\alpha_g} (\Omega_x L_g, B) = I_{\alpha_g} (0,B) \frac{1 + \tau_6^2 \Omega_x^2 L_g^2}{(1 + \tau_4^2 \Omega_x^2 L_g^2) (1 + \tau_5^2 \Omega_x^2 L_g^2)} , \tag{29}$$

where $L_g = L_{w_g}$. The expression $I_{\alpha_g} (0,B)$ is presented as a function of B in Fig. 10 and Fig. 12 presents τ_4, τ_5 and τ_6 as functions of B.
Table 2 presents the numerical values of these variables.
The expressions (25), (26) and (27) also apply to the filter transfer functions $H_{a_5} (j\omega)$, $H_{b_5} (j\omega)$ and $H_{c_5} (j\omega)$ of the vertical turbulence velocity $\alpha_{g_{asym}}$ (Fig. 3), except that in the constants A up to and including N in these transfer functions:

$I\hat{}_{u_g}(0,B)$ should be replaced by $I_{\alpha_g}(0,B)$;
L_{u_g} should be replaced by L_{w_g};
τ_1 should be replaced by τ_4;
τ_2 should be replaced by τ_5;
τ_3 should be replaced by τ_6.

The patchy turbulence simulation described above, runs in real-time on the Gould SEL 32/87 computer of the Faculty of Aerospace Engineering, in combination with the modular flight simulation software of the disciplinary group for 'Stability and Control'.

Coupling of the patchy turbulence simulation and the mathematical model of the airplane

The coupling of the patchy turbulence simulation with the aircraft mathematical model, to compute the dimensionless force and moment coefficients due to atmospheric turbulence, has been derived in[7] for the symmetric and in[8] for the asymmetric airplane motions. As a result, the expressions for the force and moment coefficients in the linearized equations of airplane motion, due to atmospheric turbulence, read:

$$
\begin{aligned}
C_{X_g} &= C_{X_u} \cdot \hat{u}_{g_{sym}} + C_{X_\alpha} \cdot \alpha_{g_{sym}} \\
C_{Y_g} &= C_{Y_\beta} \cdot \beta_g \\
C_{Z_g} &= C_{Z_u} \cdot \hat{u}_{g_{sym}} + C_{Z_\alpha} \cdot \alpha_{g_{sym}} \\
C_{\ell_g} &= -C_{\ell_{r_w}} \cdot \hat{u}_{g_{asym}} + C_{\ell_\beta} \cdot \beta_g + C_{\ell_{p_w}} \cdot \alpha_{g_{asym}} \\
C_{m_g} &= C_{m_u} \cdot \hat{u}_{g_{sym}} + C_{m_{\dot{u}_g}} \cdot \frac{\dot{u}_g \bar{c}}{V} + C_{m_\alpha} \cdot \alpha_{g_{sym}} + C_{m_{\dot{\alpha}_g}} \frac{\dot{\alpha}_g \bar{c}}{V} \\
C_{n_g} &= -C_{n_{r_w}} \cdot \hat{u}_{g_{asym}} + C_{n_\beta} \cdot \beta_g + C_{n_{p_w}} \cdot \alpha_{g_{asym}}
\end{aligned}
\qquad (30)
$$

In the equations (30) $C_{m_{\dot{u}_g}}$ and $C_{m_{\dot{\alpha}_g}}$ are[7]:

$$C_{m_{\dot{u}_g}} = -2\, C_{m_h} \cdot \frac{\ell_h}{\bar{c}}$$

(where: C_{m_h} is the contribution to C_m, due to the horizontal tail)

$$C_{m_{\dot{\alpha}_g}} = C_{m_{\dot{\alpha}}} - C_{m_q}$$

In the case of a non-linear mathematical model of the airplane, covering the complete flight envelope, the coupling of the patchy turbulence model is more complex, as the stability derivatives in the equations (30) are no longer constants.

Wind Shear and Wind Profiles

During an actual approach to landing of an airplane there usually is some wind in the lower atmosphere. Of major importance to the pilot is the variation with altitude of the wind velocity and direction, known as the wind shear, as experienced by the airplane.
The combined effect of two atmospheric disturbance components represents the total wind shear, see Fig. 13:

1. The variation of the mean or steady-state wind velocity with altitude, as determined from the wind profile and the change in wind direction with altitude.
2. A stochastic component, which is the result of the prevailing patchy atmospheric turbulence as described above.

Experimental data indicate that the atmospheric stability influences wind profiles, and large wind shears are known to occur, especially if the atmosphere is very stable. Since the mathematical model of the steady-state wind variation with altitude, presented below is a function of the atmospheric stability, this parameter is discussed first.

The rate of change of air temperature with altitude, dT/dh is one of the major factors affecting atmospheric stability. Excluding temperature inversions, the air temperature decreases with increasing altitude. So, the so-called' lapse rate, dT/dh, is normally negative. Atmospheric stability characteristics are usually given for three atmospheric conditions:

1. Stable: $-dT/dh < 0.005$ °C/m
2. Neutral: $0.005 \leq -dT/dh \leq 0.01$ °C/m
3. Unstable: $-dT/dh > 0.01$ °C/m

Both the wind profile model and values of some parameters defining the turbulence model, presented earlier in this Chapter, depend on the atmospheric stability, see Figs. 4, 5, 8 and 9.

Assuming that the mean or steady-state wind velocity has no vertical component at low altitude, the horizontal wind velocity vector $\bar{V}_w$ is defined by its magnitude V_w and its direction ψ_w, both of which can vary with altitude. The change of wind direction with increasing altitude over coastal planes in the northern hemisphere normally is clockwise. On the average it amounts to 0.04°/m up to an altitude of 900 m[2]. Actual variations in wind direction may be much larger than 0.04°/m in the so-called shear conditions, due to factors such as a locally irregular temperature profile, occurring in particular in very stable air[12].

The wind velocity vector magnitude, or wind speed, is modelled by expressions matched to experimental data. In unstable atmospheric conditions a logarithmic law seems to fit the experimental data quite well. Employing the notation as given in[10,11]:

$$u(z) = \frac{u^*}{k} \cdot \ln \left(\frac{z}{z_o}\right) \qquad (31)$$

where:

$u(z)$ = wind speed at height z.
u^* = friction velocity = 0.47 m/s, being constant up to a height, z, of at least 100 m;
k = Von Karman constant = 0.4;
z_o = aerodynamic roughness height = 0.1 m.

In order to bring the wind shear and turbulence models on a common basis, the wind speed is expressed as a function of the wind velocity at a reference height of 9.15 m (30 ft). The following expression for the wind speed V_w can be found from equation (31), using a different notation[3]:

$$V_w = V_{w_{9.15}} (0.43 \log_{10} h + 0.572) \qquad 0 < h < 300 \text{ m}$$

$$V_w = 1.637 \cdot V_{w_{9.15}} \qquad h \geq 300 \text{ m}$$

where:

V_w = wind speed at height h (m/sec);

$V_{w_{9.15}}$ = wind speed at 9.15 m altitude (m/sec);

h = altitude above the terrain (m).

The shape of the wind profile depends more critically on the lapse rate in neutral and stable atmospheric conditions. In these cases the wind profile can be represented by a power law[11]:

$$V_w = V_{w_{9.15}} \cdot \frac{h^p - h_o^p}{9.15^p - h_o^p} \qquad 0 < h < 300 \text{ m}$$

$$V_w = V_{w_{300}} \qquad h \geq 300 \text{ m}$$

where:

h_o = 0.03 m;

p = 0.43 + 27 dT/dh;

$V_{w_{300}}$ = wind speed at 300 m altitude (m/sec)

Fig. 14 shows the wind profiles, according to the above expressions, for -dT/dh > 0.01, -dT/dh = 0.0065 and -dT/dh = 0.003, representing unstable, neutral and stable atmospheric conditions, respectively.
A cumulative probability of reported mean wind and cross wind at the reference height of 9.15 m is shown in Fig. 15[3]. The data presented in this figure may provide an estimate of the mean wind speed at 9.15 m altitude required to utilize the curves in Figs. 4 and 8 in order to generate patchy atmospheric turbulence.

Other meteorological phenomena causing dangerous windshears to aircraft are the thunderstorm and the microburst. Windshear profiles occurring during a thunderstorm are measured and modelled[5] for use in flight training simulation. Examples are the wind shear profiles, which occurred during:

- the Logan/Iberian, 1973, accident;
- the Kennedy/Eastern, 1975, accident.

What might happen to an aircraft that tries to take-off or approach to land,respectively, in thunderstorm shears, is shown in Fig. 16.

Microbursts are small but intense downdrafts that last only a short period of time. Close to the ground they cause severe head and tail winds and are of great concern to the pilot, when encountered during final approach or just after lift off at altitudes below 2000 ft. The Joint Weather Studies (JAWS) field experiment[6], conducted at Stapleton Airport near Denver in 1982, provided radar measured data of some 190 microbursts less than 2 nautical miles in diameter. Aproach and take-off wind shear profiles as a result of the JAWS-data, are programmed and used in flight training simulators. The so-called 'ring-vortex downburst model' provides a mathematical model for the simulation of microbursts[9].

Conclusion

The generation of 'patchy' atmospheric turbulence and windshear for pilot-in-the-loop, real-time flight simulation has been described. Dependencies of the standard deviations and scale lengths of the turbulence velocities on airplane altitude were shown. The non-Gaussian characteristics of atmospheric turbulence

were described by the 'Kurtosis' and a 'patchiness parameter'. The influence of these two parameters on the tubulence velocities was shown.
Real-time flight simulation experiments, using the Delft University moving-base visual flight simulator, have shown that the generated turbulence and windshear has received good pilot acceptance.
Future research will be focussed on the flexibility of large airplanes and their interaction with atmospheric turbulence and windshear.

References

1. Anon. -AGARD- (1975). Approach and Landing Simulation. AGARD Report No. 632. North Atlantic Treaty Organization.

2. Anon. (1960). Handbook of Geophysics. USAF Air Research and Development Command, McMillan Book Company, New York.

3. Anon. (1970). Airworthiness Requirements for Automatic Landing in Restricted Visibility Down to Category III. British Civil Airworthiness Requirements Paper No. 367, Issue 3.

4. Dryden, H.L. (1961). A Review of the Statistical Theory of Turbulence. In: Turbulence Classic Papers on Statistical Theory. Interstate Publishers, New York.

5. Frost, W., Crosby, B., Camp, D.W. (1979). Flight through thunderstorm outflow. In: Journal of Aircraft, Vol. 16, No. 11.

6. Frost, W., Chang, H.P., McCarthy, J., Elmore, K.L. (1984). Simulated flight through JAWS wind shear: In-depth analysis results. Paper: AIAA-84-0276.

7. Gerlach, O.H. (1966). Calculation of the response of an aircraft to random aimospheric turbulence. Part I: Symmetric motions. Report VTH-138, Delft University of Technology, Delft, The Netherlands.

8. Gerlach, O.H. and Baarspul, M. (1968). Calculation of the response of an aircraft to random atmospheric turbulence. Part II: Asymmetric motions. Report VTH-139, Delft University of Technology, Delft, The Netherlands.

9. Ivan, M. (1986). A ring-vortex downburst model for flight simulations. In: Journal of Aircraft, Vol. 23, No. 3.

10. Kurkowski, R.L., et al. (1971). Development of Turbulence and Wind Shear Models for Simulator Applications. In: NASA Aircraft Safety and Operating Problems Conference, NASA SP-270, National Aeronautics and Space Administration, Washington D.C., USA.

11. Lappe, O.U. (1965). A low altitude tubulence model for estimating gust loads on aircraft. In: AIAA 2nd Aerospace Science Meeting. Paper No. 65-14.

12. Luers, J.K. (1973). A Model of Wind Shear and Turbulence in the Surface Boundary Layer. NASA CR-2288, National Aeronautics and Space Administration, Washington D.C., USA.

13. Moesdijk, G.A.J. van de, (1975). The Description of Patchy Atmospheric Turbulence, Based on a Non-Gaussian Simulation Technique. Report VTH-192, Delft University of Technology, Delft, The Netherlands.

14. Moesdijk, G.A.J. van de, (1978). Non-Gaussian Structure of the Simulated Turbulent Environment in Piloted Flight Simulation. Memorandum M-304, Delft University of Technology, Delft, The Netherlands.

15. Reeves, P.M. (1969). A Non-Gaussian Turbulence Simulation. Air Force Flight Dynamics Technical Report AFFDL-TR-69-67.

16. Reeves, P.M., Joppa, R.G. and Ganzer, V.M. (1976). A Non-Gaussian Model of Continuous Atmospheric Turbulence for use in Aircraft Design. NASA CR-2639, National Aeronautics and Space Administration.

B	$\frac{I_{\hat{u}_g}(0,B)}{\overline{\hat{u}_g^2}}$	τ_1	τ_2	τ_3
0,50	0,250084	0,662562	2,311377	2,298718
0,45	0,223658	0,607202	1,241514	1,204641
0,40	0,196050	0,544252	1,016470	0,949548
0,35	0,167491	0,472419	0,895606	0,793271
0,30	0,138317	0,406748	0,832718	0,703821
0,25	0,109001	0,346800	0,788367	0,642029
0,20	0,080211	0,288690	0,747955	0,590812
0,15	0,052906	0,231815	0,706023	0,545338
0,125	0,040229	0,202945	0,682303	0,522628
0,10	0,028509	0,172928	0,653908	0,497035
0,075	0,018059	0,141145	0,618429	0,467082
0,0625	0,013436	0,124455	0,596290	0,448961
0,05	0,009303	0,106813	0,569551	0,427748
0,03125	0,004215	0,077782	0,512936	0,383390
0,015625	0,001268	0,048239	0,423350	0,312979

Table 1 $\frac{I_{\hat{u}_g}(0,B)}{\overline{\hat{u}_g^2}}$, τ_1, τ_2 and τ_3 as functions of B.

B	$\frac{I_{\alpha_g}(0,B)}{\overline{\alpha_g^2}}$	τ_4	τ_5	τ_6
0,50	0,171258	0,480764	1,492572	1,527124
0,45	0,154164	0,458294	1,332911	1,358464
0,40	0,136015	0,426746	1,120000	1,140000
0,35	0,116959	0,386097	0,787000	0,773000
0,30	0,097219	0,337007	0,589747	0,552325
0,25	0,077119	0,279943	0,551119	0,482539
0,20	0,057131	0,218703	0,488882	0,390730
0,15	0,037945	0,162684	0,440944	0,324153
0,125	0,028958	0,136627	0,417279	0,296144
0,10	0,020599	0,111941	0,392720	0,271229
0,075	0,013101	0,087681	0,365723	0,247885
0,0625	0,009769	0,076006	0,351389	0,237504
0,05	0,006779	0,064521	0,336211	0,227862
0,03125	0,003084	0,047613	0,310788	0,214478
0,015625	0,000932	0,033226	0,283501	0,202983

Table 2 $\frac{I_{\alpha_g}(0,B)}{\overline{\alpha_g^2}}$, τ_4, τ_5 and τ_6 as functions of B.

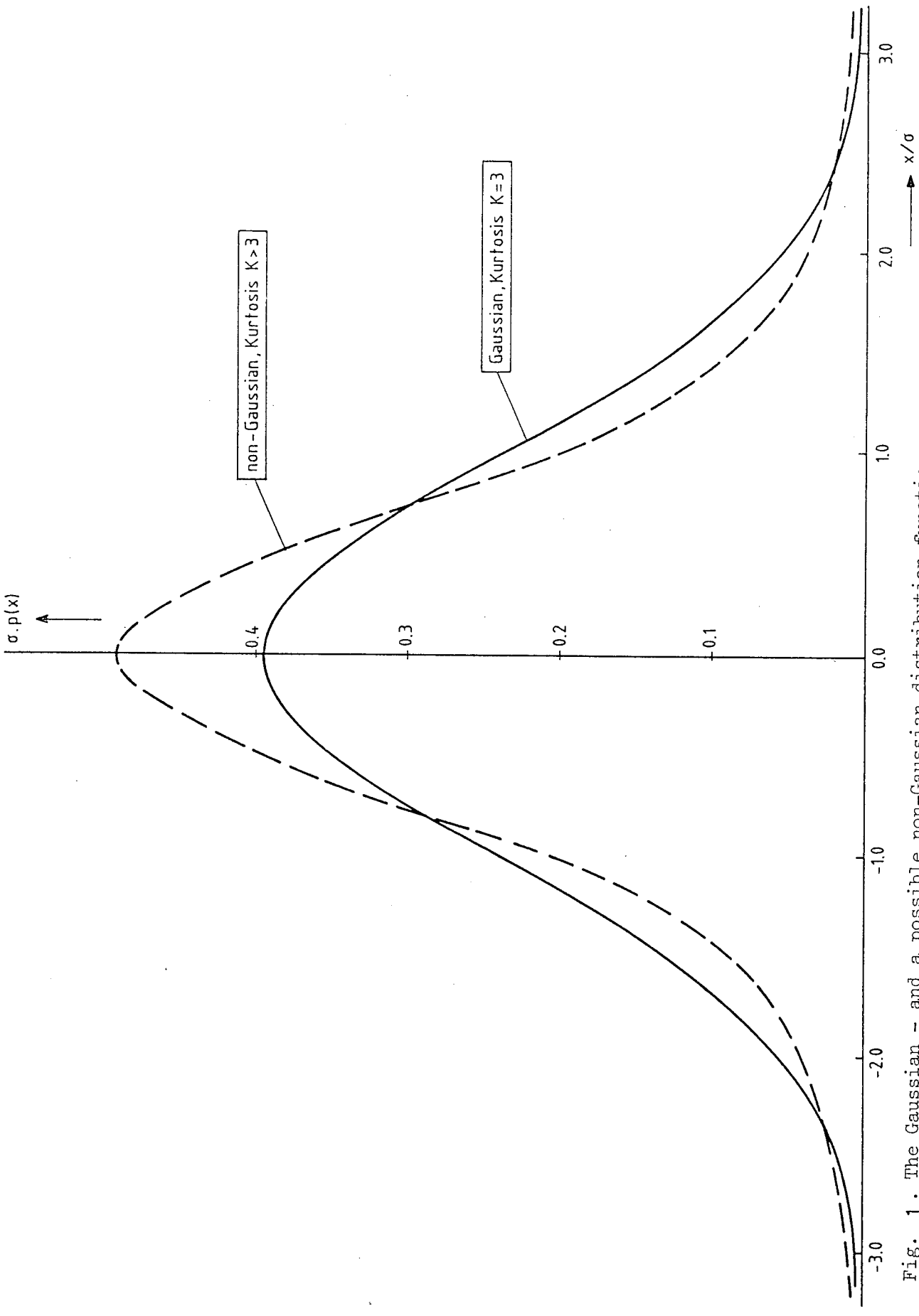

Fig. 1. The Gaussian - and a possible non-Gaussian distribution function

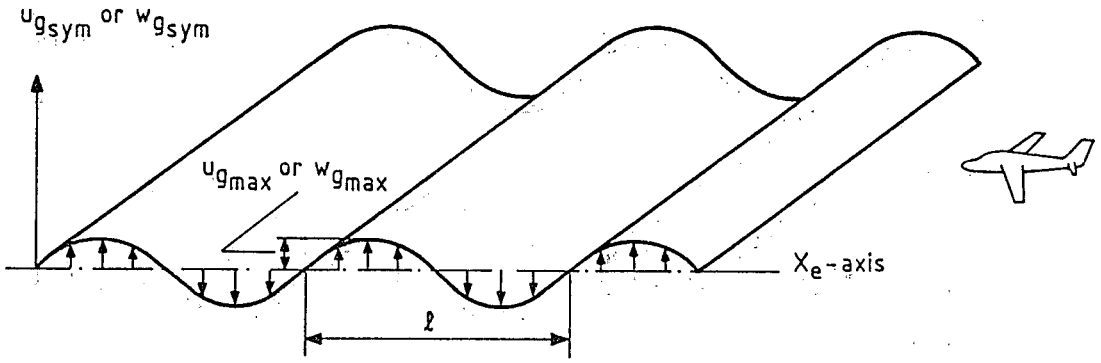

Fig. 2[a] . Sinusoidal elementary field of flow.
$u_{g_{sym}}$ and $w_{g_{sym}}$ vary only along the X_e-axis,
the wavelength in spanwise direction is assumed to be infinite.

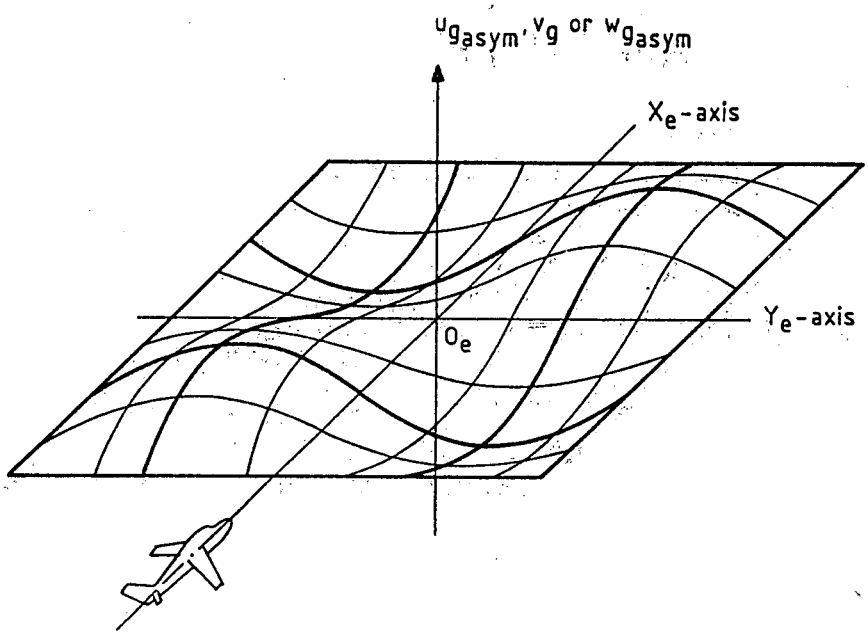

Fig. 2[b] . Two-dimensional elementary flowfield
(Fig.45a is a simplified case of this flowfield).
The turbulence velocities $u_{g_{asym}}$, and v_g and $w_{g_{asym}}$
change sinusoidally in the X_e- as well as in the Y_e-direction.

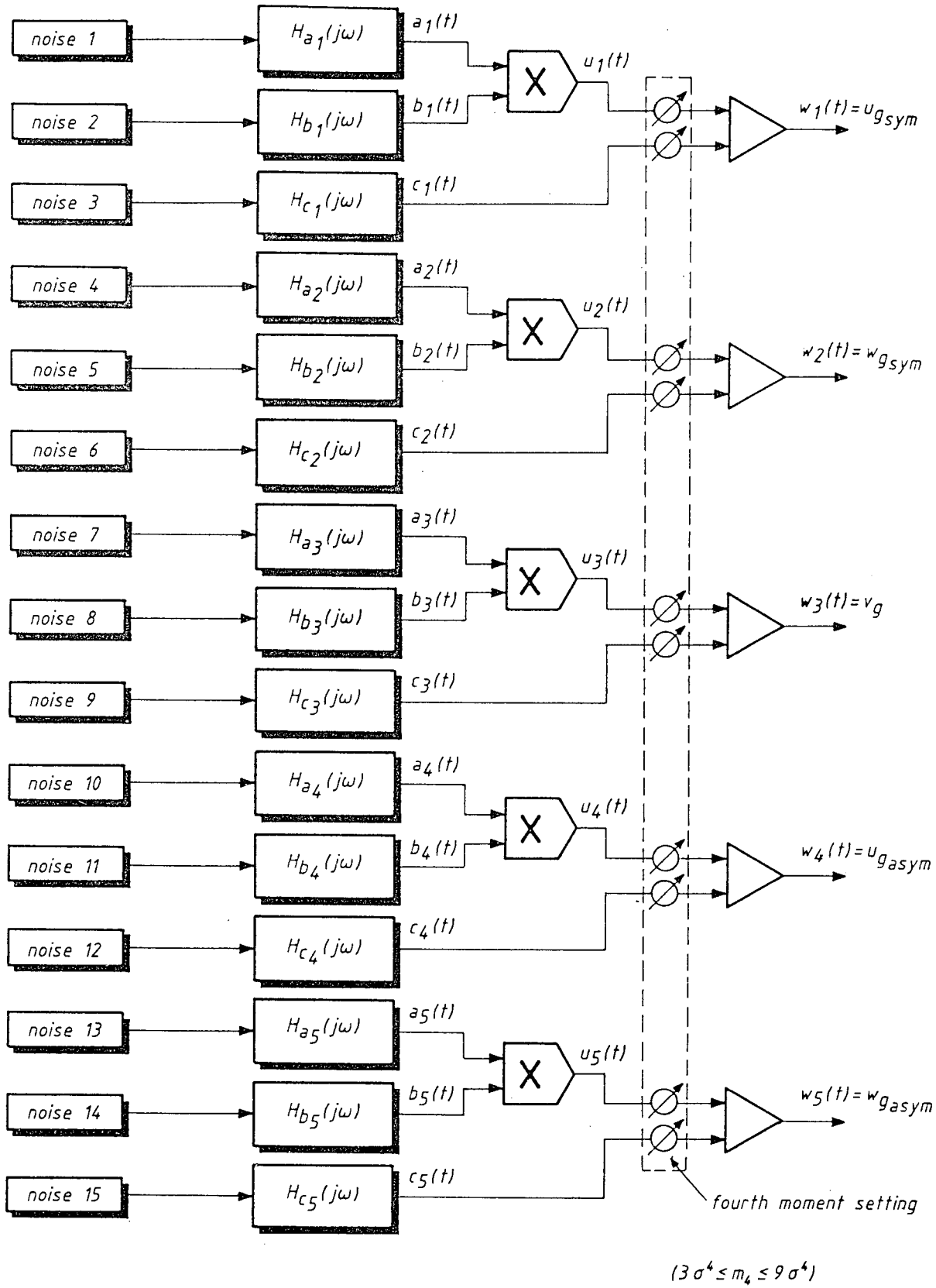

Fig. 3 . The generation of 'Patchy' atmospheric turbulence for real-time flight simulation.

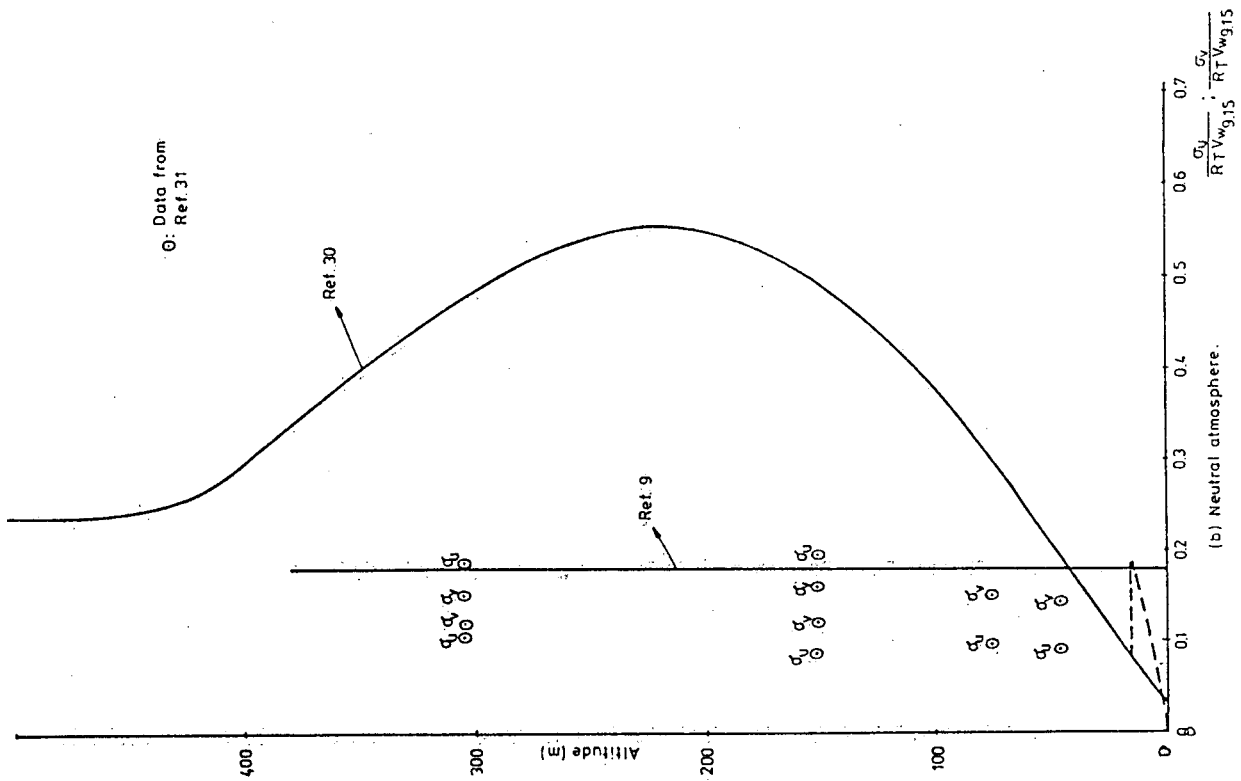

Fig. 4 . (Continued)

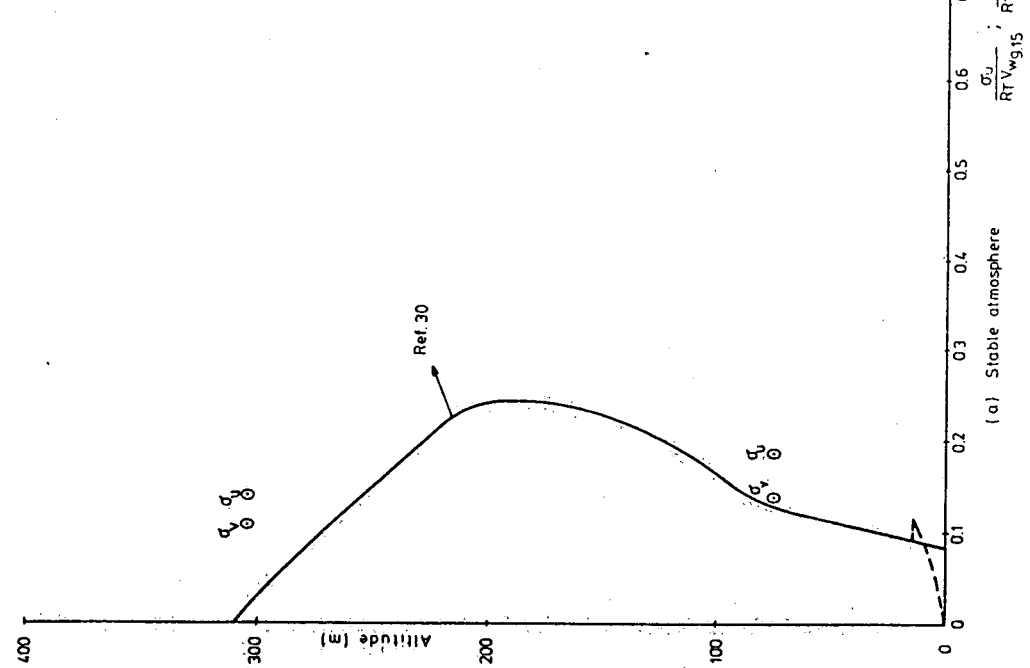

Fig. 4 . Standard deviation of longitudinal and lateral turbulence velocities

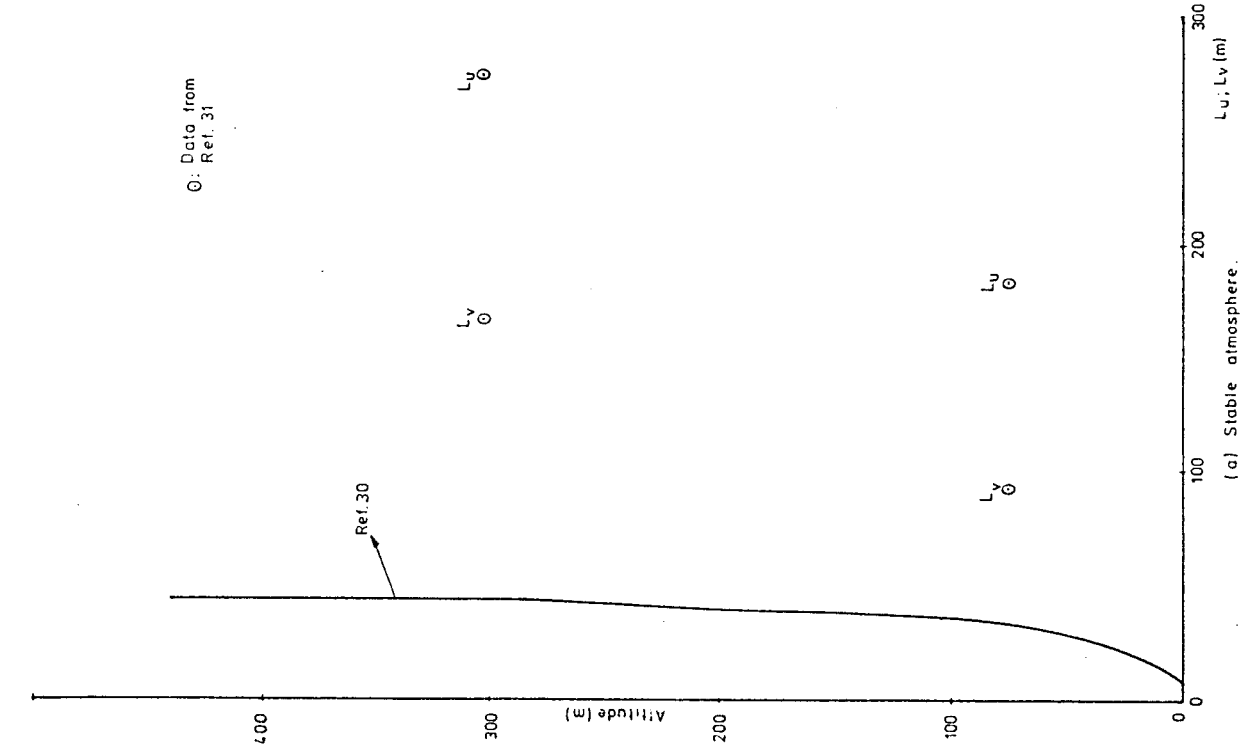

Fig. 4 . (Continued)

Fig. 5 . Scale lengths of longitudinal and lateral turbulence velocities

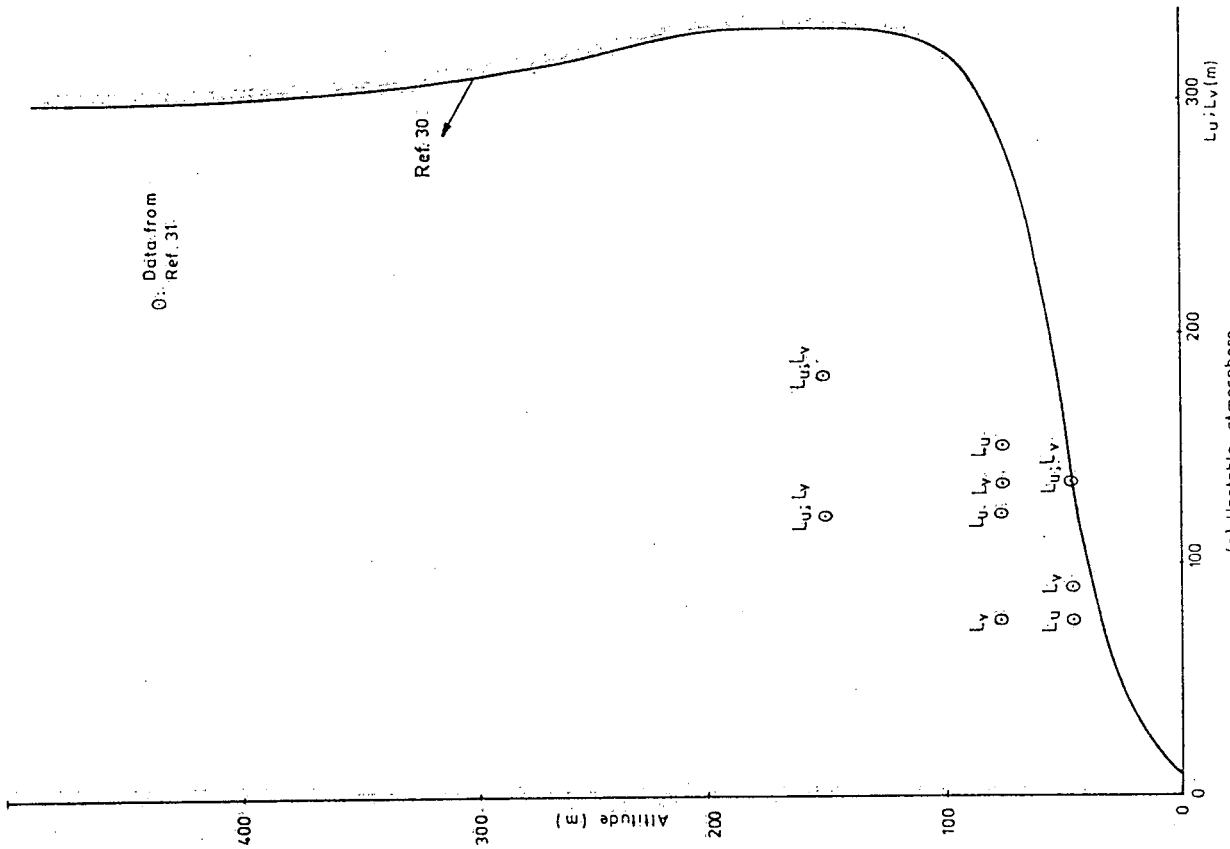

Fig. 5 · (Continued)

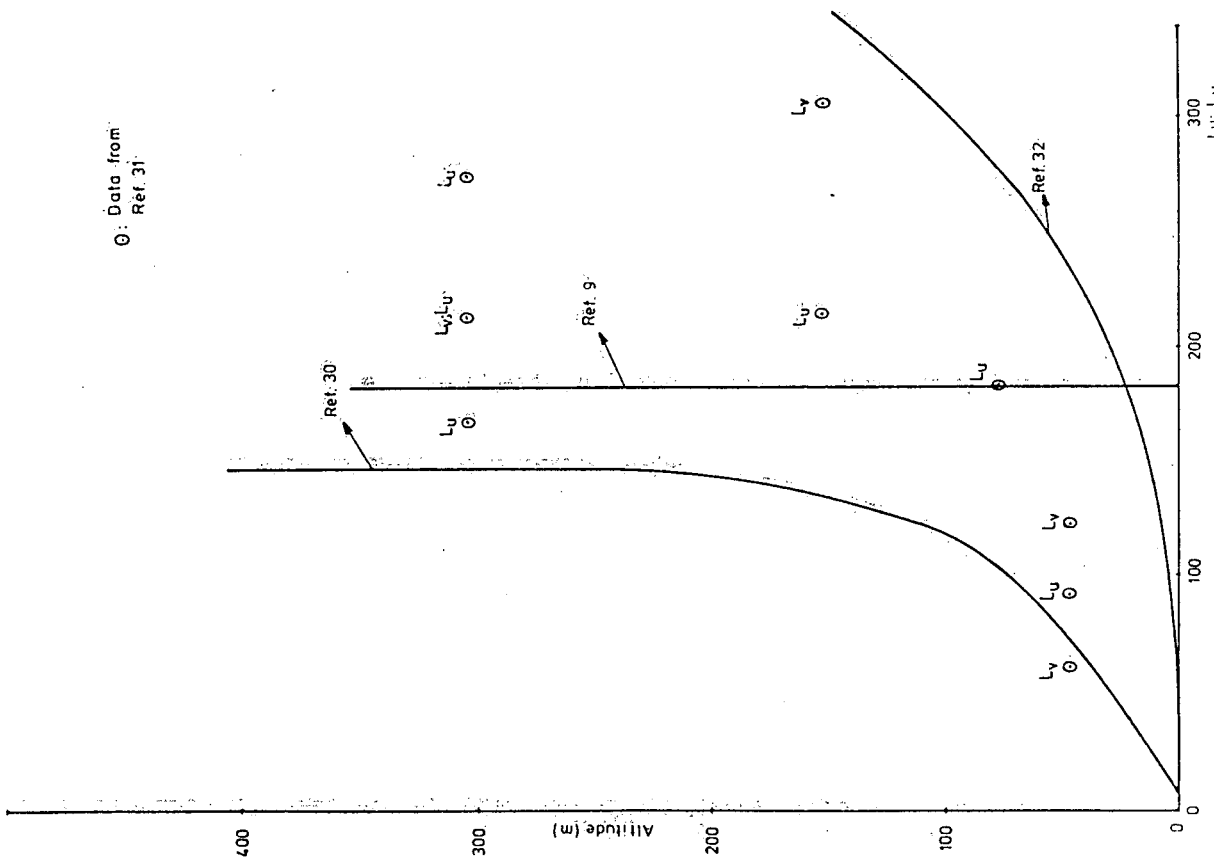

Fig. 5 .(Continued)

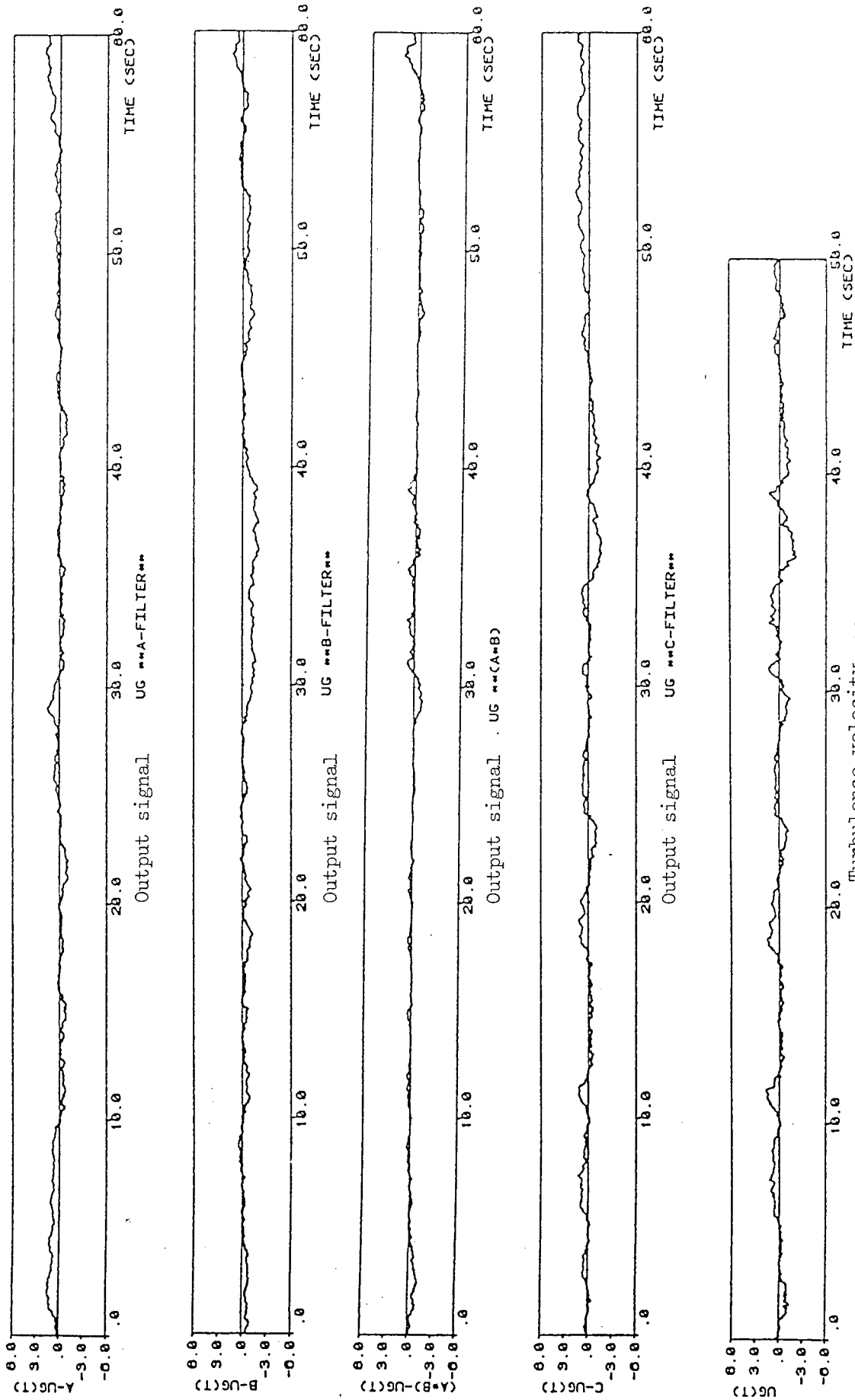

Fig. 6. Composition of the longitudinal turbulence velocity $u_{g_{sym}}$ for R=1.0 and Q=1.0.

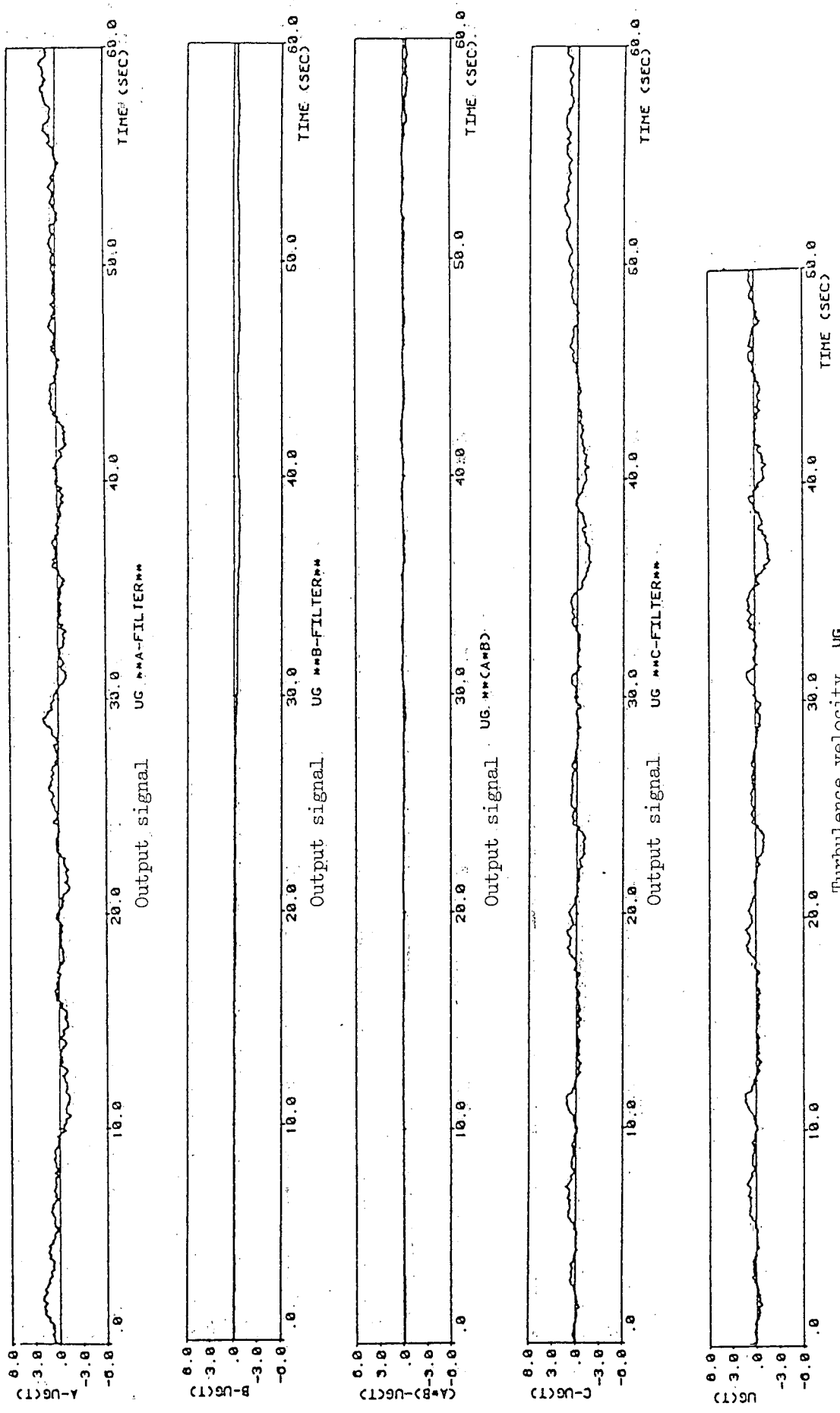

Fig. 7 . Composition of the longitudinal turbulence velocity $u_{g_{sym}}$ for R=0.01 and Q=1.0.

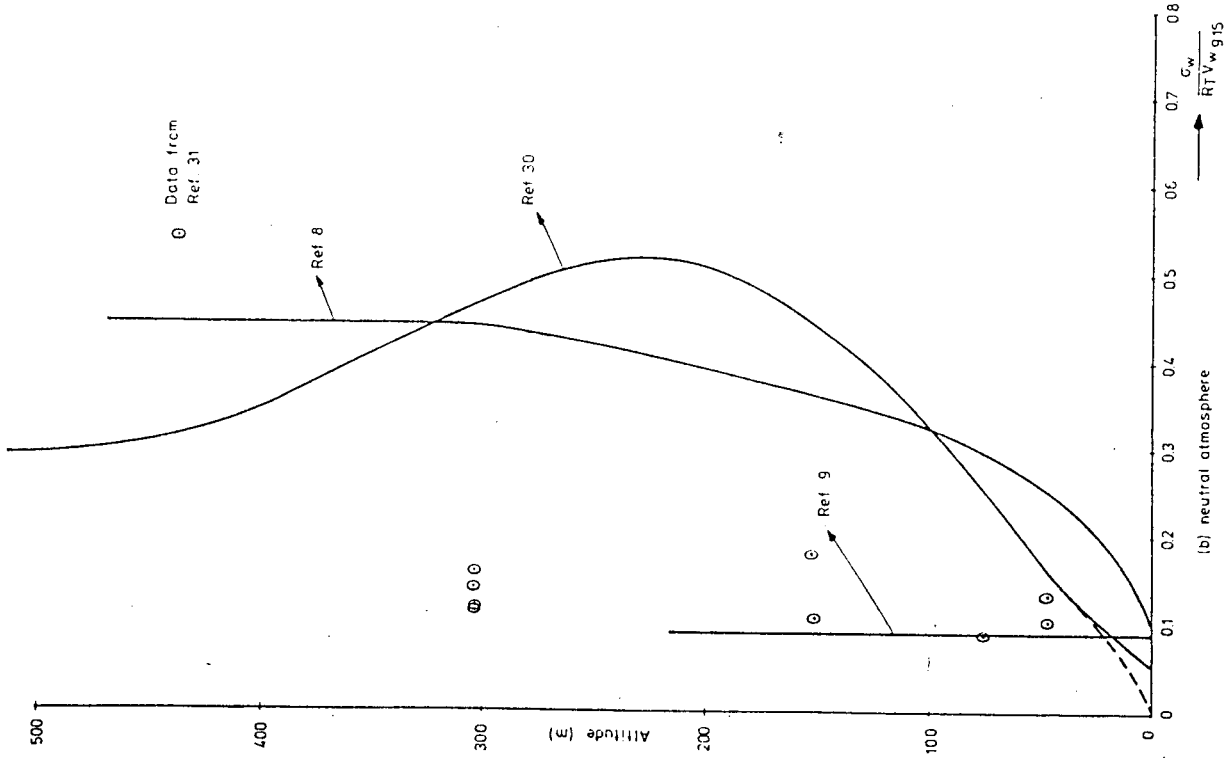

Fig. 8 .(Continued)

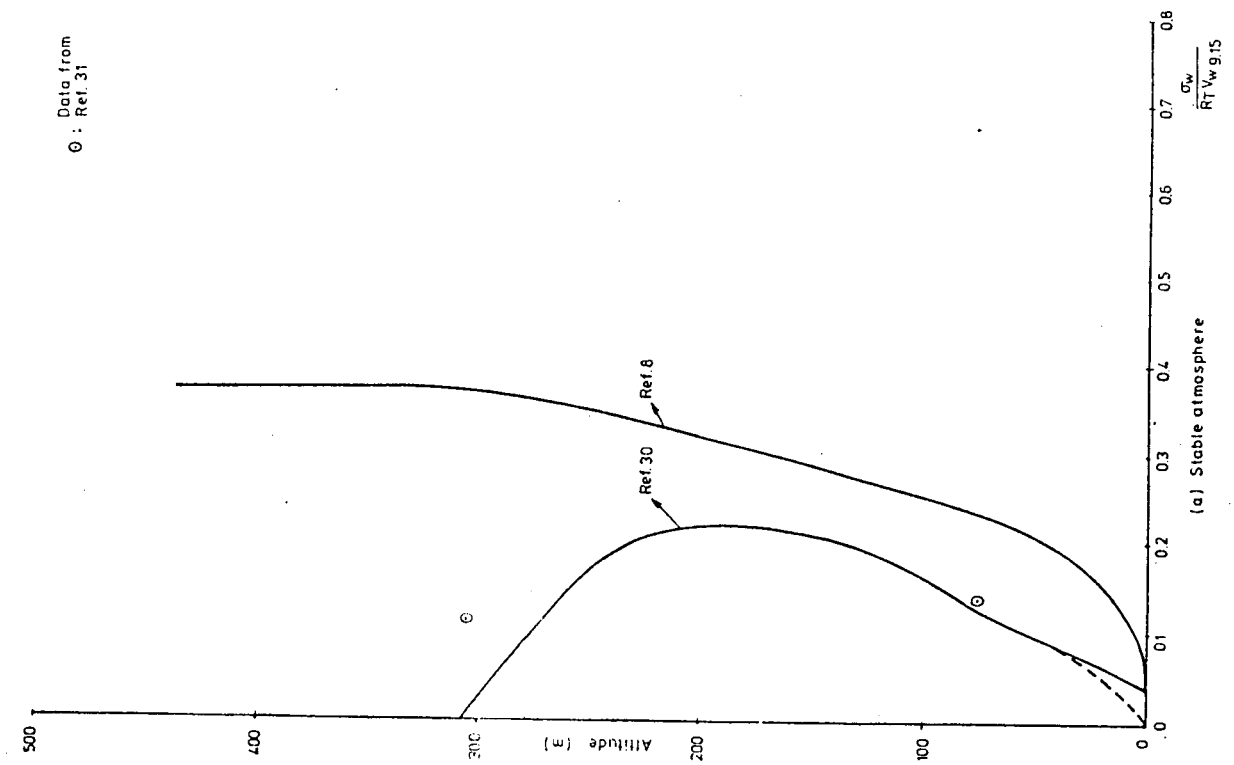

Fig. 8 Standard deviation of vertical turbulence velocity

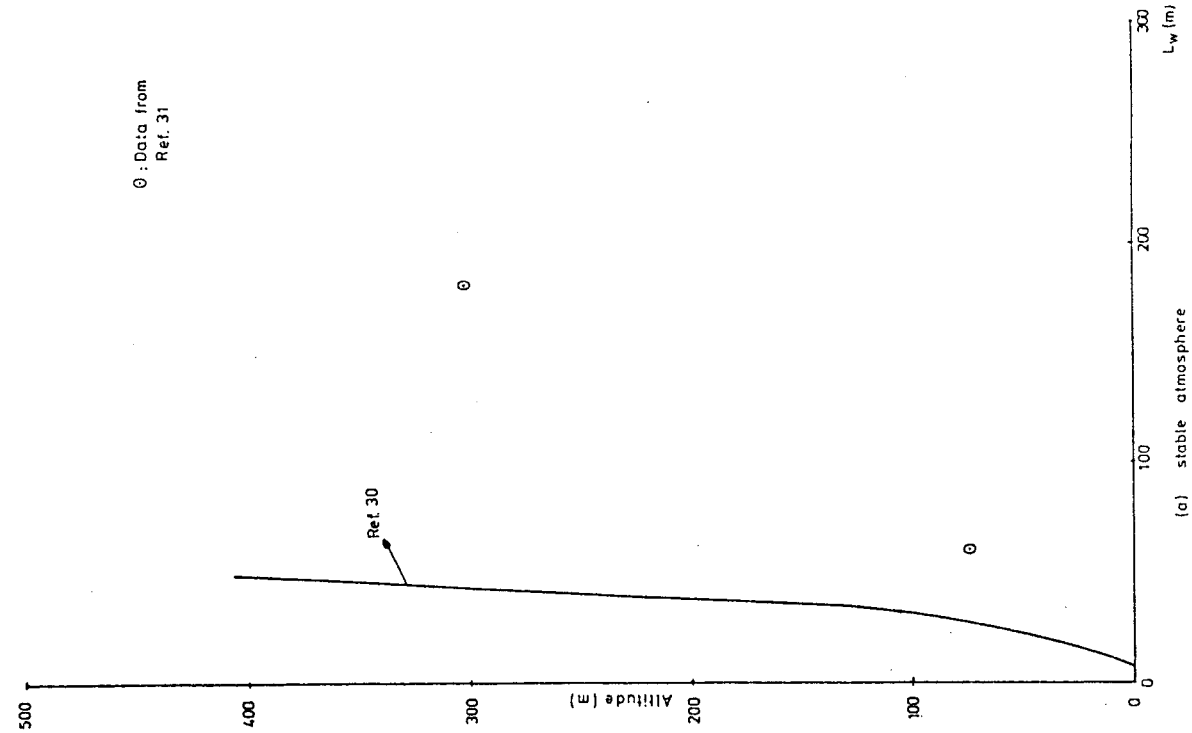

Fig. 9 .Scale length of vertical turbulence velocity

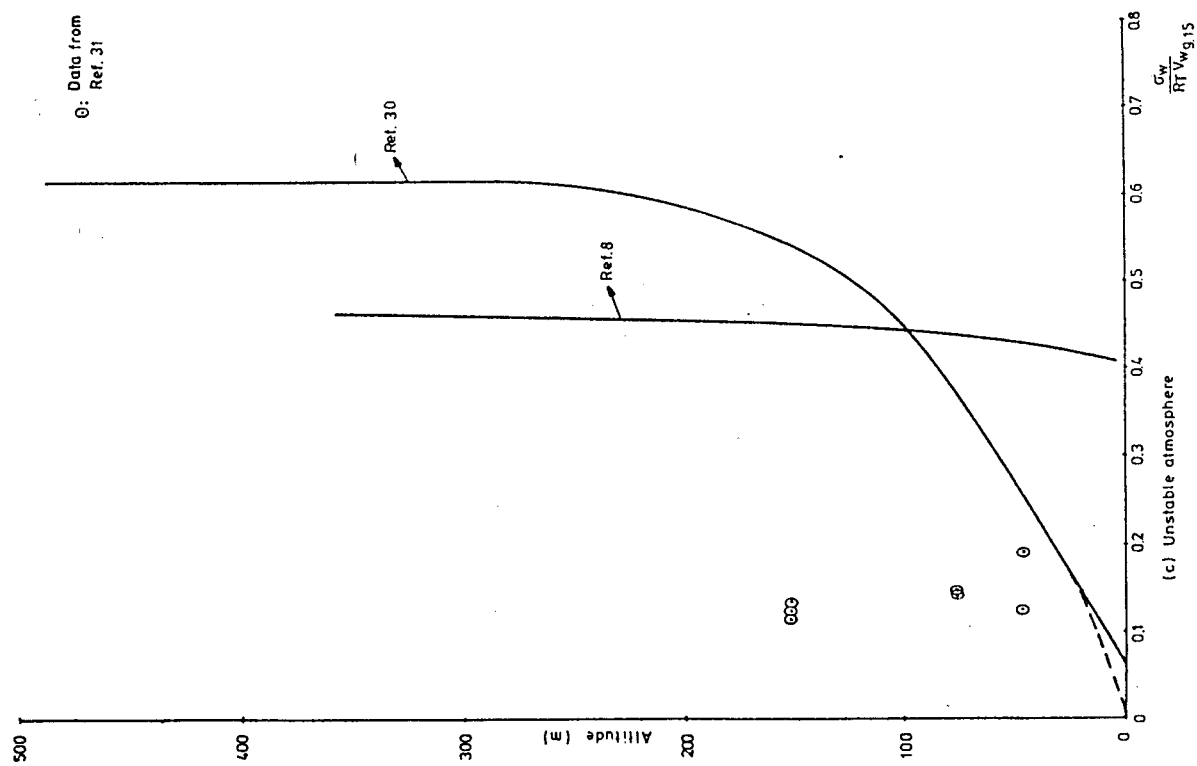

Fig. 8 (Continued)

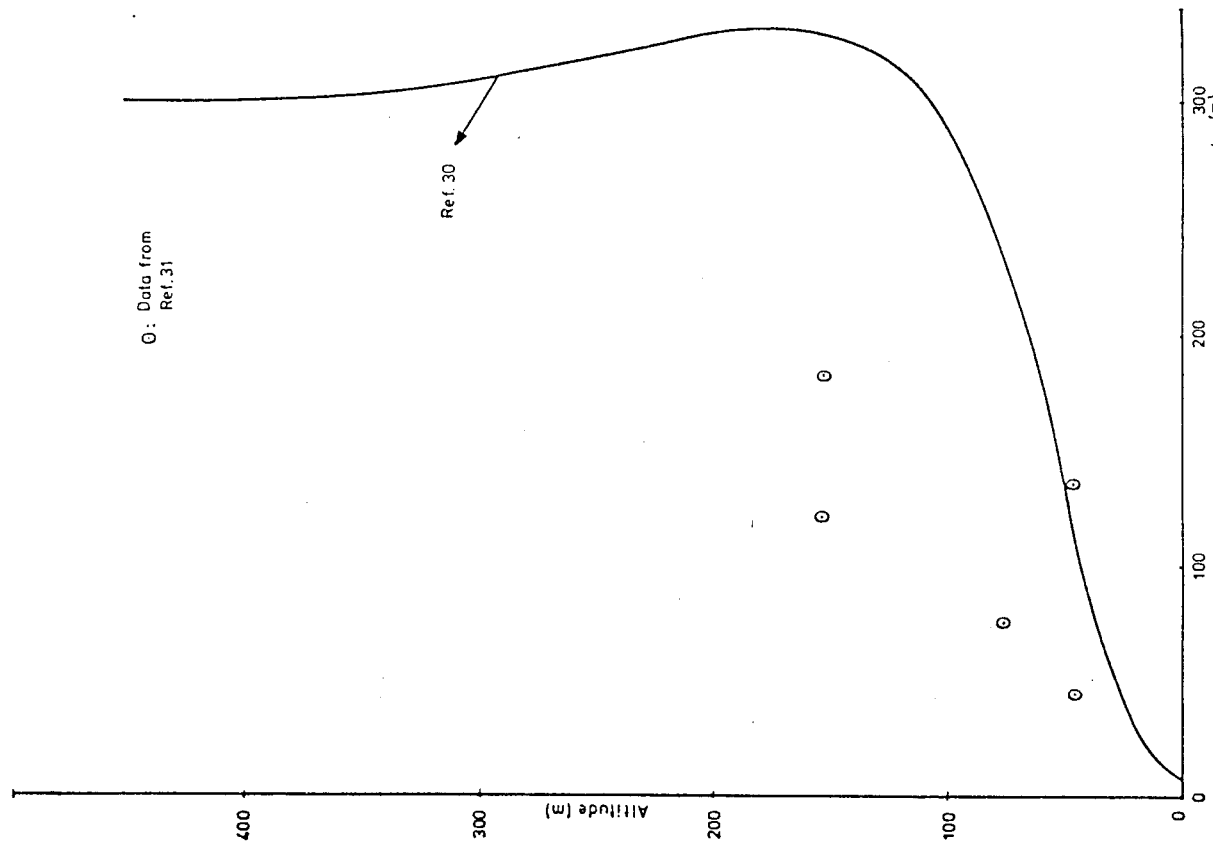

Fig. 9 .(Continued)

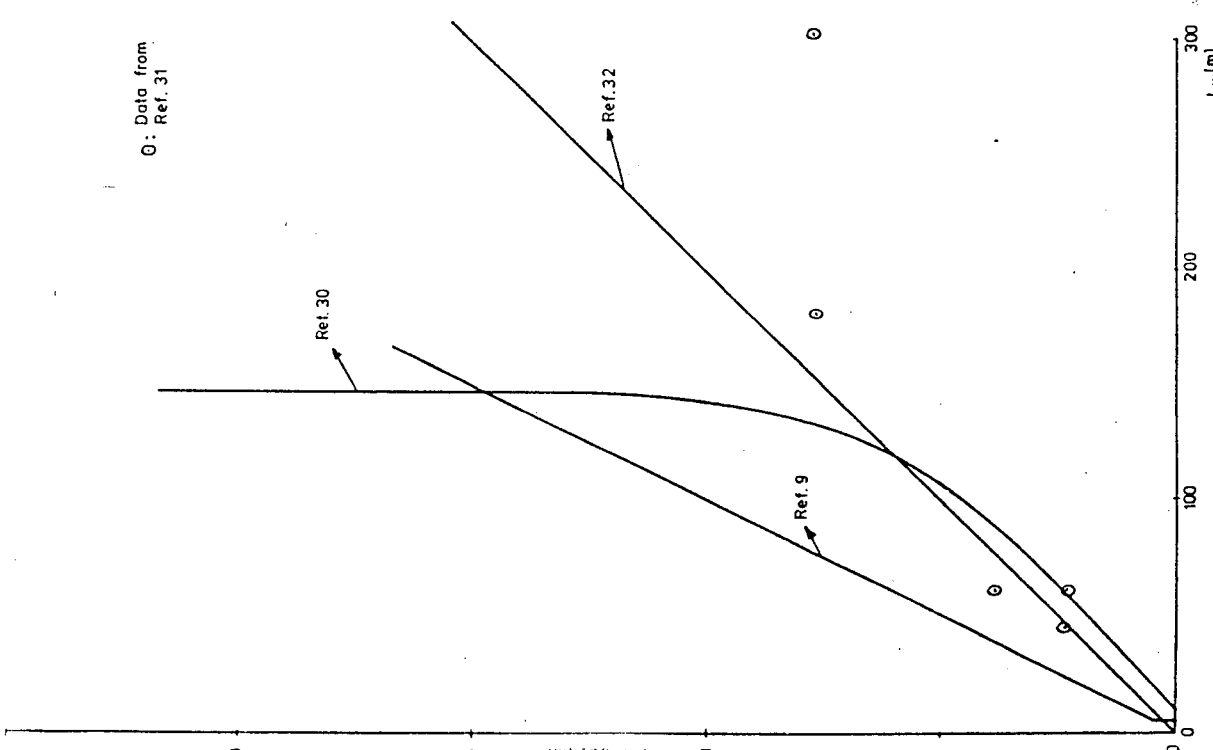

Fig. 9 .(Continued)

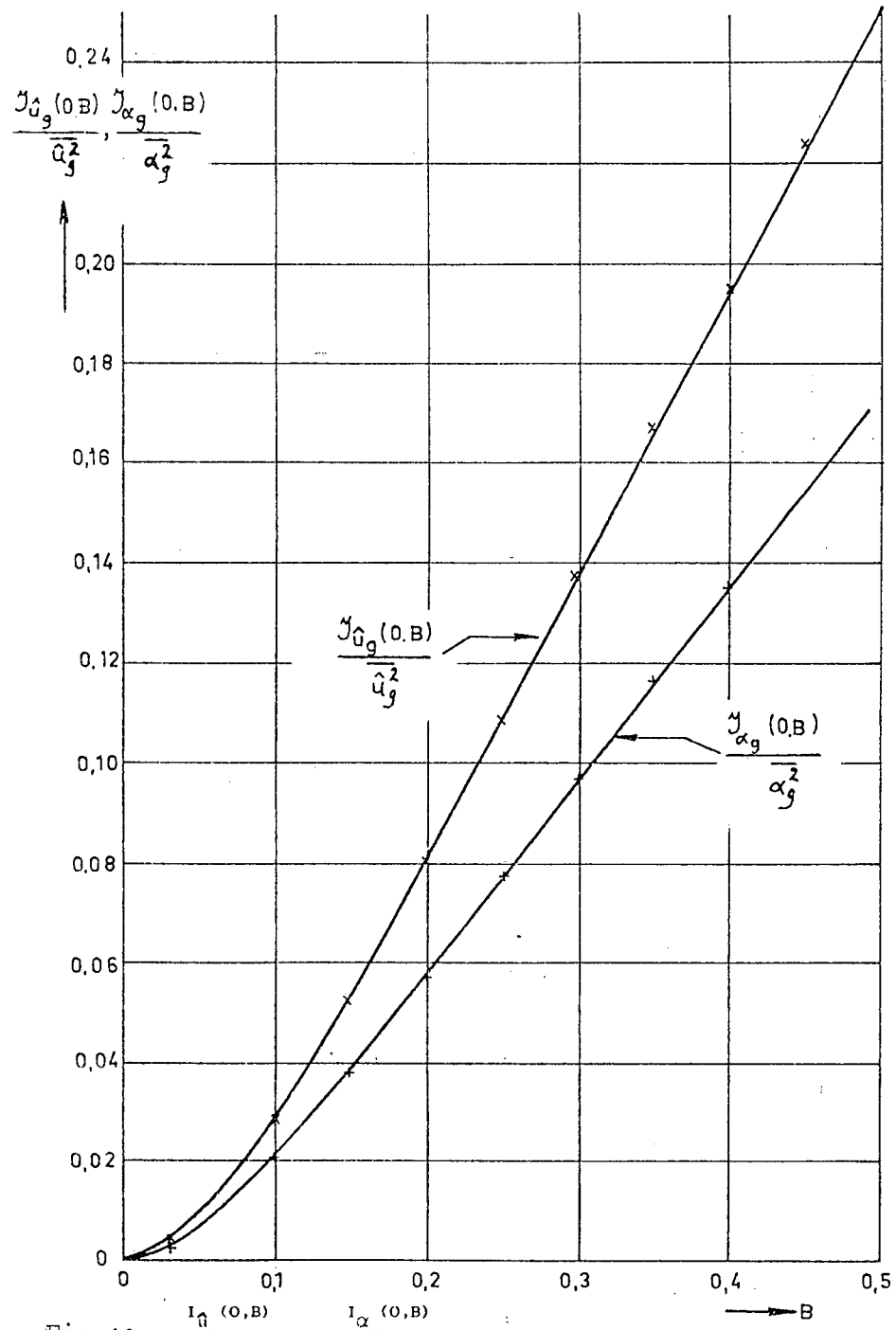

Fig. 10 · $\frac{I_{\hat{u}_g}(0,B)}{\hat{u}_g^2}$ and $\frac{I_{\alpha_g}(0,B)}{\alpha_g^2}$ as functions of B.

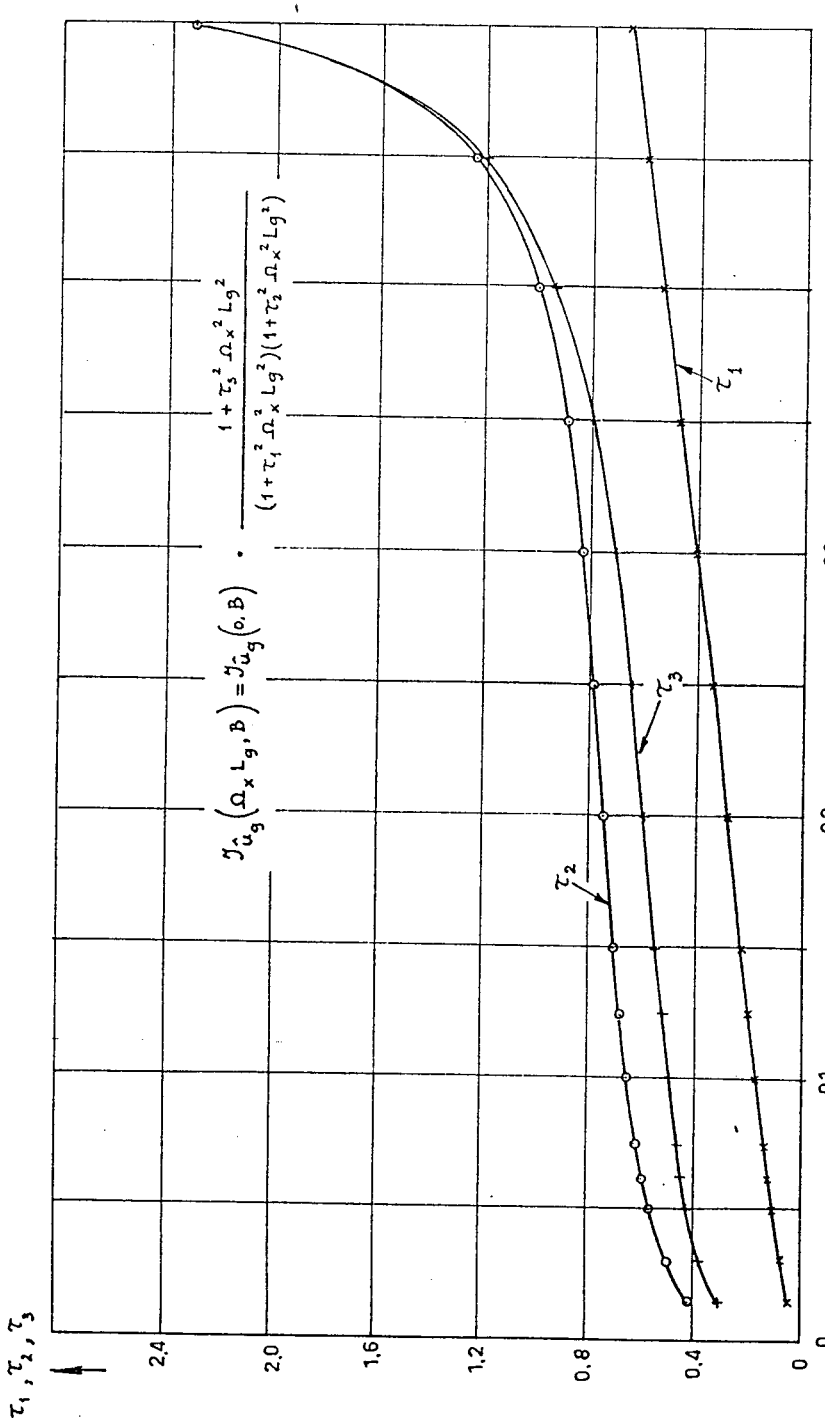

Fig. 11. τ_1, τ_2 and τ_3 in the approximated power spectral density function of the horizontal gust velocity, as functions of B.

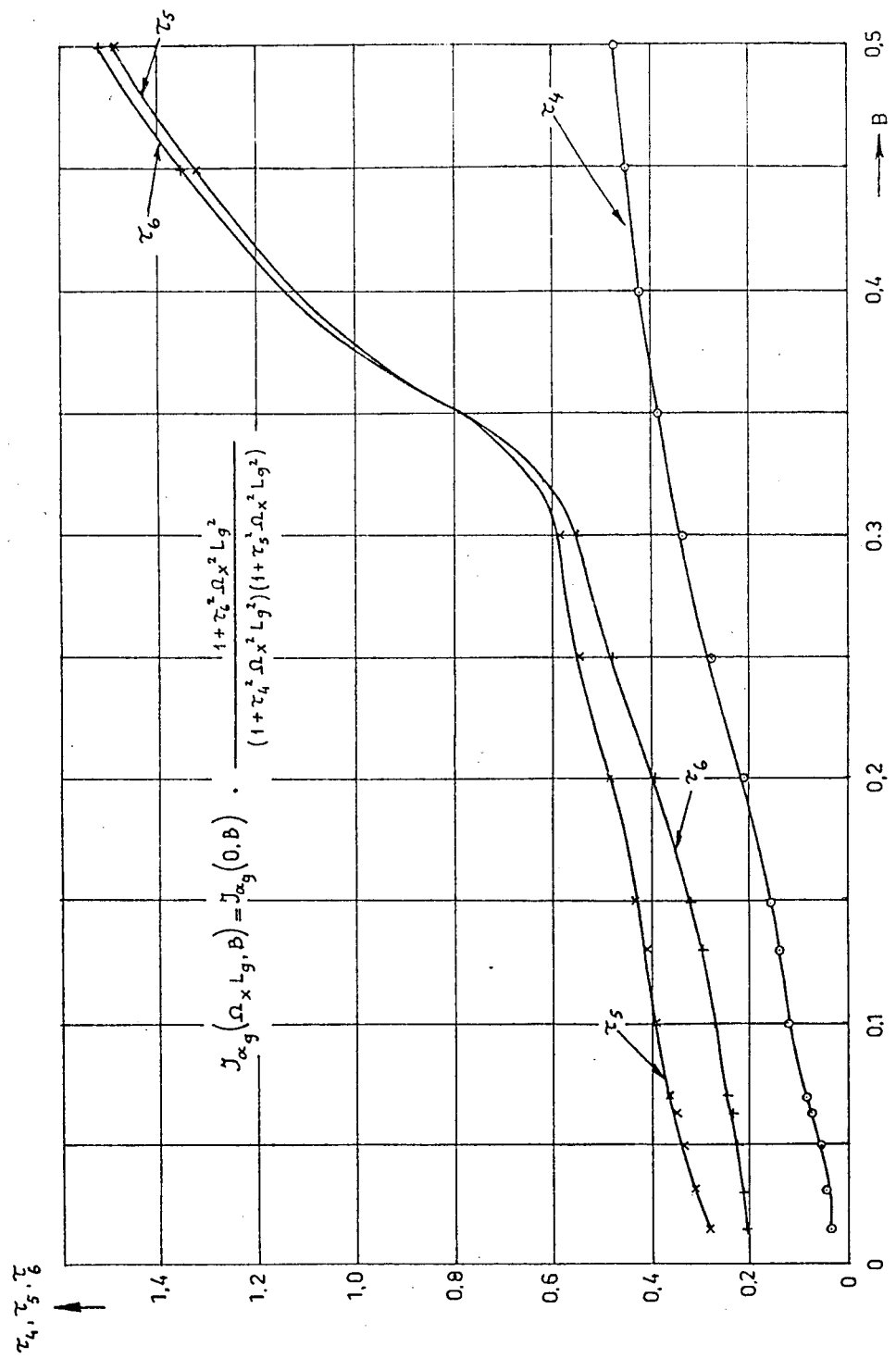

Fig. 12. τ_4, τ_5 and τ_6 in the approximated power spectral density function of the vertical gust velocity as functions of B.

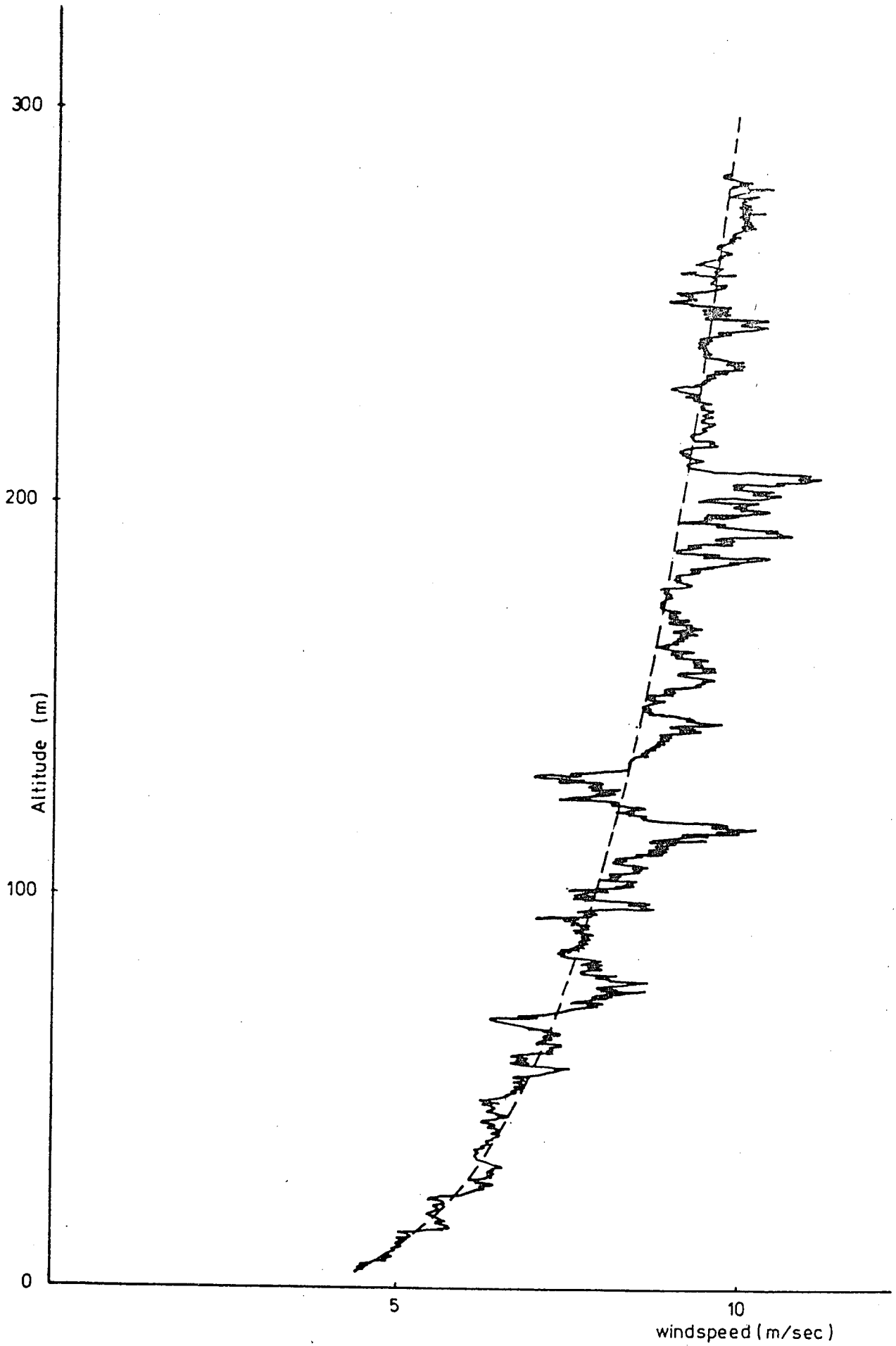

Fig. 13. Superposition of the wind profile and turbulence

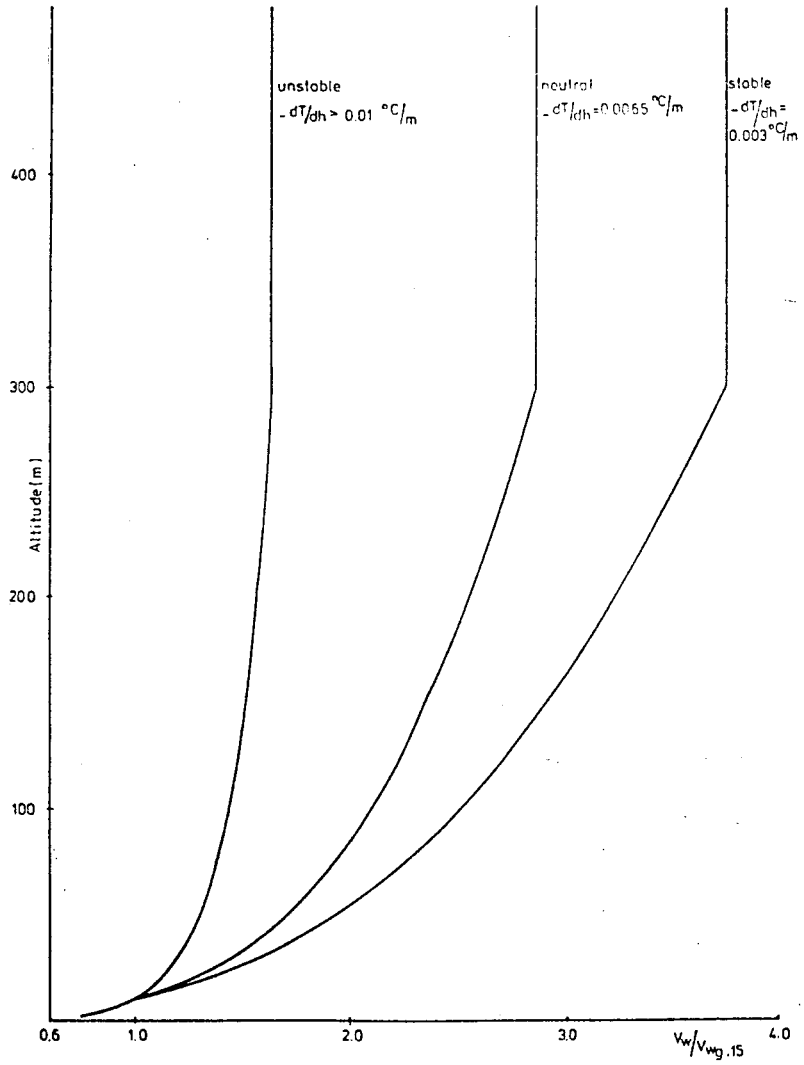

Fig.14 Wind profiles for three atmospheric stability conditions

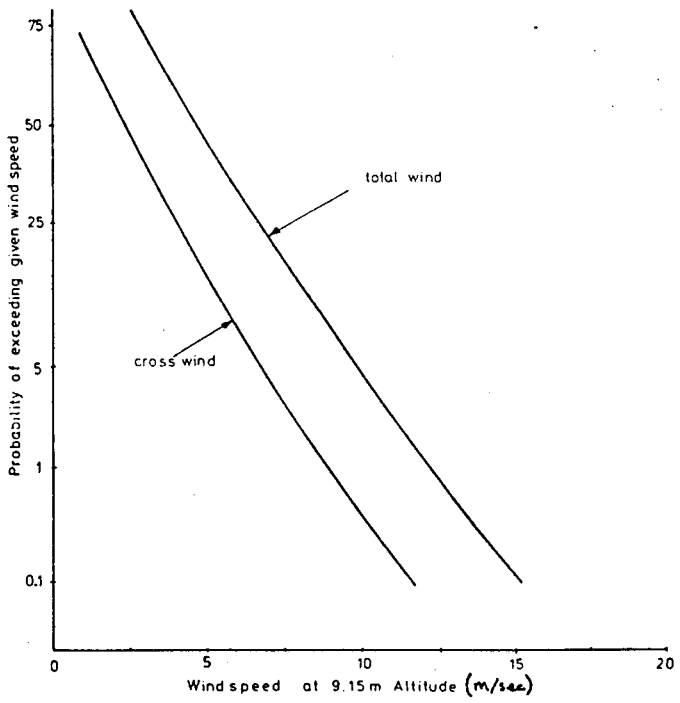

Fig.15 Cumulative probability of reported mean wind and cross wind

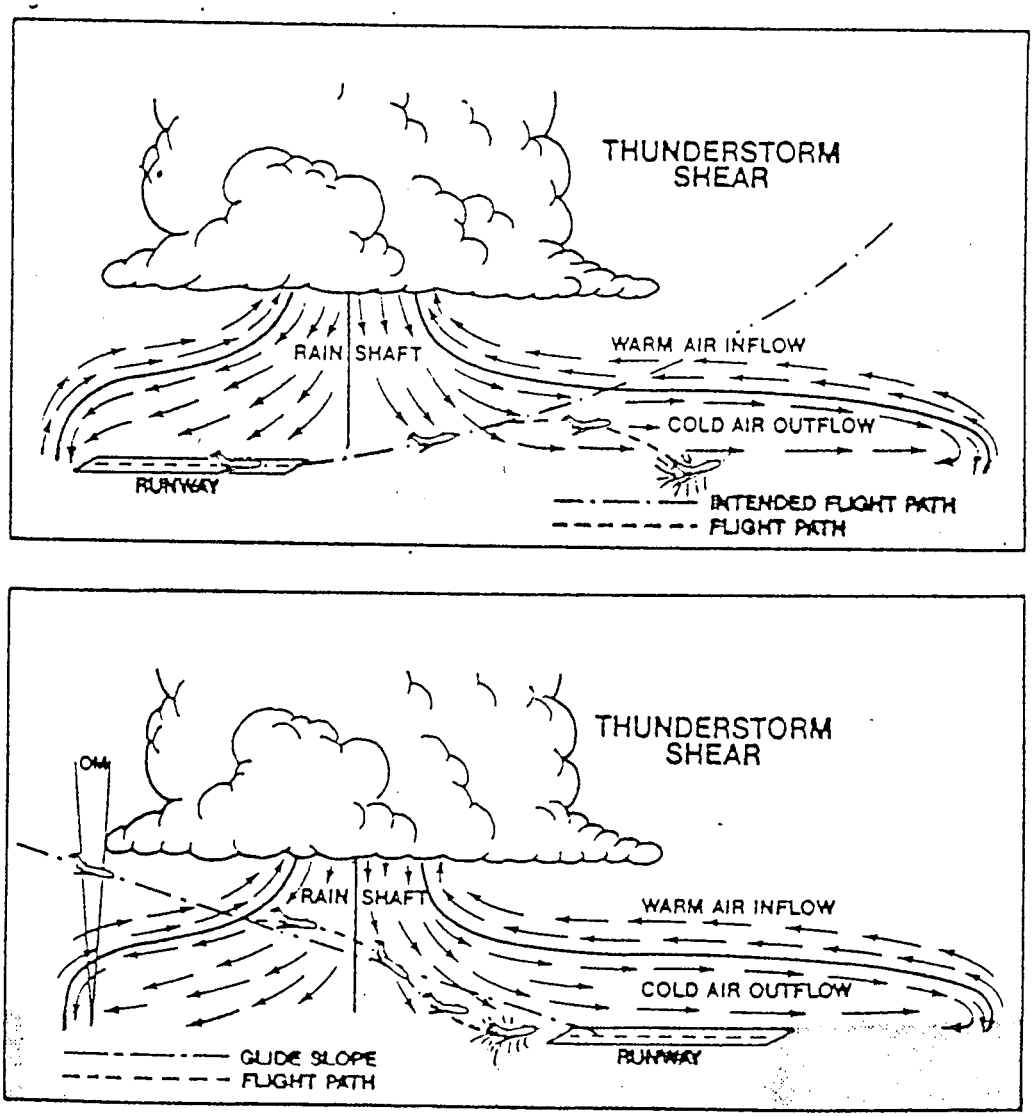

Fig. 16. Thunderstorm Shear